THE DURABILITY OF GLASS FIBRE REINFORCED CEMENTS MADE WITH NEW CEMENTITIOUS MATRICES

PHILIP PURNELL

Doctor of Philosophy

ASTON UNIVERSITY

April 1998

ASTON UNIVERSITY

"The Durability of Glass Fibre Reinforced Cements made with New Cementitious Matrices": **Philip Purnell; PhD, 1998.**

THESIS SUMMARY.

Widespread use of glass fibre reinforced cement (GRC) has been impeded by concerns over its durability. Three degradation mechanisms are proposed - fibre corrosion, $Ca(OH)_2$ precipitation and matrix densification - although their relative importance is debated. Matrices with reduced alkalinities and $Ca(OH)_2$ contents are being developed; the aim of this study was to investigate their hydration and interaction with alkali-resistant fibres to determine the factors controlling their long-term durability, and assess the relevancy of accelerated ageing. The matrices studied were;

- OPC/calcium-sulphoaluminate cement plus metakaolin (**C**),
- OPC plus metakaolin (**M**),
- blast-furnace slag cement plus a micro-silica based additive (**D**).
- OPC (**O**).

Accelerated ageing included hot water and cyclic regimes prior to tensile testing. Investigations included pore solution expression, XRD, DTA/TG, SEM and optical petrography. Bond strength was determined from crack spacings using microstructural parameters obtained from a unique image analysis technique. It was found that, for the new matrices;

- pore solution alkalinities were lower,
- $Ca(OH)_2$ was absent or quickly consumed,
- different hydrates were formed at higher immersion temperatures,
- degradation under 65°C immersion was an order of magnitude slower,
- no interfilamental $Ca(OH)_2$ was observed.

Sporadic rather than massive interfilamental $Ca(OH)_2$ precipitation was observed in O-GRC. Immersion ageing at 20 and 38°C caused no degradation. Bond strength was found to quickly reach a terminal value which decreased as the ageing temperature increased.

It was concluded that;

- fibre weakening caused by flaw growth was the primary degradation mechanism and was successfully modelled on stress corrosion/static fatigue principles. OPC inferiority was attributed partly to its higher alkalinity but chiefly to the growth of $Ca(OH)_2$ aggravating the degradation;
- hot water ageing although useful in model formulation and contrasting the matrices, changed the intrinsic nature of the composites rather than simply accelerating the degradation mechanisms.

Keywords: ***degradation, model, accelerated ageing, bond strength, image analysis.***

DEDICATION.

To those who said I should and those who said I couldn't.

To my wife, for her tolerance.

ACKNOWLEDGEMENTS.

I am deeply indebted to my supervisor, Dr. Neil Short, for his continual support, advice and patience but most importantly supervision without interference (an exceedingly rare commodity). Both this work and myself would have been much poorer but for his academic, administrative and personal support. Thanks are also due to a great many people within the department, especially Prof. C.L. Page for his insight, guidance and lengthy discussions, Colin Thompson for his invaluable remedial assistance with regard to my laboratory skills and knowledge of analytical techniques, Bill and Pete in the workshop for all the excellent kit built at the drop of a hat with only envelope backs and handwaving to go on, our sterling office staff, Al Buchanan for his help in developing the image analysis technique and Dr. M. Page for her help and advice. I also wish to thank those at the BRE who were involved in the project, especially Dr. A.J. Majumdar for bringing his unparalleled knowledge of GRC to bear on the project and Dr. P.L. Walton for his extensive assistance with regard to mechanical testing, and analysis and interpretation of results thereof. Thanks are also due to Dr K. Quillin for his assistance with XRD analysis and Dr. R.G. Sibbick for his advice on petrology and optical microscopy, and to Prof. P. Bartoš of Paisley University for his most valuable input and criticism.

The financial support from EPSRC (# GR/K 05436) and contributions from CemFIL International and Blue Circle are also gratefully acknowledged.

LIST OF CONTENTS

APPENDICES:

LIST OF TABLES AND FIGURES

TABLES

FIGURES

1. INTRODUCTION.

1.1. Glass fibre reinforced cement (GRC).

Glass fibre reinforced cement (GRC) is a versatile, modern construction material, generally produced in thin sheet form, with a wide variety of uses. It is particularly suited to non-structural applications such as cladding, roofing, permanent formwork and façade renovation. It is also increasingly employed as a substitute for traditional asbestos cement sheet following the widely publicised revelations concerning the health hazards associated with asbestos fibres.

1.1.1. Historical.

GRC was first manufactured in the former USSR by Biryukovich *et al* (1964) using low-alkali cements and glass fibre used for electrical insulation (E-glass). Further work, carried out by Majumdar and Ryder (1968) at the Building Research Establishment (BRE), was aimed at improving the alkali resistance of the glass fibres to improve their performance in ordinary Portland cement (OPC) matrices, facilitating wider application of GRC. The resulting alkali-resistant (AR) fibres, containing large amounts of zirconia were commercially developed by Pilkington plc.

1.1.2. Production.

Typical commercial GRC products contain around 5% of AR fibre by volume. The fibre, normally supplied in a continuous roving of 32 or 64 strands, each of about 200 filaments, is then chopped into pre-determined lengths during production. The fibre may occasionally be supplied pre-chopped or in woven mat form. Fine aggregate (i.e. sand) is added to the (normally Portland) cement matrix in varying quantities from none to 50% to reduce specific cost and shrinkage. Complex combination super-plasticisers/retarders are employed to control workability and setting behaviour.

The most common production process for thin sheets is spraying, where continuous roving and a cement or mortar slurry are supplied to a dual nozzle gun. An integrated chopper unit cuts the roving into carefully controlled lengths. The roving disperses into strands on contact with the slurry, producing a random 2-d fibre orientation. Other production processes include winding (e.g. for pipes), hand lay-up for small

batches, extrusion and premix formulations. While still 'green', the flat sheets may undergo further forming as in the production of corrugated sections or sandwich panels. The resultant panels are normally 8-12mm thick and have been manufactured in sizes up to 7.5 × 3m.

1.1.3. Durability.

The growth in the market for GRC, although given a significant boost by the widespread outlawing of asbestos, has been impeded by concerns over its long term durability, especially in wet environments. It has been widely documented that over timespans less than that of a reasonable service life, 'traditional' GRC made with AR fibre and OPC suffers a marked reduction in tensile strength and ductility in the presence of moisture and particularly under Northern European type weathering conditions. It is generally accepted that the major degradation mechanisms are hydroxyl corrosion of the glass fibre reinforcement in the highly alkaline cement matrix environment and precipitation of hydration products (principally $Ca(OH)_2$ [portlandite] crystals) within the fibre bundles. A number of secondary mechanisms (generally explained using fracture mechanics principles) caused by the densification of the matrix in the interfacial zone are also frequently proposed. Comprehensive reviews and discussion of the literature can be found in Majumdar & Laws (1991) and Bentur & Mindess (1990).

GRC is a relatively young material. As a result of the concerns about durability and the obvious lack of long term performance data for the composite, accelerated ageing techniques were developed to help assess the likely behaviour of GRC after long periods in service. The most common and widely accepted of these tests, where coupons of the composite are submerged in water at elevated temperatures for varying times, is based on a bending-strength predictive model allowing a particular ageing regime to be correlated with a 'true' natural ageing period in a given climate (Litherland *et al.,* 1981). It should be noted that only bending strength predictions are valid from this model; no inference as to the likely impact strength or failure strain after ageing can be directly made.

This model was originally developed for OPC/first generation fibre composites. Whether the model can be extended to composites containing modified cements and second-generation fibres has yet to be confirmed. Other accelerated ageing systems include hot/cold or wet/dry cycling and freeze-thaw cycling. No predictive models appear to have been advanced regarding their relationships to natural weathering.

1.1.4. Fibre development.

Two obvious approaches to improving the durability of GRC present themselves: increasing the alkali resistance of the fibres and modifying the composition of the matrix in order to reduce its alkalinity and/or its tendency to precipitate portlandite within the fibre bundles. Research has previously tended to concentrate on the former approach, with the result that a number of 'second generation' fibres are commercially available. These fibres combine high alkali resistance with complex organic coatings ('sizes') which purport to modify the hydration processes in the interfacial region. This results in a retardation or elimination of portlandite intrusion into the inter-filamental spaces and also retards densification of the matrix at the interface.

1.1.5. Matrix development.

Despite the fact that since its conception GRC has been made with non-Portland cement matrices, little further work on matrix improvement has taken place until recently. Much attention has focused on additives for OPC, generally pozzolanic in nature, which reduce both the matrix alkalinity and the production of free lime. Pulverised fuel ash (pfa), condensed silica fume (microsilica or CSF) and ground granulated blast furnace slag (ggbs) have been widely investigated. More recently, calcined china clay or metakaolin has come under investigation as a useful additive for GRC. Acrylic co-polymer emulsions have also become a popular additive to help improve durability, often in conjunction with one or more of the other additives mentioned above.

Of the non-Portland cements, high-alumina cement (HAC) and blast furnace slag cements have been considered suitable for GRC production, mainly due to their lower alkalinity. Interest is growing in the use of calcium sulpho-aluminate cements, which

have the added advantage of a rapid set and hence a shorter mould cycle, allowing faster product turnover.

The improved apparent durability of GRC made with these novel cementitious mixtures compared with OPC-GRC is normally simply attributed to either lower matrix alkalinity (hence less fibre corrosion) or reduced free lime production (hence less inter-filamental portlandite precipitation). There is still considerable debate concerning the relative importance of these two conditions. Moreover, little is known of the more detailed cement/glass interfacial processes underlying the improved durability of novel matrix GRC.

As with all composites, the interfacial zone is of fundamental importance in the behaviour of GRC. A greater understanding of its changing nature with ageing and continued matrix hydration is needed in order that the long-term behaviour of the new GRCs can be more confidently predicted. This should lead to increased utilisation of this versatile construction material.

1.2. Aims and objectives.

The primary objective of this project was to determine the factors that control the long term durability of a number of modern GRC formulations under various ageing regimes. This was achieved through investigation of the hydration chemistry of these new cement matrices and their interactions with AR glass fibre.

The primary facets of the project were:

- *Investigation of the hydration chemistry of the new matrices including determination of the pore solution and solid phase compositions.* Pore solution composition was determined using high pressure extraction techniques refined over a number of years at the University. Solid phase analysis was performed using standard x-ray diffraction and x-ray fluorescence (XRD/XRF), traditional optical petrography and differential thermal/ thermogravimetric analyses (DTA/TGA). Some traditional 'wet' chemistry techniques were used as appropriate.

- *Investigation of the micro- and macro-scopic interactions between the new matrices and AR glass fibre and the relationship of these interactions with the long term durability of GRC.* Continuous aligned grc composites were manufactured and aged using accepted methods of accelerated ageing. Samples were then subjected to direct tensile tests. Macroscopic results (ie. stress/strain curves and crack spacings) were analysed alongside microscopic investigations of the glass/cement interfaces after varying ageing regimes to provide an insight into the mechanisms by which GRC degrades.
- *Appraisal of the relevance of conventional accelerated ageing tests to the determination of parameters controlling long term durability in service environments.* Conclusions drawn from the investigations outlined above, compared with the known in service behaviour of GRC, permitted a critique of current widespread ageing techniques to be advanced.

2. LITERATURE REVIEW.

2.1. Introduction.

The concept of improving the performance of brittle materials with fibres has been known since biblical times. Reinforcement of clay bricks with straw, plaster with horsehair and mud with twigs and branches (wattle and daub) has been commonplace for centuries. Although the strength of the matrices may be only marginally increased, the great advantage comes from the post-cracking 'pseudo-ductility' provided by the fibres. The mode of failure is changed from a brittle, 'fast' fracture at peak stress to a mode where some cracking can be tolerated without catastrophic rupture.

Brittle cements appeared to lend themselves to fibre reinforcement; the first important material thus developed being the ubiquitous asbestos cement. This was first commercially produced in about 1900 with the development (from paper making technology) of the Hatschek process (Hannant, 1978). Despite its poor impact strength, asbestos cement was extensively employed in sheet form world-wide until information concerning the considerable carcinogenic hazard posed by asbestos fibres began to surface.

These health concerns provided the main spur for research into alternative fibres for cement reinforcement. A large number of different fibrous materials have been considered; in his review, Majumdar (1992) lists fourteen types including glass, carbon, various polymers, natural or processed vegetable fibres and steel.

Apart from strength and a reasonable failure strain, the primary attribute of any cement reinforcement material must be its resistance to attack from the highly alkaline matrix. Although steel possesses these physical attributes, it is economically difficult to produce fine fibres suitable for use in thin sheet products. In view of these concerns, it would appear that at present glass fibres provide the most economical alternative to asbestos fibres for manufacture of thin sheet fibre reinforced cement composites (although as polymer research advances, it is possible that synthetic organic fibres will become increasingly attractive).

Following initial research in the 1960s (Biryukovich *et al.*, 1964; Majumdar & Ryder, 1968) and the development of commercially viable alkali-resistant (AR) glass fibre by Pilkington Brothers PLC in 1971, the GRC industry grew large enough to merit the formation of a trade association, the Glassfibre Reinforced Cement Association in 1975. The development of second-generation fibres in the early 1980s further accelerated use of GRC. Today GRC is a multi-million pound industry of enormous diversity, both in application and geography; from artificial rock faces for Swiss film sets, to the decorative screenwork of the Bank of Oman in Doha, Qatar, to column cladding in the Santiago Bernabau Stadium, home of Real Madrid FC (CemFIL News 1995, 1996).

2.1.1. Properties.

One of the advantages of GRC is the ability to tailor its engineering and aesthetic properties for different applications by varying fibre content, length and orientation. Its properties are also time dependent to varying degrees. The table below gives some typical properties but is not exhaustive.

Table 2.1. Typical unaged GRC properties.

Property	**Range**
Tensile strength, MPa	8 - 18
Flexural strength, MPa	12 - 50
Initial Modulus, GPa	8 - 25
Post-cracking modulus, GPa	0.6 - 1.0
Strain to Failure, %	0.8 - 1.7

More qualitative properties include:

- it has the ability to reproduce fine surface detail - ideal for natural stonework renovation;
- it can be moulded into corrugated or more complex shapes and used in sandwich panels;
- it is easily coloured;
- it provides good acoustic insulation, especially in sandwich panels;

- it is inherently incombustible and provides good fire resistance.

(Data collected from Majumdar & Laws [1991], Oakley & Proctor [1975], Marikunte et al. [1997] and CemFIL News 1995, 1996).

2.2. Theoretical mechanics of GRC.

The mechanics of GRC can be considered in two stages: pre- and post cracking.

2.2.1. Composite rule of mixtures.

The initial, pre-cracked behaviour of GRC is generally modelled using the standard composites 'rule of mixtures' approach (e.g. Askeland, 1990);

$$E_c = V_f.E_f + V_m.E_m \qquad 2.1$$

where E is modulus and V volume fraction, the subscripts c, f and m denoting composite, fibre and matrix properties respectively. A similar formula applies to calculating composite strength (σ_C) substituting stress terms for the modulus terms.

This formula is only strictly valid for continuous uniaxially aligned fibres; for modelling commercial GRC with its short random fibres, efficiency factors are introduced (Majumdar, 1974a);

$$E_c = \eta_o \eta_l E_f V_f + E_m V_m \qquad 2.2$$

$$\sigma_c = \eta_o' \eta_l' \sigma_f V_f + \sigma_m V_m \qquad 2.3$$

where η_o, η_o' and η_l, η_l' are the efficiency factors for orientation and length respectively.

Substitution of typical values of matrix properties, fibre properties and the volume fractions typical of GRC (<5%) demonstrate that regardless of the values of η used, the improvement in **pre-cracking** composite modulus or strength over that of the unreinforced matrix will certainly be less than 20% (Bentur & Mindess, 1990), may be as low as 2% (Majumdar & Laws, 1991) and has no practical significance.

2.2.2. ACK model and multiple cracking.

The primary influence of the fibres is in the post cracking zone. Aveston, Cooper and Kelly (1971) expressed the behaviour of a brittle matrix composite with continuous

aligned fibres as a function of fibre volume using the mixture rule. This formed the basis of the **ACK model**.

If the fibre volume fraction of the composite is too low, when the matrix cracks during stressing of the composite the fibres will be unable to carry the load transferred to them. The composite will undergo catastrophic failure. At higher fibre volume fractions, the fibres will support this load and the composite will be imbued with some post cracking capability. The minimum fibre volume fraction required to avoid catastrophic failure is known as the **critical fibre volume** (V_{fcrit}) and can be deduced from the ACK model;

$$\sigma_{mu} \cdot V_{fcrit} > E_c \cdot \varepsilon_{mu} \qquad 2.4$$

which may be approximately expressed as;

$$V_{fcrit} = \sigma_{mu}/\sigma_{fu} \qquad 2.5$$

where σ_{mu} and σ_{fu} are the failure stresses of the matrix and fibres respectively, and ε_{mu} is the matrix failure strain.

Brittle matrix composites (i.e. GRC) with $V_f > V_{fcrit}$ exhibit a stress/strain curve with three distinct segments; a linear or quasi-linear elastic region (pre-cracking), a region of roughly constant stress but increasing strain (multiple cracking) and a final, less steep quasi-linear region up to failure (where the fibres alone bear the load) as shown in Fig. 2.1.

Figure 2.1. Idealised stress/strain curve for GRC.

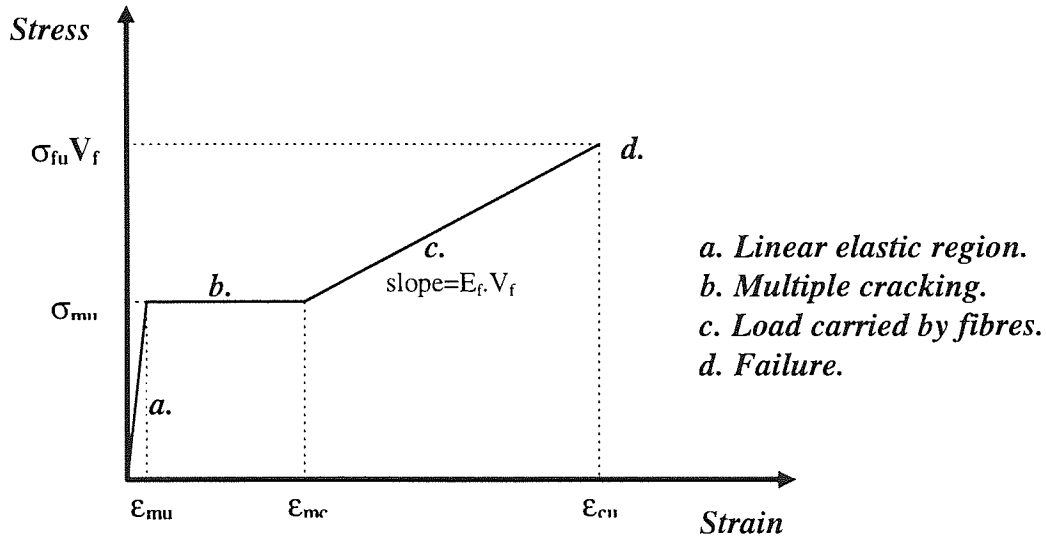

Aveston *et al.* (1971) developed a model of this process, paying particular attention to the multiple cracking region. Under tensile load above σ_{mu} , they showed that the matrix will break into blocks of length between x′ and 2x′; x′ is determined by the rate of stress transfer between the fibre and the matrix, which is in turn governed by the bond strength τ;

$$2N\pi r\tau x' = \sigma_{mu}V_f \qquad 2.6$$

where N is the number of fibres per unit area and r is the fibre radius. This yields for x′;

$$x' = (V_m / V_f).(\sigma_{mu} r / 2\tau) \qquad 2.7$$

since $N=V_f/\pi r^2$.

Multiple cracking will continue until the block length (i.e. crack spacing) becomes such that, for a given bond strength τ, insufficient load can be transferred from the fibres to the matrix to produce further cracking. The strain at this point (ε_{mc}) is given by;

$$\varepsilon_{mu}(1 + \tfrac{1}{2}\, a) < \varepsilon_{mc} < \varepsilon_{mu}(1 + \tfrac{3}{4}\, a) \qquad 2.8$$

where $a = (E_m V_m)/(E_f V_f)$.

Further loading of the composite will result in the fibres stretching and slipping through the matrix blocks and the modulus of the composite will become E_fV_f until failure at $\sigma_{fu}V_f$.

One of the assumptions of this model is that stress transfer between the fibre and the matrix is purely frictional with no adhesive or 'elastic' bonding. In their expansion of the basic ACK theory, Aveston and Kelly (1973) derive expressions for brittle matrix composites and showed that the model is not sensitive to the assumed nature of the bond provided that the elastic bond strength does not exceed σ_{mu} , which is highly unlikely. More recently, Naaman *et al.* (1991) analysed the relative significance of frictional slip over elastic 'adhesion' bond for fibre reinforced cement systems. By comparing their respective contributions to the energy absorbed during pullout tests both analytically and experimentally they conclude that frictional stress transfer (i.e. bond) is the dominant component. These findings validate the use of the 'simple' 1971 ACK theory for modelling GRC.

2.2.2.1. Fibre length and orientation - efficiency factors.

The ACK model and its derivatives are based on analysis of composites reinforced with uniaxially aligned continuous fibre. This project was concerned almost exclusively with GRC of this nature. However, any discussion of the mechanics of GRC would be incomplete without at least a brief synopsis of the mechanics of composites with finite fibre lengths and random or semi-random fibre orientations, similar to those found in commercial products.

The 'critical fibre length' (l_c) is the minimum fibre length required for the fibre to fracture under composite load. If the fibre is shorter than l_c , it will pull-out of the matrix rather than fail by fracture. l_c is a function of fibre strength, geometry and bond strength. Fibres with lengths of >> $2l_c$ (*long fibres)* will behave very similarly to continuous fibres.

The ultimate tensile strength of the composite is normally expressed as;

$$\sigma_{cu} = \eta_o \eta_l \sigma_f V_f \qquad \textbf{2.9}$$

similarly to equation 2.3 above (although the efficiency factors are not necessarily the same numerically) (Majumdar & Laws, 1991). Different authors conflict as to the values of these coefficients. They are derived from analysis of the number of fibres crossing a crack, their average embedment lengths and their alignments relative to the crack.

For the orientation factor, Aveston *et al.* (1974) derived 0.5 and $2/3\pi$ for random 2D and 3D orientations respectively; Laws (1971) quoted 0.375 and 0.2. The length factor has been variously quoted e.g. by Krenchel as $\mathbf{1-(l_c / l)}$ (Laws, 1971) and by Aveston *et al.* (1974) as $\mathbf{1-(l_c /2l)}$ for the 2D random orientation applicable to most thin sheet GRC product. Laws also showed that the two factors are not independent and derived combined strength factors for short fibre 2D 'mat' reinforcement;

$$\eta_{(o,l)} = \mathbf{0.1125}(l/l_c) \qquad (l < 5l_c/3)$$

$$\eta_{(o,l)} = \mathbf{0.375}(1-\mathbf{0.833}l_c/l) \qquad (l > 5l_c/3)$$

2.10

which are clearly not the product of the separate factors. Despite the limitations of the model pointed out by Hannant (1978) concerning the 'full bond assumptions', these factors appear to have become accepted as reasonable, although some authors have taken different approaches (Proctor, 1985; Pera *et al.*, 1993).

These factors must also be applied to the calculation of V_{fcrit} for typical GRC products. For example, a typical V_{fcrit} for an aligned GRC might be 0.4% (Hannant, 1978); with reference to equation 2.10 above, the corresponding V_{fcrit} for a 2D randomly orientated 'long' fibre composite would be (0.4/0.375)% = 1.07%. For a similar short fibre composite, V_{fcrit} will depend on l_c and the fibre length. As an example, one commercial manufacturer supplies pre-chopped fibre in 25mm lengths; l_c is often quoted as around 12 to 15mm (e.g. Bartoš, 1980; Oakley & Proctor, 1975) giving $V_{fcrit} \approx 2\%$ i.e. an efficiency factor of ≈ 0.2.

2.2.3. Bond strength.

In any model of aligned or random GRC, the strength of the bond between the fibre and the matrix is a controlling parameter. There are two obvious methods of measuring bond strength;

- directly e.g. from pullout tests on single filaments, strands or groups of strands,
- indirectly from analysis of the crack spacings produced in GRC under tensile load, by using ACK theory (equation 2.7 above).

Determination of bond strength is complicated by the fact that the reinforcement in GRC exists not as discrete elements of definite radius, but as bundles of relatively loosely packed filaments into which the matrix does not completely penetrate. This makes the determination of cross-sectional geometry parameters (i.e. the **r** term in equation 2.7 above or the surface area used in pullout tests) very difficult.

The product of bond strength and strand perimeter τp (i.e. shear force per unit length) appears frequently in the literature as it can be deduced without reference to cross-sectional geometry parameters. It is generally encountered during discussion of bond strength behaviour in pullout tests (e.g. Oakley & Proctor, 1975; Bartoš, 1980; Gray, 1984; Laws *et al.*, 1986). Bartoš called this quantity the 'shear flow, **q**', a term that seems to have been taken up by most subsequent authors.

2.2.3.1. Strand perimeter determination.

Few authors have attempted to determine strand perimeters in order to fully quantify bond strengths. Oakley and Proctor (1975) examined microscopic sections of GRC and deduced a perimeter (for the 'standard' 204 filament strand) of 2.83mm although they do not give their method. This value seems to have been used without question by later authors (e.g. Laws, 1982; Laws *et al.*, 1986). Recently, Kakemi *et al.* (1996) took backscattered SEM photos of polished cross-sections of GRC, traced the "shapes of the glass fibre strands" onto tracing paper and analysed the traces using a Quantimet 920 image analyser. They deduced a perimeter of 1.097mm (SD 0.143mm) for a 100 filament strand. Assuming that strand perimeter is proportional to number of filaments this would appear to be a broadly similar result to Oakley and Proctor's. They also estimated that the glass occupied 66% of the strand volume.

Although the approach of Kakemi *et al.* uses image analysis techniques it still depends on a manual tracing of the glass fibre cross-section and is therefore subject to operator judgement. A more consistent approach is required that is less prone to such subjectivity. Such an approach is outlined in section 3.5.3.

2.2.3.2. Direct bond strength measurement.

Direct measurement of bond strength is generally performed using a pull-out test where a fibre strand (or occasionally filament) is pulled out of a 'button' of matrix (Majumdar & Laws, 1991) and a load/displacement curve obtained.

Analysis of these curves is more complex than might be assumed. The ACK model predicts that the bond strength is constant along the embedded length and consequently pullout load will be directly proportional to embedded length. Experimental results do not support this (Majumdar & Laws, 1991).

The analysis of Lawrence (1972) showed that the shear stress developed during a pullout test is maximum at the entry point of the fibre and when the stress at this point reaches the bond strength (τ_s) the fibre will debond completely. Experiment shows however that there is still resistance to pullout after this point and Lawrence attributed this to the action of a frictional bond strength (τ_i). He further showed that pullout load is sensitive to embedded length and the ratio τ_s / τ_i. Laws (1982) later suggested that in fact frictional bond was more important in determining composite properties than 'total' bond (i.e. elastic plus frictional), a point later reinforced by the work of Naaman *et al.* (1991).

Kelly & Zweben (1976) proposed that large scatter may be exhibited in pullout tests due to unstable debonding caused by the mismatch in Poisson's ratio between fibre and matrix. They also showed that the effect of this mismatch will be different for single fibres and arrays of fibres.

Bartoš (1980) demonstrated the existence of three key embedment lengths;

- L_p : maximum length at which the fibre will debond and pullout instantaneously;
- L_c : minimum length at which fibre will fracture rather than pullout (i.e. critical length, see section 2.2.2.1.);
- L_f : minimum length at which fibre will fracture with no debonding.

He also experimentally determined the frictional and ultimate shear flows in GRC as **1.8** and **6.2** N/mm respectively for single strands; these represent $p\tau_i$ and $p\tau_s$. In a later paper Bartoš (1985) showed schematically the changing distribution of shear stress along a fibre during a pullout test.

Laws *et al.* (1986) developed a pullout test which used an array of 16 strands rather than a single strand to more accurately model actual composite behaviour. They produced average shear flows of **1.4** to **>8** N/mm depending on storage conditions. Their results exhibit a large scatter possibly due to the effects proposed by Kelly & Zweben (1976).

More recent developments include the finite element analysis model of Morrison *et al.* (1988), the energy/fracture mechanics approach of Naaman *et al.* (1991) which included the description of a 'pull through' test and the introduction of the 'telescopic pullout' mode described by Bartoš (1985) and Zhu & Bartoš (1993). Very recently Bartoš & Zhu (1996) have developed 'micro-indentation' apparatus which allows single filaments of glass to be pushed through the matrix and load/displacement graphs plotted. This equipment is beginning to yield interesting results, particularly regarding the role of fibre-fibre bond within the fibre strands in GRC. (It does not as yet however allow either shear flow or bond strength to be directly deduced). They conclude that the fibre strand should itself be treated as a composite.

2.2.3.3. Indirect bond strength measurement.

Rather less data is extant in the literature concerning bond strengths derived from crack spacing patterns. Rearranging equation 2.7 above yields;

$$\tau = \tfrac{1}{2}r.(V_m/V_f).(\sigma_{mu}/x'). \qquad 2.11$$

This value of τ will be equivalent to τ_i , the frictional bond strength. An expression for calculating the elastic bond was included in the extension of the ACK theory (Aveston

& Kelly, 1973) but since most of the available literature suggests that it plays a limited role in GRC composite behaviour it is not considered here.

Two minor modifications are normally made to equation 2.11. The first concerns the crack spacing. Under tensile loading, the matrix breaks into blocks of length between x′ and 2x′. Using the statistical 'car parking analogy' the average observed crack spacing can be shown to be 1.364x′ (Gale, cited in Aveston *et al.* 1974). The second concerns the radius term; obviously a radius cannot be found for a fibre strand consequently equation 2.11 is usually written;

$$\tau = 1.364(V_m/V_f).(\sigma_{mu}/X).(A_f/P_f) \qquad 2.12$$

where X is the average observed crack spacing, A_f is the cross-sectional area of the glass and P_f is the perimeter of the strand.

Although shear flow values ($p\tau$) values can be deduced from equation 2.12 and compared with the values found in pullout tests, most authors who have taken this approach have attempted to quantify the fibre perimeter in order to derive a bond strength rather than a shear flow parameter. Oakley & Proctor (1975) calculated bond strength values generally between **0.6** and **1.6** MPa; Kakemi *et al.* (1996) obtained **1.4** to **2.2** MPa. Multiplying these with the respective authors' perimeter measurements (see section 2.2.3.1.) gives $p\tau$ values of 1.7 to 4.5 for Oakley & Proctor, and (assuming a linear correction for number of filaments, see section 2.2.3.1.) 3.1 to 4.8 for Kakemi *et al.* which are within the range suggested by pullout test results.

It is interesting to note that the quantity σ_{mu}/X is directly proportional to τ and is easily determined. It could therefore be used to compare relative bond strengths without reference to radius or perimeter terms in a similar manner to $p\tau$, but is not found in the literature.

2.2.4. Fracture mechanics.

There exists a considerable body of literature concerning the fracture mechanics of fibre reinforced cement. The effects of fibre/crack interaction fall into three categories;

- *Crack suppression* - in the pre-cracking zone, the increase in the stress required to initiate cracking of the matrix (σ_{mu}) over and above that predicted by the mixture rule;
- *Crack stabilisation* - the retardation of continued propagation of cracks beginning to cross the fibres provided by the fibre array;
- *Fibre/matrix debonding* - the modelling of debonding as crack propagation along the fibre/matrix interface.

The application of fracture mechanics to FRC systems is summarised by Bentur & Mindess (1990).

2.2.4.1. Crack suppression.

Linear elastic fracture mechanics (LEFM) was first applied to FRC systems by Romualdi & Batson (1963). They showed that as cracks begin to form between the fibres there is a strain mismatch between the matrix and the fibres caused by the stress concentrations at the crack tip. This mismatch causes the fibre to exert a 'pinching force' (Bentur & Mindess, 1990) which reduces the stress intensity factor of the crack and increases the stress required for propagation (i.e. σ_{mu}). The effect is controlled by a parameter known as the spacing factor S;

$$S = 2.76r(1/V_f)^{1/2} \qquad 2.13$$

to which the first crack stress of the matrix is inversely proportional. The theory was later modified by Swamy *et al.* (1974) to take into account fibre geometry and bond considerations. Nevertheless, a value of r is still required for analysis and the same problems apply to its derivation as those outlined above.

The original ACK theory (Aveston *et al.*, 1971) derived the first crack strain (ε_{mu}) from energy considerations; this also predicts an increase in ε_{mu} over that deduced from the mixture rule. Bentur & Mindess (1990) point out that '[in] essence, this is another way of predicting the degree of crack suppression...in accordance with spacing factor concepts.' This also requires a knowledge of r as well as such exotics as the surface energy of the crack area, so it is difficult to apply.

2.2.4.2. Crack stabilisation.

In the crack stabilisation phase LEFM can no longer be used to model the process, as the fibres bridging the crack generate a closing pressure (Wecharatana & Shah, 1983). This invalidates the 'traction free crack' assumption on which LEFM is based.

Wecharatana & Shah (1983) and Naaman & Shah (1979) proposed an ideal crack model divided into three zones along its length; the traction free zone (wide end) where no fibres bridge the crack, the fibre bridging zone and the aggregate bridging zone (narrow end). This last zone is often called the 'process zone'.

Figure 2.2 Ideal crack model (after Wecharatana & Shah, 1983).

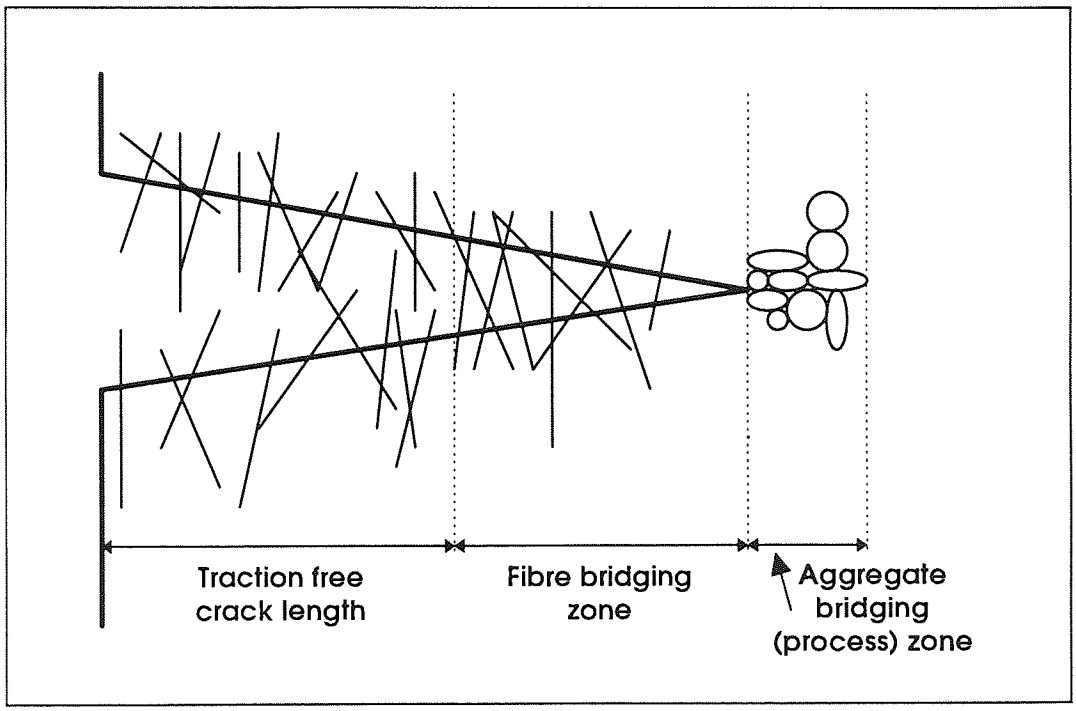

The analytical treatment of this model involves knowing the 'material parameters' of the crack closing pressure/opening displacement relationship and the critical crack opening displacement (CCOD). The resultant R-curves (strain energy release rate vs. crack extension) were compared with a limited set of experimental data.

The complex model proposed by Li *et al.* (1992) predicts multiple cracking behaviour and the stress at the end of the multiple cracking region. Despite its elegance, the theory is derived with steel fibre reinforcement in mind and depends on a number of assumptions that are invalid for GRC.

In general, the fracture mechanics theories concerning the post-cracking region tend to over-complicate a process that is adequately explained by ACK theory. As noted by Majumdar & Laws (1991), neither do they clearly identify useful design parameters or 'new' material parameters.

2.2.4.3. Fibre/matrix debonding.

Griffith's theory analysis supported by finite element analysis (FEA) of the fibre/matrix interface was undertaken by Morrison *et al.* (1988). The model differs from classical models in that it takes into account the frictional pull-out resistance. It showed that the strain energy release rate for debonding is generally lower than that which would be expected for plain mortar i.e. a crack should preferentially propagate along the fibre/matrix interface. This is not a wholly unexpected result - we would expect the interfacial zone to be weaker - but it does confirm the importance of the interface in controlling composite behaviour.

2.3. The durability problem.

The primary obstacle to more widespread specification of GRC, especially as a structural or load bearing material, is concern over its long term durability in certain environments. Many authors from the early 1970s onwards (e.g. Majumdar, 1975; Diamond, 1985; Bentur, 1985; Majumdar & Singh, 1990) have documented that over timespans less than that of a reasonable service life, standard OPC matrix GRC suffers from a marked reduction in tensile strength and more importantly ductility, especially in environments where moisture is present (i.e. temperate climates); this is shown in Table 2.2.

Table 2.2. Long term GRC properties.

Age	28 days	1 year	5 years	10 years	17 years
TS (MPa)	14 - 17	11 - 14	7 - 8	7 - 8	4 - 7
Failure strain (%)	1.0	0.5	0.05	-	-

TS: Tensile strength. Spray de-watered GRC, 5% w/w Cem-FIL fibre 34-38mm length, natural UK weathering. Summarised from data in Majumdar & Laws (1991)

Figure 2.3. Idealised stress/strain curve for GRC under various storage conditions (after Majumdar & Laws, 1991).

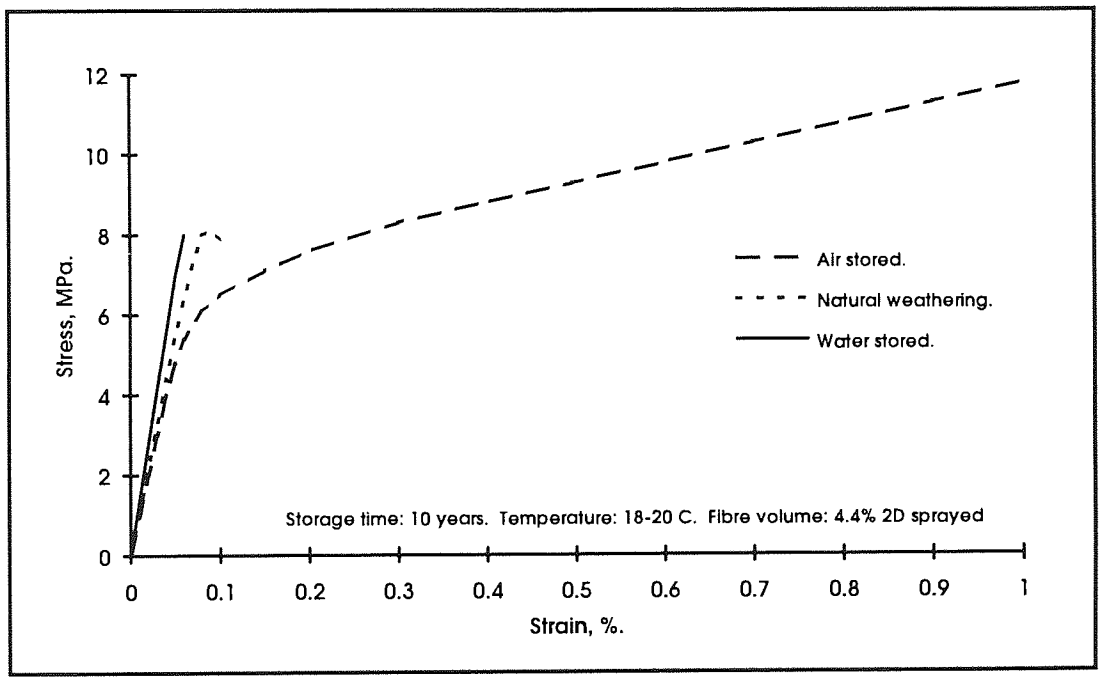

It is generally accepted that there are three mechanisms which are responsible for this degradation;

- fibre corrosion by OH ions in the matrix pore solution;
- matrix densification and bond enhancement with continued hydration, and
- precipitation of hydration products in the void spaces within the fibre strands.

These mechanisms are discussed in detail in sections 2.3.2.1 to 3.

2.3.1. Accelerated ageing.

Before any elaboration of the degradation mechanisms of GRC, it is necessary to discuss the processes by which many of the published results concerning its durability have been obtained. As with many relatively young, rapidly developing materials, there is a lack of long term data concerning the variation in GRC properties with time and certainly no consensus as to its 'ultimate' properties. Consequently, a number of accelerated ageing tests have been proposed.

The simplest and most widely used of these is where samples of GRC are immersed in 'hot' water for relatively short periods of time (typically 25-80°C for 1-12 months). The theoretical basis for this test was developed from the 'strand in cement' (SIC) test by Litherland et. al. (1981), which involves casting a small block of cement around a single glass fibre strand (see Figure 2.4 below). The cement was cured for 24 hours at room temperature at 100% RH and then aged under various temperature-time regimes (5-80°C and up to 1000 days). After ageing the strand is tested in direct tension and the reduction in tensile strength of the strand (presumed to be due to fibre corrosion) derived.

Figure 2.4. SIC test specimen (after Litherland *et al.*, 1981)

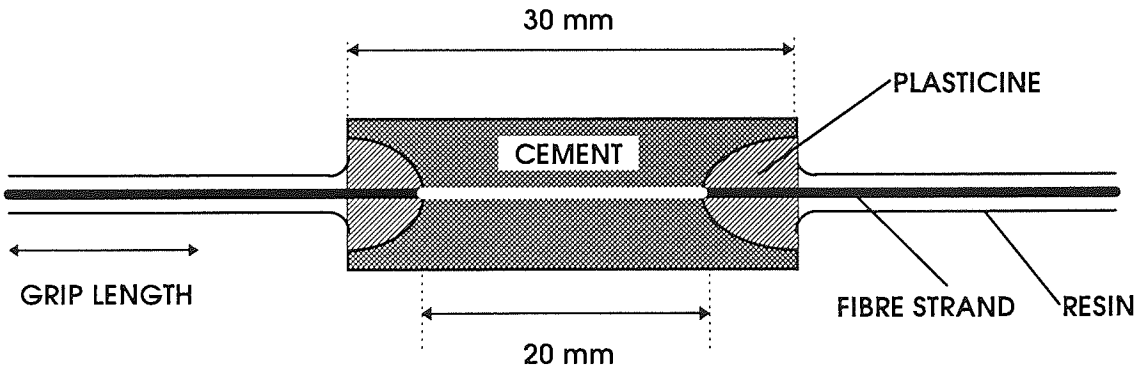

Similar ageing was carried out on ordinary GRC samples and the reduction in flexural strength analysed. This analysis showed a pattern of early strength loss followed by a region of constant strength in both composite and SIC tests. The reduction in strength with ageing time and temperature was then plotted assuming an Arrhenius relationship between the parameters (log[*time taken for strength to fall to any given value*] $\propto$ 1/temp). Since the family of lines for a reduction to a given strength level on the

Arrhenius plot were parallel the results were normalised by correlation with the 'standard' ageing temperature of 50°C (323K) , and represented on a single diagram (Figure 2.5 below).

Figure 2.5. Normalised Arrhenius plot of GRC strength loss, accelerated ageing. (from data in Litherland *et al.*, 1981 & Proctor *et al.*, 1982)

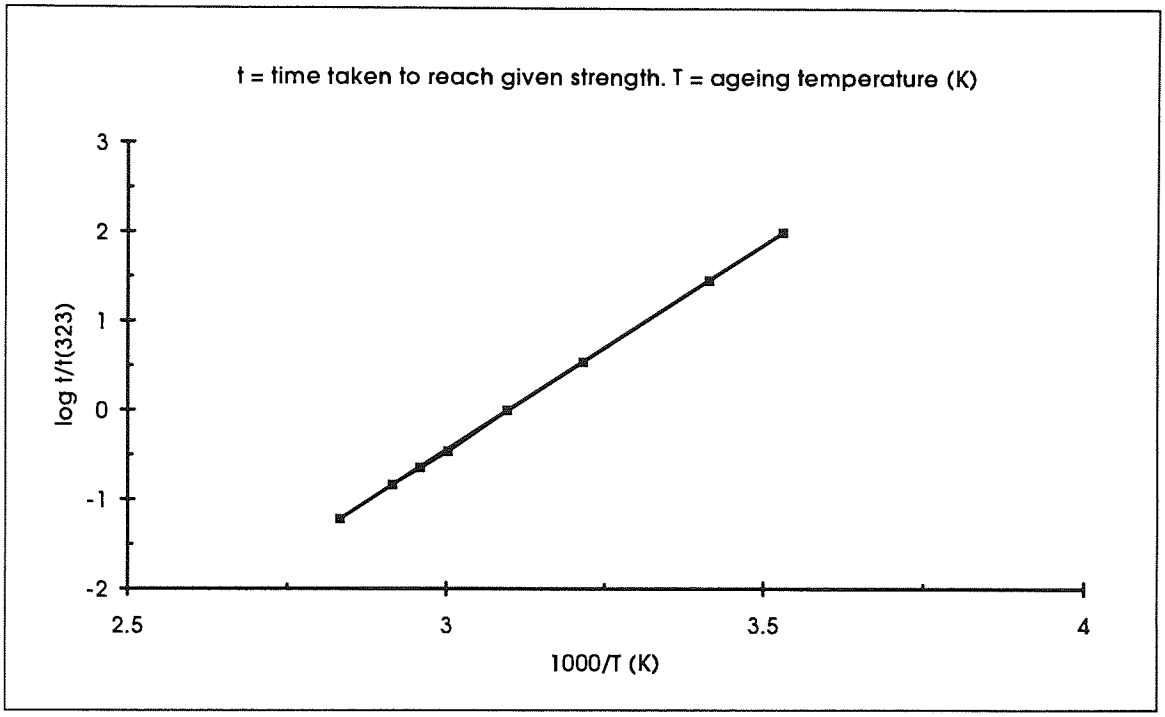

This allowed direct comparison of accelerated ageing tests performed at different temperatures. In an allied paper (Proctor *et al.*, 1982) results from 'real-time' weathered composites were compared to the model with reasonable success. Predictions were advanced as to the 'equivalence' of periods of ageing at elevated temperature with corresponding longer periods of real weathering via the application of 'acceleration factors' (with UK annual temperature taken as 10.4°C, Table 2.3).

Acceleration factors for other climates were also advanced. The model was further reinforced by a later study of systems with second-generation AR fibre (Litherland, 1985).

Table 2.3. Acceleration factors relative to UK climatic exposure (after Proctor *et al.*, 1982)

1 day @ 80°C	**x 1672**	**4.6 years**
1 day @ 70°C	**x 693**	**1.9 years**
1 day @ 60°C	**x 272**	**9 months**
1 day @ 50°C	**x 101**	**3½ months**

The major drawback of this theory is that only changes in flexural strength can be predicted. No predictions can be advanced as to the likely changes in failure strain or impact strength with time. It also assumes that loss of composite strength is solely due to fibre corrosion, which may be an invalid assumption as outlined in the following sub-section (2.3.2.). Despite this, the strong correlation obtained from experimental data and the lack of any other coherent predictive accelerated ageing model ensure that hot water ageing remains by far the most commonly used procedure for durability analysis.

Hot/wet/cool/dry cyclic accelerated ageing is occasionally encountered in the literature (e.g. Thiery *et al.*, 1991). This generally involves sub-cycles of water immersion, forced drying, cooling and re-immersion. At the time of writing a draft EC pre-standard was in existence concerning cyclic ageing of GRC (see section 3.4.3.2.). Thiery *et al.* also quote a French standard "NF-851-263" used by the wood and asbestos industries which they adapted. The same authors, together with Daniel *et al.* (1985), also describe freeze-thaw cyclic tests based on ASTM-C666. Neither of these cyclic regimes contain any predictive component and should only be treated as quality-control type tests.

2.3.2. Mechanisms.

The three degradation mechanisms outlined in section 2.3. all involve microstructural processes at the fibre-cement interface. The microstructure of GRC has been extensively studied (e.g. Jaras & Litherland, 1975; Stucke & Majumdar, 1976; Page, 1982; Bentur, 1985; Diamond, 1985; Majumdar & Singh, 1990), generally using scanning electron microscopy. Despite this large volume of work, there is still a great deal of debate concerning which of the three processes is primarily responsible for the

weakening and embrittlement of GRC in moist environments. The relevant evidence, microstructural and otherwise, for each of the mechanisms is discussed below.

2.3.2.1. Fibre corrosion.

Ordinary silicate glasses (E or A glass) are highly susceptible to attack by strongly alkaline solutions similar to those found in the pore solution of portland cements. The siloxane bonds in the silica network of the glass are broken and hydrolysed by OH ions;

$$\equiv Si—O—Si\equiv + OH^- \rightarrow \equiv Si—OH_{solid} + O^-—Si\equiv_{in\ solution}$$

This causes surface flaws (pits), making them unsuitable as reinforcement for GRC as they quickly lose strength, degrading the composite. AR zirconia-based fibre such as CemFIL reacts similarly, but the Zr-O bonds are less favourable to attack than the Si-O bonds. Silica is preferentially leached out and in consequence the contact area becomes zirconia enriched. The Zr-O bonds are mildly attacked, but the reaction products are relatively insoluble. This results in a protective 'passivating' surface layer which provides the alkali resistance. (Chakraborty, 1979; Scholze, 1982; Yilmaz & Glasser, 1991a)

The chemical interactions between AR fibres stored in alkaline solutions and 'cement extract' solutions (supposedly simulating pore solutions) have been considered by many authors. Majumdar (1974) measured the network breakdown of E and AR glass in cement extract solutions at 80, 65 and 50°C for up to 112 days. AR glass showed an order of magnitude improvement (1% cf. 12%) over E glass with little increase in breakdown with time or temperature. A substantial strength advantage was also reported. SEM examination of the fibre surfaces showed E-glass to be heavily pitted and AR glass to be almost unmarked. Franke and Overbecke (1987) reported negligible loss of strength of CemFIL fibres in a variety of highly alkaline media after 1000 hours at 70°C. A similar lack of decay was reported by Vanis & Komlos (1985). It should be noted however that the applicability of these results to the corrosion of in-situ fibres is uncertain for a number of reasons, as discussed by Yilmaz and Glasser (1991a). These include inadequate buffering of the solutions, reduction of calcium solubility in NaOH or KOH solutions owing to the common ion effect, the absence of

any notching effect, uncertainty as to the 'accuracy' of the cement extract solutions and the much greater diversity of attack modes in cements cf. aqueous solutions.

Tensile tests on fibres removed from aged GRC have been performed (Cohen & Diamond, 1975; Majumdar & Laws, 1991). Results seem to conflict between investigators; the difficulty in removing a representative filament from the bundle is the likely cause of the discrepancies.

SEM examination of in situ fibres can provide qualitative information. Jaras and Litherland (1975) contrasted the heavily pitted surface appearance of E-glass fibres after one year 'indoor storage' of the composite with the smooth appearance of CemFIL fibres after 5 years. Cohen and Constantiner (1985) reported a similar pattern after 69 days in water at 23°C (despite the addition of alkaline additives to accelerate the corrosion), as do most other authors. The same authors postulate the formation of a colloidal zirconium hydroxide layer on the glass. Bentur (1985) reports extensive damage to AR fibres after 5 months composite immersion in water at 50°C, but none at 20°C. Yilmaz & Glasser (1991a) have reported that after 60 days immersion at 20°C, the fibre carries an adherent layer of mixed and varying composition, generally containing CSH, calcium hydroxide and ettringite. The underlying fibre is smooth. After 90 days at 55°C, a layer of reaction product covers the fibre giving it a rough appearance. The layer appears to have a duplex formation with the inner layer consisting of hydroxlated glass and the outer of cement hydration products.

As a footnote, research is continuing into fibre development. The chief disadvantage of zirconia based AR fibre is that (compared to standard glasses) the addition of zirconia increases the liquidus temperature and hence makes fiberisation more expensive. The composition of AR glass is therefore a compromise between the enhanced alkali resistance imparted by increasing zirconia content and the economic need to keep the liquidus temperature low. Other glass systems have therefore been investigated e.g. SiO_2-PbO-Al_2O_3, (Datta *et al.* 1986) but with limited success.

2.3.2.2. Matrix densification and bond enhancement.

The heading above refers to a number of detrimental effects caused by the continued hydration of the cement matrix.

As the matrix hydrates it becomes stronger i.e. σ_{mu} increases; by inspection of equations 2.4 and 2.5 above it can be seen that this will increase the amount of fibre required to carry the load on fracture of the matrix (V_{fcrit}). If the composite is initially designed with V_f only slightly higher than V_{fcrit} then the composite may lose its post-cracking capabilities as the matrix strengthens. This can be easily avoided by careful composite design.

Stucke and Majumdar (1976) noted in a detailed SEM study that the fibre in mechanically tested GRC appeared to have failed in a bending manner. Fibres bridging a transverse crack have a region of length l where the fibres are bent through an angle θ. l is related to the radius of curvature. The stress induced in the fibre is in inverse relation with l. In young or air stored GRC, the matrix immediately adjacent to the fibre is relatively weak, composed of whisker-like crystals of ettringite or CSH(II). It can 'crumble' during the bending of the fibre, keeping l large ($\approx$200 microns) and the induced stress small. The matrix at the interface densifies with age or wet storage, becoming composed of "fully dense" $Ca(OH)_2$ (hereafter referred to as CH) with a few residual whiskers. The ability of the matrix to crumble is reduced, l becomes small (a few microns) and the induced stress is greatly increased for a given angle θ. Bentur (1985) has shown that some local flexure of fibres traversing a crack occurs even in fibre strands spanning the crack at right angles due to shifting crack paths.

It is also generally accepted that the fibre/matrix bond strength is likely to increase with time. Many microstructural studies have shown that the initial interfacial contact zone is porous but with continued ageing the contact area increases drastically (e.g. Jaras & Litherland, 1975; Stucke & Majumdar, 1976; Majumdar & Laws, 1991) . For short fibre reinforced composites, this will reduce the critical embedment length l_c and may change the failure mode from fibre pullout to fibre fracture. This will mostly concern the post-peak behaviour of the composite but is also likely to decrease its toughness, as fibre pullout expends more energy then fibre fracture. Changes in l_c will

also change the values of the efficiency factors used to model the behaviour of non-aligned and short fibre composites (see section 2.2.2.1.)

2.3.2.3. Inter-filamental precipitation and fibre notching.

Many of the microstructural studies mentioned above have also noted that as well as the densification of the interfacial area, in wet environments hydration products are also precipitated within the fibre bundles (strands). These hydration products are almost exclusively crystalline CH. This precipitation has two major effects. The first is to reduce the flexibility of the fibre strands. In order for the composite to perform well, the reinforcement must be able to accommodate significant flexural deformations of the type described above. If the inter-filamental spaces are filled with hydration product, the filaments within the fibre strand lose the ability to move relative to each other in a rope-like manner; they behave monolithically and with reduced flexibility.

The second and more recently acknowledged effect concerns the 'telescopic pullout' mode first identified by Bartoš (1985). In a bundle of filaments (i.e. a strand) the outer filaments are better bonded to the matrix than the inner filaments. These outer filaments fracture while the inner core pulls out. The outer filaments of this core are similarly preferentially bonded and a still smaller core is pulled out. The process repeats generally three or four times and a characteristic quasi-conical array of fibres can be seen emerging from the fracture surface. The precipitation of CH within the bundles prevents this behaviour and decreases the toughness of the composite (Zhu & Bartoš, 1993). Using novel micro-indentation equipment to assess relative fibre-fibre and fibre-matrix bond, Bartoš and Zhu (1996) have also shown that embrittlement of aged composites is associated with an increase in 'micro-strength' at the interface and within the fibre bundle.

Some authors also postulate that growth of CH crystals at the interface and within the strands may cause notching of the fibre. Mills (1981) reported that CH, when precipitating out of hydrating OPC has 'a remarkable affinity' for nucleating on AR-glass surfaces in preference to many other substrates. He further reports that the hexagonal plate-like crystals form with their short axis parallel to the longitudinal axis

of the fibre (i.e. edge-on) and that these may cause notching. Yilmaz and Glasser (1991a,b) report that the contact areas between large CH crystals and the fibre surface show signs of "accelerated attack...thus the fibres are being notched by CH." Other authors (Proctor & Yale, 1980) have indicated that this notching may not simply be mechanical as they report that CH slurries are more damaging to fibres than saturated CH solutions.

The inhibitive organic coatings or 'sizes', often of the polyhyrdroxy phenol family (Majumdar & Laws, 1991), applied to second generation AR fibres such as CemFIL 2 are generally considered to delay the formation of CH and other hydration products at the interface (Procter *et al.*, 1982; Litherland & Proctor, 1985). This helps to reduce the effect of the processes described in this and the previous subsection, allowing longer retention of tensile strength and strain to failure. This improvement (over a nine-year ageing period) has been demonstrated by Majumdar and Singh (1990) both microstructurally and by mechanical testing and is considered to "...give grounds for cautious optimism."

2.3.3. Discussion

Although the existence of most of the decay mechanisms described above is not in question, considerable and heated debate continues concerning their relative importance. Opinion tends to polarise between the fibre corrosion and matrix densification/bundle filling mechanisms. The huge number of SEM micrographs extant in the literature showing fibre strands filled with hydration product and greatly reduced fibre pullout at first glance tend to support the latter camp. The generally smooth surfaces of AR fibres (especially compared to E-glass fibres) examined after immersion in hot caustic solutions and within aged composites adds further support. Contrary to this is the clear correlation achieved by Litherland *et al.* and Proctor *et al.* between SIC tests (which are based purely on a fibre corrosion model of degradation) and real composites. Majumdar and Laws (1991) also point out that the strength of a glass fibre is governed by flaw size and population i.e. fracture mechanics, rather than strength loss through reduction of section. A fibre that appears smooth under naked eye or optical microscope examination may well contain very small but significant 'Griffiths' flaws which will promote crack propogation within

the fibre. They further point out that according to current models a bond strength in the order of 50 MPa would be necessary to stress the reinforcing fibre to its ultimate. The formation of bond of this magnitude is highly unlikely. The debate is further confused by authors who, whilst rejecting fibre corrosion as a primary decay mechanism, attest to the validity of hot water ageing for making long-term strength predictions.

It should also be noted that the vast majority of mechanical testing evidence has been obtained from short/random fibre reinforced GRC rather than its continuous uniaxially reinforced counterpart. The accepted theories (i.e. ACK theory and its developments) can only be applied *without* the use of efficiency factors (which are themselves the subject of some disagreement) to this latter class of composites. When such material has been tested, it was in flexure rather than pure tension, and the simple "beam" theory relating flexure to tensile stress is not valid for GRC due to its non-elastic behaviour. Several of the 'secondary' effects such as pull-out and localised fibre flexure should be greatly reduced or absent in continuous uniaxially reinforced GRC tested in pure tension, producing clearer results. The study of this more fundamental material forms the basis of this project and will provide information on the intrinsic nature of the durability mechanisms in GRC that is absent from the literature.

2.4. Improvement of GRC by matrix modification

Since it was first manufactured, non-OPC matrices have been used for GRC, but most early research concentrated on fibre alkali resistance development to allow the use of relatively cheap and widely available OPC. Since the advent of second generation AR fibre which would appear to represent the current economical limit of alkali resistance, research has returned to modification the matrix of GRC to improve its durability.

These new matrices can be broadly divided into two categories: those formed from the addition of supplementary materials to OPC, and those presented as new cements.

2.4.1. Additives to PC matrices.

Additives to the OPC matrix generally consist of finely divided siliceous material. They purport to improve the matrix *vis a vis* durability by acting in a pozzolanic manner, consuming the CH and alkalis released during hydration to form secondary silicate hydrates;

(in CH solution; Larbi et al., 1990)

$$SiO_{2\,(s)} + H_2O_{(l)} \rightarrow H_4SiO_{4\,(aq)}$$ *(followed by...)*

$$H_4SiO_{4\,(aq)} + Ca^{2+}{}_{(aq)} + 2OH^-{}_{(aq)} \rightarrow n_1CaO.SiO_2.n_2H_2O$$

$$SiO_{2\,(s)} + Ca^{2+}{}_{(aq)} + 2OH^-{}_{(aq)} \rightarrow n_1CaO.SiO_2.n_2H_2O.$$

This action has the dual advantage of reducing the alkalinity of the pore solution (and hence fibre corrosion) and greatly reducing or even eliminating CH from the matrix (and hence reducing bundle filling). Some of the more common additives are described below.

2.4.1.1. Ground granulated blast furnace slag (GGBS).

GGBS contains around 30-40% active silica by weight. It is added at relatively high addition rates of up to 70%. It is known that GGBS can substantially reduce the alkalinity of cement pore solution (Canham *et al.,* 1987; Duchesne & Berube, 1994). Kumar and Roy (1985) reported that a 65% addition of GGBS to autoclaved GRC samples eliminates fibre corrosion and greatly reduces the formation of CH as detected by XRD. Lower addition rates seem to have little effect. GRC made with high addition levels of GGBS seems to have improved durability cf. OPC over a nine year weathering period (Majumdar & Laws, 1991).

2.4.1.2. Microsilica (condensed silica fume, CSF).

CSF is waste product of the silicon industry and contains 95-99% active silica by weight. It is generally added at lower rates than GGBS, about 10-20%. This is in part due to the adverse effect CSF has on workability. It has an exceptionally fine particle size (10-500 nm) and as such is able to penetrate into the spaces between the cement particles, reducing porosity and this accounts for the very fine microstructure observed

in CSF-GRC (Kumar & Roy, 1985). The high specific surface increases the rate of the pozzolanic reaction and also that of hydration generally, probably due to the small CSF particles acting as nucleation sites for hydration. The alkalinity of the pore solution is greatly reduced (Larbi *et al.*, 1990; Duchesne & Berube 1994). There is some disagreement as to the degree of CH depletion and performance enhancement caused by CSF. Cohen and Constantiner (1985) report that a 10% addition had little effect on the early microstructure and did not prevent CH 'stacking' on the fibres. Bartoš and Zhu (1996) reported that 10% addition of CSF could only slightly delay the degradation of GRC composites under accelerated ageing. Marikunte *et al.* (1997) have reported similar results for a 20% addition rate. Kumar and Roy (1985) however reported the virtual elimination of CH from the matrix with a 20% addition rate, and Bentur and Diamond (1985) reported little microstructural bundle filling and improved flexural performance for a 10% addition rate. It should be noted that some of these studies were complicated by the addition of polymer emulsions (briefly explained in 2.4.1.4. below) to the mix and the combined effects are not always clear.

Some authors have experimented with adding CSF to the fibre bundles by immersing them in CSF slurries prior to their incorporation in GRC (Bentur & Diamond, 1985; Zhu & Bartoš, 1993; Bartoš & Zhu, 1996). The rationale behind this procedure is that the fine CSF particles will penetrate into the inter-filamental spaces and prevent bundle filling by physically blocking the precipitation of CH. Initial results seem to be encouraging although what effect the inevitable eventual hydration of this interfilamental material will have has not been discussed.

2.4.1.3. Metakaolin (MK).

There has been much recent interest in the GRC community regarding the addition to OPC of a calcined china clay (approximate formula AS_2), known as metakaolin, to improve durability. Coleman and Page (1997) have reported a marked reduction in the pore solution alkalinity of cement pastes with 10 and 20% additions of MK. Studies of the action of 'cement extract' solution derived from MK/OPC on E glass fibres has shown a marked reduction in fibre corrosion although CH deposition has not been eliminated (Murat & Al Cheikh, 1989). Thiery *et al.* (1991) report that metakaolin modified GRC retains its tensile and ductile properties after 84 days at 50°C, 50

cycles of cyclic ageing (as described in 2.3.1. above) and after freeze/thaw ageing. It should be noted that this paper and several others that attest to the benefits of MK addition refer to the so-called "St. Gobain" or "5/5" matrix, which consists of 5% polymer and 5% short AR fibre plus an unspecified amount of MK added to OPC (e.g. Glinicki *et al.,* 1993; Soukatchoff *et al.,* 1993). Zhu and Bartoš (1993) also report improved performance for 25% MK addition, and have also tried to pre-treat the fibre strands with MK similarly to the CSF treatment described above. Pera and Ambroise (1994) detected no intrusion of CH into the strands in a composite with a 40% MK addition, although again a polymer was also added.

2.4.1.4. Other additives.

Another commonly used supplementary cementing material, pulverised fuel ash (PFA) has also been added to GRC. It has similar attributes to the other pozzolans described above. It is outside the brief of this project, but is well documented and many of the publications referred to previously contain information on its effects on GRC durability (e.g. Jaras & Litherland, 1975; Canham *et al.,* 1987; Majumdar & Laws, 1991; Duchesne & Berube, 1994).

As previously mentioned, acrylic polymer dispersions are also added to GRC matrices, often in conjunction with other additives e.g. in the ubiquitous "5/5" matrix. Their primary purpose is to reduce water loss by evaporation during curing and hence minimise drying shrinkage. They also purport to improve mix workability and the durability of the composite. The mechanisms by which this durability improvement is achieved is not altogether clear although the penetration of polymer into the fibre bundle, preventing precipitation of CH therein, is often cited. It has been postulated that the polymer may form a protective layer on the fibre, although the work of Daniel and Schultze (1985) does not support this. Further research is required and is ongoing, but again is outside the brief of this project and the reader is referred to other publications (e.g. Majumdar & Laws, 1991; van der Plas, 1991; Zhu & Bartoš, 1993; Ball & Wackers, 1993; Duchesne & Berube, 1994; Bartoš & Zhu, 1996).

2.4.2. Non-PC matrices.

Many non-Portland cements currently in use in the construction industry produce a less alkaline environment than OPC and would seem well suited to GRC manufacture. Many also produce far less CH during hydration. Prior to the advent of AR fibres these were often used to produce E-glass GRC. Since it has become clear that AR-fibres do not completely solve the durability problem research interest has been re-established in these materials (Majumdar & Laws, 1991). High-alumina cement (HAC) is the most frequently encountered matrix and has been mooted as a possible improvement over OPC for some time (Majumdar, 1974; Litherland & Proctor, 1985). Super-sulphated cement (SSC) has also been used (Litherland & Proctor, 1985). Tests on aged samples made with these matrices indicate a better retention of properties than for OPC-GRC. However, the conversion reaction (HAC) and carbonation (SSC) reduce the integrity of these matrices, especially at moderately raised temperatures similar to those used to age GRC and specification of such cements should be undertaken with great caution (Majumdar & Laws, 1991). Other proprietary and more exotic systems are described in the literature (e.g. Molloy *et al.,* 1993; Hommertgen & Odler, 1991).

Much interest is presently being shown in cements based on calcium sulpho-aluminates. These cements, as well as having lower alkalinities, develop practically no CH during hydration, which is generally considered to be beneficial. One such recently developed cement (Gartshore *et al,* 1991) uses a blend of OPC, calcium sulpho-aluminate clinker, anhydrite and MK. Composites made with this new cement appear to have increased durability *vis a vis* OPC. As a further benefit, these cements tend to be very rapid setting; composite boards can be demoulded within 2 hours of manufacture. This has obvious commercial advantages. However, since the only data concerning the properties of this matrix have been published by the manufacturers, independent research will be required to increase confidence in its use.

2.4.3. Discussion.

Much of the recent literature, especially that concerning non-Portland cements and MK addition, tends to concentrate on documenting the improved properties of GRC made with these new matrices with little regard for the microstructural changes

responsible for these purported improvements. It also concentrates solely on short-fibre random 2-D oriented composites with no analysis of the more fundamental information that can derived from the testing of continuously aligned samples. This fundamental information is vital in order to permit structured research and development of GRC composites made with 'new' matrices.

It is also unclear whether the hot-water accelerated ageing regime predictions advanced by Litherland and co-workers for OPC-GRC are relevant to 'new'-matrix GRC with its differing durability characteristics. Since these materials often show little or no degradation during relatively short periods of hot water ageing, more 'punishing' cyclic ageing regimes have been formulated by some commercial researchers. The parameters affected by these regimes have not been identified and no correlation between accelerated and natural ageing is possible. These parameters must be identified before service life predictions can be formulated and GRC can be specified by designers with reasonable confidence.

3. MATERIALS AND EXPERIMENTAL TECHNIQUES.

3.1. Matrices.

Three new cementitious matrices were used in the manufacture of composites for this study, chosen to be representative of the cementitious materials currently being investigated internationally for commercial use. A more limited study was undertaken using an OPC matrix GRC for comparative purposes. These materials are described in more detail below.

After consultation with the BRE, it was decided that no fine aggregate should be added to the matrix formulations. The effects of fine aggregate addition on the properties of GRC are complex, depending on particle size, aggregate/cement ratio, grading and other factors. It was felt that these considerations would unnecessarily complicate interpretation of results.

3.1.1. Description.

These matrices have all been designed specifically for GRC. More detailed analyses of them and their constituents (e.g. oxide analyses) are presented in section 4.1.

3.1.1.1. Matrix O.

Matrix O was a 'neat' standard OPC matrix. The same OPC was used in the formulation of matrix M described below.

3.1.1.2. Matrix M.

Matrix M was formed by the addition of Cem-Star metakaolin (marketed and supplied by Cem-FIL International Ltd.) to OPC. The constituents were supplied separately and blended as needed. After consultation with the suppliers, the mix formulation was set at 20:80 metakaolin:OPC.

3.1.1.3. Matrix C.

Matrix C was a rapid setting shrinkage compensated cement based on calcium sulpho-aluminate. It was developed from cements originally used for specialist mining

applications. The base material (a blend of OPC, calcium sulpho-aluminate clinker and anhydrite) is blended with metakaolin. It was supplied ready to use.

A distinctive feature of matrix C was its very short setting time. At normal water cement ratios, the paste was workable for only 10 to 20 minutes. In commercial use, this phenomenon was previously circumvented by using very high w/c ratios and suction dewatering after spraying. The quick set then becomes an advantage in that the product can be demoulded in about 2 hours. More current practice involves using complex compound plasticiser/retarder additives to tailor the workability and setting time to specific processes.

Chemical means of retardation for matrix C (such as citric acid addition) have an uncertain effect on the hydration chemistry of the cement. To avoid any distortion of the results by such methods, it was decided to achieve retardation by chilling the mix constituents and mixing equipment to 5°C prior to sample manufacture. This provided a sufficient extension to the workability of the paste (for up to 40 minutes).

3.1.1.4. Matrix D.

Matrix D was formed by the addition of Durapact Concentrate (a very fine grey powder based on microsilica, marketed and supplied by Durapact GmbH, Germany) to blast furnace slag cement. A suitable cement (DIN 1164 Hocheffenzement) was supplied along with the Concentrate. The constituents were supplied separately and mixed as needed.

Initial information presented with the materials suggested that the two constituents should be mixed in the ratio 1:1; this proved to be impracticable as a result of insufficient workability (a stiff, dough-like consistency at normal w/c ratios) and excessive shrinkage during hardening causing disintegration of the boards. Subsequent discussions with the manufacturers led to a revised mix design of 2:1 blast furnace slag cement to Concentrate. The delay in resolving the problem with the manufacturers meant that matrix D composites were unable to be accommodated in the main schedule of work, hence only a limited investigation could be undertaken.

3.1.2. Water/cement ratio and plasticiser.

Preliminary experiments with the various matrices established that at normal w/c ratios (0.3 - 0.4) none of the new cements possessed sufficient workability for composite manufacture. It was decided, after consultation with the BRE, that the use of a superplasticiser would be preferable to employing abnormally high w/c ratios to attain the required workability. A commercial naphthalene sulphonate based superplasticiser (Conplast SP430, supplied by Fosroc) was used throughout.

Only matrix D was supplied with any specific instructions regarding a suitable w/c ratio. The figure specified (equivalent to w/c = 0.38) was used as a starting point for establishing the necessary superplasticiser addition level for all matrices. The w/c ratio was subsequently altered to 0.4 to bring the addition level within the levels suggested by the superplasticiser manufacturer. The adjusted addition levels were then used throughout the project and are tabulated in Table 3.1.

Table 3.1. Superplasticiser addition levels for equivalent workability at w/c = 0.4

Matrix	ml/kg cement	w/w cement, %	v/v mix water, %
O	1.7	0.24	0.53
M	12	1.44	3.16
C	17	1.92	4.21
D	33	4.01	8.77

These addition levels were determined to ensure that the slurries were of a consistency such that they would just pour freely but not exhibit excessive bleeding during trowelling of the surface. A support project was undertaken to investigate the effect of superplasticiser addition on the rheology of the slurries (Gill, 1996; Markou, 1996).

3.1.3. Analytical techniques.

3.1.3.1. Pore solution extraction and analysis.

All cement pastes contain a certain amount of 'free water' existing in the pore structure. Dissolved within it are a number of ionic species (depending on the composition of the cement) and this 'water' is often termed *pore solution*. Since it

would be reasonable to assume that this pore solution is likely to be in contact with the glass fibres in GRC, its composition is of great interest.

Samples of the cement matrices were cast at w/c=0.4 into cylindrical moulds (47 ∅ × 74mm), demoulded after 2 days, cured for a further 26 days at >95% RH and then either tested immediately as '0 day' (unaged) control samples or aged under various ageing regimes. (For a description of the ageing regimes used, see subsection 3.4.3.)

After ageing, the samples were placed into a steel press (shown schematically in Fig. 3.1) and a force applied via a hydraulic ram onto the piston, creating pressures within the press of up to 370 MPa. These pressures were typically held for about an hour until sufficient pore solution (2-3 ml) had been extracted for analysis.

The pore solution was analysed immediately after extraction (to prevent atmospheric carbonation of the highly alkaline solution) for OH^- content by titration against 0.01 molar HNO_3. Analysis for other ions (normally K^+, Na^+ and Ca^{2+}) was performed within a few days using flame photometry.

Figure 3.1.: Schematic Section of Pore Press Assembly

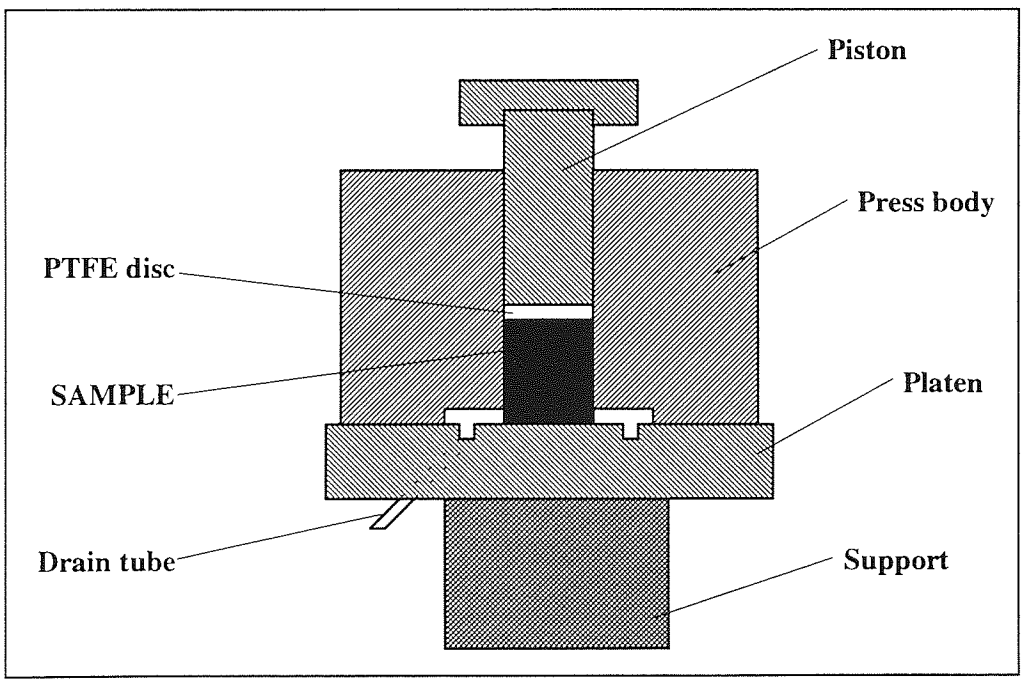

3.1.3.2. XRF/XRD.

X-ray fluoroscopy (XRF) was used as a quantitative technique to determine the elemental composition of the original cementitious powders. Preparation of samples for XRF is complex, requiring mixing with a lanthanum flux and heating to >1000°C to melt the cement and form a glass bead. All volatiles (e.g. carbonates and hydrates) are driven off in this process, leaving only oxides. This glass bead is then bombarded with X-rays, exciting the atoms of the constituent elements. These fluoresce with characteristic wavelengths, and analysis of the relative intensities of the wavelengths emitted allows the elemental (i.e. oxide) composition of the bead to be determined. The elements analysed for were; Si, Al, Ti, Fe, Mg, Ca, Na, K, P and Mn.

X-ray diffraction (XRD) was used as a primarily qualitative technique to detect crystalline compounds within the hydrated cements after various ageing regimes. A small quantity of ground sample is spread flat, and an X-ray beam fired at it. Crystals of specific compounds will diffract the beam, producing a diffraction pattern with peaks at a number of characteristic angles (θ) according to Bragg's Law:

$$n\lambda = 2d.\sin\theta \quad (n=1,2,3...)$$

where λ is the wavelength of the x-rays and d is the 'basal spacing' or distance between the crystal layers. The wavelength used in these studies was 1.5406 Å.

The sample stage is rotated, and the intensity of X-rays is determined as a function of angular displacement or basal spacing. The resulting trace will show families of peaks corresponding to specific compounds. The traces were presented in 2θ° vs. number of counts (i.e. intensity) format. The angular resolution was 0.05°.

The analysis of these peaks to identify constituents is highly complex and greatly aided by a computer. XRD testing was performed by the BRE on a Siemens D500 diffractometer using Cu Kα radiation at 40 KV and 30 mA. They also provided guidance on interpretation by comparison with the JCPDS (Joint Committee on Powder Diffraction Standards) computer database using Siemens software.

3.1.3.3. DTA/TG.

Differential thermal analysis (DTA) and thermogravimetry (TG) were used as semi-quantitative techniques to determine the natures and relative amounts of hydrated compounds present in the cement pastes after various ageing regimes.

In DTA, a small (≈ 60 mg) ground sample of hydrated cement is packed into a crucible and placed in a furnace alongside an inert reference sample. The two samples are then subjected to a carefully controlled temperature rise (ambient up to 1000°C at 20°C per minute). If no physico-chemical changes occur in the cement, the temperature of the cement sample relative to the reference sample (ΔT) will be zero. When reactions do take place in the cement sample (e.g. loss of chemically bound water, or de-carbonation), ΔT (measured with a pair of matched thermocouples) will change. The sign of ΔT indicates whether the reaction is exo- or endothermic. Plotting ΔT against time (i.e. furnace temperature) will produce a graph with peaks and troughs each characteristic of certain compounds.

TG is normally performed alongside DTA. As the furnace temperature rises, the mass of the cement sample will change as water or gas is driven off during reactions. Plotting the weight on the same scale as the DTA trace allows the weight loss during each reaction (i.e. corresponding to each DTA peak/trough) to be determined and hence the quantity of compound present in the sample.

3.1.3.4. Other techniques.

Sulphate analysis - the raw cementitious materials were analysed for sulphate content gravimetrically. 1 gram of cementitious powder was dissolved in HCl, boiled and filtered. The pH of the solution was then adjusted with ammonia and concentrated HCl and reboiled. Boiling $BaCl_2$ solution was added, producing a $BaSO_4$ precipitate. This was then filtered, dried and weighed to determine the sulphate content.

Ion chromatography - some of the pore solution expressions were tested for anions other than OH, primarily sulphate. A Dionex 2000i/SP dual column chromatograph coupled with a HP 3390A Integrator was used for the analysis.

Ion chromatography is a complex process. Samples are diluted and passed through a column containing an ion exchange resin which strips out the anions. The column is then 'washed' with an eluent solution. The eluent will remove different anions from the column at different rates, dependent on the balance between the particular anion's affinities for the column and the eluent. Consequently, the eluent will become contaminated with particular anions at different times. If the conductivity of the eluent leaving the column is plotted against time, a number of peaks will be displayed, each at a time corresponding to a different anion. By comparison of the appearance time and areas of these peaks with plots derived from standard solutions, quantitative analysis of the anions in a pore solution expression can be obtained.

Pore solution dilutions of 1:100 and a $NaCO_3$-$NaHCO_3$ solution eluent were used. Samples were analysed for sulphate, fluoride, chloride, nitrite, bromide, phosphate and sulphate.

3.2. Commercial GRC product.

A small quantity of commercial GRC was supplied by BRE for limited testing alongside the main programme. This corrugated sheet product was unusual in that as well as employing the standard spray-formed 2-d short randomly orientated fibres it was further reinforced in the peaks and troughs of the corrugation with continuous aligned glass fibre rovings. It also used a novel matrix, believed to be based on a mixture of blast furnace slag cement and microsilica. The matrix also contained fine aggregate as is normal with commercial GRC.

The product was supplied in two forms; 'fresh' unaged sample (stored in ambient laboratory conditions) and naturally weathered (approximately 4 years outdoor exposure at the BRE's Garston exposure site).

Owing to the corrugated section of the commercial material, it was impossible to perform direct tensile tests on samples. As an alternative, bending tests were carried out at the BRE.

3.3. Fibres.

Cem-FIL 2 AR glass 250/5B fibres, supplied by CemFil International were used in the manufacture of all composites in this study. Cem-FIL 2 is a second-generation alkali resistant glass fibre designed specifically for the manufacture of GRC, and is based on glasses in the Na_2O-CaO-ZrO_2-SiO_2 system. The 250/5B variant is a continuous roving of 32 strands. Each strand is composed of about 200 filaments, which average 14 μm in diameter. Manufacturers' data for the fibre is given in table 3.2.

Table 3.2. Manufacturer's data for Cem-FIL 2 250/5B fibres.

Industrial strand tensile strength	1.7 GPa
Young's Modulus	72 GPa
Strand strain to failure	2.4%
Roving tex	2450 g/km

The fibre strands are coated with a size to preserve strand integrity before component fabrication and to offer some protection against abrasion damage during handling. This size is impregnated with a chemical 'inhibitor' that is slowly released into the surrounding matrix. It modifies the hydration of the interfacial zone in such a manner as to reduce fibre cement interaction and preserve composite strength in the long term.

3.4. Composites.

3.4.1 Manufacturing method design considerations.

A number of factors had to be considered before the final manufacturing method could be formulated. First was whether individual test samples ('coupons') or larger boards (from which to cut the coupons) should be manufactured. Although coupon manufacture has some advantages, e.g. the fibre volume can be more precisely controlled, it was felt that in view of the large number of samples involved manufacture of large boards would be more efficient. This method has other advantages; it is closer to the methods used in industrial applications, and it allows a large number of samples to be quickly manufactured from a single matrix batch. Due to the quick-setting nature of matrix C, a batch of matrix could not be kept workable for much more than 30 minutes. A board size of 500 x 500mm was decided upon, as

experience at the BRE indicated that boards of greater size are difficult to lay-up by hand.

Fibre volume fraction (V_f) had to be set at a high enough level to ensure that the critical fibre volume (V_{fcrit}) was exceeded, but not so high as to make manufacture awkward. Initial calculations suggested that a board thickness of 10mm and a roving spacing of 10mm would give V_f = 0.9%, comfortably exceeding the V_{fcrit} of about 0.3% calculated using law of mixtures principles. Boards were manufactured to these specifications. Tensile testing of coupons cut from these trial boards suggested that although V_{fcrit} had certainly been exceeded, the stress-strain traces would be clearer if a higher volume fraction was used. It was also found that the fibre strands did not disperse well throughout the thickness of the specimens. To help overcome both these problems, the sheet thickness was reduced to 6mm, increasing V_f to 1.5%. The manufacturing method was also adjusted, the fibres being laid in two layers rather than in one go.

This V_f of 1.5% may seem low compared with the typical commercial value of 5%. However, continuous aligned fibre as used in this project is usually quoted (e.g. Bentur & Mindess, 1990) as being about 3 times more efficient than the short randomly oriented fibres found in a commercial product.

Two approaches can be taken with regard to controlling the fibre volume fraction within the composite. A mass fraction can be determined and the corresponding quantity of fibre weighed out prior to manufacture of a board, or a 'length requirement' can be determined, i.e. a set length of fibre can be incorporated in each board. It was decided that, since V_f would remain constant throughout the project, the latter approach would be most convenient. It removes the need for weighing and reduces unnecessary handling of the fibre rovings prior to manufacture.

3.4.2. Board preparation.

3.4.2.1. Mould design.

The mould design is shown in the figure in Appendix 4. The base was manufactured from marine plywood, the edge formers and slotted formers from softwood and the two thin formers from PVC sheet. The assembly was screwed together. The moulds were re-used three or four times, with new slotted formers used each time. A partially prepared mould is shown in Figure 3.2.

Figure 3.2. Partially prepared GRC board mould.

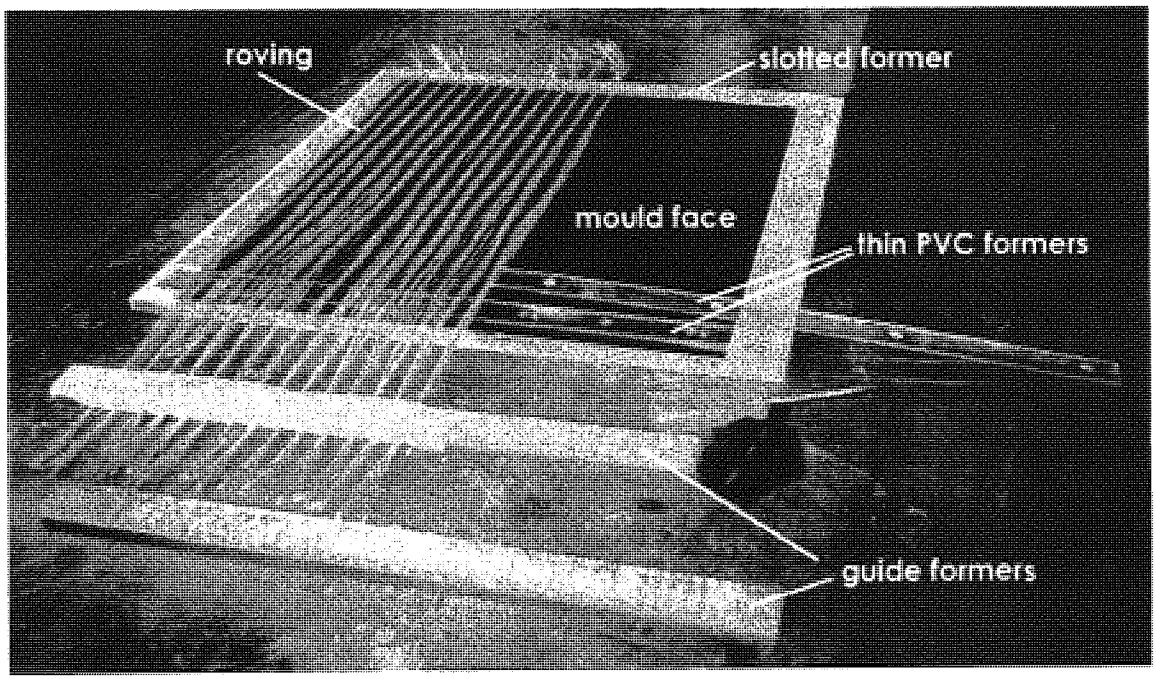

(Adapted from Fig 3.2., Gambles, 1997).

3.4.2.2. Manufacturing process.

After cutting a piece of roving to length, a knot was tied at one end which was then placed into the slotted former on the mould. The other end of the roving was placed (un-knotted) into a spare slotted guide former positioned about 200mm from the opposite edge of the board. This was repeated such that a length of roving was positioned in alternate slots. The rovings were then loosely anchored in the spare slotted former with a length of wide masking tape. This procedure was then repeated for the remaining slots using another spare slotted former placed on top of the first, hence producing two layers of equally spaced rovings. The knotted ends were then secured with more tape and the two roving assemblies moved clear of the body of the

mould. The top thin PVC former was then removed and the mould sprayed lightly with PTFE aerosol to aid demoulding.

A quantity of matrix was then mixed, first by hand and then for 5 minutes in a Hobart mixer. After a short period of mild vibration to remove any large air pockets, 1.5 litres of slurry was measured into a jug. About a third of this was poured into the mould and spread with a plasterer's trowel. The first layer of roving was lowered onto the layer of slurry and very gently pressed into it with the fingers until covered. The second third of the slurry was then poured and spread, the second layer of rovings installed and the top thin PVC former replaced. The remaining slurry was poured in and surfaced finished with the trowel. The mould was then tapped vigorously with a small steel bar to remove any large air voids. Finally the green board was contact covered with very thin PVC sheet and transferred to a curing cabinet at 20°C and 95% RH for 28 days, after which it was demoulded. The board was immediately cut into 205 x 50 mm coupons with a diamond wheel. These coupons were then transferred to various ageing regimes. A certain number of coupons from each batch were immediately tested to provide the control data, which are referred to in this project as '0 day' samples.

3.4.3. Ageing.

The ageing regimes outlined below were designed in consultation with the BRE and after review of the substantial literature on the subject. Tensile test coupons were aged in quadruplicate, whilst matrix samples ie. the cylinders for pore pressing (see subsection 3.1.3.1) were aged in duplicate.

3.4.3.1. Hot water.

Hot water ageing is the simplest and consequently most common accelerated ageing regime used for GRC.

Samples were placed into small (1 to 5 litre) tanks of de-ionised water at 20°C, 38°C and 65°C for varying exposure times, summarised in Table 3.3.

Table 3.3. Hot water ageing regimes.

Temp., °C	7 days	14 days	28 days	56 days	6 months	12 months
20	OCM*	not used	OCM*	OCM*	OCMD	OCM*
38	CMD	CMD	CMD	CMD	CMD	CM*
65	OCMD	OCM*	OCMHD	OCMD	OCMD	OCM*

*H: pre-fabricated commercial GRC samples. * = tensile samples only (ie. not pore expressions).*

(Note: in the text of the thesis, where reference is made to an ageing regime described solely by a temperature, it refers to the water immersion ageing regime at that temperature.)

3.4.3.2. Cyclic.

The cyclic test regime used in this project was based on Draft European Pre-standard Final Draft - prENV 1170-8: 1994 drawn up by Technical Committee CEN/TC 229. The document specifies a 48-hour cycle as follows:

- 24 hours immersion in water at 20 ± 2°C;
- 30 minutes forced drying at a temperature of 70 ± 5°C and an airspeed of 1 m/s;
- 23 hours in circulating hot air of 70 ± 5°C (air renewal: 30 times the air volume in one hour);
- 30 minutes forced cooling at a temperature of 20 ± 2°C.

A Fisons environmental cabinet equipped with air circulation and a refrigeration unit was available. This cabinet was adapted to take an additional hot air supply from an external variable hot air 'gun' and a movable thermocouple to monitor the internal temperature directly over the samples. A standard temperature controlled water bath was also acquired. Stacking stainless steel racks were manufactured, each holding 12 samples, to allow easy transfer from cabinet to bath. The racks spaced the samples 50mm apart as specified in the standard.

Three ageing regimes were used; 28 day, 56 day and 6 months. Samples were aged in quadruplicate. Pore pressing style cylinders were not aged in this manner, pieces of matrix taken from the composite coupons were used for XRD, etc.

3.4.3.3. Carbonation.

Since degrees and rates of carbonation were beyond the scope of this project, a simple carbonation regime was used. Samples were placed in a small sealed tank over a saturated solution of sodium nitrite to provide the optimum RH (*vis a vis* carbonation) of 65%. This tank was then slowly flushed twice a day with pure CO_2. Spare samples were removed at weekly intervals. These samples were then fractured and the fresh surface treated with phenolphthalein to determine the degree of carbonation. When the samples were fully carbonated they were removed from the tank and tested.

Samples were aged in quadruplicate. Pore pressing style cylinders were not aged in this manner, pieces of matrix taken from the composite coupons were used for XRD, etc.

3.4.4. Mechanical testing.

Much of the literature concerning mechanical testing of GRC advocates three- or four-point bending tests, normally because they are simple to perform. Although they provide an excellent quality control measure, the analysis of results from these tests is less straightforward than the analysis of direct tensile test results. This is mainly because only one half of the specimen is in tension and the behaviour of cementitious materials in compression is very different to that in tension. It was decided that direct tensile testing would be more appropriate to a fundamental study of this nature.

3.4.4.1. Equipment and method.

An Instron 1197 tensile test machine fitted with a 100kN load cell was used for the testing, modified to PC control using Deltalab/Nene Materials Test Program software. The machine was fitted with adjustable combination hand tightened/ wedge action jaws (provided by the BRE). Strain was measured using a 50mm gauge length 'clip-on' extensometer. The software allowed the sample dimensions (i.e. width and thickness) to be inputted and output was given as stress/strain values rather than load/extension values. Output was taken from the PC as ASCII text files, each of around 3000 data pairs and subsequently plotted and analysed using other software, although some analysis (post-cracking modulus) was performed using the on-board software.

The equipment allowed a stress resolution of ≈0.05 MPa. Strain measurement was analogue but the sampling rate restricted resolution to ≈10μ (0.001%). Maximum measurable strain was 3.4%. Preliminary experiments showed that a crosshead speed of 0.6 mm/min (equivalent to $200\mu\varepsilon.s^{-1}$) gave the most reliable results.

To prevent sample failure in the machine jaws (due to stress concentrations at surface imperfections) it was necessary to bond grip plates to the ends of the coupons. After trials with a number of systems, hardboard plates (50 x 40 x 1mm) were used, bonded to the coupons with an epoxy resin. Occasional gross imperfections in the sample surface were gently ground off by hand prior to application. Careful application of these plates also allowed correction of non-parallel end surfaces.

As the grips were tightened onto the sample, it was found that their wedge action caused the application of a small preload. To counteract this, tightening was performed slowly in stages, the preload being taken off by a small crosshead adjustment after each stage. The extensometer was then attached and the test started. During the test, the developing stress/strain curve was displayed on the computer screen.

On completion of the test, any on-board analysis required was carried out and the ASCII test data loaded onto 3½ inch diskette for later analysis. Up to 6 tests could be completed in an hour.

3.4.4.2. Analytical tools.

The large quantity of data generated by the tensile test software (up to 70 Kbytes per test) necessitated the use of computer software for its analysis. The tensile test machine's on-board software, although useful for certain functions, was not designed to deal with the relatively unusual stress/strain traces generated by GRC. It was also inconvenient to use for long periods of study as the PC could not be easily detached from the tensile test machine.

It was decided to make use of some software specifically developed for GRC by Dr. P. Walton of the BRE. This software (LOPFinder) reads a file consisting of two columns of ASCII format stress/strain data pairs and determines a number of parameters, namely;

- peak stress, and strain at peak stress;
- LOP, and strain at LOP;
- BOP, and strain at BOP;
- elastic moduli up to LOP, and up to BOP.

These values can then be pasted into a commercial spreadsheet package. The raw data can also be processed by a commercial spreadsheet package for plotting graphs and for functions that are not available in LOPFinder (such as computing the energy absorbed to failure).

The software was also adapted to 'reduce' the data. The raw data from the tensile test machine contained a large number of redundant data pairs caused by its strain resolution being substantially greater than its stress resolution. The software detects and removes these data pairs, reducing the file size by up to a factor of four. This allowed quicker processing of the data when used with a commercial spreadsheet package.

3.4.5. Crack spacing analysis.

During tensile testing, uniaxially aligned GRC samples develop a system of parallel transverse cracks (multiple cracking). Analysis of the spacing of these cracks can provide information about the fibre/cement bond strength.

Initially, attempts were made to highlight the cracks (using dyes) in order that the crack spacings might be studied macroscopically. This approach proved unsuccessful, mainly due to the narrowness of the cracks (generally of sub-micron width). Microscopic examination of dyed samples at 100X magnification showed that the dye was not highlighting all the cracks. Consequently it was decided that a microscope equipped with a travelling stage would be used for the crack spacing analysis.

Samples were placed on the stage mould face uppermost and lit from above. The viewfield crosshairs were centred on a crack and the stage traversed through 75mm. The number of cracks passing the crosshairs during the traverse was recorded. The traverse was repeated four times in different places on each sample and an average number of cracks encountered (C) calculated. The crack spacing for the sample was then calculated as (75/C)mm.

3.5. Microstructure.

The performance of GRC is largely dictated by parameters such as the fibre/cement bond, strand 'bundle filling' mechanisms and corrosion of the fibres themselves. All these parameters concern the fibre/matrix interface and are manifest at the microstructural level. The techniques used to follow the interfacial development are described below.

3.5.1. SEM.

The primary advantage of scanning electron microscopy (SEM) is in its far superior depth of field ability compared to optical microscopy. This allows fracture surfaces to be observed rather than polished sections.

Samples were cut to a height of <6mm and mounted on an aluminium stub with the fracture surface uppermost. They were then dried over silica gel and sputter coated with gold in vacuum. Micrographs were then taken at various magnifications, providing views of the whole surface, the strands and the individual filaments. Particular attention was paid to the interfacial area and the filament surfaces.

(Note: a number of problems were encountered during SEM study of the composites which are described in section 6.2.)

3.5.2. Thin section (optical) microscopy.

Thin sections of the aged coupons were prepared with the intention of supporting and elaborating upon the findings of the SEM work. Also, there is little if any analysis of GRC thin sections described in the literature.

Tensile test coupons were cut into short pieces, stacked three high and vacuum-impregnated with araldite. A cross-section (normal to the fibre alignment) of this 'sandwich' was then polished and mounted on a glass slide. The specimen was roughly ground to a thickness of about 0.5 mm, then finely ground (using a non-aqueous abrasive medium) to standard petrographic thickness (30μm) and a cover slip placed over the specimen. (This preparation was carried out by Birmingham University who have extensive experience in the preparation of thin sections).

The manufacture of slides of sections parallel to the fibre alignment proved fruitless, as the polishing process tended to pull the filaments out of the matrix.

The thin sections were examined using a petrographic microscope to determine the nature of any interfacial or inter-filamental deposits and to examine the general nature of the fibre/cement interface. Further description appears in section 6.1.

3.5.3. Image analysis.

The petrological microscope used to examine the thin sections was also equipped with video camera attached to a PC, allowing images to be captured and digitally analysed. The most useful application of this facility was in estimating the effective perimeter of the fibre strands in contact with the cement matrix. This perimeter is essential if quantitative bond strength calculations are to be made from crack spacing data.

Images were captured on disk as 512 x 512 pixel 16 million colour tagged image file format (TIFF) images. These were converted to grey-scale (256 grey level) TIFFs for analysis using the Unix-based GRASS image analysis software.

The software processes the image in a number of stages. First, the image is 'reclassed'. The fibres appear much brighter than the surrounding matrix. A threshold value (T) of brightness can therefore be chosen; parts of the image with a brightness value above T are assumed to represent fibre and those below to represent matrix. The program processes the image and replots it in binary (i.e. black and white) on the basis of the threshold value. Each pixel is assigned a value of either 1 (fibre) or 0 (matrix)

depending on whether its original grey-scale (0 to 255) value was above or below T. This is also known as 'density slicing'. (The rationale behind choosing a threshold value is discussed in 7.3).

Secondly, the image must be 'clumped'. Unwanted artefacts in the original image (e.g. pores, small crystals in the matrix, microcracks) may also have appeared brighter than T and hence been erroneously classed as fibres. The image will have a large number (typically a few thousand) small groups ('clumps') of continuously adjoining white pixels as well as the large clump representing the fibre strand. The program scans the image for these clumps and replots the image, assigning each clump a different colour value. The 'clumped' image is then examined and the colour value of the clump representing the fibre strand noted. The image is then reclassed in binary again with the colour value of the fibre clump used as the threshold value, hence removing all the extraneous pixels.

It is important to note here that if the strand is well flattened then there may be more than one clump that represents fibre as all the pixels may not be continuous, hence this step must be carried out with some care and interpretation.

The image now consists of just one clump of pixels on a background, and using a small program written by A. Buchanan of the Aston University Remote Sensing Group, the total number of pixels (i.e. the area) and the number of pixels in the perimeter was found, which acted as rough guide and lower bound to the perimeter. The image was again replotted with just the perimeter pixels displayed. This is then 'vectorised' using GRASS and the perimeter established.

The entire process is further explained and illustrated in Chapter 7.

3.6. Sample labelling code.

Occasional reference is made to sample numbers in this thesis. The code for the samples was derived as follows:

(matrix)/(ageing regime)/(ageing time)/(sample number)

The matrix code may be followed by a letter qualifying the type of sample; P for pore pressing style cylinder, T for tensile test sample, TP for cylinder made directly from a batch of matrix material used in manufacture of a board, TX for prefabricated bending sample.

Ageing regime codes: 20, 38, 65 = 20, 38 and 65°C hot water ageing; C = cyclic ageing; CO = carbonation; N = natural weathering.

Ageing time codes: a number alone indicated ageing time in days, suffixed by m for months or y for years. Note that carbonation samples have no time code as they were all aged for 4 months.

Examples:

- CP/65/56/1: Matrix C cylinder sample aged for 56 days at 65°C, sample #1.
- MT/C/6m/3: Matrix M composite sample cyclically aged for 6 months, sample #3.

4. RESULTS; MATRICES.

A note on the presentation of matrix results: *Sections 4.1 to 4.4 present the results on a matrix-by-matrix basis and generally contain only 'factual' notes. Section 4.6 discusses the results with emphasis on comparison and contrast of matrices and their behaviour. This sectioning of the presentation is necessary owing to the difficulty in presenting the substantial number of pore expression results in a coherent manner.*

4.1. Unhydrated cement compositions.

The constituents of the various unhydrated cementitious materials used for the GRC matrices were analysed using XRF, XRD and 'wet' sulphate analysis. A description of the techniques is given in the previous chapter. The results from these analyses were used in stoichiometric calculations (often referred to as 'Bogue' calculations) to derive the compound compositions given below. An example of such a calculation is given in Appendix 1. Further examples can be found in most cement chemistry texts (e.g. Lea, 1970). Compounds are described using cement chemistry notation, a brief key to which is included in Appendix 1. The XRD traces for the unhydrated cementitious components are given in Appendix 2.

4.1.1. Matrix O.

XRD traces for unhydrated matrix O show the presence of C_3S, C_2S, C_3A and C_4AF, with C_3S the most prominent component owing to its strong XRD signature. Traces of quartz and possibly $C_3A.(CaCO_3).H_{11}$ were also detected. The XRF oxide analysis is given in Table 4.1, along with the manufacturers analysis.

Table 4.1. XRF analysis; Matrix O.

Oxide	SiO_2	Al_2O_3	Fe_2O_3	MgO	CaO	Na_2O	K_2O	LOI
MD % w/w	19.3	5.14	2.91	1.36	63.4	0.1	0.78	na
XRF % w/w	22.0	5.7	2.9	1.7	65.0	0.0	0.9	3.2

LOI = Loss on ignition (volatiles). MD = manufacturers data.

SO_3 : MD = 3.28%, our analysis = 3.0%

Although XRF analysis is accurate enough for most purposes, the Bogue calculations are extremely sensitive to the CaO/SiO_2 ratio in the oxide analysis. The manufacturer's figures are used in the derived compound composition given below as they are considered to be more accurate with regard to CaO and SiO_2.

Table 4.2. Compound composition, Matrix O (% w/w).

C_3S	C_2S	C_3A	C_4AF	CaO	MgO	Gypsum	Alkalis	Minors
56.6	12.6	8.7	8.8	1.6	1.4	7.0	0.9	2.4

4.1.2. Matrix M.

Matrix M was a blend of the OPC detailed above and metakaolin. The peaks manifested in the XRD traces for the metakaolin did not correspond to any common compound in the BRE XRD database. The major peaks were at 26.8, 8.8, 20.9 and 28.4° 2θ. The XRF oxide analysis is given in Table 4.3.

Table 4.3. XRF analysis; Cemstar meta-kaolin.

Oxide	SiO_2	Al_2O_3	Fe_2O_3	MgO	CaO	Na_2O	K_2O	LOI
% w/w	55.3	41.3	0.6	0.3	0.1	0.1	2.5	1.3

LOI = Loss on ignition (volatiles).

No sulphate was detected. This corresponds to an approximate molar formula of AS_2 (as expected), possibly slightly enriched in silica, plus minor phases. The AS_2 phase accounts for at least 90% of the total. The analysis of unhydrated matrix M will therefore be as that for matrix O but 'diluted' with a 20% w/w addition of metakaolin. As an example, assuming that the meta-kaolin is 90% AS_2, the matrix composition would be as in Table 4.4.

Table 4.4. Compound composition; Matrix M (%w/w).

C_3S	C_2S	AS_2	C_3A	C_4AF
45.3	10.1	18.0	7.0	7.0
CaO	**MgO**	**Gypsum**	**Alkalis**	**Minors**
1.3	1.1	5.6	1.2	3.4

Note that the high alkali content of the meta-kaolin has increased the alkali content of the matrix cf. matrix O (Table 4.2).

4.1.3. Matrix C.

The XRD traces for unhydrated matrix C show the presence of C_3S, C_2S, C_3A, anhydrite and a phase identified as 'ye'elimite' ($C_4A_3\check{S}$). Gehlenite (C_2AS) was identified in the hydrated samples (as a unhydrated remnant rather than a hydration product) and was certainly present in the unhydrated material, but with its major peak masked by the strong anhydrite peak. The complete consumption of anhydrite on hydration uncovers the gehlenite peak. Traces of C_4AF and possibly $C_3A.(CaCO_3).H_{11}$ were also detected. The XRF oxide analysis is given in Table 4.5.

Table 4.5. XRF analysis; Matrix C.

Oxide	SiO_2	Al_2O_3	Fe_2O_3	MgO	CaO	Na_2O	K_2O	LOI
% w/w	19.0	16.5	1.9	0.9	53.6	0.0	0.6	0.7
	±0.4	±0.0	±0.0	±0.1	±0.1	±0.0	±0.0	±0.1

LOI = Loss on ignition (volatiles).

Two XRF samples were tested for matrix C owing to concerns about its small scale homogeneity. The maximum departure from the mean is presented with the values.

The sulphate analysis yielded **8.2%** (expressed as w/w SO_3).

According to the manufacturers (Gartshore *et al.*, 1991), matrix C is a mixture of a mining cement plus an unspecified amount of metakaolin. The mining cement blend consists of Portland cement, calcium sulpho-aluminate clinker and anhydrite in the

ratio 8:3:1 by weight. The composition of the calcium sulpho-aluminate clinker was given as in Table 4.6.

Table 4.6. Published calcium sulpho-aluminate clinker phase composition, %w/w (Gartshore *et al.*, 1991).

$C_4A_3\check{S}$	CA	C_2AS	$C_{12}A_7$	C_4AF	CT
60	15	15	1	4	4

T = TiO_2.

It was not possible to deduce the compound composition of matrix C from our own results alone owing to the large number of similar phases, hence this published analysis was used in analyisis. Discussions with the manufacturers confirmed that the addition level was 10% metakaolin w/w i.e. 1:9 metakaolin to mining cement, which was confirmed by Bogue style stoichiometric analysis. The derived compound composition for matrix C is given in Table 4.7.

Table 4.7. Compound composition, Matrix C (%w/w).

C_3S	C_2S	$C_4A_3\check{S}$	$C\check{S}$	AS_2	C_4AF	C_3A
34.0	7.6	13.5	7.5	9.0	6.2	5.2
Gypsum	**CA**	**C_2AS**	**CaO**	**MgO**	**Alkalis**	**Minors**
4.2	3.4	3.4	1.0	0.9	0.6	≈ 4

4.1.4. Matrix D.

Matrix D was formed from a 50:50 mixture of German Hocheffenzement (blast furnace slag cement) and Durapact Concentrate. The ingredients of the concentrate were not divulged.

The XRD traces for the cement indicate the presence of C_2S, C_3S, C_4AF, C_2AS (gehlenite) and relatively large amounts of anhydrite. The large hump in the baseline of the XRD traces between about 28 and 35° 2θ is most likely attributable to glassy blast furnace slag. The concentrate traces show C_2S, C_3S and anhydrite, with a very large baseline hump between about 17 and 28° 2θ probably indicating the presence of micro-silica. The XRF oxide analysis of the components is given in Table 4.8.

Table 4.8. XRF analysis, Matrix D (% w/w).

	SiO_2	Al_2O_3	Fe_2O_3	MgO	CaO	Na_2O	K_2O	LOI
BFSC	30.4	8.2	1.9	6.8	47.9	0.2	0.6	0.3
D-pact	68.4	10.1	3.5	1.4	11.7	0.5	2.0	3.2

BFSC = blast furnace slag cement; D-pact = Durapact Concentrate.

The sulphate analyses yielded **3.2% (BFSC)** and **0.8% (D-pact)**, although total sulphur analysis performed by the BRE gave 5.5 and 1.1% equivalent SO_3 w/w respectively. This may be owing to the presence of iron sulphides in the slag which were not detected in the 'wet' sulphate analyses.

Without further information on the composition of the Hocheffenzement (e.g. the compositions of the components of the cement [ggbs and OPC]), it was not possible to derive its detailed compound composition. The German standard for cement (DIN 1164-1: Oct. 1994) dictates that Hocheffenzement contains 36 to 80% ggbs by weight. By comparison with typical German blast furnace slag compositions (Lea, 1970), the high magnesia and silica contents revealed in the XRF analysis would tend to indicate a slag content in the upper end of this range (i.e. a type III/B hocheffenzement with between 66 and 80% slag).

Similarly, the lack of information on the general composition of the Concentrate precludes derivation of its detailed compound composition. Exploratory investigations revealed that the Concentrate is weakly hydraulic on its own. It is probably formed from a mixture of microsilica, a hydraulic cementitious material and anhydrite in uncertain proportion.

4.2. Hydrated cement compositions: XRD analysis.

XRD was used to study the hydration behaviour of the different matrices under various ageing regimes. The consumption or evolution of compounds was determined qualitatively by comparing peak heights relative to those at the unhydrated and '0 day' ageing stages. The detailed analysis was performed by compiling annotated tables; one for each ageing regime (i.e. in water at 20 and 65°C, cyclic, and 4 months of

carbonation) with separate columns for each ageing period. Summaries of the tables are presented below. Annotated copies of the key XRD traces are presented in Appendix 2. After preliminary investigations, it was decided not to perform detailed analysis on the samples aged at 38°C as the differences between the traces for these and samples aged at 20°C were insignificant.

4.2.1. Notes on the analysis.

CSH of various forms is almost certainly present in all samples. However, XRD is a technique dependent on the existence of crystal structures; as such, it is very difficult to detect CSH owing to its poorly crystalline, gel-like structure. There will be little discussion of CSH in the following XRD summaries.

The consumption of C_2S may be difficult to track with XRD as its characteristic peaks are often obscured by the strong and numerous C_3S peaks.

Despite the extensive number of 'masks' (compound templates) applied to the traces by the BRE, nearly all samples display a substantial untagged peak at 31.0° 2θ. After discussion with the BRE, it was decided that this peak is most likely attributable to C_2S although if an associate peak is also present at 10.7° 2θ then it can be attributed to calcium 'low' carbo-aluminate hydrate ($Ca_4Al_2O_6(CO_3)_{½}OH.11½H_2O$ or low-CCAH), which will obscure the C_2S peak. This is confirmed by traces where the 31.0° peak appears to become stronger after hydration, which is improbable if it is solely attributed to C_2S.

The 56 day hot water aged samples appear to have undergone unwanted carbonation between the preparation and testing stages and consequently display spurious traces of calcite. It is interesting to note that these samples appear to contain reduced amounts of the CCAHs, particularly the 'high' form ($C_3A.(CaCO_3).H_{11}$), perhaps indicating that these compounds are unstable and 'decay' to calcite under carbonating conditions.

4.2.2. Matrix O.

4.2.2.1. Water immersion, 20°C

C_2S:	Unhydrated to 0 days; peak heights reduced by x2 0 days to 1 year; peak heights reduced by x2.
C_3S:	Unhydrated to 0 days; peak heights reduced by x4, then stable up to 1 year.
C_3A:	Unhydrated to 0 days; peak heights reduced by x4, then stable up to 1 year.
C_4AF:	Present at unhydrated stage but detection uncertain during hydration.
CSH:	Difficult to detect with XRD (see 4.2.1 above)
Ettringite:	Main crystalline hydration product. Amounts stable during hydration, possibly up slightly after 1 year.
C_3AH_6 hydrogarnet:	Trace amounts, more at 6 months and 1 year.
Portlandite:	Present in large stable quantities throughout hydration.
Calcite:	Traces present after 1 year.
$C_3A.CaCO_3.H_{11}$:	Traces present in unhydrated cement, larger amounts after hydration. Less where calcite is present.
Quartz:	Traces detected in all samples.

4.2.2.2. Water immersion, 65°C

As 20°C except;

C_2S:	0 days to 1 year; peak heights reduced by x5. Only traces present at 1 year.
C_3S:	Slightly depleted between 0 days and 1 year.
C_3AH_6 hydrogarnet:	Traces smaller after 6 months hydration cf. 20°C.
Calcite:	Traces present at 6 months, larger at 1 year.
$C_3A.CaCO_3.H_{11}$:	Not present after 0 days.

4.2.2.3. Cyclic ageing.

Up to 6 months ageing. As 20°C except;

Portlandite:	0 days to 56 days; peak heights reduced by x2. Further slight depletion at 6 months.
Calcite:	Large amounts present at 56 days, more at 6 months
$C_3A.CaCO_3.H_{11}$:	Not present after 0 days.

4.2.2.4. Carbonation.

The traces for carbonated samples are almost identical to those for 6 month cyclically aged samples with the exception of an unidentified peak at 26.7° 2θ. This peak does not correspond to vaterite or aragonite as might be expected and may be attributable to a more exotic carbonate.

4.2.3. Matrix M.

(Note; the unhydrated mixture of OPC and meta-kaolin (MK) was not subjected to XRD analysis owing to the difficulties in preparing a reliable, well mixed sample on such a small scale. The initial (i.e. unhydrated to 0 day) depletions of C_3S and C_3A were similar to those for matrix O. The depletion of C_2S could not be tracked owing to the obscuring of its characteristic 31.0° peak by the presence of low-CCAH. As noted previously (4.1.2), the major MK peak occurs at 26.8° 2θ and the depletion of this peak could be tracked during hydration.)

4.2.3.1. Water immersion, 20°C.

C_2S:	Probably present throughout but difficult to track.
C_3S:	Present throughout, possibly slightly depleted at 1 year cf. 0 days.
C_3A:	Present and stable throughout.
C_4AF:	Could not be reliably detected.
MK (26.8° peak):	Steadily depleted, 0 days to 1 year; peak heights reduced by x2.
CSH:	Difficult to detect with XRD.
Ettringite:	Main crystalline hydration product. Slight depletion between 0 days and 1 year.

C_2ASH_8 stratlingite: Present after 56 days. 56 days to 1 year; peak heights increased by x2.

Portlandite: Steadily depleted, 0 days to 1 year; peak heights reduced by x2 to 3.

Calcite: Present after 1 year.

$C_3A.CaCO_3.H_{11}$: Present throughout, converted to calcite at 1 year.

$C_4A.½CO_2.H_{12}$: Present throughout, converted to calcite at 1 year.

Quartz: Traces present throughout.

4.2.3.2. Water immersion, 65°C.

As 20°C except;

C_3S: 0 days to 6 months; peak heights reduced by x2. 6 months to 1 year; no change.

MK: 0 days to 56 days; peak heights reduced by x2. 56 days to 1 year; no change.

Ettringite: Steadily depleted. 0 days to 6 months; peak heights reduced by x3. Only trace remained at 1 year.

Monosulphate: Strong traces appeared at 1 year.

C_2ASH_8 stratlingite: Not detected.

C_3ASH_4 hyd'garnet: Appeared at 56 days. Increased between 56 days and 6 months. (not present under 20°C ageing).

Portlandite: 0 days to 56 days; peak heights reduced by x3. Not detected at 6 months or 1 year.

Calcite: Present after 56 days.

$C_3A.CaCO_3.H_{11}$: Depleted to trace quantities, 0 days to 1 yr.

$C_4A.½CO_2.H_{12}$: Not present after 56 days.

4.2.3.3. Cyclic ageing.

Up to 6 months ageing. As 20°C except;

C_3S: Slightly depleted at 6 months cf. 0 days.

C_3A: Slightly depleted at 6 months cf. 0 days.

MK: 0 days to 6 months; peak heights reduced by x3.

Ettringite:	Steadily depleted, 0 days to 6 months; peak heights reduced by x3.
Monosulphate:	Present after 56 days.
C_2ASH_8 stratlingite:	Not detected.
Portlandite:	0 days to 56 days; peak heights reduced by x5. Not detected at 6 months.
Calcite:	Large amounts at 56 days. 56 days to 6 months; peak heights increased by x2.
$C_3A.CaCO_3.H_{11}$:	Not detected after 0 days.
$C_4A.½CO_2.H_{12}$:	Not detected after 0 days.

4.2.3.4. Carbonation.

(0 days and 4 months only) As 20°C except;

C_2S, C_3A, C_4AF:	Peaks obscured by those of carbonation products.
C_3S:	Slight depletion after carbonation.
Ettringite:	0 days to 4 months; peak heights reduced by x2.
C_2ASH_8 Stratlingite:	Not detected.
Portlandite:	0 days to 4 months; peak heights reduced by x5.
Calcite:	Very large amounts after carbonation.
Vaterite:	Large amounts after carbonation.

4.2.4. Matrix C.

4.2.4.1. Water immersion, 20°C

C_2S:	Difficult to track during hydration, main peak obscured by carbo-aluminate peak.
C_3S:	Unhydrated to 0 days; peak heights reduced by x2. Further slight depletion between 0 days and 1 year.
C_3A:	Slightly depleted between unhydrated and 0 days but stable during ageing.
C_4AF:	Probably present throughout in small quantities.

Anhydrite ($C\check{S}$) & 'Ye'elimite' ($C_4A_3\check{S}$) Not detected in any hydrated samples i.e. were all consumed during initial curing.

C_2AS Gehlenite: (see 4.1.3) Present throughout ageing, slight depletion between 0 days and 1 year.

CSH: Difficult to detect with XRD.

Ettringite: Main crystalline hydration product. Slight depletion between 0 days and 1 year.

C_2ASH_8 Stratlingite: Traces detected at 6 months and 1 year.

C_3ASH_4 Hyd'garnet: Traces possibly present throughout.

Portlandite: Not detected.

Calcite: Occasional traces.

$C_3A.CaCO_3.H_{11}$: Present in unhydrated cement but not after hydration.

$C_4A.½CO_2.H_{12}$: Not present in unhydrated cement but probably present during ageing.

Vaterite/aragonite: Both present in small amounts at 1 year.

Two unidentified peaks were apparent at 14.7° and 29.4° 2θ, probably attributable to the same compound.

4.2.4.2. Water immersion, 65°C.

As 20°C except;

C_3S: 0 days to 6 months; peak heights reduced by x3. Only traces remained at 1 year.

C_2AS Gehlenite: 0 days to 6 months; peak heights reduced by x3. Only traces remained at 1 year.

Ettringite: Slightly more depleted at 1 year cf. 20°C.

C_2ASH_8 Stratlingite: Not detected.

C_3ASH_4 Hyd'garnet: Large amounts detected at 6 months, further increased at 1 year.

No **Calcite, Vaterite** or **Aragonite** were detected.

4.2.4.3. Cyclic ageing.

As 20°C except:

C_3S: 0 days to 6 months; peak heights reduced by x2.

C_2AS Gehlenite: Not depleted at 6 months cf. 0 days.

Ettringite: 0 days to 6 months; peak heights reduced by x4.

C_2ASH_8 Stratlingite: Not detected.

Calcite: Large amounts detected at 56 days, increased at 6 months.

No **carbo-aluminates, vaterite** or **aragonite** were detected.

4.2.4.4.Carbonation.

(0 days and 4 months only) As 20°C except;

C_2S, C_3A, C_4AF: Peaks obscured by those of carbonation products.

C_3S: 0 days to 4 months; peak heights reduced by x2.

C_2AS Gehlenite: Not depleted.

Ettringite: Not detected after carbonation.

C_3ASH_4 Hyd'garnet: Not detected.

Calcite, vaterite and **aragonite** were all detected in large amounts after carbonation in that order of abundance. No **carbo-aluminates** were detected after carbonation.

4.2.5. Matrix D

As detailed in 3.1.1.4, only a limited study of matrix D could be undertaken. Samples aged for 6 months at 20, 38 and 65°C were analysed. The results presented are for a matrix containing a 50:50 mix of hocheffenzement to concentrate.

After 6 months hydration: at all temperatures, gehlenite, anhydrite, C_2S, C_3A and C_4AF have all become undetectable. C_3S is depleted by a factor of at least 3 at 20°C and is depleted to trace quantities at 38 and 65°C. The baseline 'humps' attributed to microsilica and glassy slag observed in the unhydrated traces are no longer present in any trace.

Ettringite is the main crystalline hydration product. C-S-H is also present, betrayed by a broad, messy peak between 29 and 30° 2θ. Since it is normally difficult to detect with XRD owing to its gel-like structure, the appearance of its trace indicates that either very large quantities are being formed, or that the C-S-H formed by matrix D has a different, more ordered structure compared to that formed by the other matrices. Slightly more C-S-H may be formed at the higher ageing temperatures. High-CCAH was also detected at 65°C.

In general, ageing temperature seemed to have little effect on matrix D XRD traces.

4.3. Hydrated cement compositions: DTA/TG.

DTA/TG thermograms were obtained for matrices O, C and M for the following ageing regimes:

- 0 days*,
- 6 months water immersion at 20°C†, 38°C†, 65°C† and cyclic ageing*,
- 1 year water immersion at 20°C* and 65°C*,
- after the carbonation period (4 months)*.

(* indicates that matrix samples were taken from composite coupons, † that matrix samples i.e. cylinders containing no fibres were tested.)

The 38°C water immersion thermograms are not included in this summary as they show little difference from the 20°C curves.

DTA/TG thermograms for matrix D were obtained after 6 months water immersion at 20, 38 and 65°C.

Qualitative data only (i.e. compound presence indicated by characteristic temperature peaks) was derived from the DTA traces, while quantitative analysis was performed using the TG traces. Temperatures are quoted to the nearest 5°C.

The analysis of the DTA traces was performed with extensive reference to Ramachandran (1969), with occasional additional information derived from Lea (1970).

Note that in keeping with the presentation style, traces in this section are presented for each matrix individually. Figures 4.29 and 4.30 in section 4.6.1 show traces for each matrix on the same axes for comparative purposes.

4.3.1. Qualitative - DTA.

4.3.1.1. Matrix O.

Figure 4.1. DTA/TG thermogram for Matrix O, 0 days.

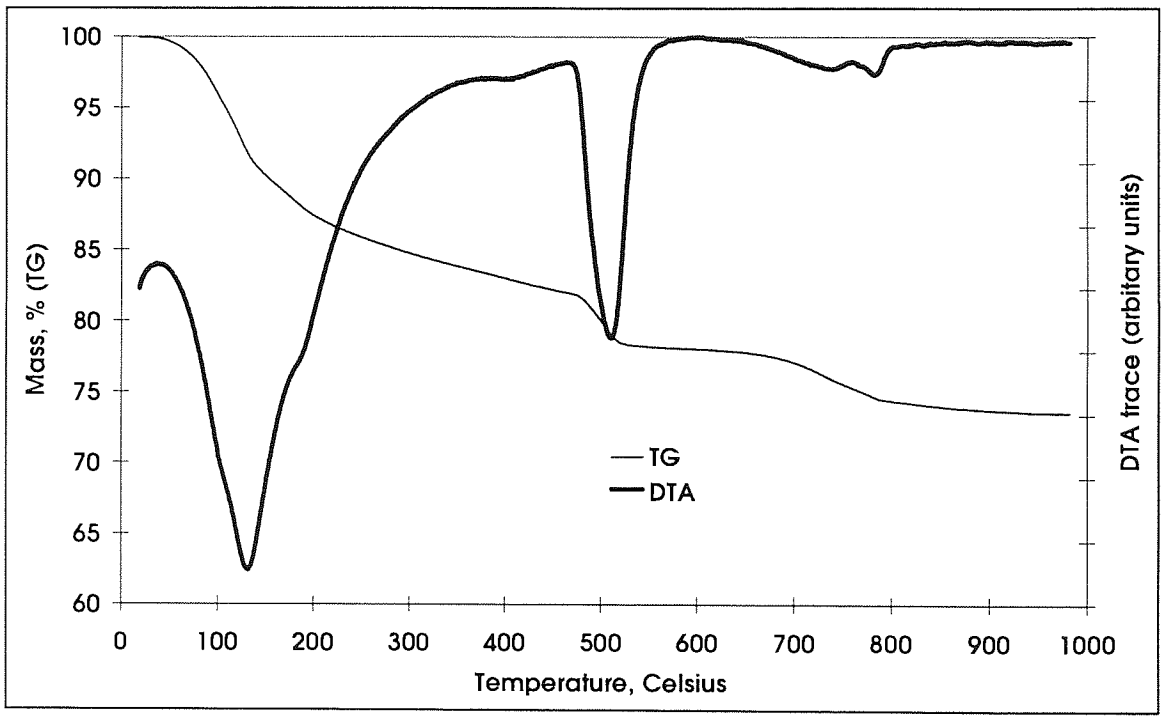

Figure 4.1 shows the three primary endotherms typical of OPC DTA, namely a low (<200°C) temperature effect, a sharp peak at about 500°C and a high (750 to 800°C) temperature effect. The corresponding perturbations in the TG trace can also be seen. There is also a minor endotherm at ≈400°C.

The low temperature effect appeared to consist of three overlapping peaks, manifested as a strong central peak (130°C) with a shoulder on each side. The shoulder temperatures were taken at the inflexion points, 100 and 180°C respectively. The peak

temperatures corresponding to these are likely to be different by up to 20° (higher for the low shoulder and vice versa). It is generally accepted (e.g. Ramachandran, 1969; Lea, 1970) that this triple effect is caused by evaporation of physically bound water, dehydration of C-S-H gel and dehydration of ettringite. Although exact interpretation is difficult, these three effects were assigned to the peaks/shoulders at ≈100, 130 and ≈180°C respectively.

Interpretation of the 495 to 505°C peak is far easier, being universally attributed to the dehydration of $Ca(OH)_2$ (portlandite).

The 800°C effect is attributed to the decomposition of $CaCO_3$. The minor endotherm prior to the main effect may be attributable to the expulsion of CO_2 from poorly crystalline calcium carbonate.

Under the hot water ageing regimes, the traces showed little variation with time apart from some intensification of the 800°C peak owing to minor atmospheric carbonation in the samples taken from composite coupons. The ettringite shoulder became less distinct with increased ageing time and temperature.

Traces from samples aged under the cyclic and carbonation (Fig. 4.2) regimes were very similar and showed more pronounced changes from the hot water aged traces. The portlandite peak was markedly reduced in intensity in both cases and the calcite peak correspondingly enhanced. The ettringite shoulders could not be discerned. For the carbonated samples, the calcium carbonate effect at 800°C formed a doublet and the small pre-calcite endotherm was not observed (Fig. 4.2).

Figure 4.2. DTA/TG thermogram for Matrix O, carbonated.

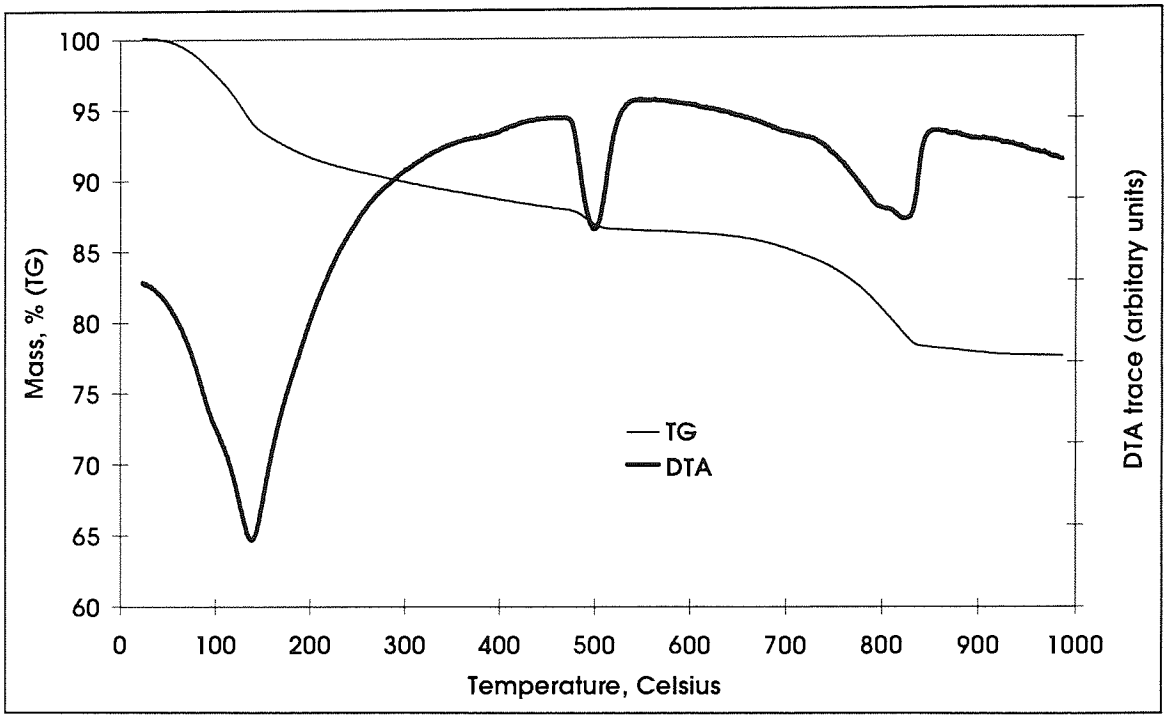

4.3.1.2. Matrix M.

Figure 4.3. DTA/TG thermogram for Matrix M, 0 days.

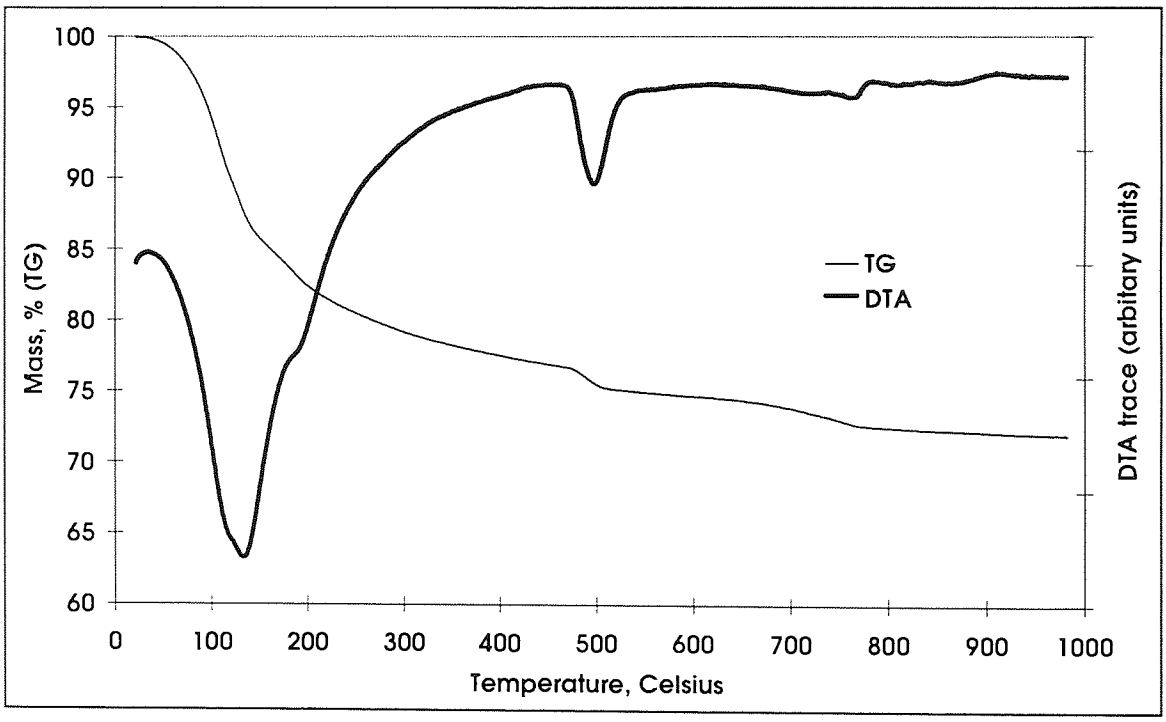

The DTA traces for matrix M (Fig. 4.3) samples showed effects similar in nature and characteristic temperature to those for matrix O (Fig. 4.1). The first shoulder on the triple peak occurred at a slightly higher temperature and the ettringite shoulder is more

distinct. The portlandite peak was less intense than for matrix O samples, as was the carbonate effect.

The low and high temperature effects remained essentially unchanged under the hot water ageing regimes. The portlandite peak became less intense with ageing time and temperature (Fig. 4.4) and was completely eliminated after 1 year at 65°C.

Figure 4.4. Variation of DTA trace portlandite peak for Matrix M.

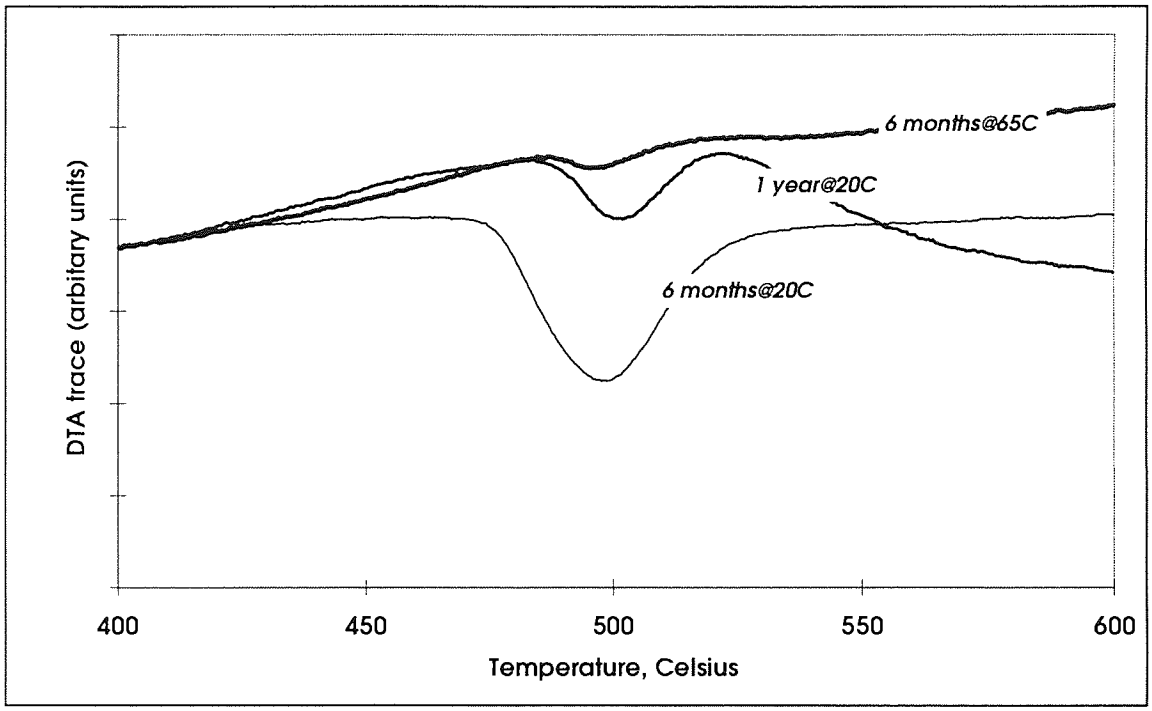

Under the cyclic ageing regime, the triple peak remained unchanged, the portlandite peak virtually disappeared and the carbonate peak became well defined. Although the peak appeared less substantial than in the matrix O thermograms, it had a similar effect on the TG trace.

The thermogram for the carbonated sample (Fig. 4.5) was very similar to that for the cyclically aged sample except that the ettringite shoulder could not be discerned.

Figure 4.5. DTA/TG thermogram for Matrix M, carbonated.

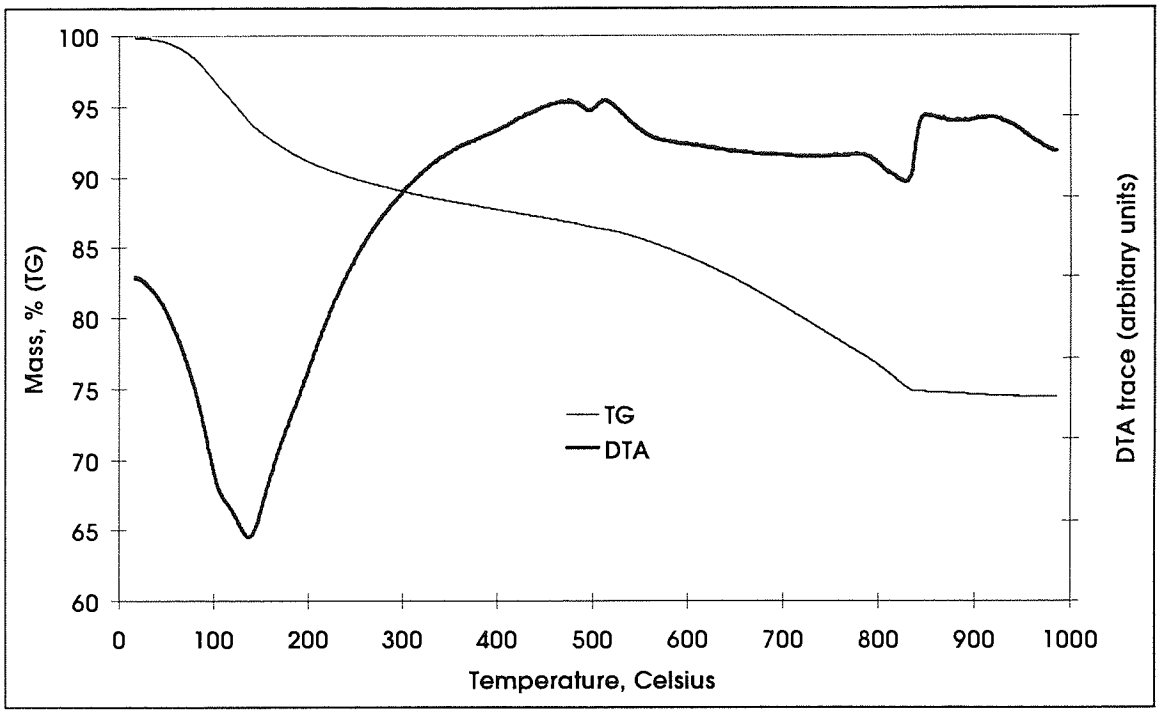

4.3.1.3. Matrix C.

Figure 4.6. DTA/TG thermogram for Matrix C, 0 days.

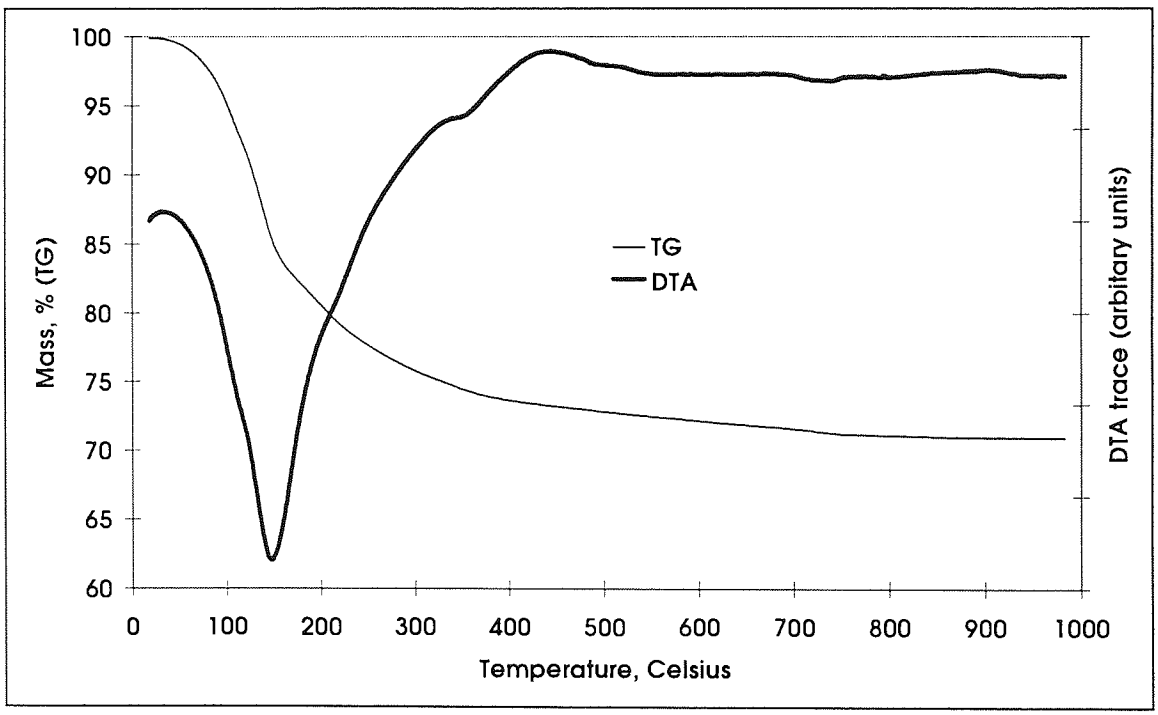

The thermograms for matrix C (Fig. 4.6) were rather different from those for matrices O and M (Figs. 4.1, 4.3). The characteristic temperature of the major peak was higher and less stable, varying between 140 and 150°C cf. a relatively steady 130°C for matrices O and M. The high shoulder was less distinct and difficult to ascribe a temperature to. These differences may be explained by the formation of a C-S-H gel of different composition to that formed in matrices O and M, whose peak interferes with that of ettringite (which XRD confirms is present and is expected from the hydration of the sulpho-aluminate clinker component of the cement).

A distinct shoulder occurred at 350°C which may be attributed to the dehydration of C_3ASH_4 hydrogarnet. Initially, there were no effects at any higher temperature, indicating that portlandite and carbonate were not present in significant quantities.

In general, hot water ageing had little effect on the DTA traces except for a gradual enhancement of the hydrogarnet shoulder with increased ageing time and temperature. It became a clear bulge after 1 year at 65°C (Fig. 4.7).

Figure 4.7. Variation of DTA hydrogarnet shoulder for Matrix C.

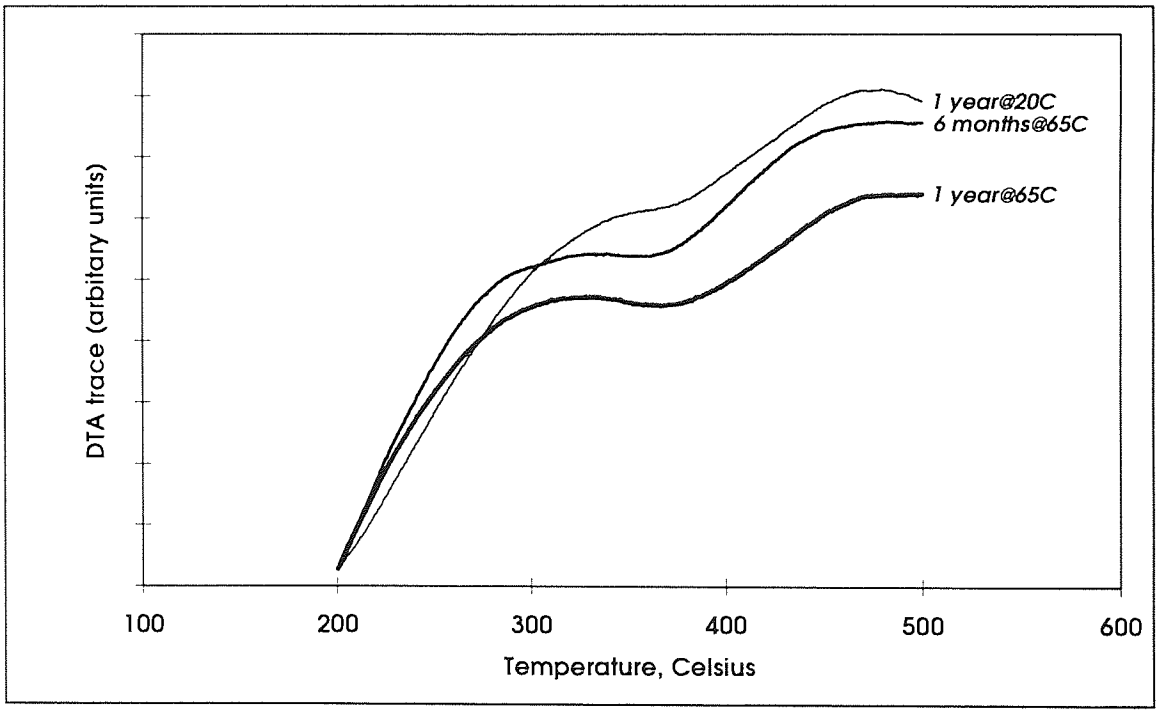

A blip also appears at ≈780°C after this ageing regime indicating some carbonation has taken place.

The DTA behaviour of carbonated and cyclically aged matrix C is shown in Fig. 4.8. A number of previously unobserved effects are apparent.

Figure 4.8. DTA traces for carbonated and cyclically aged Matrix C.

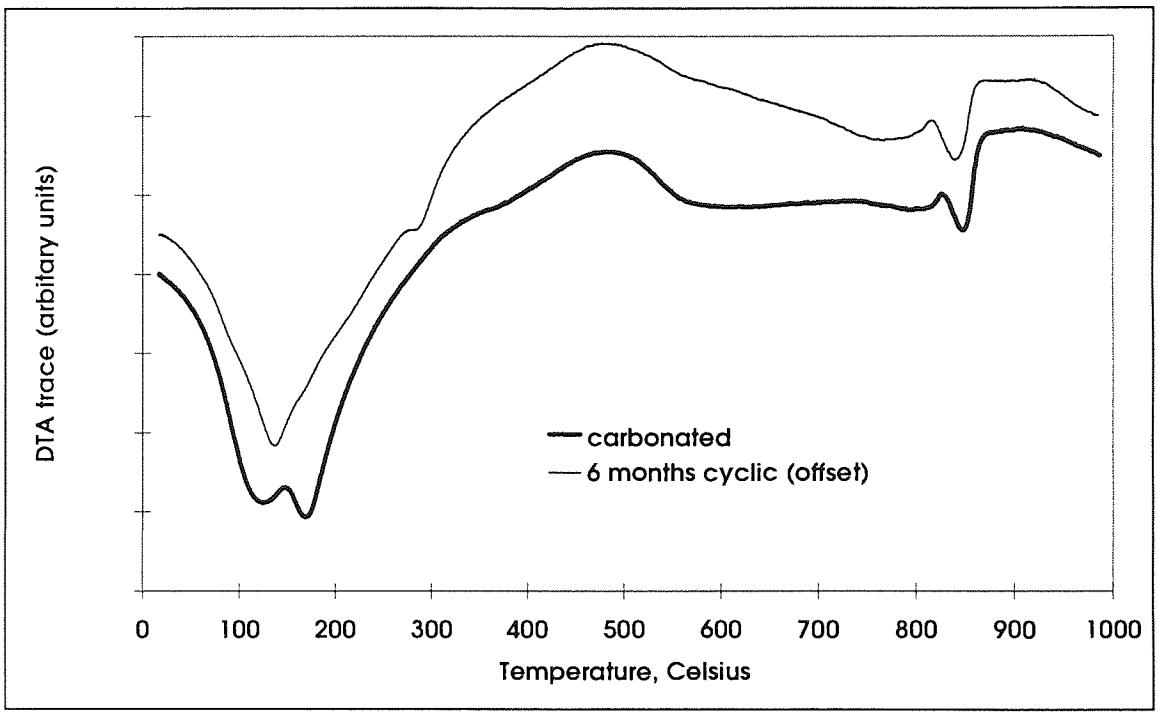

The expected carbonate peak (and corresponding TG mass loss) was apparent in both traces. In the cyclic trace, the low temperature peak became less sharp and an unusually shaped shoulder was observed at 280°C. This could not be correlated with any expected compound and may be a test artefact.

The carbonated sample showed a clear doublet in the low temperature region, with peaks at 125 and 170°C compared with the normal single low temperature peak at 140 to 150°C. This indicates that under carbonating conditions, one or more of the hydrates associated with the low temperature peaks (i.e. ettringite and C-S-H) are consumed to form the carbonate, allowing previously masked peaks to be observed.

4.3.1.4. Matrix D.

Figure 4.9. DTA/TG thermogram for Matrix D, 6 months at 20°C.

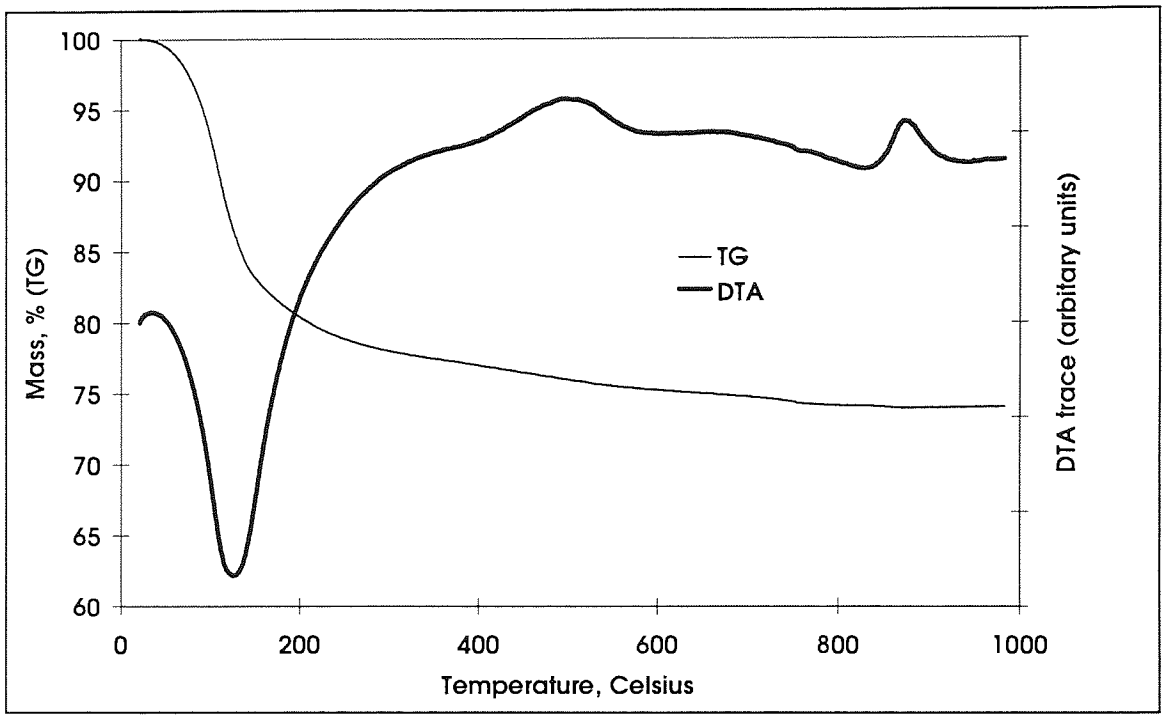

The thermograms for matrix D showed a low temperature effect at 125°C with no discernible shoulders most likely attributable to C-S-H gel. The exotherm at 860°C is attributable to the devitrification of the glassy slag in the hocheffenzement. No carbonate or portlandite peaks were apparent. The broad exotherm at 490°C was not accompanied by significant mass changes (TG trace) and remains unidentified. A less prominent but similar exotherm can be seen in the matrix C traces (Fig. 4.8 above).

Thermograms for matrix D aged for 6 months at 38 and 65°C were practically identical to Fig. 4.9 above.

4.3.2. Quantitative - TG.

Quantitative comparisons between the different ageing regimes can be made by determining the total weight loss, and the loss during the three major reactions:

- the dehydration of the 'primary' hydration products ettringite and C-S-H between 50 and 250°C;
- the dehydration of $Ca(OH)_2$ between 450 and 550°C;

- the decarbonation of $CaCO_3$ between 700 and 850°C.

It should be noted prior to any analysis that the TG traces have a continuous general downward slope. Between any two temperatures there will be a 'background' weight loss as well as any specific effect caused by dehydration/decarbonation of the compound of interest. Changes of less than 1% should be considered insignificant. In accurate work, this background loss must be accounted for.

The traces and charts below are coded to save space; 'cyc' represents cyclic ageing and 'carb' represents carbonated samples.

4.3.2.1. Matrix O.

Figure 4.10. TG traces, Matrix O.

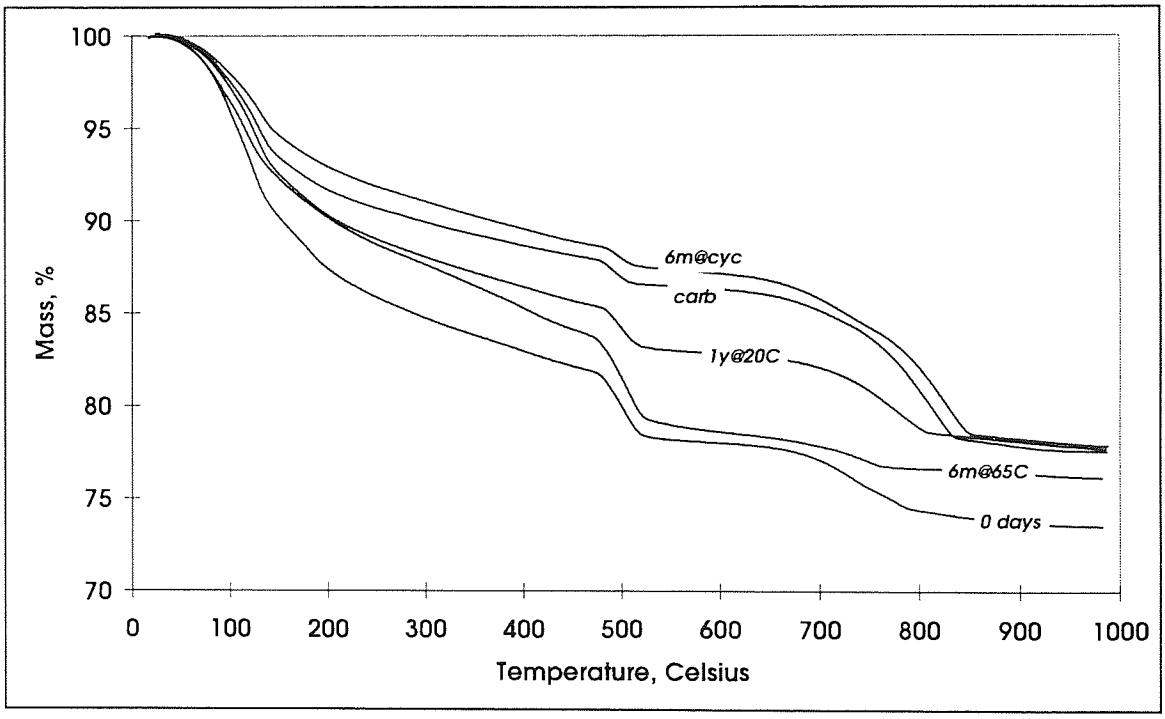

Figure 4.11. TG mass loss chart, Matrix O.

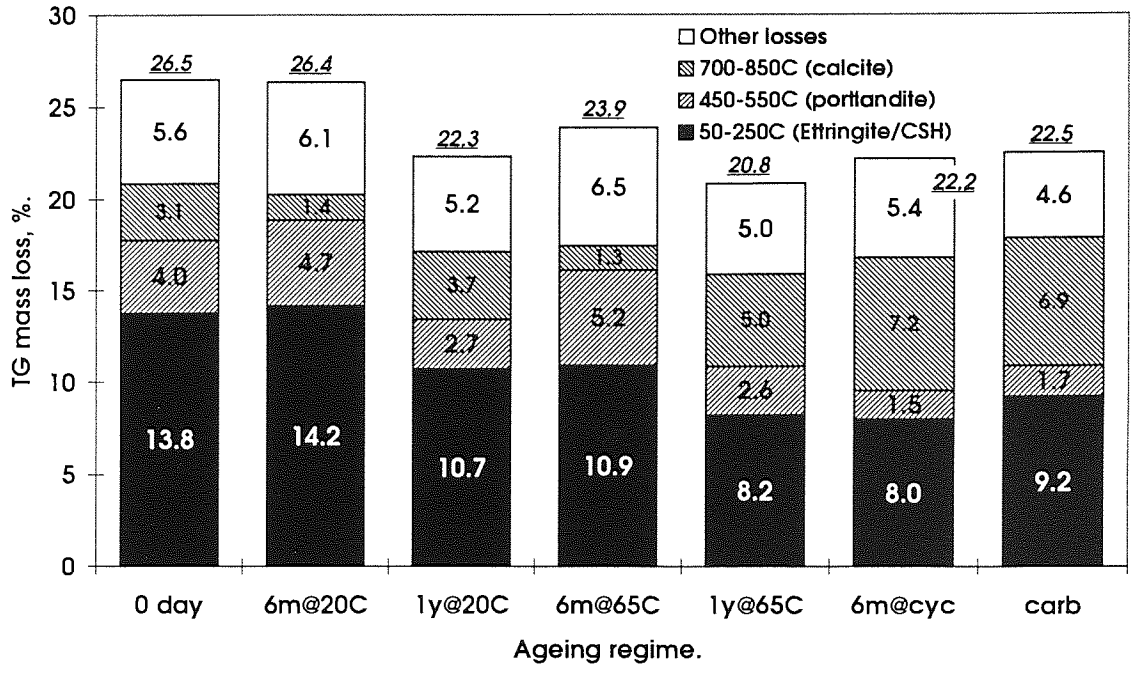

The amount of 'primary' hydrates in the matrix and the total losses decreased with time and to a lesser extent, increased ageing temperature. Portlandite content did not appear to be affected, except where carbonation had taken place (by design or accident). Rises in calcite content were accompanied by decreasing portlandite content. In the samples carbonated by design (i.e. cyclically aged and carbonated) the portlandite content was drastically reduced and a marked depletion of primary hydrates was apparent. The total weight loss less the loss attributable to primary hydrates remained constant.

4.3.2.2. Matrix M.

Figure 4.12. TG traces, Matrix M.

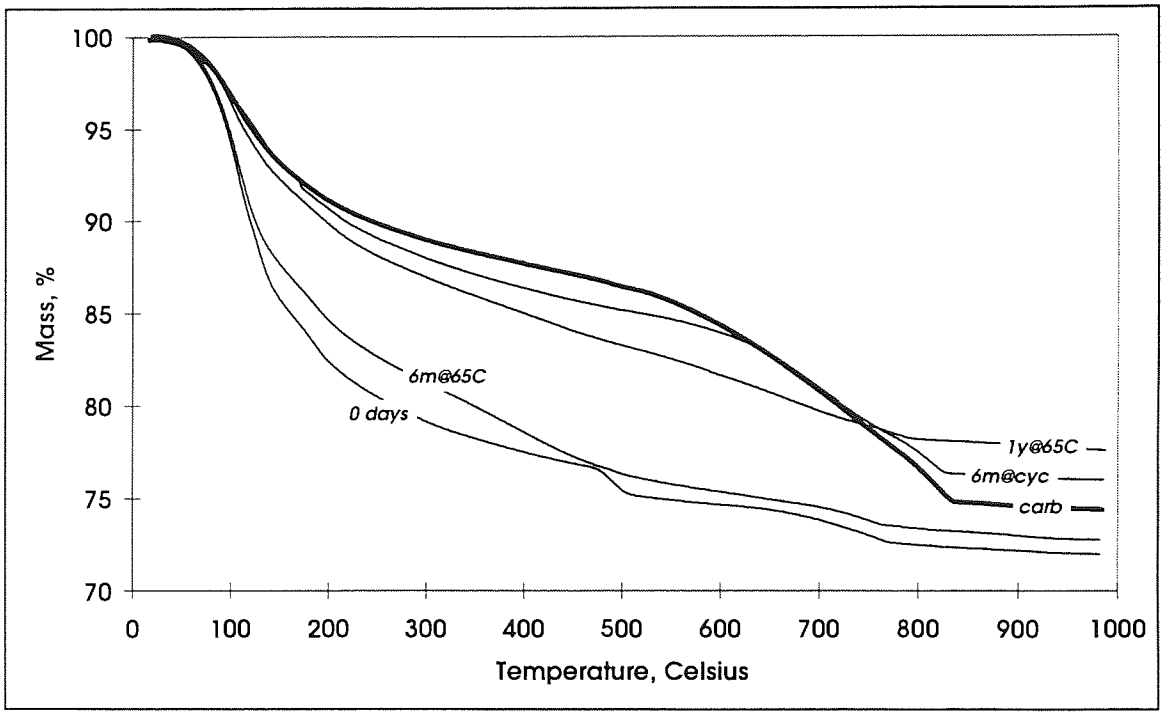

Figure 4.13. TG mass loss chart, Matrix M.

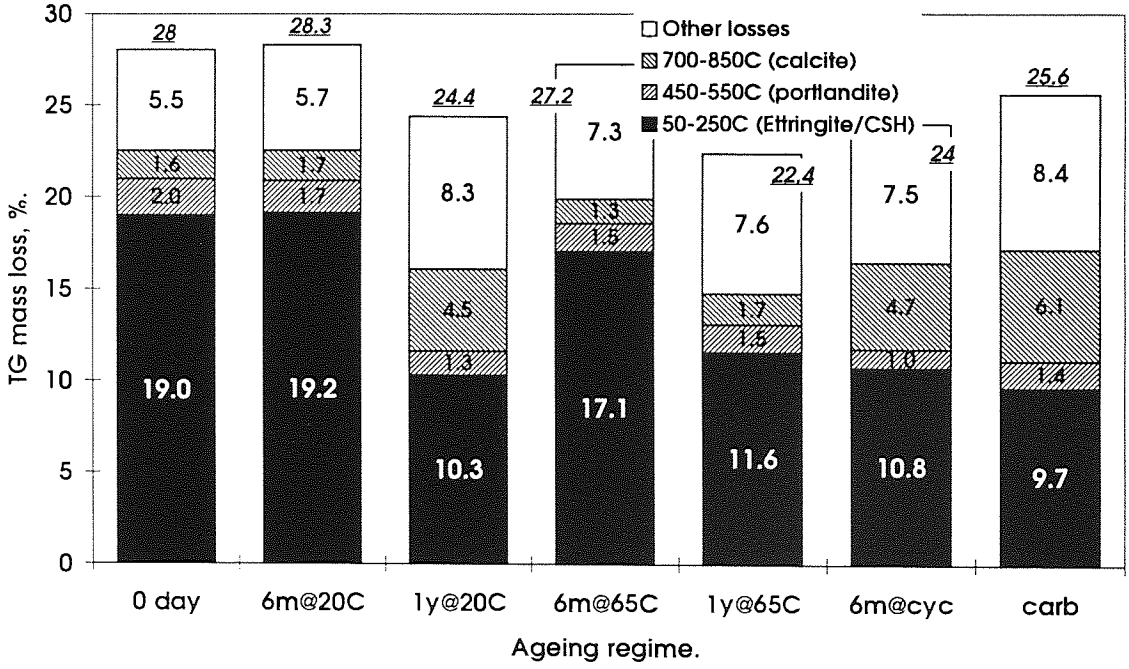

Only the 0 day and 6m@20C thermograms (Fig. 4.12) show any significant DTA/TG portlandite effect. The 450 to 550°C mass loss for the other regimes detailed in Fig. 4.13 above was attributable to the background effect described in 4.3.2.

The total loss and the loss attributable to primary hydrates decreased with ageing time but ageing temperature seemed to have little effect. Under the carbonating regimes, primary hydrate weight losses were halved.

4.3.2.3. Matrix C.

Figure 4.14. TG traces, Matrix C.

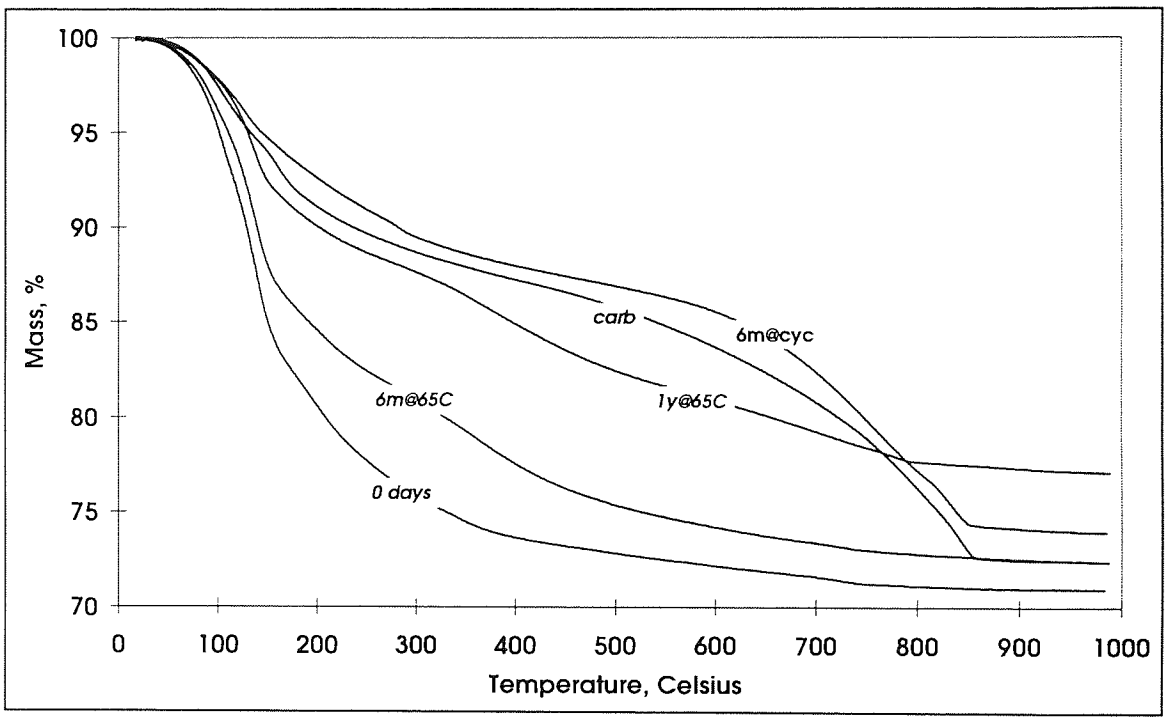

Figure 4.15. TG mass loss chart, Matrix C.

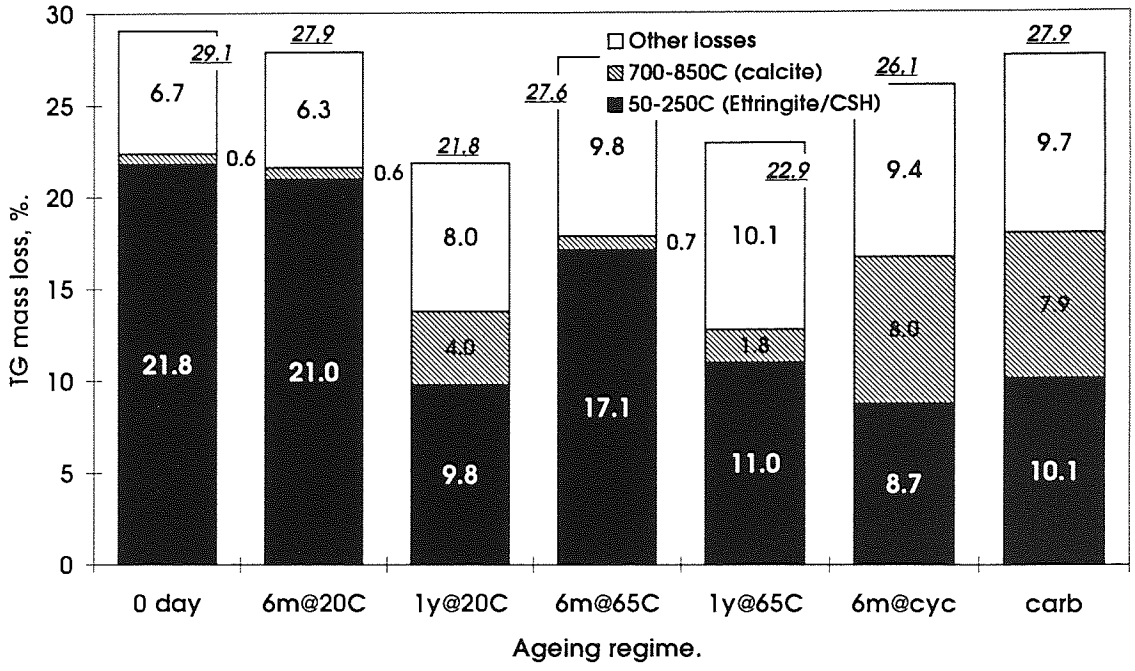

Portlandite losses are not shown in Fig. 4.15 for matrix C as the DTA/TG thermograms showed no effect in the 450 to 550°C region (Figs. 4.6, 4.8).

Primary hydrate and total losses decreased with ageing time and to a lesser extent, with increased ageing temperature. Under carbonating ageing regimes, the primary hydrate weight loss is more than halved.

4.3.2.4. Matrix D.

Note: The matrix D TG trace (for 6 months at 20°C) is shown in Fig. 4.9. There were no significant differences between this trace and those for different ageing regimes.

Matrix D samples lost 19 to 22% mass between 50 and 250°C. No portlandite, calcite or other effects were observed and the total mass loss was 25 to 28%. There were no discernible trends between the ageing regimes.

4.4. Hydrated cement compositions: Pore fluid expression analysis.

The mean values from two tests are presented. The variation from the mean was generally less than 5% but where greater error was encountered or only one sample

could be tested this is shown in the tables. Cyclically aged and carbonated samples were not pore pressed since it is unlikely that the required cylindrical samples would be similarly penetrated by the regime as the thin tensile test coupons.

4.4.1. Matrix O.

Table 4.9 and Figures 4.16 & 4.17 show the variation in the concentration of the major ionic species in the matrix O pore solution with ageing time and temperature.

Table 4.9. Pore fluid ion concentrations (mmol/l): Matrix O.

Initial (0 day): [OH] = 543; [K] = 496; [Na] = 76.

Temp	Ion	7 days	28 days	56 days	6 months
65°C	OH	186	125	100	96
	K	177	99	73	76
	Na	42	27	21	16
20°C	OH	-	-	-	245
	K	-	-	-	195
	Na	-	-	-	48

Figure 4.16. Matrix O: Variation in pore solution ion concentration with time at 20°C

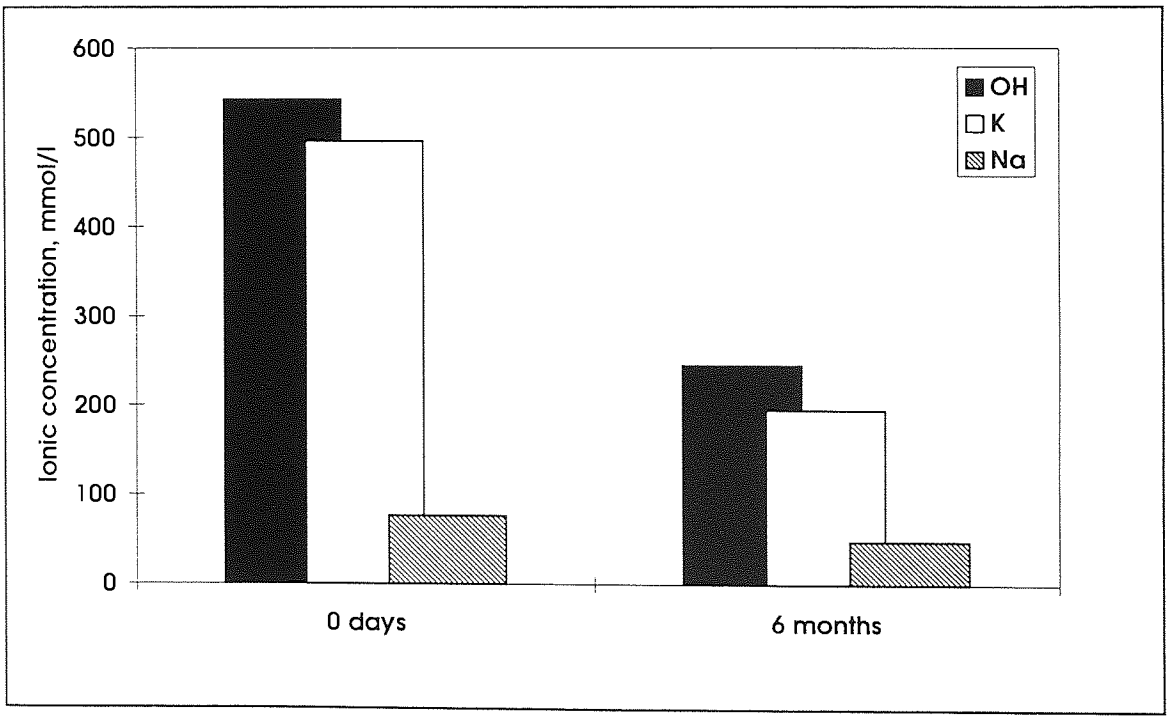

Figure 4.17 Matrix O: Variation in pore solution ion concentration with time at 65°C

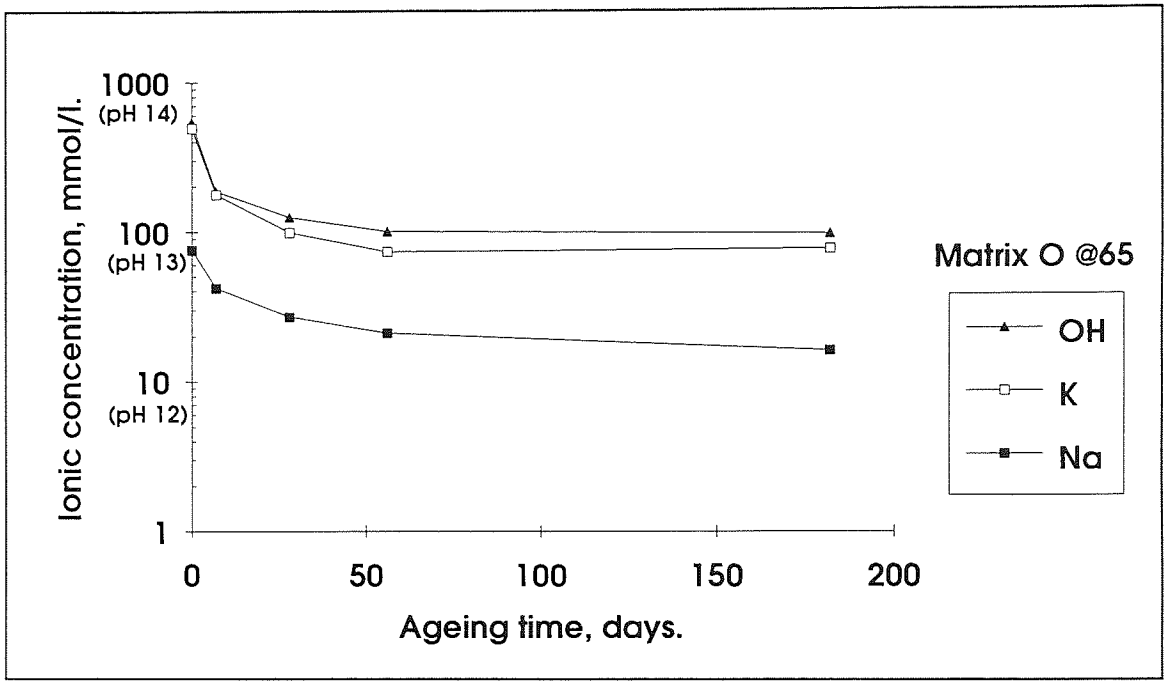

The matrix O pore solution alkalinity (i.e. OH^- concentration) was primarily associated with potassium ions with little contribution from sodium. Concentrations of all three species followed a similar pattern. The initial pH was 13.7, dropping to pH 13.4 after 6 months at 20°C (Fig. 4.16) and 13.0 after 6 months at 65°C (Fig. 4.17). The OH ion concentration was well balanced by the K and Na ion concentration.

4.4.2. Matrix M.

Table 4.10 and Figures 4.18 to 4.20 show the variation in the concentration of the major ionic species in the matrix M pore solution with ageing time and temperature.

Table 4.10. Pore fluid ion concentrations (mmol/l): Matrix M.

Initial (0 day): [OH] = 183; [K] = 144; [Na] = 49.

Temp	Ion	7 days	14 days	28 days	56 days	6 months
65°C	OH	119	-	134	121	82
	K	91	-	95	92	61
	Na	34	-	34	33	37
38°C	OH	151	143	141	146	114 ± 12
	K	121	109	103*	102 ± 10	84 ± 12
	Na	42	38	37*	35 ± 4	48 ± 10
20°C	OH	-	-	-	-	140
	K	-	-	-	-	104
	Na	-	-	-	-	61

Figure 4.18 Matrix M: Variation in pore solution ion concentration with time at 20°C

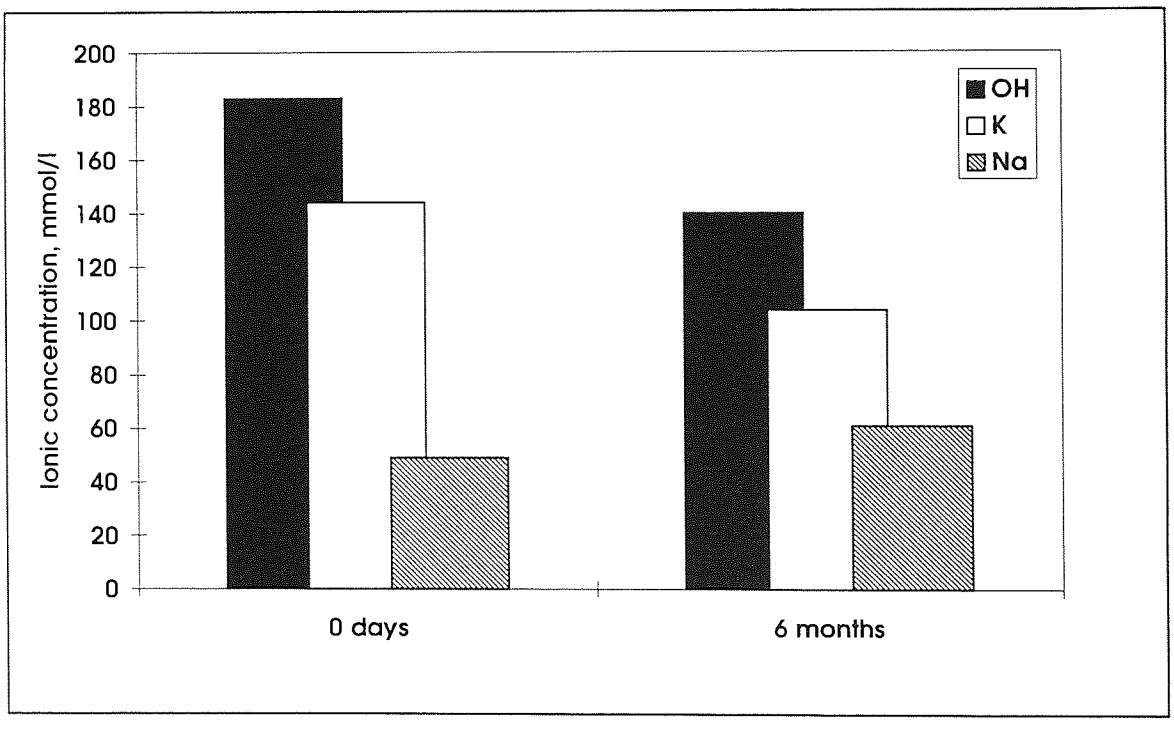

Figure 4.19 Matrix M: Variation in pore solution ion concentration with time at 38°C

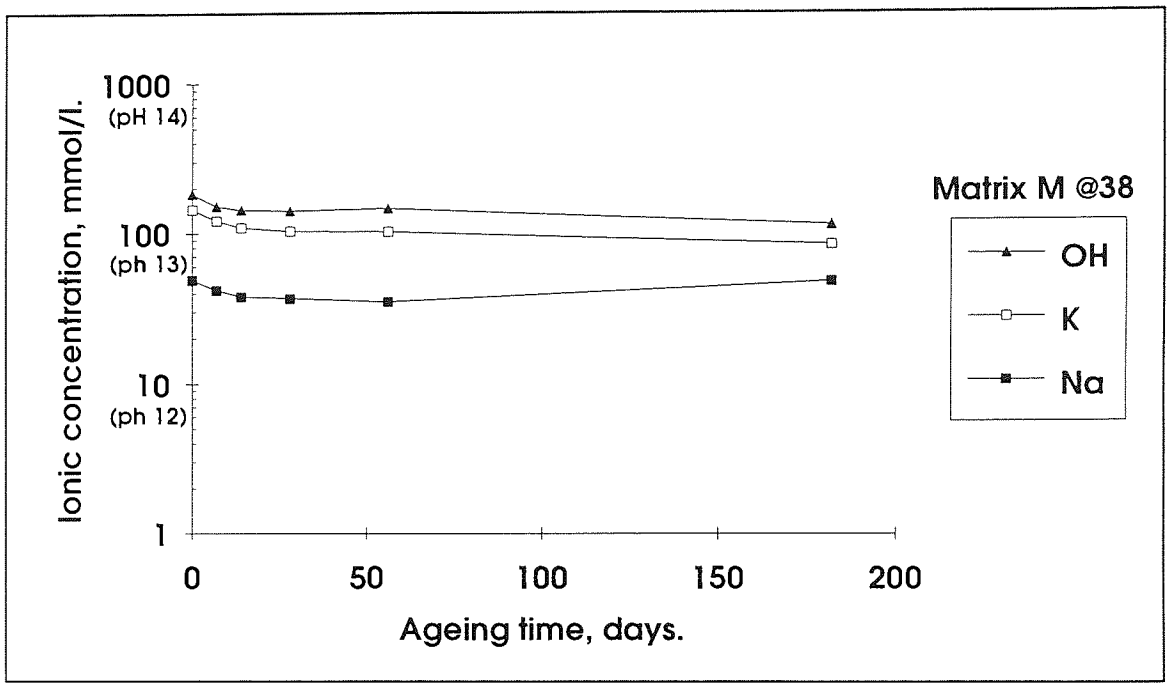

Figure 4.20 Matrix M: Variation in pore solution ion concentration with time at 65°C

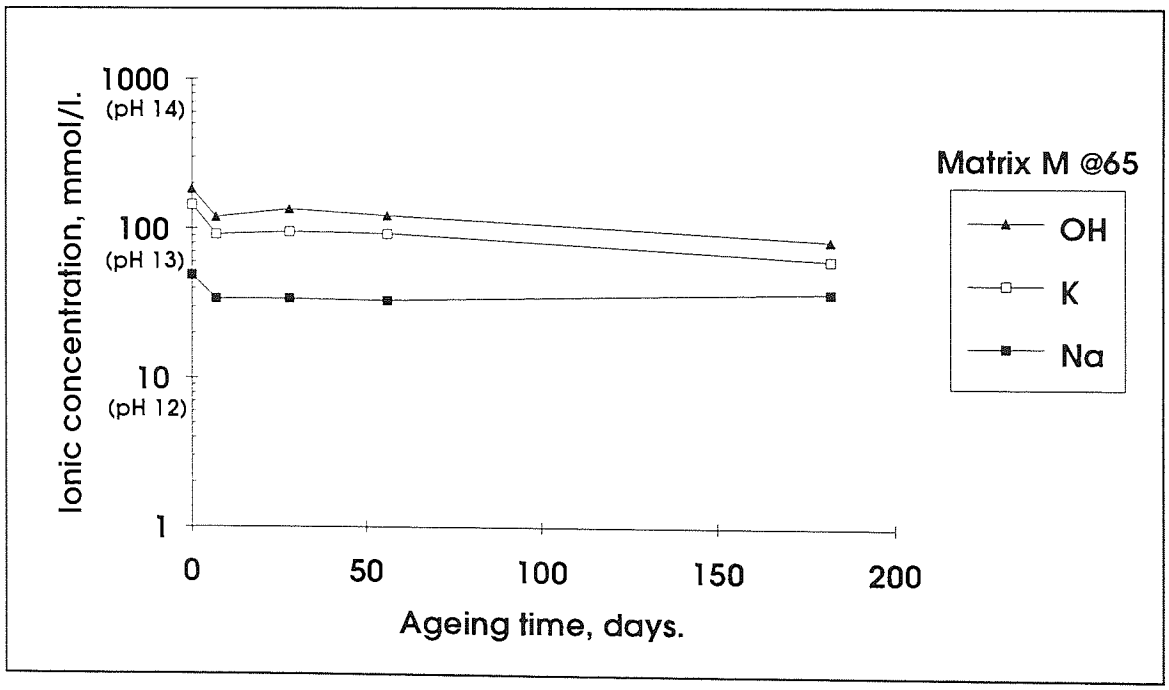

As with matrix O, the matrix M pore solution alkalinity was primarily attributable to potassium ions. The concentration of potassium ions with time followed the OH trends.

The sodium ion concentration initially followed the OH and K trend, but began to rise again between 28 and 56 days (Figs. 4.19, 4.20). The effect was more pronounced at lower ageing temperatures. For the 20°C aged samples, more Na^+ was present in solution at 6 months than at 0 days (Fig. 4.19).

The initial pH was 13.3, and dropped to 13.1, 13.0 and 12.9 after 6 months at 20, 38 and 65°C respectively. The OH ion concentration was generally well balanced by the K and Na ion concentrations, except at later ages when there was a slight 'surplus' of cations (Fig. 4.18).

4.4.3. Matrix C.

Table 4.11 and Figures 4.21 to 4.23 show the variation in the concentration of the major ionic species in the matrix C pore solution with ageing time and temperature.

Table 4.11. Pore fluid ion concentrations (mmol/l): Matrix C.

Initial (0 day): [OH] = 243; [K] = 173 ± 16; [Na] = 91 ± 7.

Temp	Ion	7 days	14 days	28 days	56 days	6 months
65°C	OH	70	-	57 ± 5	70	93
	K	60*	-	46	53	69 ± 5
	Na	41*	-	37	43	61
38°C	OH	128	121	100 ± 10	93	95
	K	98	90	64 ± 16	73	59
	Na	62	59	45 ± 9	56 ± 4	52
20°C	OH	-	-	-	-	108
	K	-	-	-	-	81
	Na	-	-	-	-	79

Figure 4.21 Matrix C: Variation in pore solution ion concentration with time at 20°C

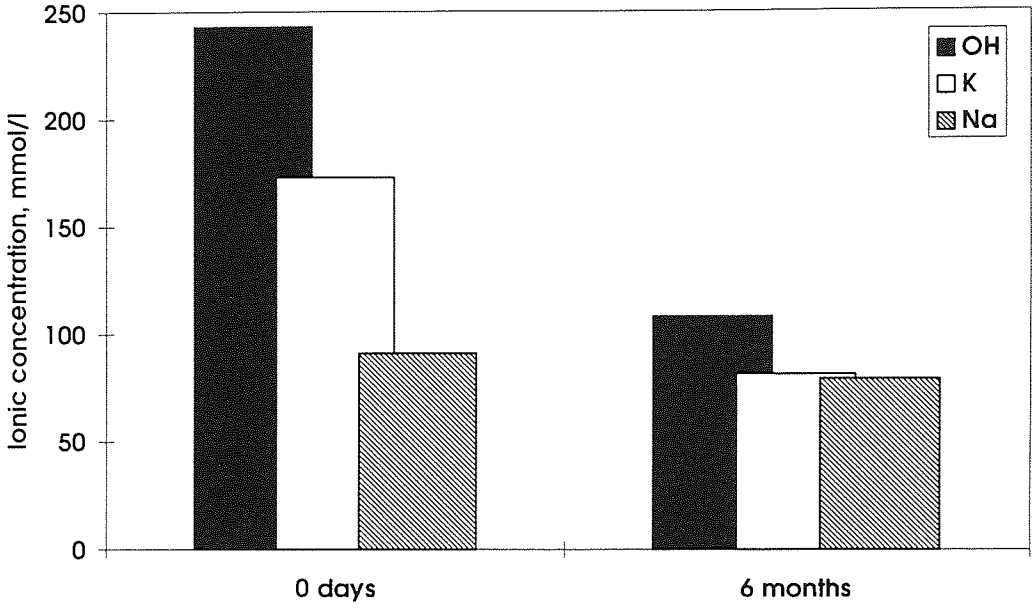

Figure 4.22 Matrix C: Variation in pore solution ion concentration with time at 38°C

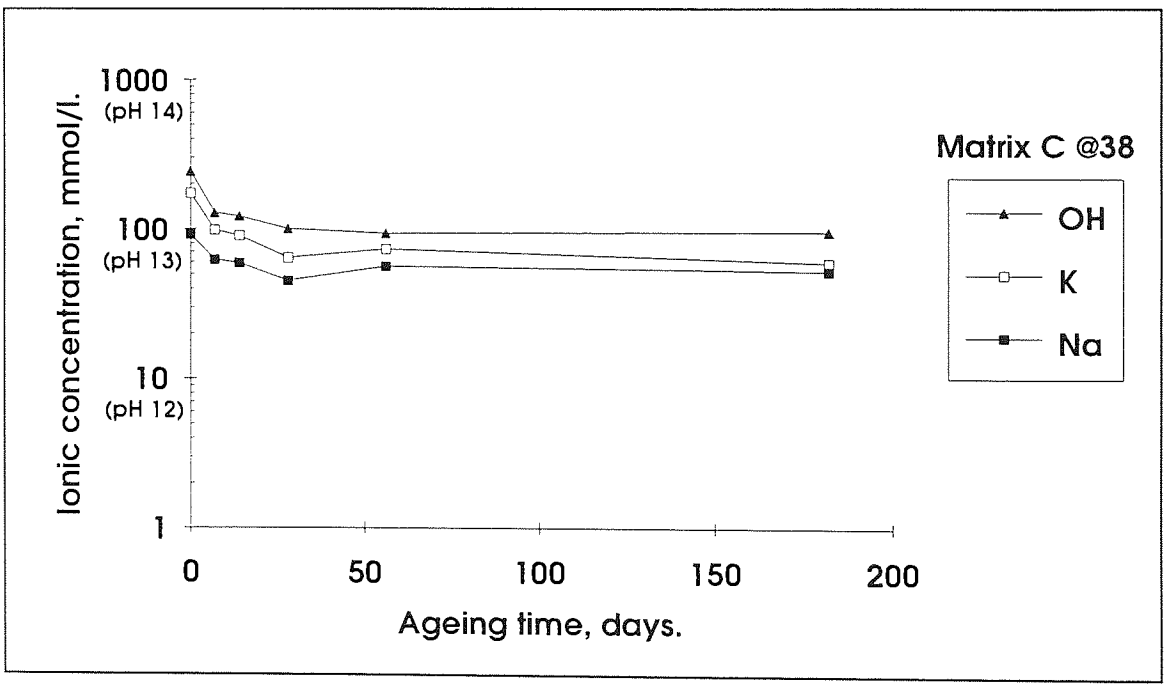

Figure 4.23 Matrix C: Variation in pore solution ion concentration with time at 65°C

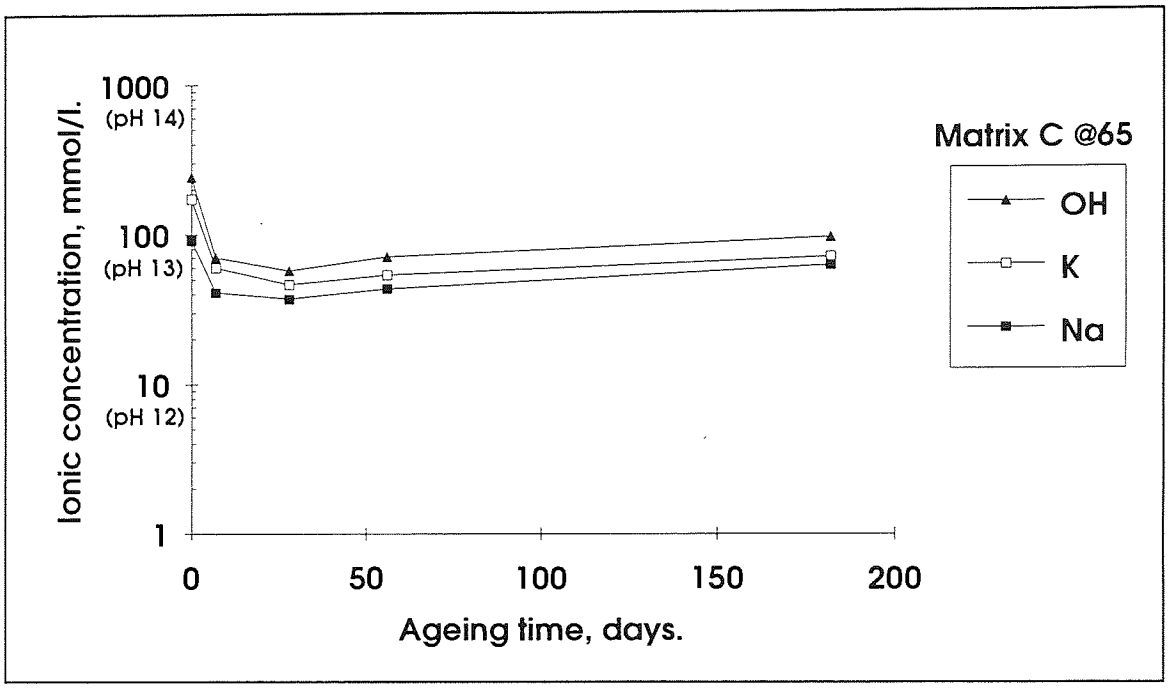

For matrix C, the concentrations of sodium ions in the pore solution was more significant, being about two-thirds that of the potassium ion concentration. The sum of the sodium and potassium concentrations was generally about 150% of the OH^- concentration i.e. there was always a cation 'surplus'. In general the sodium ion concentration decayed less slowly than the potassium concentration.

In contrast to matrices O and M, the alkalinity of the matrix C pore solution did not continuously decrease. Between 28 days and 6 months at 65°C (Fig. 4.23) , the OH^-, K^+ and Na^+ concentrations rose by about 60% although they remained well below the initial concentrations.

The initial pH of the pore solution was 13.4, dropping to 13.0 after 6 months at all ageing temperatures.

4.4.4. Matrix D.

Table 4.12 and Figures 4.24 to 4.26 show the variation in the concentration of the major ionic species in the matrix D pore solution with ageing time and temperature.

Table 4.12. Pore fluid ion concentrations (mmol/l): Matrix D.

Initial (0 day): [OH] = 5.0; [K] = 23; [Na] = 82.

Temp	Ion	7 days	14 days	28 days	56 days	6 months
65°C	OH	2.7 ± 0.3	-	2.1	1.7	1.3*
	K	13	-	6.6	5.3	4.9*
	Na	64 ± 5	-	38	31	28*
38°C	OH	3.5	2.9 ± 0.3	3.0	2.6 ± 0.3	2.1*
	K	17	13	6.6	9.0	4.9*
	Na	72	58	61	58 ± 6	50*
20°C	OH	-	-	-	-	2.2 ± 0.2
	K	-	-	-	-	8.9
	Na	-	-	-	-	43

Figure 4.24 Matrix D: Variation in pore solution ion concentration with time at 20°C

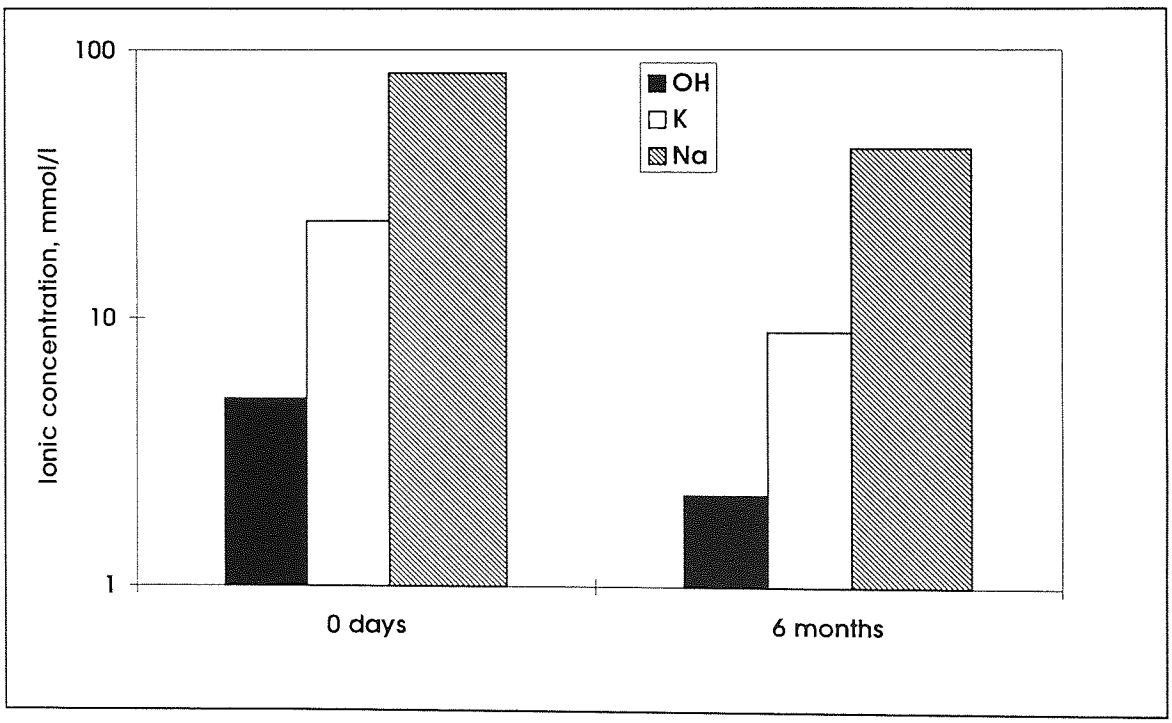

Figure 4.25 Matrix D: Variation in pore solution ion concentration with time at 38°C

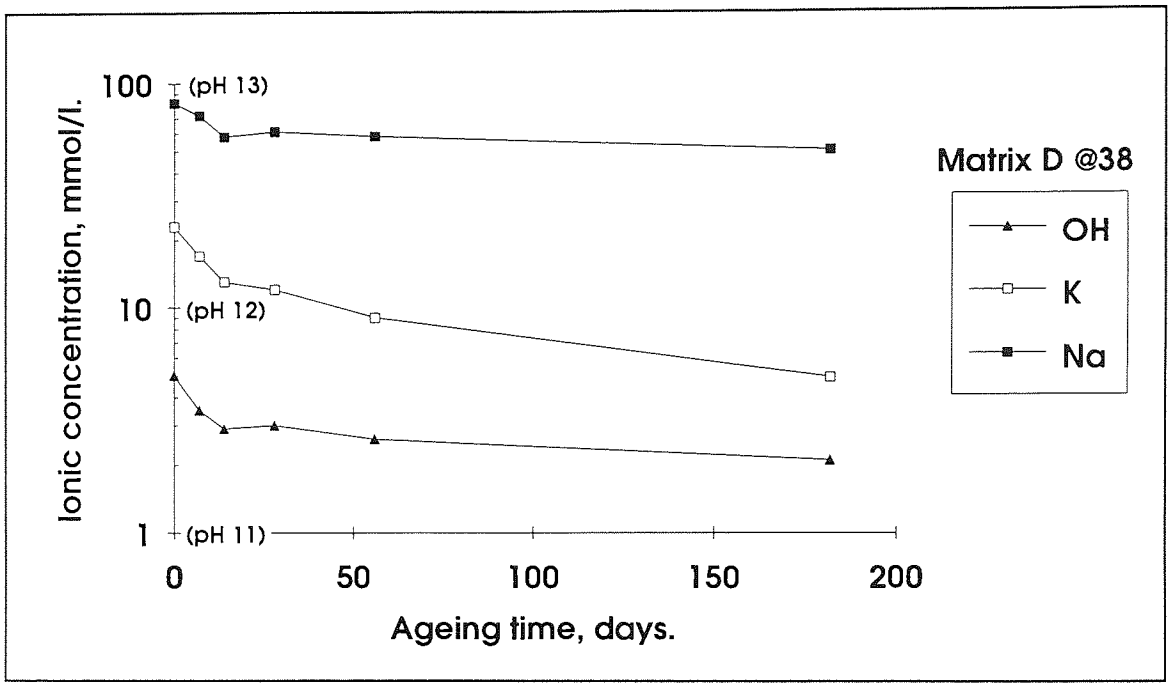

Figure 4.26 Matrix D: Variation in pore solution ion concentration with time at 65°C

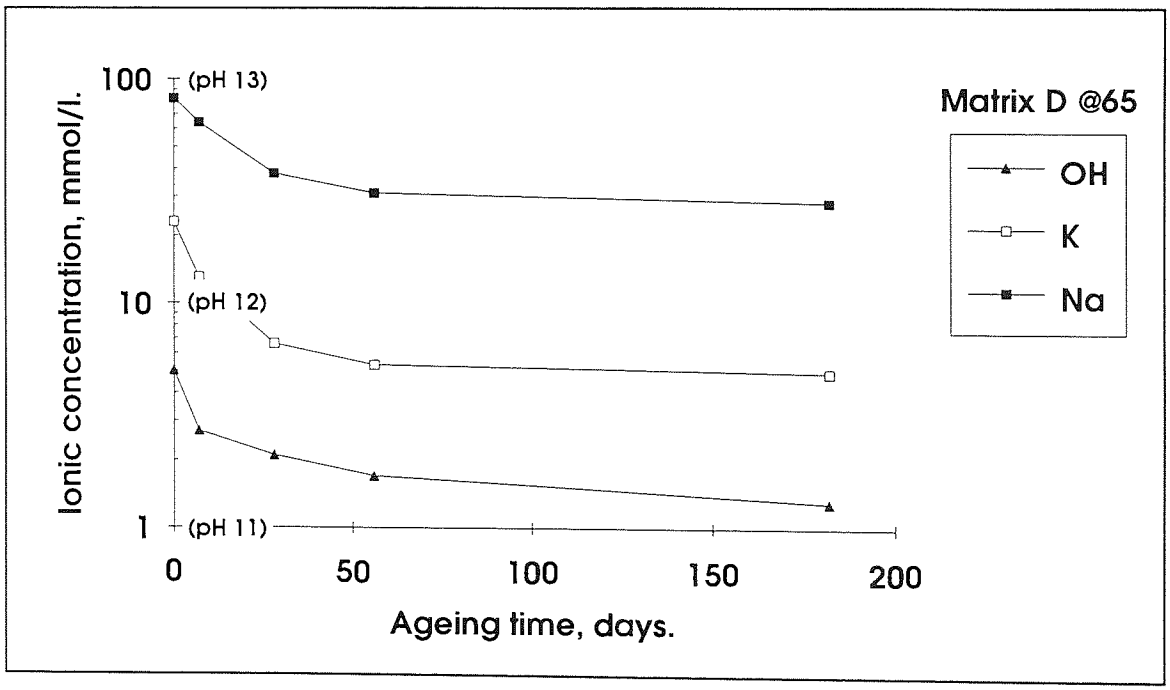

The matrix D pore solutions were very different from those of the other matrices. Their alkalinity was nearly two orders of magnitude lower (initial pH 11.7 cf. 13.3 to 13.7) and sodium was the dominant cation (being 5 times more abundant than potassium). The total cation concentration was some 30 times the hydroxyl concentration. The pH of the pore solution was 11.3, 11.3 and 11.1 after 6 months at 20, 38 and 65°C respectively.

4.5. Ion chromatography.

It was noted that for most of the pore solutions analysed, the sum of the major cation concentrations was generally balanced by the OH ion concentration, indicating that the concentrations of species other than alkali hydroxides in the pore solution was insignificant. However, matrix D (see Figs. 4.9 to 4.11) and to a lesser extent matrix C in the later ageing stages (Fig 4.6) have substantially greater concentrations of alkali ions than OH ions. For matrix D, the difference is more than an order of magnitude. Ion chromatography was performed on selected samples to determine the nature of the non-OH anions associated with the alkali 'surplus'.

It was found that the principal non-OH anions were sulphate and chloride ions, in concentrations of 1 to 40 mmol/l and 0 to 7 mmol/l respectively, with sulphate invariably the dominant species. Figure 4.27 compares the alkali surplus (sum of the concentrations of Na and K ions minus the concentration of OH ions) with the sulphate and chloride 'OH equivalent' (twice the SO_4 concentration plus the chloride concentration; the SO_4 concentration is doubled to account for its divalency).

Figure 4.27. Alkali surplus cf. OH equivalence (SO_4 & Cl).

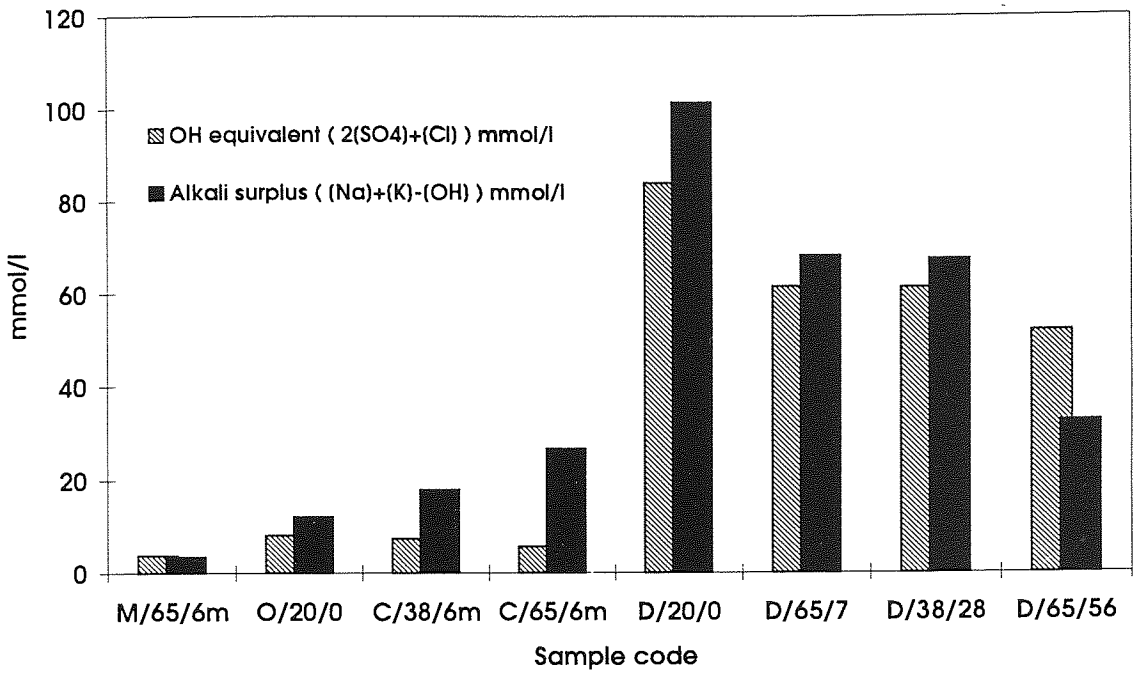

The ion chromatograms for matrices C and D also displayed an unidentified peak, appearing between the fluoride and chloride timeslots. This peak is of similar size (in ppm terms) to the chloride peak. Discussions with the equipment manufacturers suggested that this may be attributable to an organic acid, most likely a residue from the superplasticiser. This may account for the remaining discrepancy in the matrix D pore solutions, since the pastes were made with relatively large amounts of superplasticiser.

The remaining discrepancy in the matrix C pore solutions is rather larger. The pore solutions are left open to atmosphere during extraction; because of the much longer times required to extract pore solution from matrix C pastes (about 2 hours compared to about 45 minutes for the other pastes) they may therefore have undergone a relatively greater degree of atmospheric carbonation. Titration to a phenolphthalein endpoint will not completely convert carbonate ions to H_2CO_3, which may account for the discrepancy. Since a carbonate eluent is used in the chromatography, detection of carbonate in the pore solutions by this method is difficult.

4.6. Discussion of matrix analysis results.

4.6.1. Matrix compatibilities.

Fibre corrosion by OH ions and inter-filamental deposition of portlandite are generally considered to be the main causes of poor durability in OPC-GRC composites. Reduced portlandite content and pore solution alkalinity are the primary goals of new matrix formulators.

Figure 4.28 compares the pore solution alkalinity of the matrices after various ageing regimes. Note the logarithmic scale.

Figure 4.28. Comparison of pore solution alkalinities.

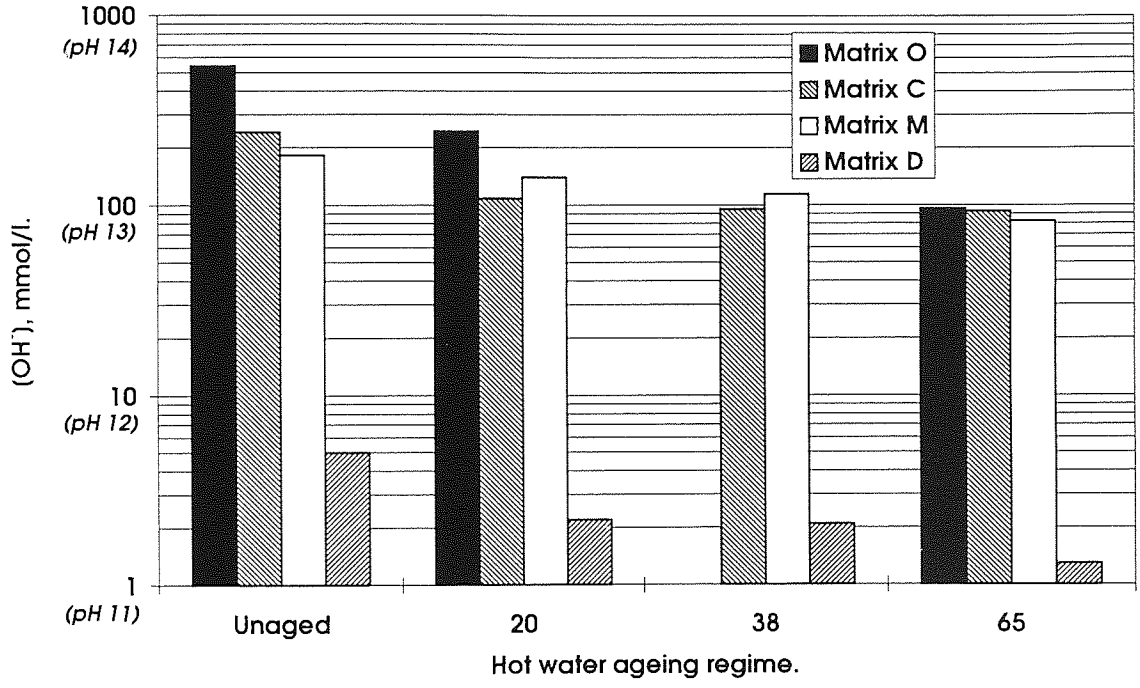

All the new matrices had a lower initial pore solution alkalinity than matrix O; matrix C by a factor of 2, matrix M by a factor of 3 and matrix D by two orders of magnitude. After 6 months ageing at 65°C, pore solution alkalinities in matrices O, C and M were reduced to a similar level of about 90 mmol/l, whereas in matrix D levels were still nearly 100 times lower.

An indication of the relative capabilities of the new matrices to consume alkali ions can be obtained by comparing the alkali oxide levels (as Na_2O equivalents) from the XRF analysis (section 4.1) with the initial pore solution alkalinities (Table 4.13).

Table 4.13. Alkali oxide contents cf. initial pore solution alkalinities.

Matrix	**O**	**C**	**M**	**D**
Alkali oxides (Na_2O_e %ww)	0.61	0.40	0.83	1.26
Initial pore solution alkalinity (mmol/l)	543	243	183	5.0
Alkalinity per weight% oxide (mmol/l)	890	608	220	4

The alkalinity contributed to the pore solution per unit weight percent sodium oxide equivalent is also given in Table 4.13 as a rough measure of the alkali consumption capability of each matrix. All the new matrices performed better than matrix O, matrix D especially so.

There is some evidence that after extended periods of ageing the matrices containing meta-kaolin begin to release additional alkali ions into the pore solution. The effect was most prominent in matrix C (Table 4.11 and Fig. 4.23) where the concentrations of Na, K and OH ions all increased significantly between 28 days and 6 months at 65°C. Although a similar increase in alkalinity was not observed in matrix M, additional Na ions were released into the pore solutions between 56 days and 6 months at all temperatures. (Figs. 4.18 to 4.20). In both cases the alkalinity of the pore solution remained well below the initial alkalinity hence these increases are probably of little concern *vis a vis* GRC.

The differences in portlandite contents of the matrices can best be seen by comparing their DTA traces. Figure 4.29 shows the DTA traces before ageing, and Fig. 4.30 after 6 months at 65°C. Portlandite can be identified by the endothermic effect at about 500°C.

Figure 4.29. Comparison of 0 day (unaged) DTA traces.

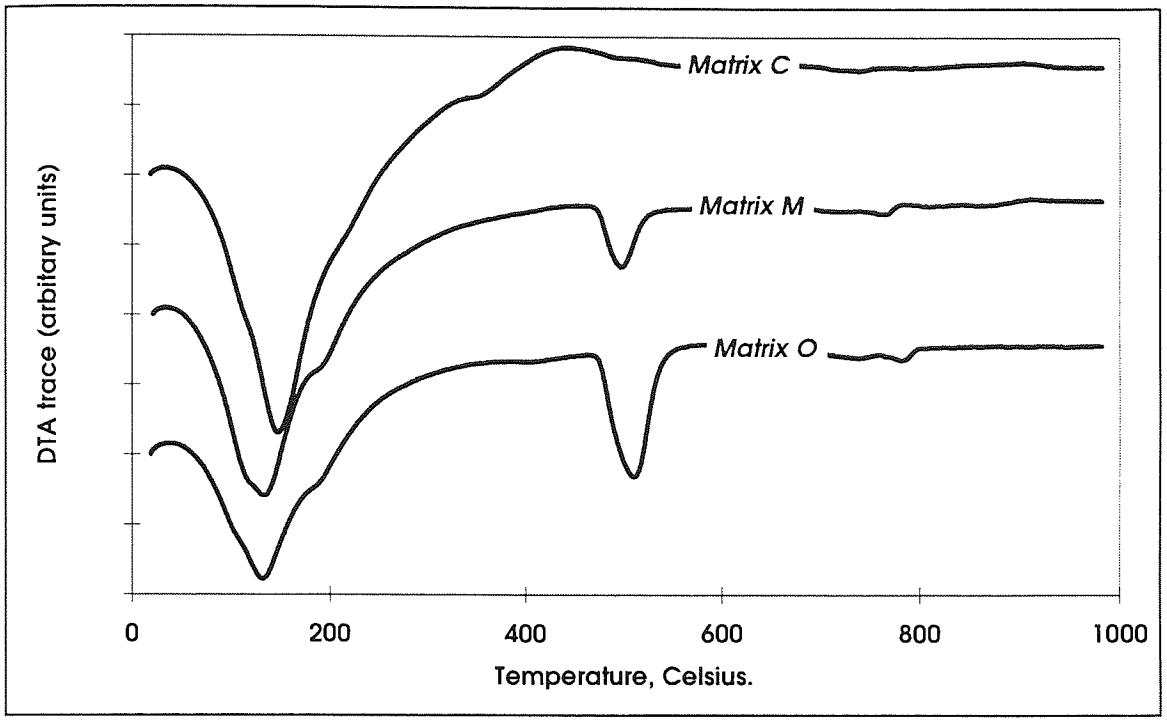

Figure 4.30. Comparison of DTA traces after 6 months at 65°C.

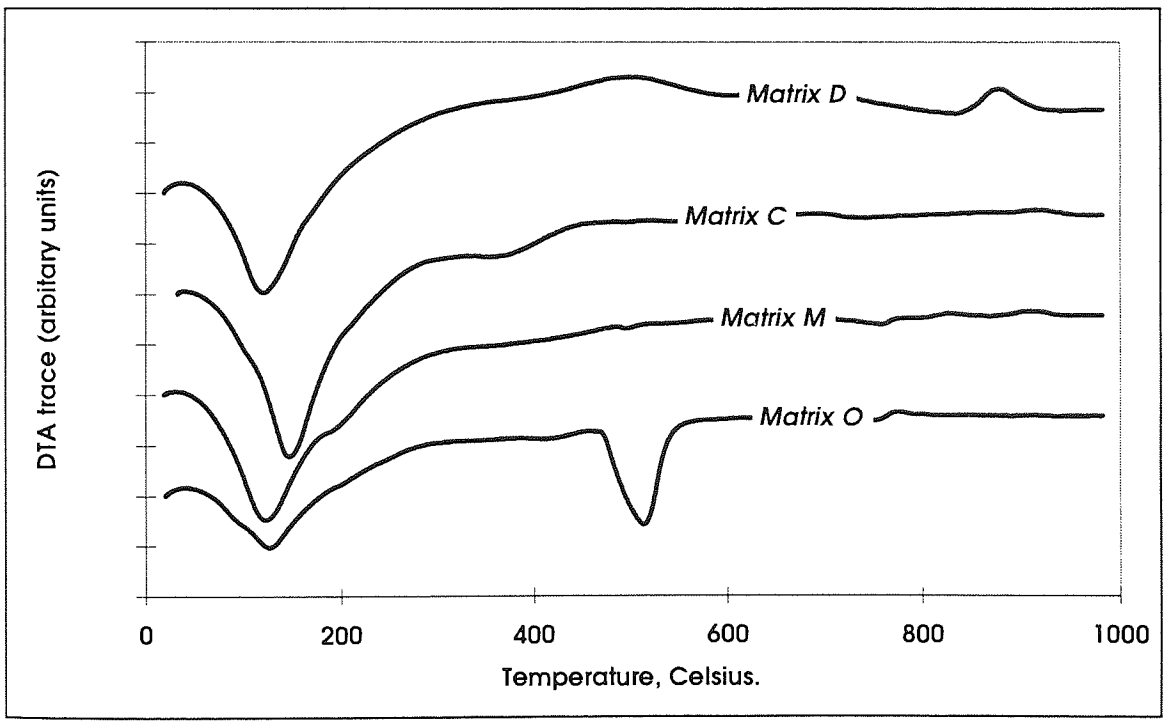

The 0 day portlandite endotherm (Fig. 4.29) is less prominent in matrix M than in matrix O. Matrix C displays no portlandite endotherm. After 6 months at 65°C, only matrix O displays any significant portlandite endotherm, the portlandite in matrix M

having been consumed by the meta-kaolin (see also Fig. 4.4). These results were confirmed by the XRD traces (Appendix 2 and Section 4.2). Analysis of the TG results (Section 4.3.2) after correction for the background drift gives initial portlandite contents of 12.8 and 5.0% by weight for matrices O and M respectively. Matrix M retains a portlandite content of 3.2% w/w after 6 months at 20°C but after more advanced ageing portlandite levels fall below the resolution of TG. Matrix O portlandite content increased with more severe ageing, being 13.2% after 6 months at 20°C and 15.6% after 6 months at 65°C although where unwanted carbonation had taken place these figures were lower.

In summary, all the new matrices studied appeared better suited chemically for use in GRC than OPC. Matrix D, with its much lower pore solution alkalinity and lack of portlandite would seem particularly well suited. It was unfortunate that the workability and shrinkage problems encountered during attempts at matrix D board manufacture owing to the erroneous mix design supplied with the materials prevented any composite samples being made to confirm this suitability.

4.6.2. Hydration chemistry.

4.6.2.1. Initial hydration.

The initial hydration chemistry (i.e. from mixing to the end of the 28 day 95%RH curing period) of matrices O and M were very similar; the chief anhydrous phases (C_2S, C_3S and C_3A) were depleted by factors of two to four (with some unreacted metakaolin remaining in the hydrated matrix M). CSH, ettringite and portlandite were the only important hydration products. The only initial difference between the two was that matrix M only formed about a third as much portlandite (see section 4.6.1) but more CSH (Fig. 4.29). Figure 4.29 also suggests that the nature of the CSH phase was similar for matrices O and M.

Initial matrix C hydration was rather different. Two of its major anhydrous phases ($C_4A_3\check{S}$ and $C\check{S}$) completely disappeared on hydration. C_3S appeared to be depleted less severely than in matrix O. Ettringite and CSH were the only hydration products and no portlandite was detected. Much larger quantities of ettringite were formed compared with matrices M and O. Figure 4.9 shows the corresponding difference in

the low temperature endotherm and suggests that the nature of the CSH formed may have been different to that in matrices O and M.

Although initial matrix D samples were not studied, XRD traces (Appendix 2) show that practically no anhydrous material remains after 6 months of hydration. Very large amounts of CSH are formed, with some ettringite. As mentioned above, there was no change in the DTA or XRD traces with increased ageing temperature. Figure 4.30 compares the DTA trace after 6 months at 65°C with the other matrices. Matrix D will not be discussed further.

4.6.2.2. Effects of hot water ageing.

There was little change in the composition of matrix O with time or ageing temperature. Ageing at 65°C did not significantly accelerate the hydration of the remaining C_3S or C_3A compared with ageing at 20°C but did accelerate the hydration of the remaining C_2S by a factor of two or three.

By contrast, in matrix C and M composites, 65°C ageing not only accelerated the hydration of the remaining unhydrated material (particularly C_3S) but caused the hydrated compounds formed to be different from those formed at 20°C. In matrix M, slight depletion of ettringite and formation of small amounts of stratlingite occured between 0 days and 1 year at 20°C. Over a similar period at 65°C, ettringite was depleted to trace quantities and large amounts of C_3ASH_4 hydrogarnets and monosulphate were formed in preference to stratlingite, which was not detected. In matrix C, 1 years ageing at 20°C had very little effect on the matrix while a similar period at 65°C again replaced much of the ettringite with hydrogarnet.

4.6.2.3. Effects of cyclic ageing and carbonation.

Cyclic ageing appeared to slightly accelerate the hydration of the anhydrous material in the matrix compared to ageing at 20°C. The most striking feature of the matrices after cyclic ageing was the degree of carbonation induced. In matrices O and C, it appeared that 6 months of cyclic ageing was at least as effective at carbonation as ageing for 4 months in CO_2 (Table 4.14).

Table 4.14. $CaCO_3$ and $Ca(OH)_2$ content comparisons after cyclic ageing and carbonation.

% w/w	Matrix O	Matrix M	Matrix C
$CaCO_3$, [$Ca(OH)_2$] contents after 6m cyclic ageing.	15 [3.9]	10 [0]	17 [0]
$CaCO_3$, [$Ca(OH)_2$] contents after 4m carbonation.	14 [4.4]	13 [0]	17 [0]
Initial $Ca(OH)_2$ content.	12.8	5.0	0.0
Expected $CaCO_3$ content from $Ca(OH)_2$ loss; 100/74 x [$Ca(OH)_2$]	12 (cyc.) 11 (carb.)	8	na

Figures calculated from TG traces.

It was also clear that for both cyclic ageing and the enhanced CO_2 regime, not only the portlandite in the matrix was being carbonated but that the ettringite and possibly gel phases were also being carbonated.

The new carbonate compounds formed differed between the cyclic and carbonation regimes. The cyclic ageing produced only calcite in all the matrices, whereas the enhanced CO_2 environment tended to also produce vaterite in matrix M, and vaterite and aragonite in matrix C. Only calcite was detected in appreciable amounts in matrix O.

4.7. Summary of main findings.

The main findings of the matrix investigations were;

- All new matrices had lower initial pore solution alkalinities than matrix O; matrices C and M by factors of 2 to 3; matrix D by 2 orders of magnitude. After extended ageing matrix O,C and M pore solution alkalinities were similar while matrix D continued to display a level two orders of magnitude lower.
- Portlandite was absent from matrices C and D and the initial low level of portlandite in matrix M (cf. matrix O) was largely consumed during the early period of ageing.

- Matrices C and M formed different hydration products under 65°C immersion ageing than at 20 or 38°C. These variations were not observed in matrices O or D.
- Cyclic ageing caused extensive carbonation of all the matrices, as did ageing in an enhanced CO_2 environment; the latter regime tended to produce different carbonation products to the former.
- Carbonation consumed 'low temperature' hydrates (i.e. ettringite and C-S-H) as well as portlandite.

5. RESULTS; MECHANICAL TESTING.

A note on the presentation of mechanical testing results: *The results in this chapter are presented in ageing regime by ageing regime format (as opposed to the matrix by matrix style of Chapter 4), since the relative severity of the regimes is generally obvious. This allows clearer demonstration of the relative performance of the different matrices.*

5.1. Normalisation.

The tensile testing software used in this project (section 3.4.4.1) produced results in stress-strain format and required input of the sample width and thickness. In the early stages of the project, the post-cracking properties of the composites (i.e. tensile strength and post-cracking modulus) were of primary importance. These properties are dependent only on fibre volume fraction and fibre properties;

$$\sigma_c = V_f.\sigma_f \; ; \; E_c = V_f.E_f \qquad \textbf{5.1.}$$

Since the method used in manufacturing the composite boards involved incorporation of a set amount of fibre into each board, the **fibre content** (i.e. amount of fibre in each sample as opposed to V_f) is dependent only on the sample width and not the thickness. This may be visualised by considering that for a given width, any tensile test coupon will contain a set amount of fibre; regardless of the thickness, it should theoretically fail at the same load. Consequently, a nominal sample thickness was used by the software for every test. This meant that the output from the software was effectively normalised with respect to sample thickness.

The thickness of the first 28 samples manufactured was analysed and found to average **6.1 mm, SD 0.46mm**. This thickness was used throughout the program as the nominal thickness.

The pre-cracking properties of most interest were;

- initial modulus (E_m);
- limit of proportionality (LOP, where the stress/strain curve begins to depart from linearity) and

- bend over point (BOP, the onset of multiple cracking often characterised by the first stress drop in the stress/strain curve).

These properties are all dependent on the sample thickness.

The output from the tensile testing software was derived from an assumed nominal thickness - a sample thicker than 6.1 mm will display artificially high E_m, LOP and BOP values and for thin samples the converse will be true. The pre-cracking results derived from the 'LOPFinder' software (see section 3.4.4.2) analyses of the tensile test software output for each sample were therefore multiplied by a 'correction factor' **k** equal to (6.1/T) where T is the measured thickness of the sample. This gave the true pre-cracking properties of the composites.

It should be noted here that the thickness variations also affect V_f - a thick sample will have a lower V_f than a thin sample. This may be disregarded for the properties described above since the effect of V_f on the pre-cracking properties is negligible (Bentur & Mindess, 1990; Majumdar & Laws, 1991; see section 2.2.1). It does become important when analysing bond strength and this is discussed in Chapter 7.

5.2. Tensile testing.

The error bars in all the graphs below represent ± 1 standard error, defined as the standard deviation divided by the square root of the number of results for each condition. The properties presented are;

- **tensile strength**, defined as the peak stress on the stress/strain curves;
- **post cracking modulus** (region c., Figure 2.1). This was derived by the tensile test software rather than the LOPFinder analysis software. Derivation involved plotting a best fit line through a chosen section of the post multiple cracking region of the stress/strain curve. Sections were chosen towards the end of the curve, well away from any residual multiple cracking effects.
- **strain to failure**, defined as the strain at the peak stress;
- **BOP**, the onset of gross matrix cracking, derived by the LOPFinder software and
- **specific toughness**, defined as the area under the stress/strain curve up to the peak stress. This was derived by inserting the ASCII tensile test data into a commercial

spreadsheet package. A number of other methods of quantifying toughness in fibre reinforced cements are available (Bentur and Mindess, 1990). Most of them are developed with steel-fibre reinforced cement and flexural testing in mind, and involve analysis of the post peak stress region, which had an unpredictable nature for the composites in this study. The simple definition above was decided as the most appropriate toughness measure in this case.

5.2.1. Typical initial stress strain curves.

Figure 5.1 shows typical stress/strain curves for 'unaged' samples made with each matrix.

Figure 5.1. Typical 0 day (unaged) stress/strain curves.

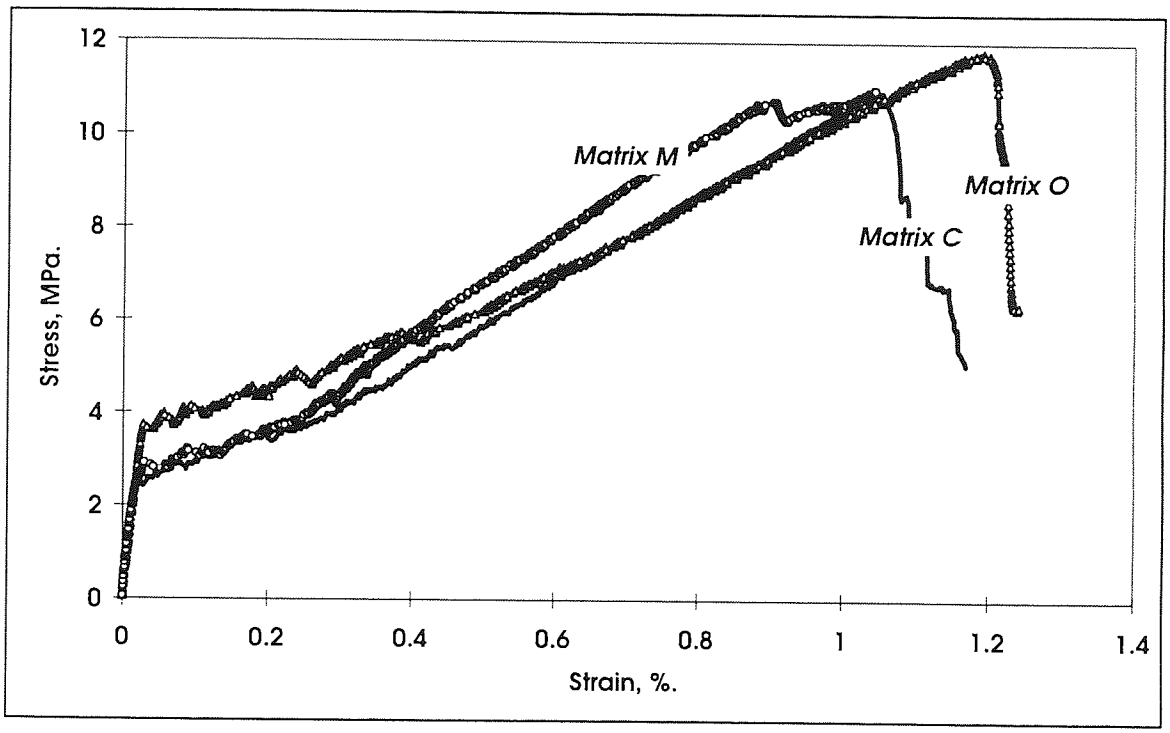

The initial elastic region, the region where the load is carried solely by the fibres (Fig. 2.1 regions a. and c.) and the onset of multiple cracking can be clearly correlated with the ideal trace. However, the multiple cracking region itself is not horizontal (i.e. at constant stress) as in Fig. 2.1 and the transition between the multiple cracking region and the E_fV_f quasi-linear region (c., Fig. 2.1) is not sharp. According to the extension of the ACK theory (Aveston & Kelly, 1973) this may be caused by the stress transfer between the fibre and matrix being partly by elastic bond rather than purely by frictional bond as assumed in the original ACK model.

5.2.2. Water immersion, 20°C

Figures 5.2 to 5.6 show the variation in the primary mechanical properties of the composites for samples aged at 20°C.

Figure 5.2. Variation of tensile strength with ageing time at 20°C.

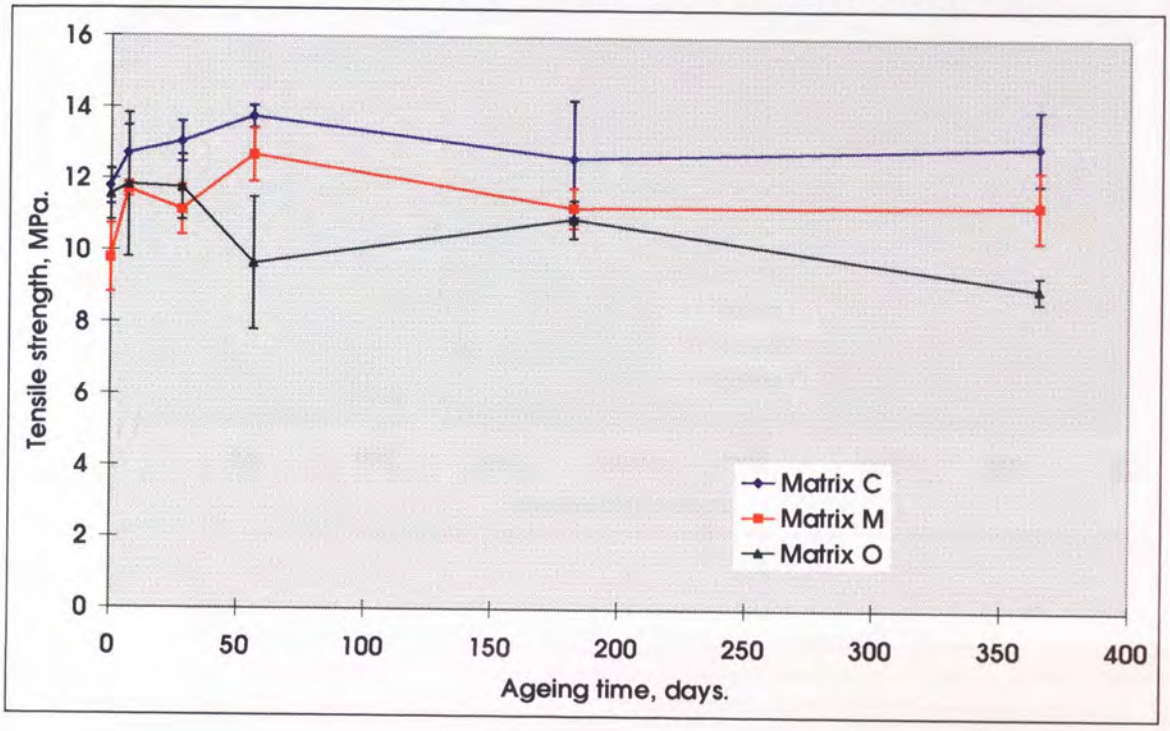

Figure 5.3. Variation of post-cracking modulus with ageing time at 20°C.

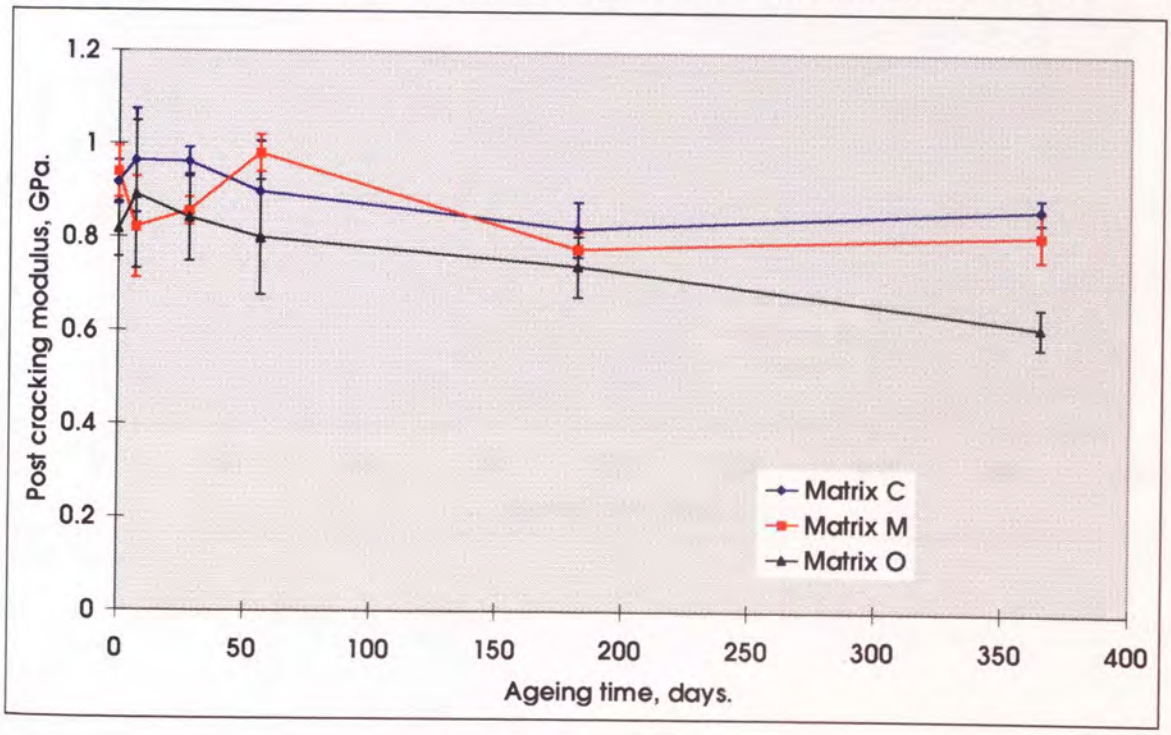

Figure 5.4. Variation of strain to failure with ageing time at 20°C.

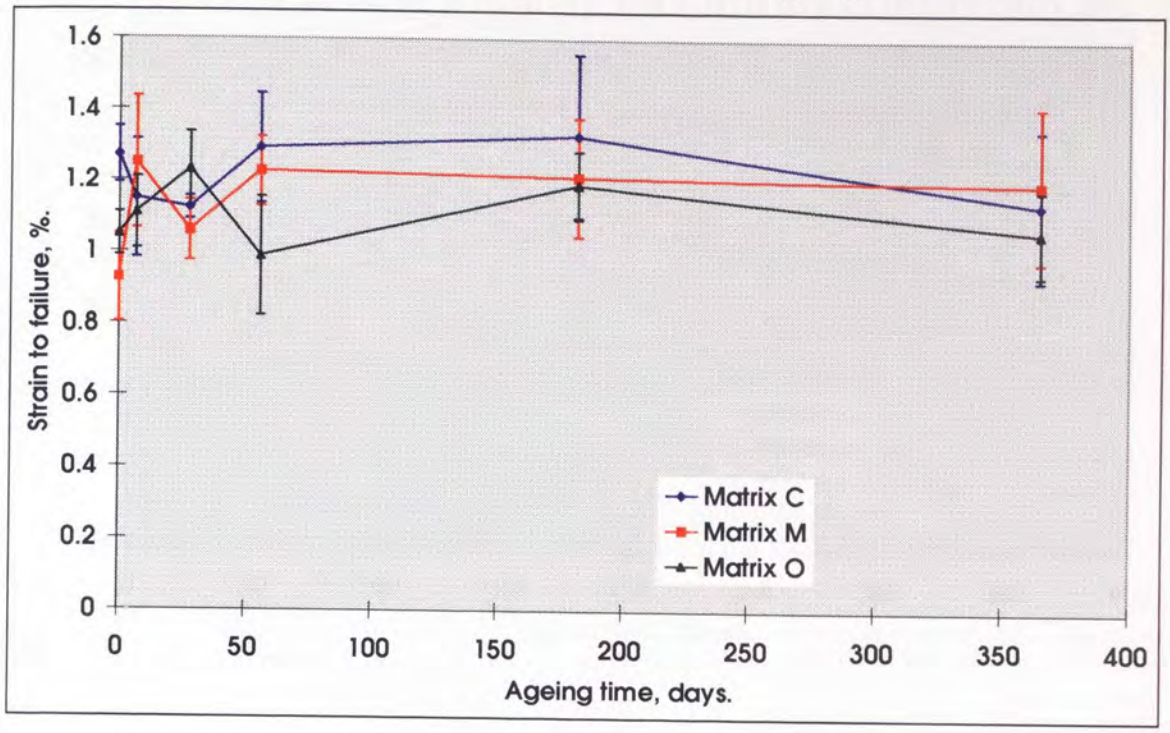

Figure 5.5. Variation of BOP with ageing time at 20°C.

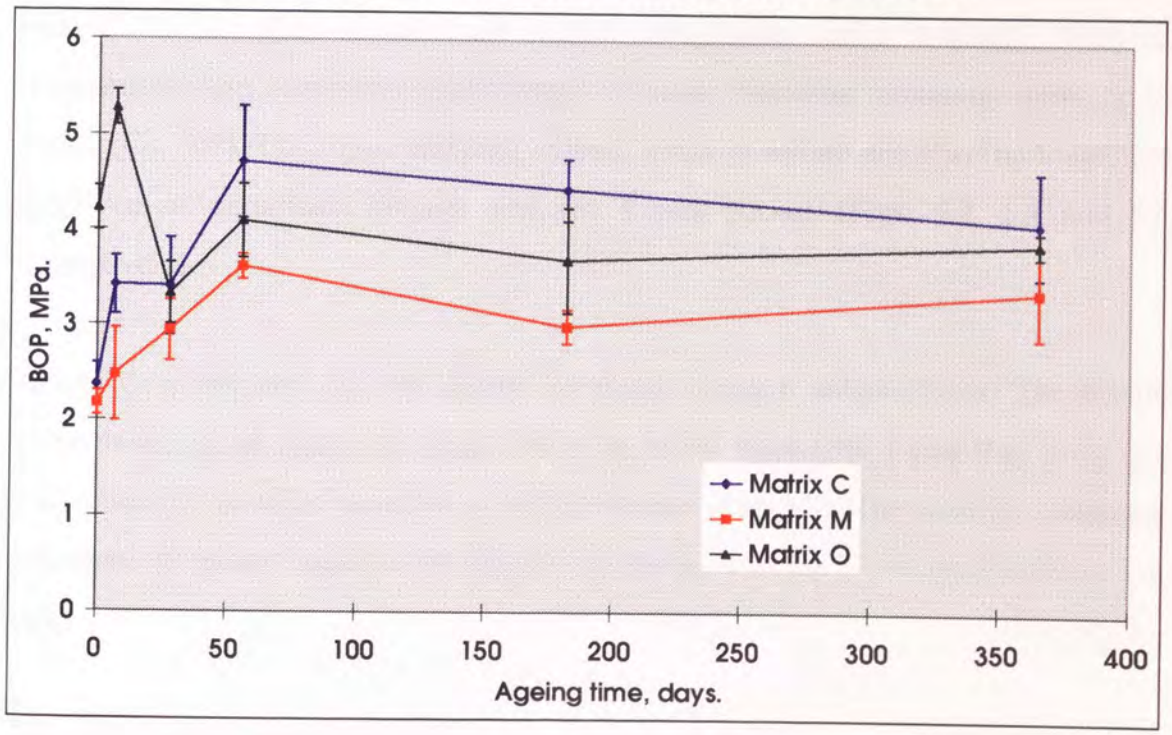

Figure 5.6. Variation of specific toughness with ageing time at 20°C.

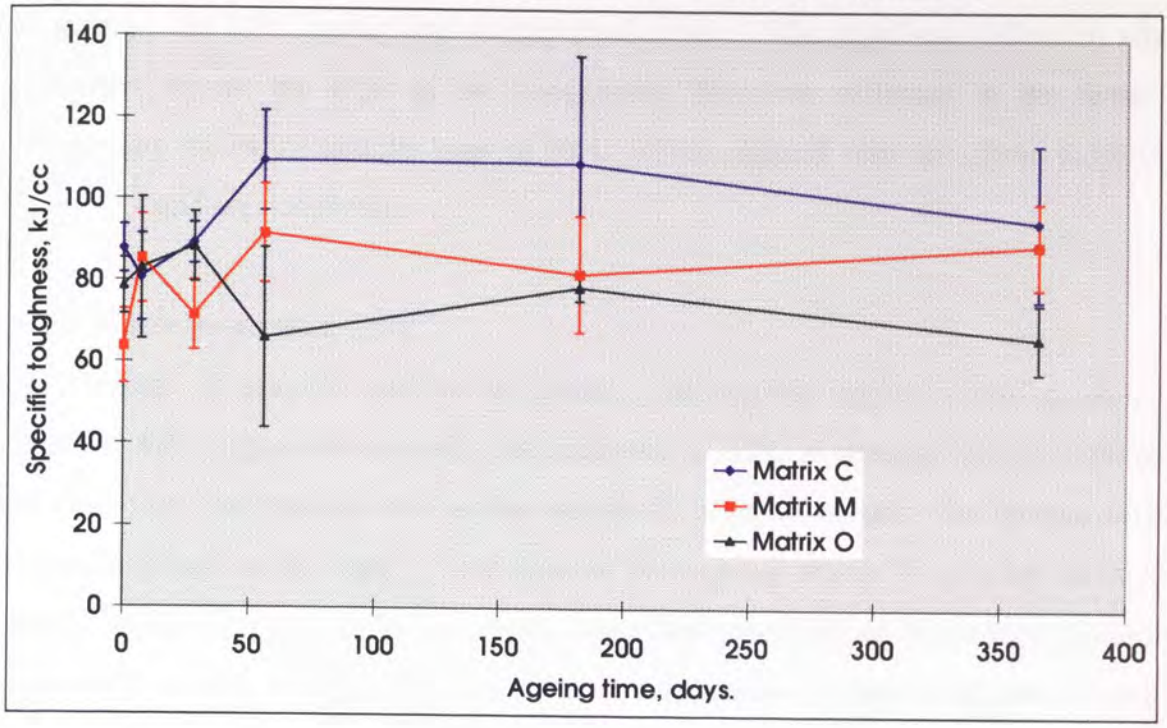

From these figures, the following observations were made.

The tensile strengths of both new matrix composites varied similarly, showing progressive slight increases (10-20%) up to 56 days, thereafter remaining stable up to 1 year (Fig. 5.2). Their post cracking moduli, strain to failure and specific toughness displayed no significant change over the 1 year period. (Figs. 5.3, 5.4 and 5.6 respectively).

Matrix O composites did not display an initial strength enhancement. The tensile strength decreased slightly to about 80% of its initial value after 1 year (Fig. 5.2). The post cracking modulus varied in a similar manner (Fig. 5.3). The specific toughness and strain to failure displayed no significant change over the 1 year period (Figs. 5.4, 5.6).

The BOPs of the new matrix composites increased steadily between 0 and 56 days - matrix C by about 80%, matrix M by about 40% - and thereafter stabilised. The matrix O composite BOP results were erratic up to 56 days and thereafter stabilised close to the initial value (Fig. 5.5).

In general, the 20°C ageing regime appeared to have little significant effect on any properties except the BOP of the composites. This was reflected in the tensile stress/strain traces for samples aged at 20°C, which differed very little from those in Figure 5.1 and are not shown.

5.2.3. Water immersion, 38°C

Note: *Matrix O samples were not subjected to this ageing regime. Initial guidance from the BRE suggested that since the behaviour of OPC composites was thought to be relatively well known, only a few matrix O 'control' samples for comparative purposes needed to be aged. It was advised that ageing matrix O samples at 38°C would add further samples to an already stretched testing schedule without yielding important results. Subsequent testing has revealed several interesting phenomena regarding matrix O composites that might be clarified by a testing of samples aged at 38°C, and this is discussed in the Further Work section of Chapter 9.*

Figures 5.7 to 5.11 show the variation in the primary mechanical properties of the composites for samples aged at 38°C.

Figure 5.7. Variation of tensile strength with ageing time at 38°C.

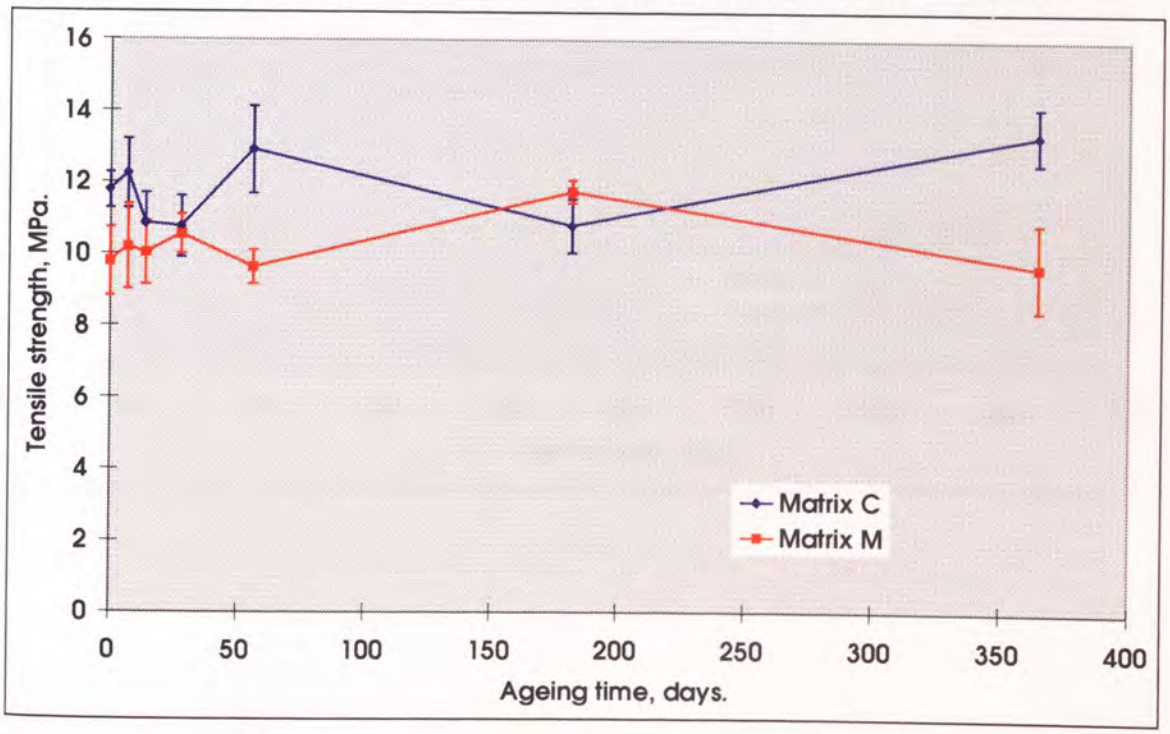

Figure 5.8. Variation of post-cracking modulus with ageing time at 38°C.

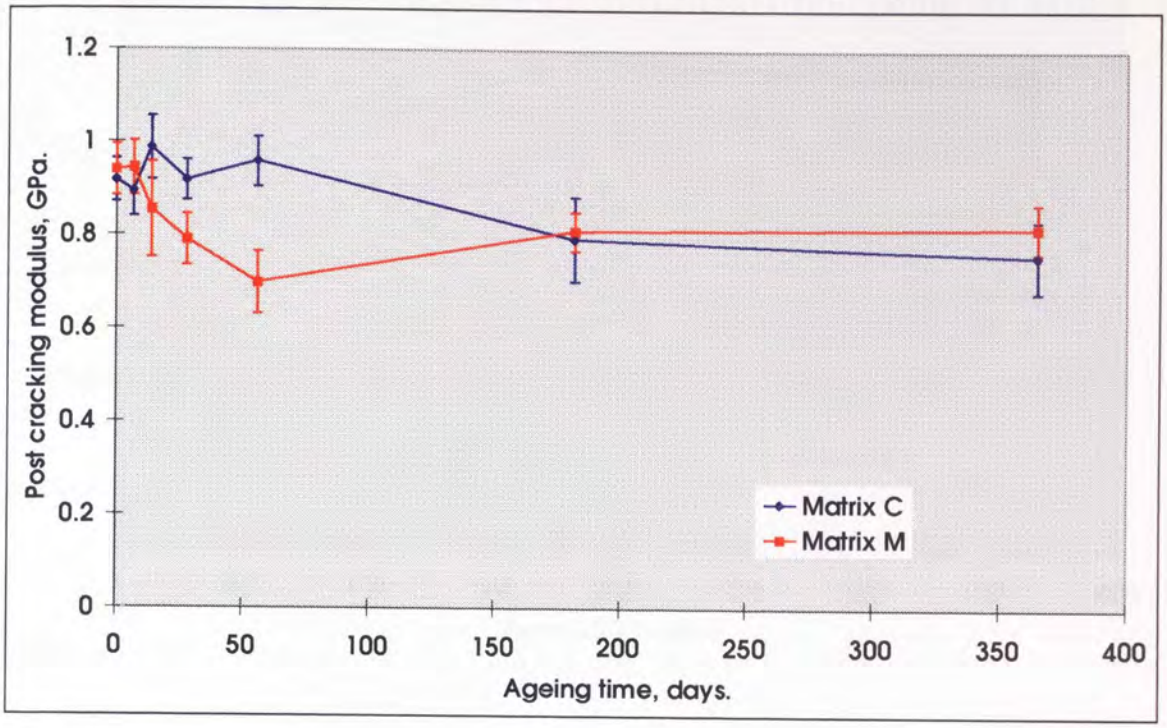

Figure 5.9. Variation of strain to failure with ageing time at 38°C.

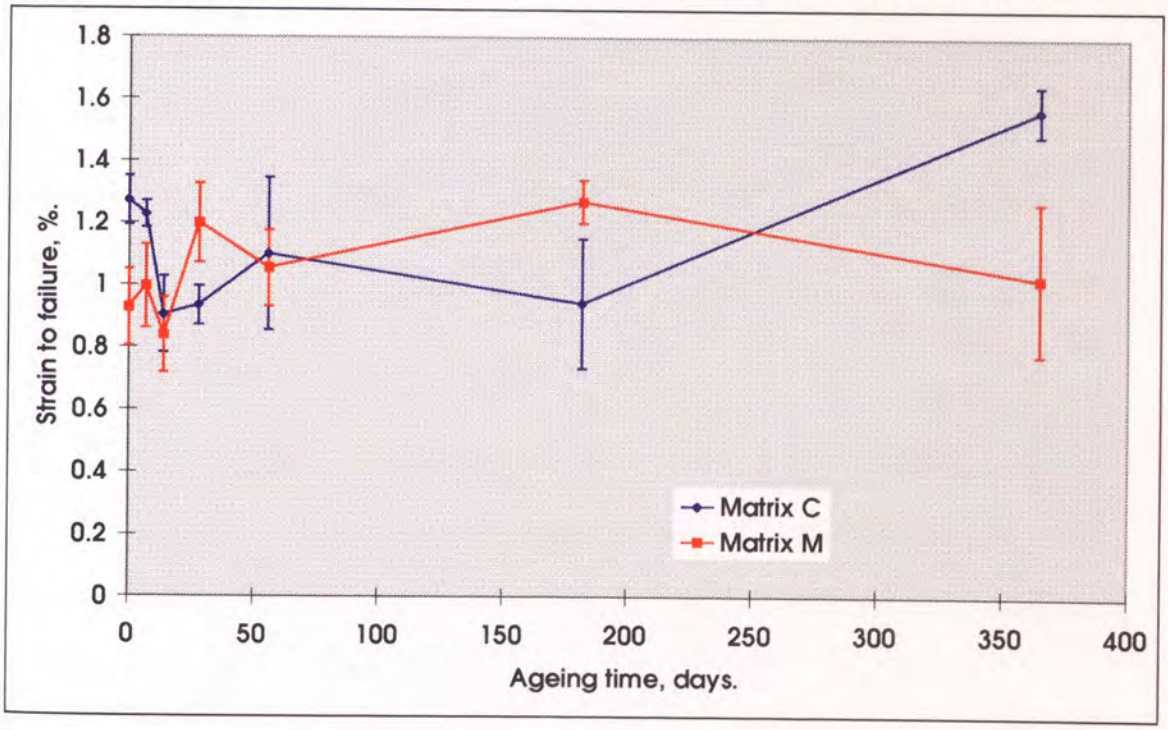

Figure 5.10. Variation of BOP with ageing time at 38°C.

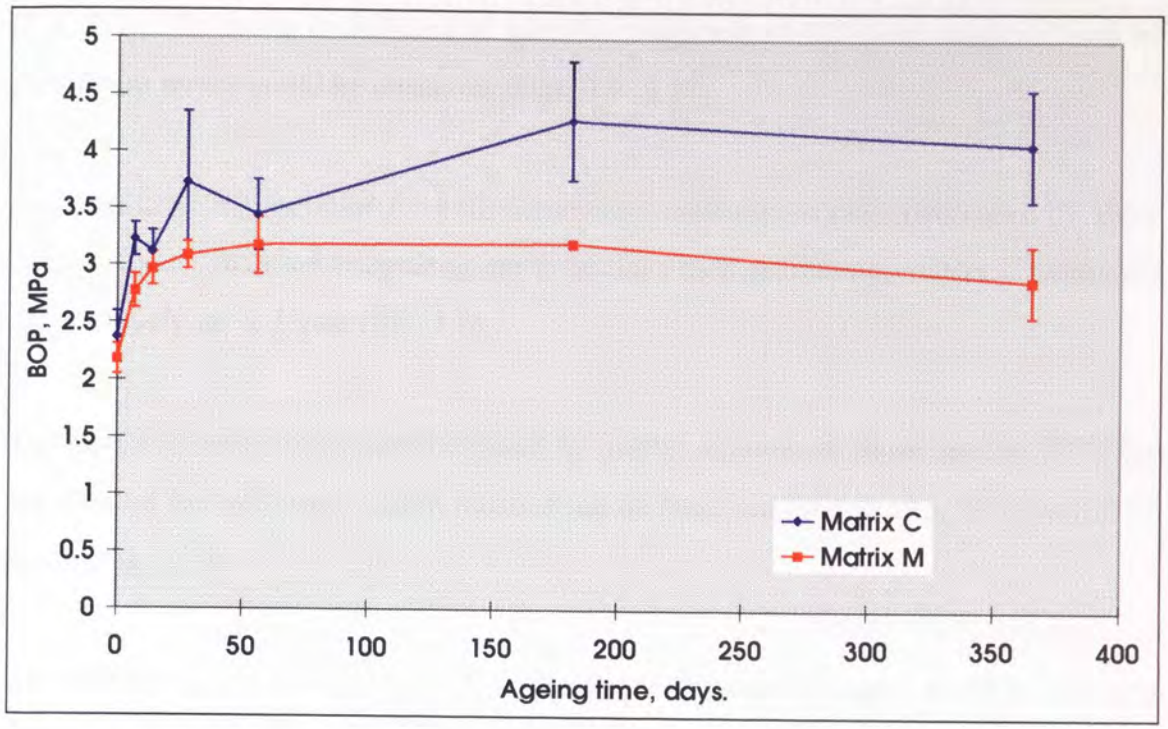

Figure 5.11. Variation of specific toughness with ageing time at 38°C.

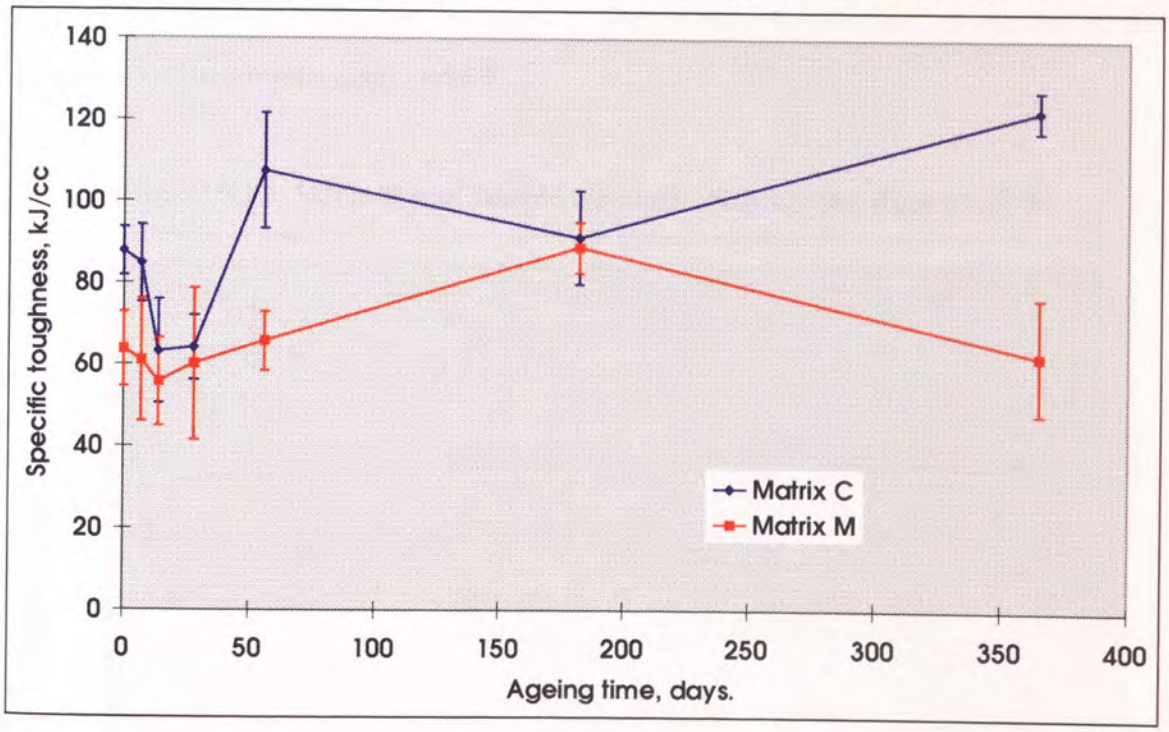

From these figures, the following observations were made.

There was no significant change in tensile strength for either composite up to 1 year (Fig. 5.7). The strain to failure and specific toughness results were scattered and no significant trends could be observed (Figs. 5.9, 5.11).

The post-cracking modulus for both composites appeared to have decreased by about 20% at 1 year, matrix M degrading up to 56 days then stabilising, matrix C degrading progressively up to 1 year (Fig. 5.8).

The BOPs of both composites increased by similar amounts to those aged at 20°C but the rates of increase were faster, most of the increase completed after 28 days (cf. 56 days) (Fig. 5.10).

As with ageing at 20°C, the stress/strain traces for samples aged at 38°C are very similar to those in Figure 5.1. Some examples are given in Fig. 5.30.

5.2.4. Water immersion, 65°C

Figures 5.12 to 5.16 show the variation in the primary mechanical properties of the composites for samples aged at 65°C.

Figure 5.12. Variation of tensile strength with ageing time at 65°C.

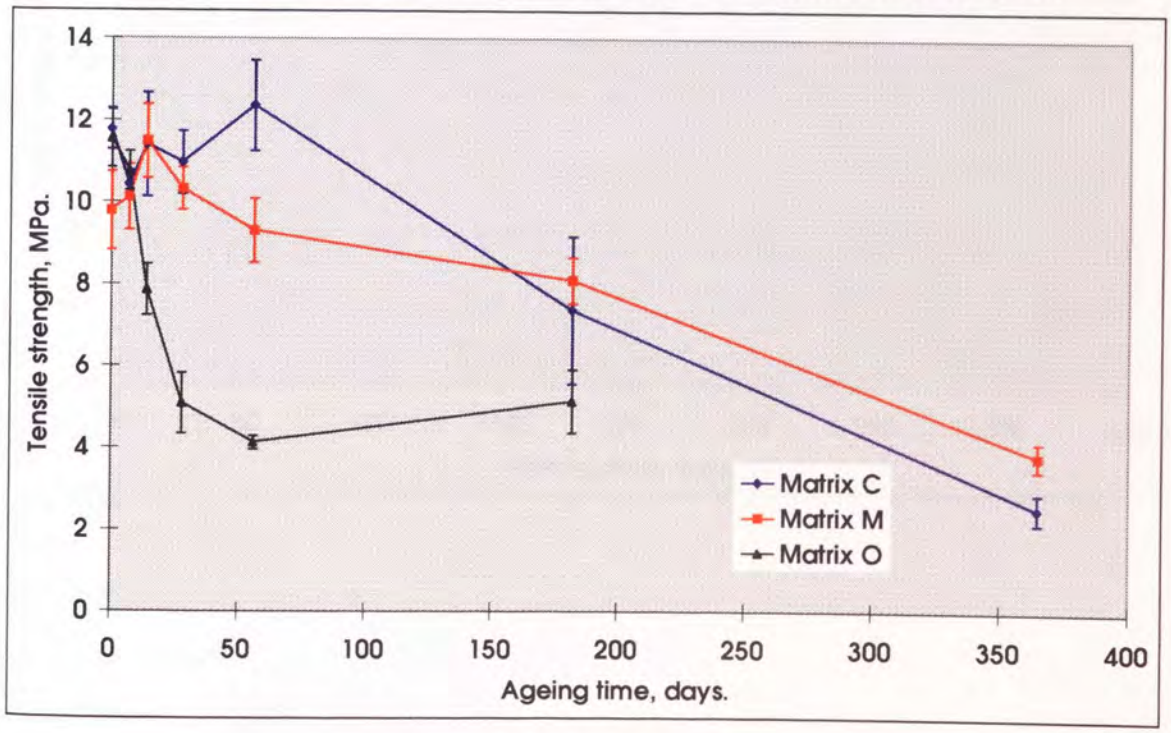

Figure 5.13. Variation of post-cracking modulus with ageing time at 65°C.

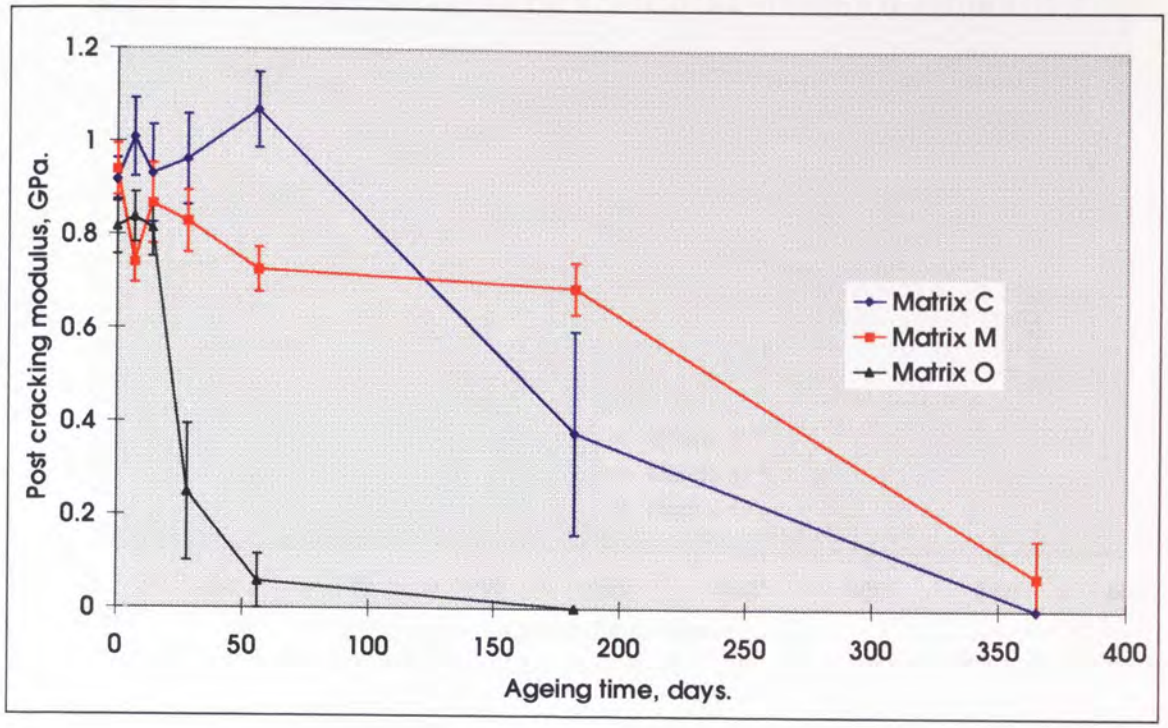

Figure 5.14. Variation of strain to failure with ageing time at 65°C.

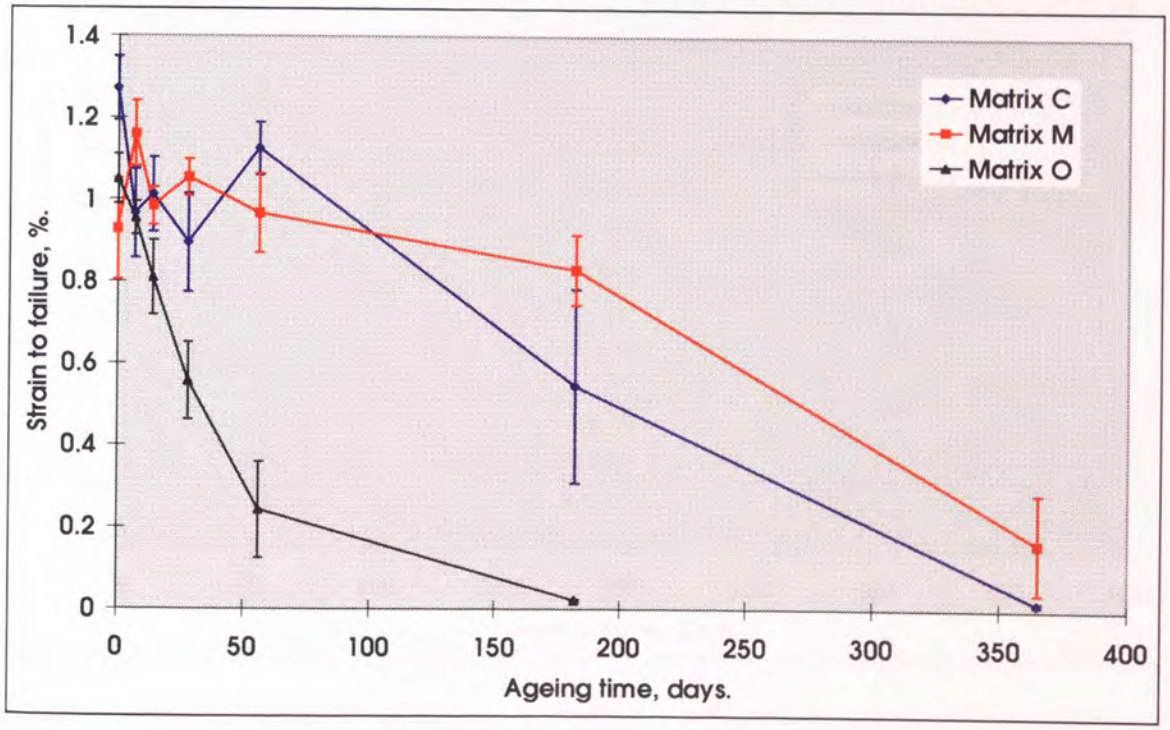

Figure 5.15. Variation of BOP with ageing time at 65°C.

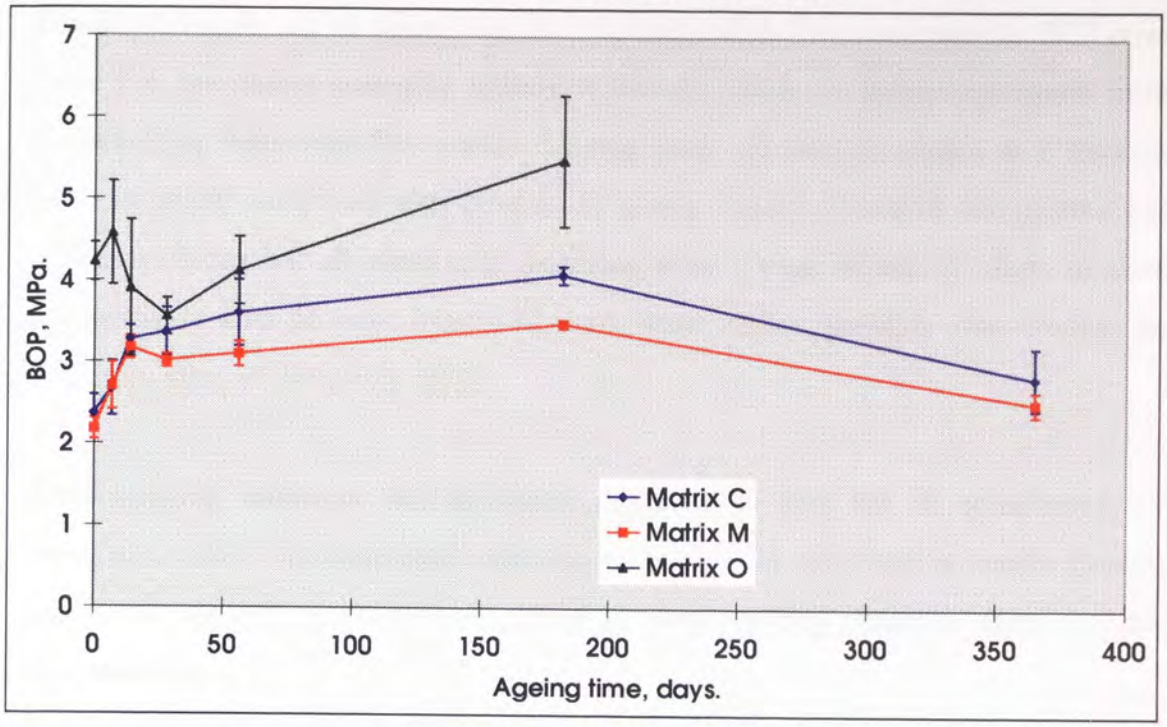

Figure 5.16. Variation of specific toughness with ageing time at 65°C.

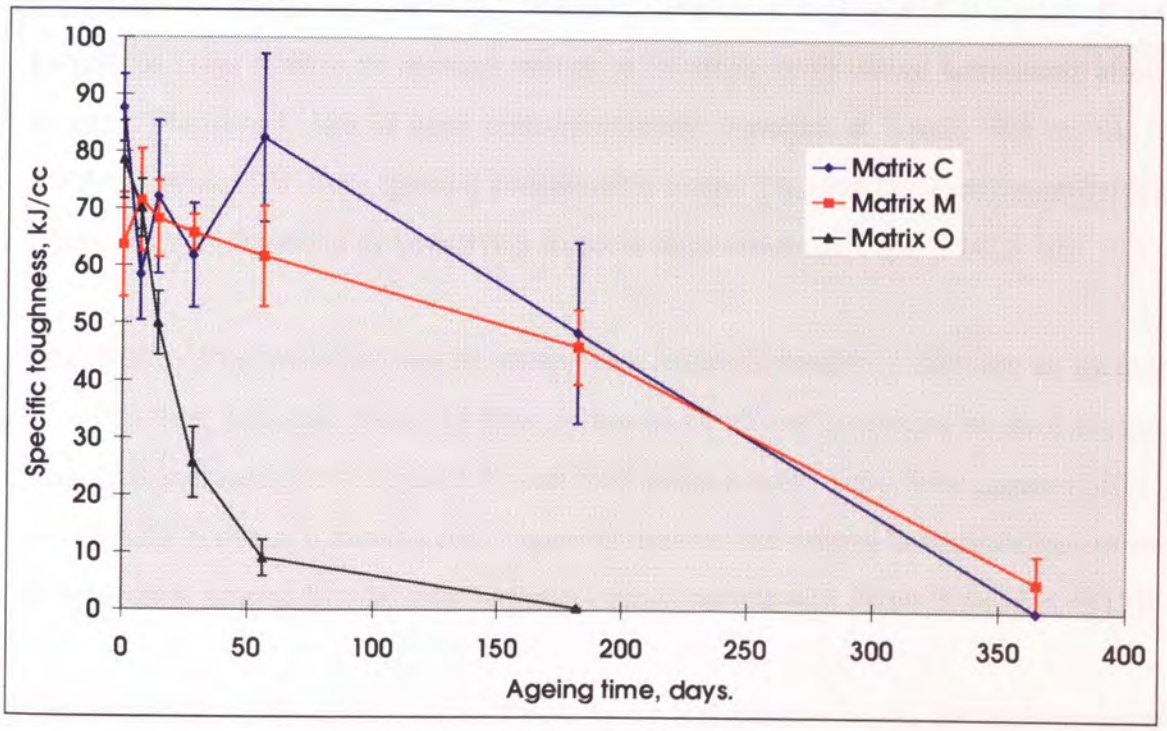

Compared to 20 and 38°C, the 65°C ageing regime has a dramatically deleterious effect on all the composites. The end effects are the same for all matrices, only the timescales differ.

Tensile strength can be considered as fully degraded when it reaches the BOP stress value (i.e. the matrix strength), indicating that the fibres no longer contribute to the post-cracking behaviour. For matrix O composites, the decline started at 7 days and was essentially completed after 28 days of ageing. Matrix C and M composites were slower to decay but all were fully degraded after 1 year. Matrix C starts to decay progressively after 56 days. Matrix M starts rather earlier, possibly after 14 days and definitely after 28 days (Fig. 5.12).

Post-cracking modulus was ultimately degraded to zero for all composites. For matrices O and C, the timescales were the same as those exhibited by tensile strength. Matrix M showed a progressive decay of post-cracking modulus from 14 days onwards (Fig. 5.13).

Strain to failure and specific toughness were both ultimately degraded over similar timescales to negligible quantities. Matrix O exhibited a progressive decay of both properties from 0 days to residual values at 56 days, with decay completed after 6 months. Matrices C and M were both completely degraded at 1 year. The results for matrix C prior to 56 days showed considerable scatter but then decayed progressively. Matrix M was degraded progressively from 28 days onwards (Figs. 5.14, 5.16).

The **BOP**s of the matrix C and M composites behaved similarly, showing an increase of about 40% between 0 and 14 days followed by slower increases up to 6 months. The total increases were about 80% and 50% respectively. They then appeared to fall off slightly between 6 months and 1 year. Results for the matrix O composites showed considerable scatter, but the total increase over 6 months was about 30% (Fig. 5.15).

These variations were reflected in the changing stress/strain traces for the composites aged at 65°C (Figs. 5.17 to 5.19). Note that at 1 year, only matrix M exhibits any true post-cracking behaviour and even this is reduced to insignificance. Most samples aged for 1 year at 65°C (6 months for matrix O) failed by single fracture.

Figure 5.17. Stress/strain curve variation with time at 65°C, Matrix O.

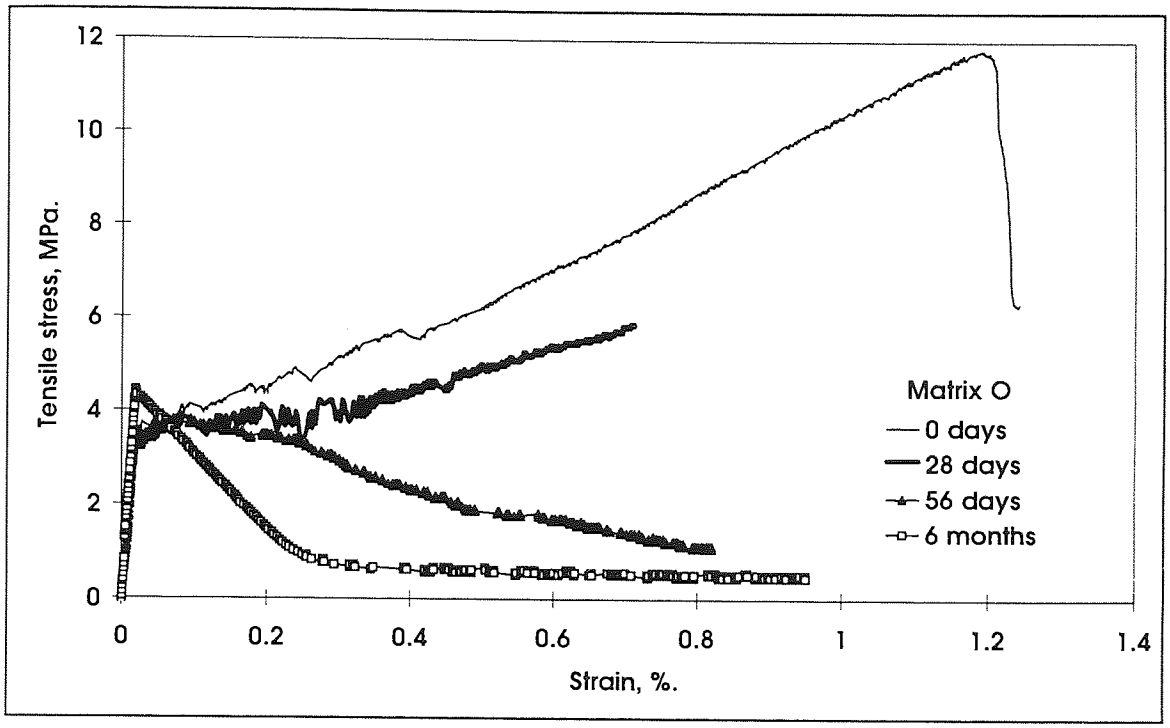

Figure 5.18. Stress/strain curve variation with time at 65°C, Matrix C.

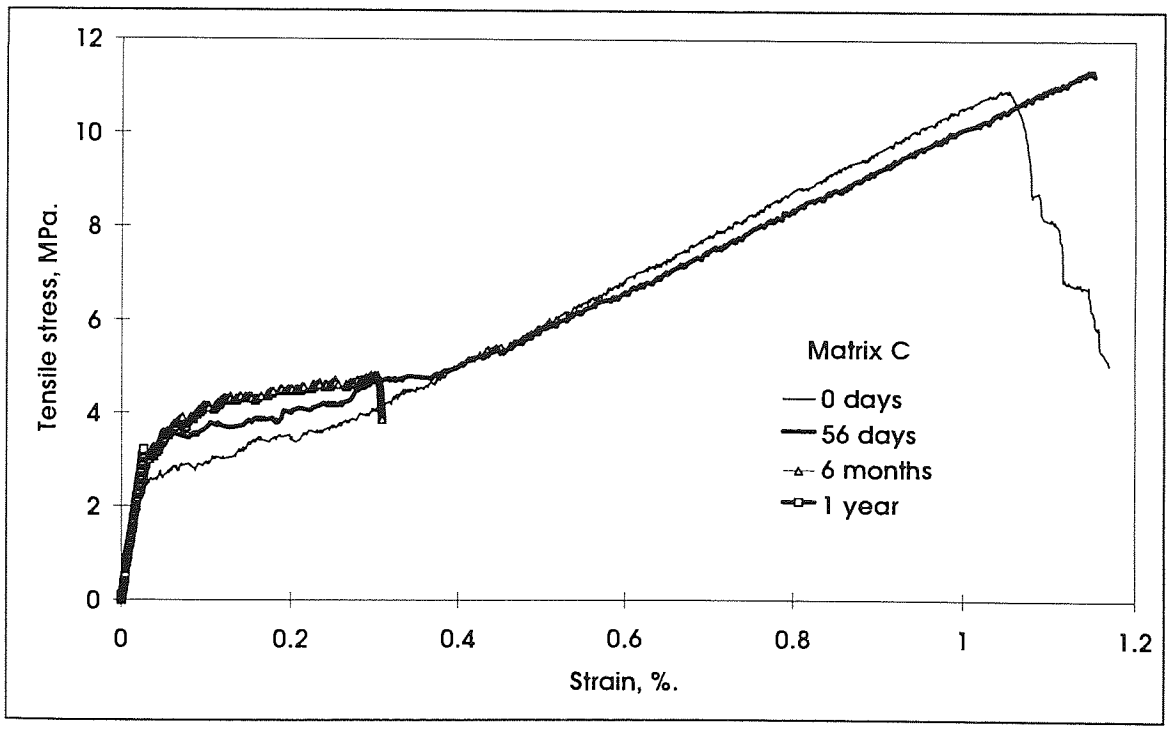

Figure 5.19. Stress/strain curve variation with time at 65°C, Matrix M.

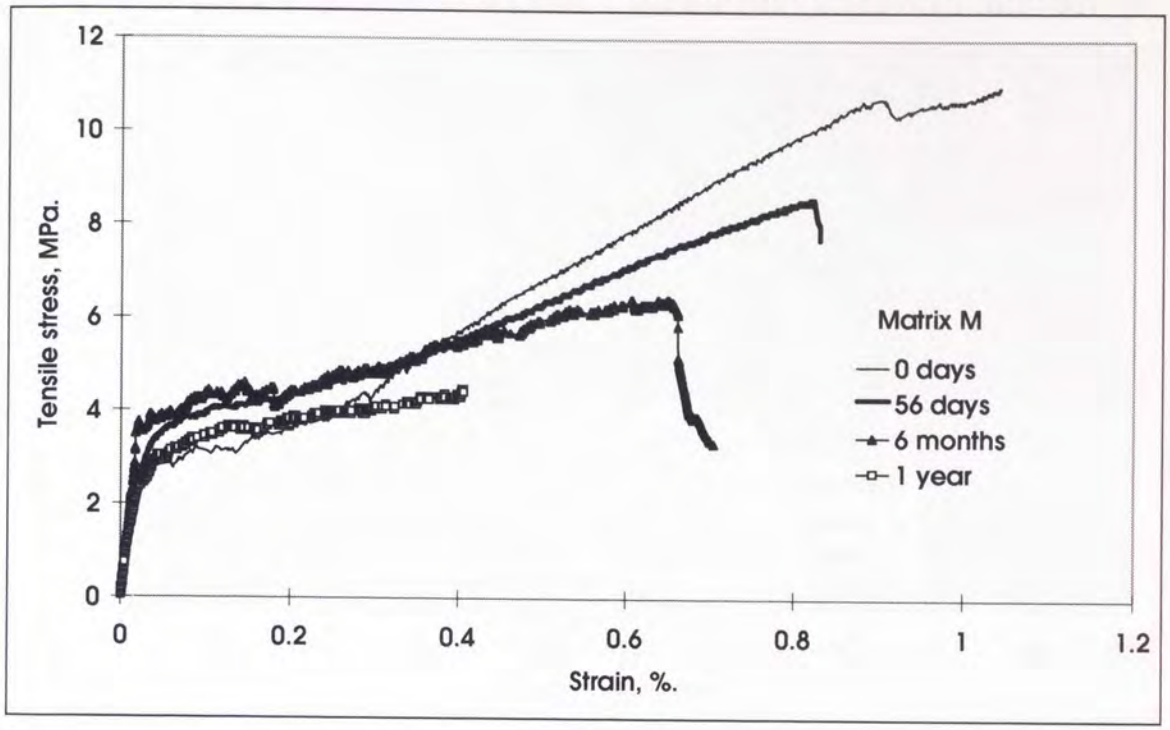

5.2.5. Cyclic ageing.

Figures 5.20 to 5.24 show the variation in the primary mechanical properties of the composites for samples subjected to cyclic ageing.

Figure 5.20. Variation of tensile strength with ageing time, cyclic ageing.

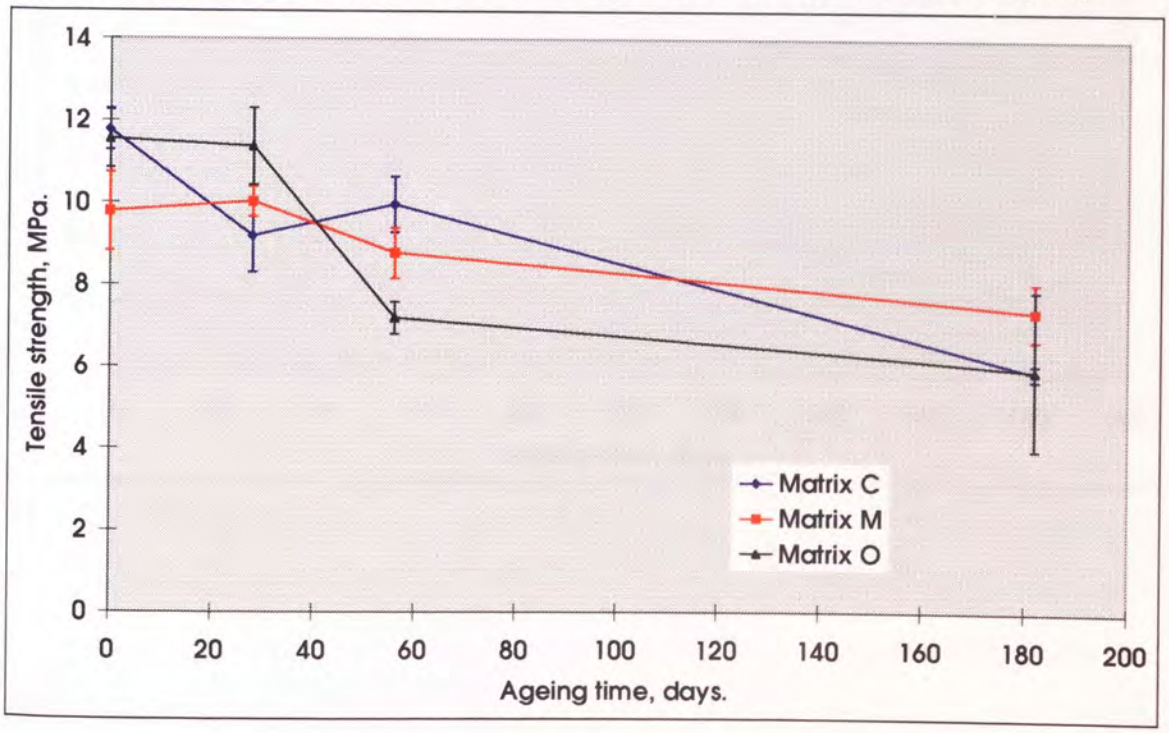

Figure 5.21. Variation of post-cracking modulus with ageing time, cyclic ageing.

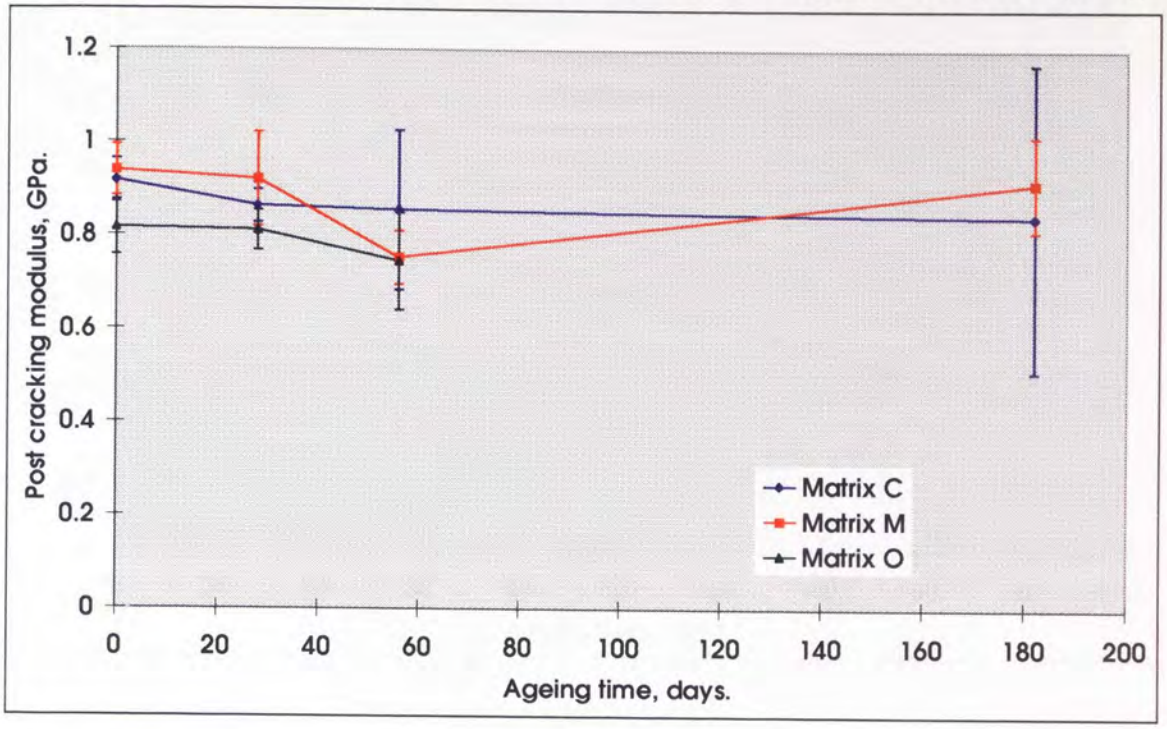

Figure 5.22. Variation of strain to failure with ageing time, cyclic ageing.

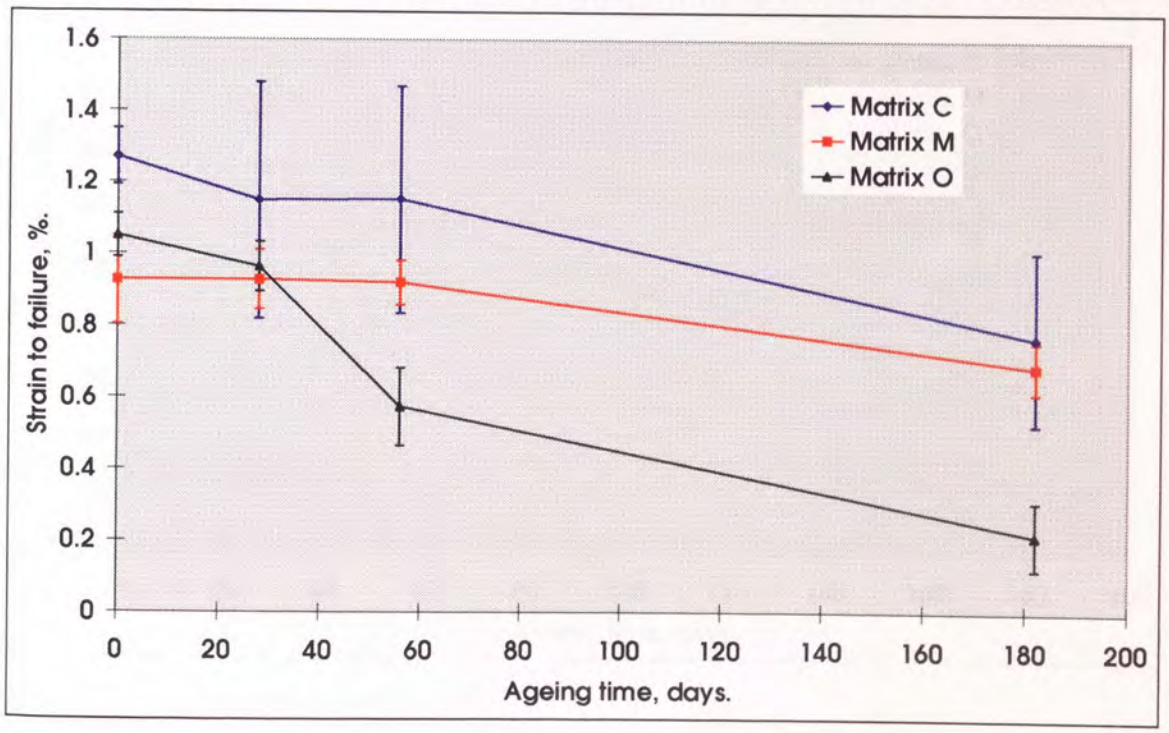

Figure 5.23. Variation of BOP with ageing time, cyclic ageing.

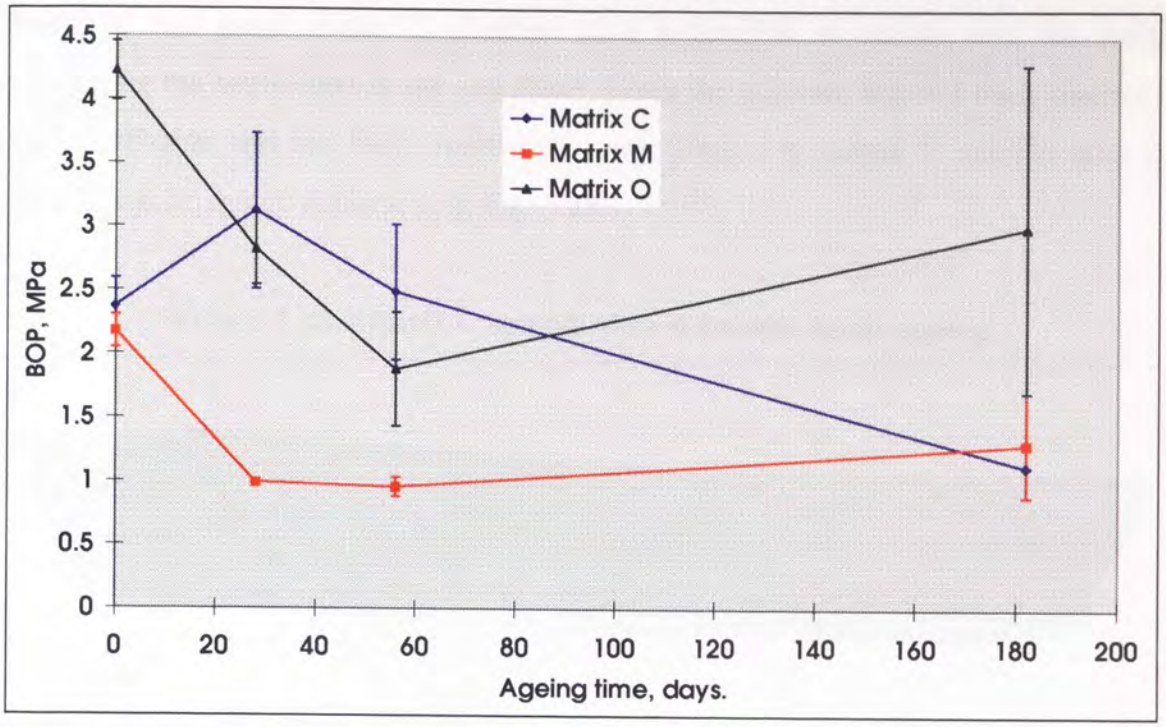

Figure 5.24. Variation of specific toughness with ageing time, cyclic ageing.

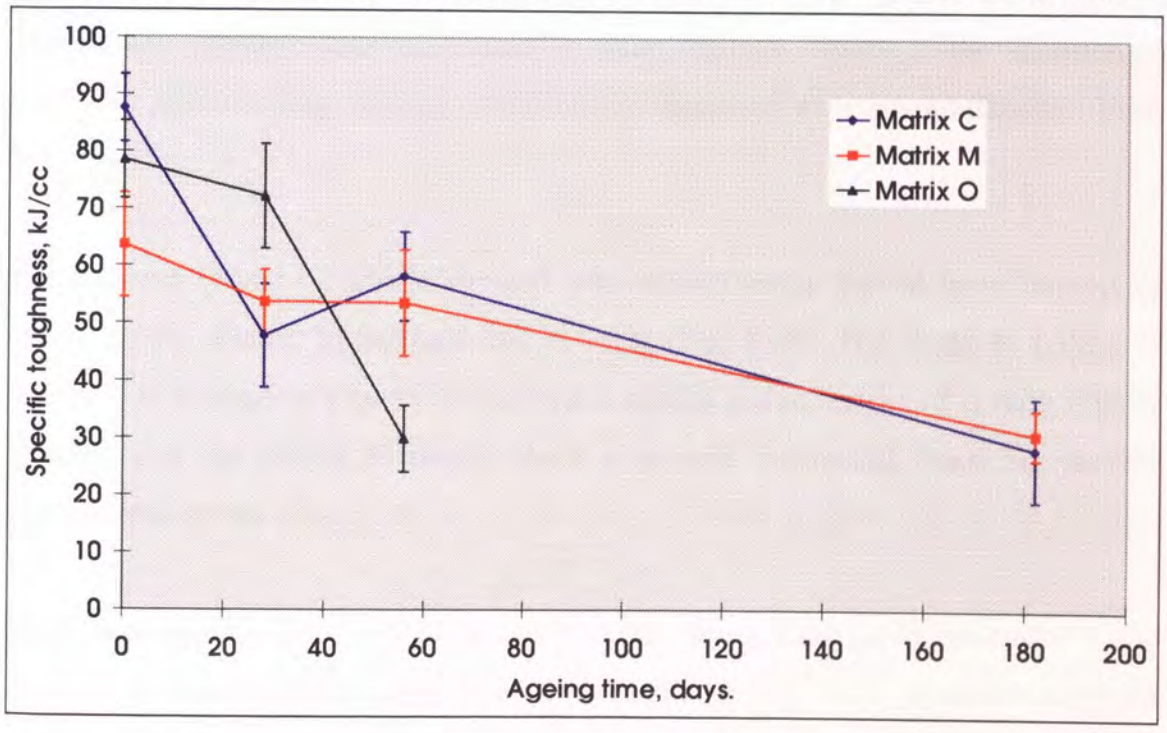

The physical appearance of cyclically aged samples was very different to those aged under other regimes. Substantial surface crazing was apparent after only a few days. Samples also tended to develop a considerable longitudinal curvature (bow). Matrix C samples were the most severely affected, losing cross-section through crumbling and

also developing a transverse curvature (warp). After 6 months of cyclic ageing, most matrix C and some matrix O samples were impossible to tensile test, the warp preventing the application of the end plates, hence the 6 month data for these matrices is less reliable and has been omitted in some graphs. A matrix C sample after 6 months cyclic ageing is pictured in Fig. 5.25.

Figure 5.25. Matrix C sample after 6 months cyclic ageing.

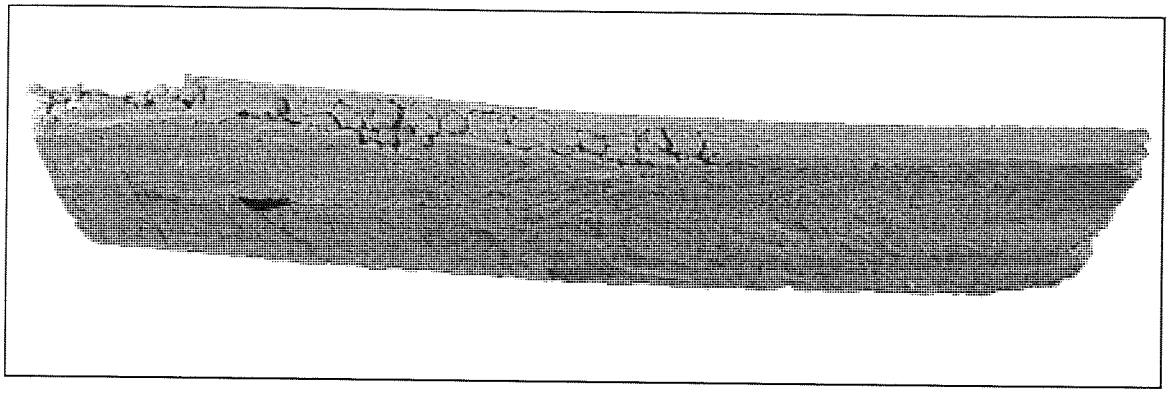

In general, the results obtained from samples aged under the cyclic regime showed considerably greater scatter than those for other regimes. Trends in the variation of BOP and post-cracking modulus could not be identified with any confidence (Figs. 5.23, 5.21).

For matrices O and C, tensile strength was approximately halved by 6 months of cyclic ageing. Matrix M suffered less severely (Fig. 5.20). The strain to failure of matrix O is reduced by a factor of four over a similar period, matrix M is only slightly affected and the matrix C results show a general downward trend but a very considerable scatter (Fig. 5.22).

Specific toughness results showed clearer trends, being reduced by factors of 2 and three for matrices M and C respectively over 6 months (Fig. 5.24). Specific toughness could not be derived for matrix O after 6 months due to the bow, friability and low strength of the samples conspiring to produce illegible stress/strain traces, but was reduced by a factor of between 2 and 3 after 56 days.

Figure 5.26. Typical stress/strain curves after 56 days of cyclic ageing.

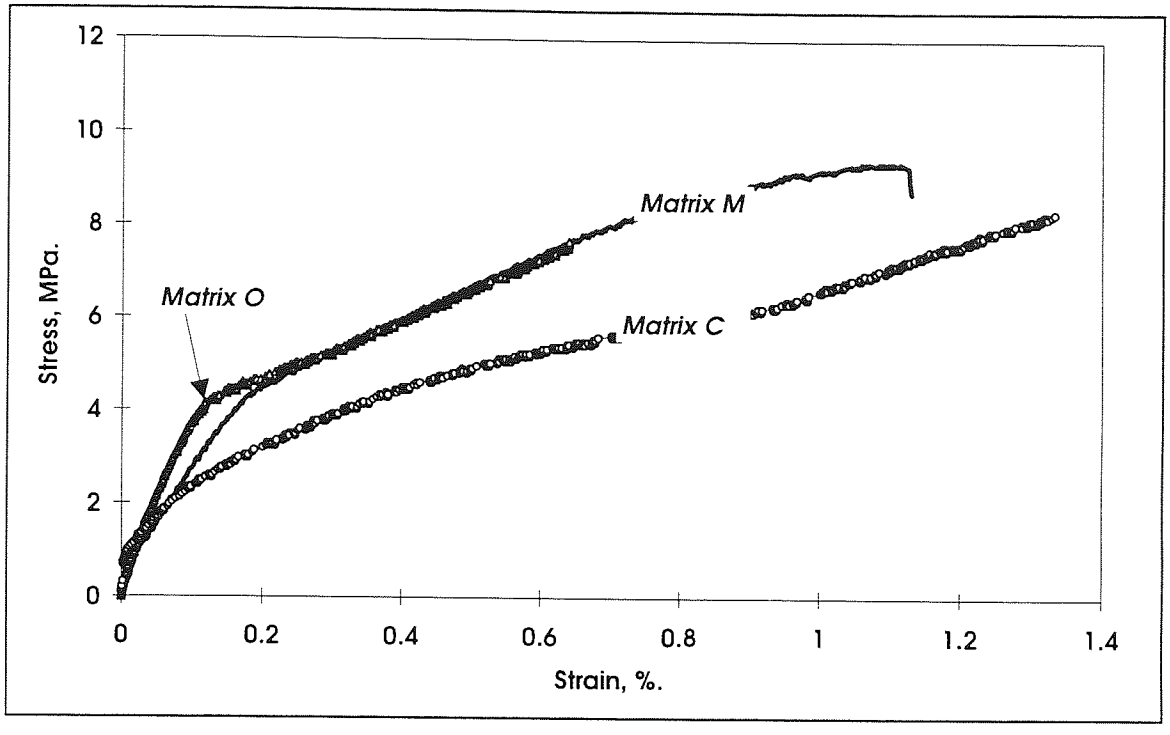

The stress/strain traces for cyclically aged samples (Fig. 5.26) were distinctly different from those shown previously. Note that, compared with traces from samples aged under other regimes (Figures 5.1, 5.17-5.19), the initial moduli are greatly reduced and no multiple cracking regions can be observed, indicating substantial matrix damage.

5.2.6. Carbonation.

The carbonation ageing regime caused perceptible bow in the tensile test samples. Untested matrix C samples were found on low power microscopic examination to have a family of parallel transverse cracks throughout their length. Matrix M samples displayed no such cracks, but it is likely that some pre-cracking was present judging by the shape of their stress strain curves (Figure 5.26a). As with cyclic ageing, the initial moduli and BOPs were reduced. The multiple cracking region is indistinct. No significant changes from the 0 day values of tensile strength, post-cracking modulus, strain to failure or specific toughness were observed for either composite.

Figure 5.26a. Typical stress/strain curves after carbonation.

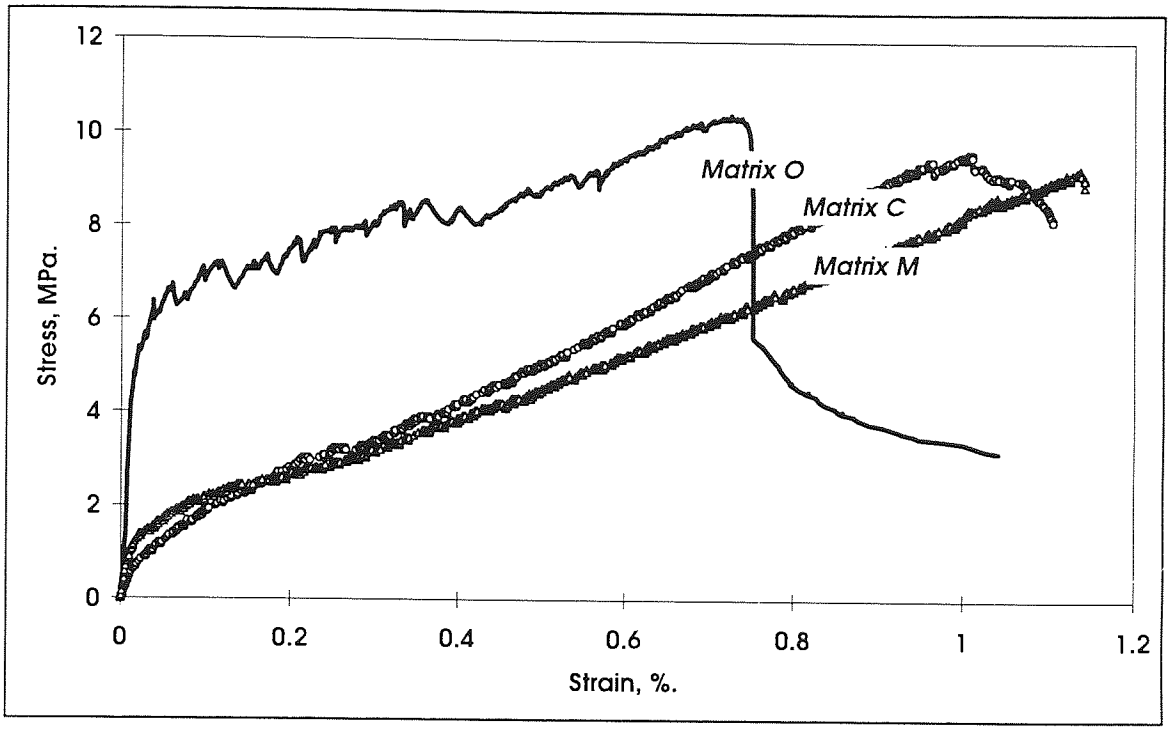

The matrix O samples also suffered slight bowing but no pre-cracking appeared to have taken place. In fact, it would seem from the stress/strain traces for the carbonated GRC that the matrix strength is substantially increased, by at least 50%, over that of the 0 day samples. Not only is the BOP higher, but the multiple cracking region occurs at a generally higher stress level than for conventionally aged samples (see Figure 5.17) and is much more distinct.

Note: *Unfortunately, small-scale noise in the stress/strain traces (believed to have been caused by either minor surface cracking as the slight bow was straightened during testing or by extensometer slippage) caused the LOPFinder software to give erroneous results for the BOP of the carbonated matrix O samples. As an example, the BOP for the typical trace in Figure 5.17 was given as 3.1 MPa which is clearly in error. Consequently the BOPs for the carbonated matrix O samples used in the bond strength analysis (Chapter 7) were derived 'by eye'.*

Their were no significant changes in the tensile strength and post-cracking modulus for the matrix O samples compared to the 0 day samples, but the strain to failure and specific toughness were both reduced by about 30%.

5.3. Other testing.

Four point bending tests were carried out on the corrugated pre-fabricated GRC samples provided by the BRE (see 3.2). Samples 250 mm long were cut from the peaks and troughs of the sections and hence contained both uni-directional and random fibre.

Figure 5.27. Section diagram of bending test samples (commercial GRC).

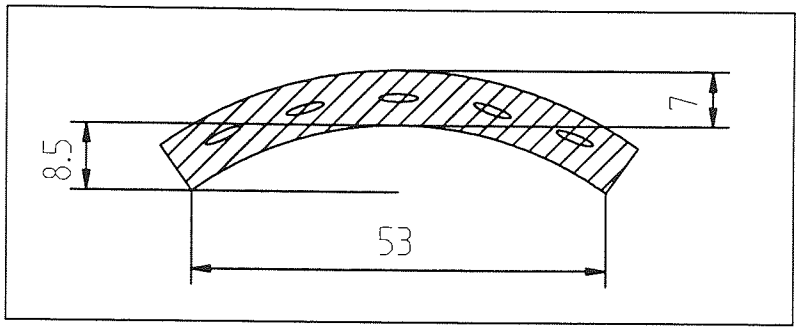

(dimensions in mm)

The cross-section (Fig. 5.27) was analytically treated as a circular torus segment to derive a section modulus $\mathbf{Z = I_{NA}/y}$ where I_{NA} is the second moment of area about the neutral axis and y is the maximum distance from the neutral axis, at which the stress due to bending is a maximum. This section modulus was used by the BRE bending software to derive the failure stresses. The full analytical treatment is presented in Appendix 3.

Two sets of material were supplied; unaged material and material subjected to 4 years natural weathering at the BRE's Garston exposure site. Samples of unaged material were subjected to 28 days of 65°C hot water ageing, and 28 days of cyclic weathering to compare the accelerated regimes with the natural weathering. Figure 5.28 presents the bending strength, strain to failure and LOP of the samples with error bars representing ±1 standard error. LOP was presented, as the software appeared not to correctly derive the BOP, often returning a value equal to the bending strength.

Figure 5.28. Properties of pre-fabricated GRC under various ageing regimes.

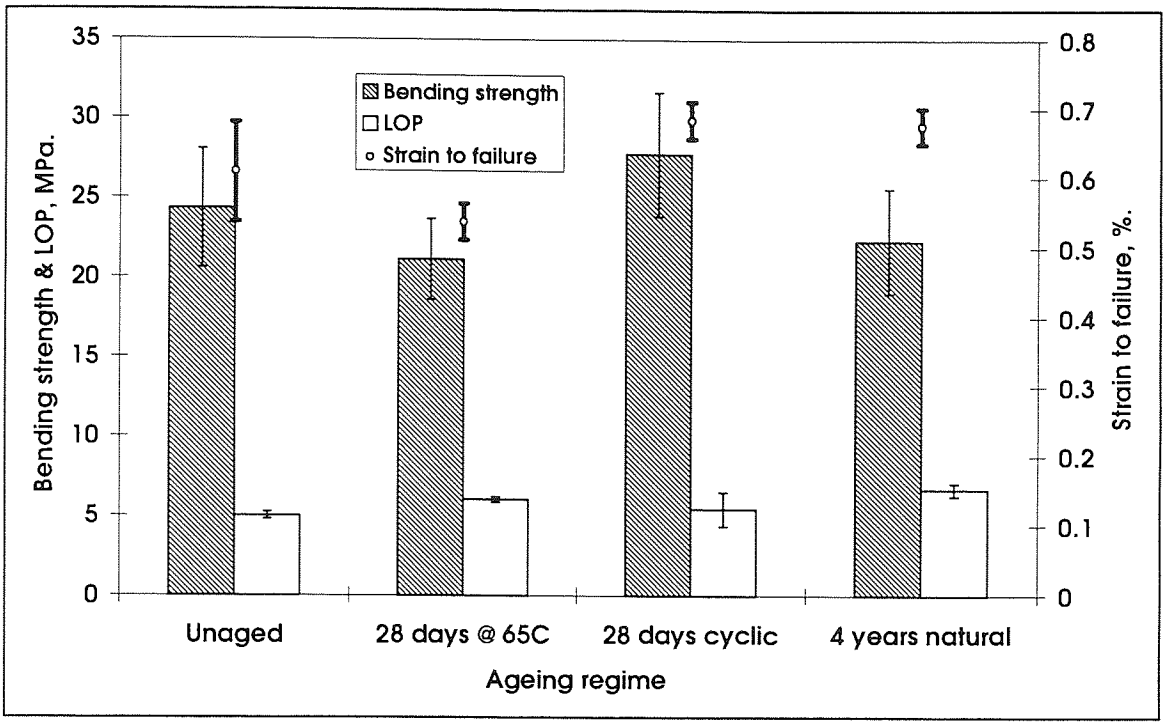

No significant trends were observed. It was concluded that the artificial ageing regimes have little effect on the properties of this GRC after 28 days, and that they are no more severe than 4 years of natural ageing.

5.4. Discussion of mechanical testing results.

5.4.1. Initial properties - comparison with theoretical predictions.

The tensile strength and post cracking modulus of the composites can be predicted from the ACK theory. Using the manufacturers' data for the fibre properties (Table 3.2) and a fibre volume fraction of 0.015 (1.5%), the tensile strength was predicted (eq. 5.1) as **25.2 MPa**. The average experimental initial strength was less than half this at 11.1 MPa.

Precise prediction of failure strain from ACK theory is less reliable as it is dependent on the failure strain and modulus of the matrix, which were difficult to measure. Using 0.02% and 15 GPa for the matrix failure strain and modulus respectively (values typical of those derived from the stress-strain curves above), ACK predicts about 2.2% i.e. slightly less than the failure strain of the fibres. The experimental results were about half this, averaging 1.1%.

In contrast to the stress and strain predictions, the predicted initial post-cracking modulus (see Fig. 2.1) was **1.08 GPa** which compared more favourably with the experimental value of 0.89 GPa.

The departure of the stress/strain values from theoretical predictions is due to two factors. Firstly, the average strand strength (1.7 GPa, Table 3.2) is likely to be higher than the roving strength; any group of strands will begin to fail at the strength of the weakest strand, instigating a tearing effect as extra load is thrown onto the remaining strands. This effect is illustrated in the difference between the manufacturers data for filament strength (3.5 GPa) compared with the 204-filament strand strength of 1.7 GPa. Secondly, the fibres are likely to have suffered some damage during board manufacture, despite careful handling. Being made of a brittle material, the fibres are very sensitive to surface flaws introduced during handling.

It is unlikely that corrosion during the 28 day curing period caused significant strength loss. Had this been so, a drop in the fibre (i.e. post-cracking composite) modulus of similar magnitude would probably have been observed.

5.4.2. Relative performance under accelerated ageing

5.4.2.1. Hot water ageing.

The new matrix (C and M) composites performed better than the matrix O composites under hot water ageing regimes. After 1 year at 20°C, the new matrix composites displayed no degradation of primary mechanical properties, while the matrix O composite lost about 20% of its tensile strength and post-cracking modulus.

At 65°C, the differences were far more significant. Although all the composites were completely degraded after 1 year, the new matrix composites retained their properties for a much longer period. The matrix O composites could be considered completely degraded by 28 days, while the others still retained some of their properties at 6 months. This is shown graphically in Figs. 5.12-5.16. Figure 5.29 compares $t_{50\%}$ for the mechanical properties of the composites aged at 65°C; $t_{50\%}$ is defined as the time taken for a given property to be reduced to half its original (i.e. 0 day) value.

Figure 5.29. $t_{50\%}$ for mechanical properties, 65°C hot water ageing.

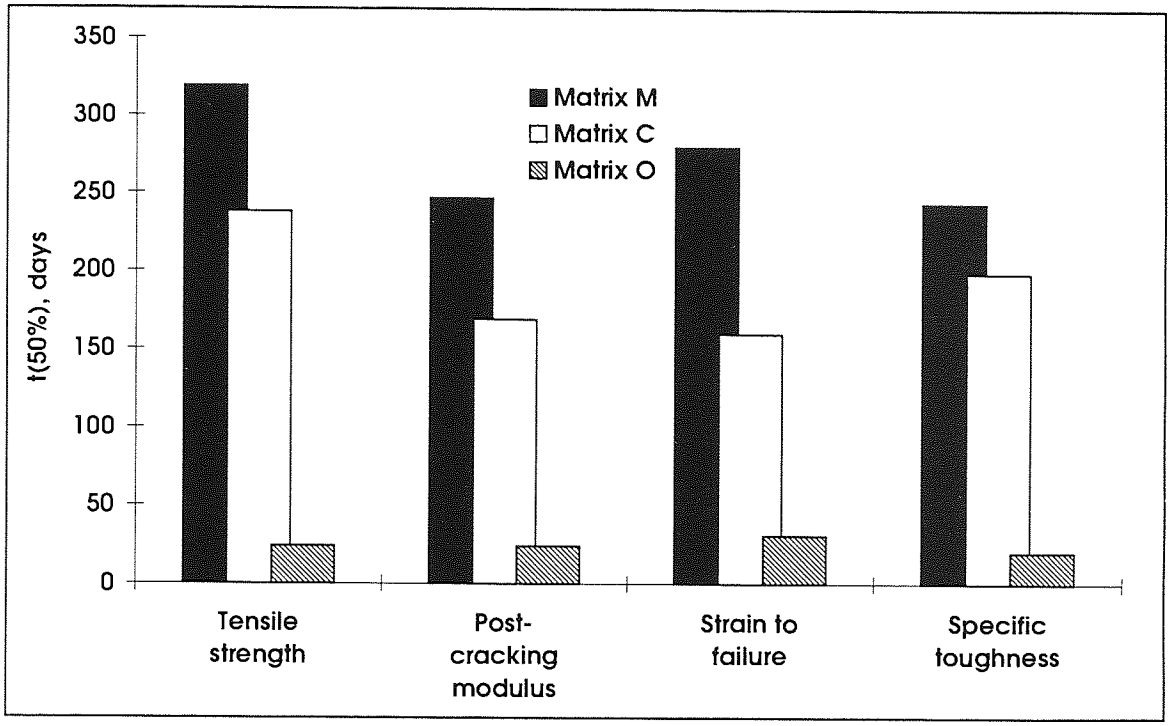

The $t_{50\%}$ times for matrix C and M composites were about 8 and 11 times longer respectively than those for matrix O composites. These factors applied broadly to all properties. If periods of hot water ageing are taken as being proportional to periods of natural weathering as first postulated by Litherland *et al.* (1981) then matrix C and M composites should perform in service longer than matrix O composites by similar factors. Similarly, matrix M should perform slightly better than matrix C (i.e. by a factor of about 11/8).

The most surprising aspect of the performance of the matrices was the resilience of the new matrices under 38°C hot water ageing. It was originally expected that a significant proportion of the initial mechanical properties would be lost under this regime and that the results could be used to assess the relevance of the model proposed by Litherland *et al.* (see 5.4.3). In the event, no significant degradation was observed, as shown by Figs. 5.7 to 5.11. This resilience is also reflected in the stress/strain curves for the new matrix GRC aged at 38°C (Fig. 5.30).

Figure 5.30. Stress/strain curves, unaged cf. 1 year at 38°C.

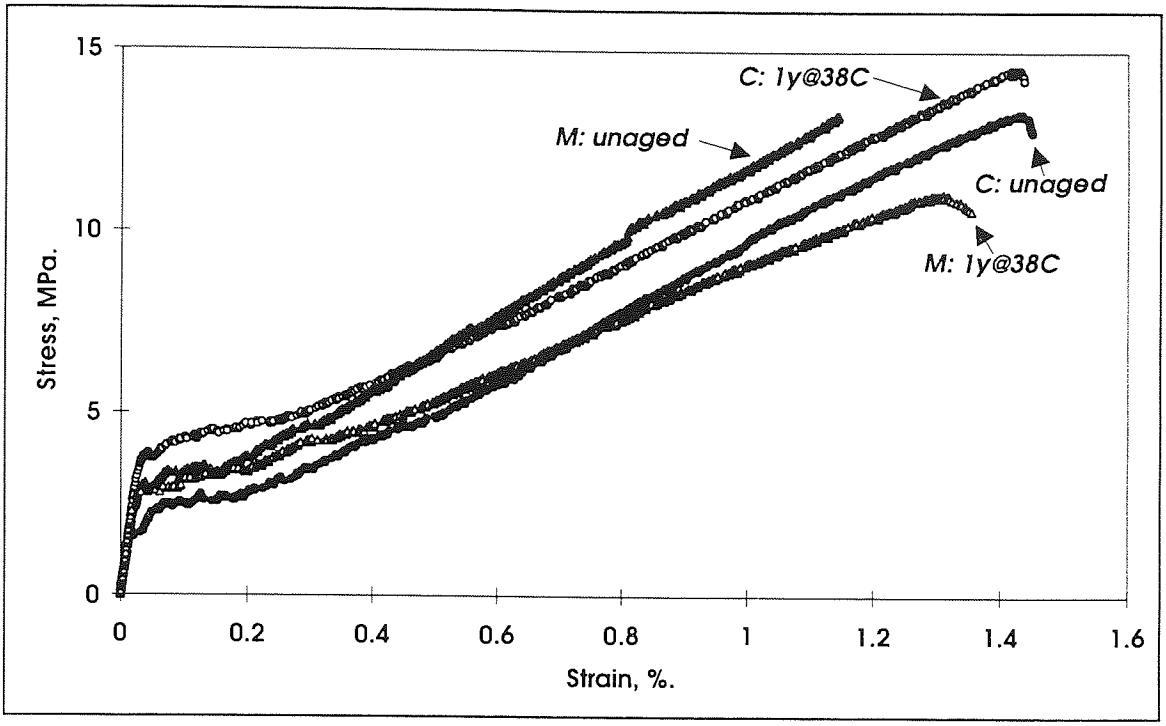

5.4.2.2. Cyclic ageing.

The scatter in the primary mechanical property results derived from cyclically aged samples precluded the derivation of similar $t_{50\%}$ statistics. The results of similar periods of ageing under the different regimes are compared in Fig. 5.31.

Bearing in mind the considerable scatter in the cyclic ageing results, it was difficult to identify clear differences between 6 months of hot water and cyclic ageing for the new matrices. Cyclic ageing appeared to have a more deleterious effect on specific toughness and a less deleterious effect on post-cracking modulus than hot water ageing. The toughness loss is due to the pre-cracking induced and hence the lack of a multiple cracking region; this reduces the total area under the stress-strain curve (Fig. 5.26 cf. Figs. 5.18, 5.19). The retention of post-cracking modulus is an indication that less fibre corrosion is taking place under cyclic ageing due to the lack of water available during the high temperature section of the test. Tensile strength was similarly affected by both regimes, as was strain to failure for matrix M. Strain to failure for matrix C was degraded less by cyclic than hot water ageing.

Figure 5.31. Comparison of similar periods of cyclic and 65°C hot water ageing.

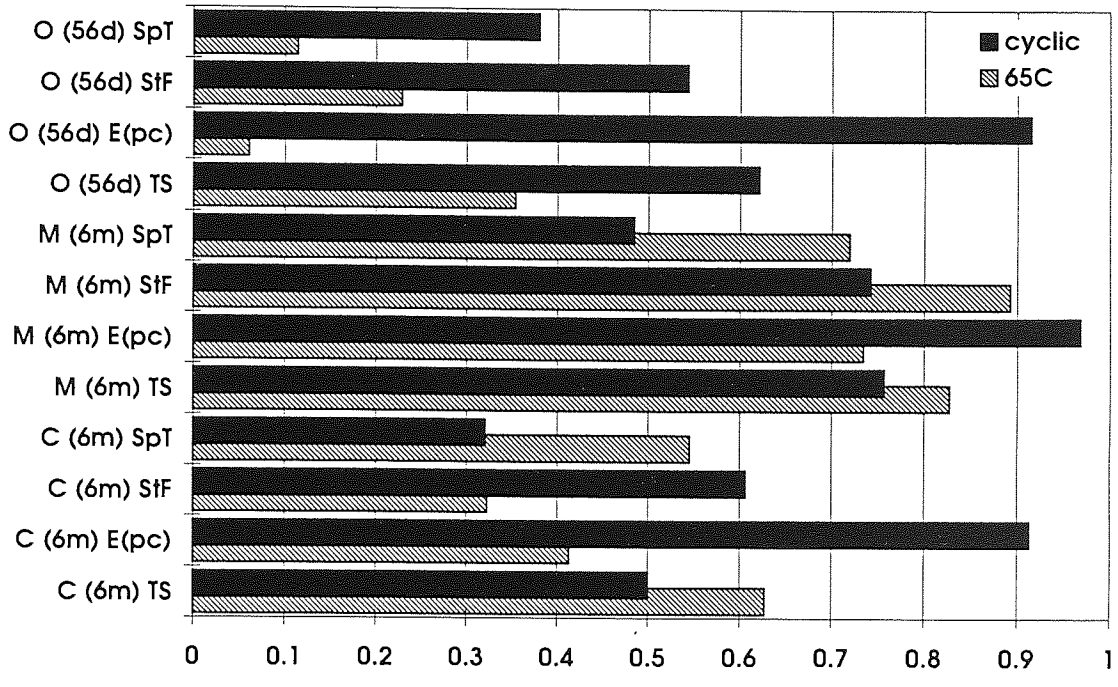

Properties expressed as proportions of those at 0 days.

SpT = specific toughness, StF = strain to failure, E(pc) = post cracking modulus, TS = tensile strength.

For matrix O (compared at 56 days of ageing), the cyclic ageing regime was very clearly less deleterious than the hot water ageing regime. All properties bar specific toughness retained at least half their original values under cyclic ageing, while all properties bar tensile strength are reduced by at least three quarters under the hot water ageing. The post cracking modulus showed the greatest difference; reduced by over 90% for 56 days at 65°C but by only 10% for 56 days of cyclic ageing.

Comparing the relative performance of the matrices, matrix O performed very similarly after 56 days to the new matrices after 6 months of cyclic ageing. The service life (i.e. relative $t_{50\%}$) factors of 8 to 11 mentioned in section 5.4.2.1. would be reduced to about 3 or 4 if cyclic ageing was considered as a guide to service life.

Although the primary mechanical properties of the cyclically aged composites remained at reasonable levels after short periods of cyclic ageing (<28 days for matrix O, <56 days for the new matrices), the effect on their serviceability was severe. Even

after a few days, the matrices were completely cracked and crazed, affecting the appearance and the water permeability of the composites. A considerable bow also quickly developed. However, these effects are likely to have been a result of the uni-directional fibre not being perfectly equally distributed across the cross-section due to the batch nature of the manufacturing process, and the absence of fine aggregate. This would have resulted in non-uniform constraint of the shrinkage caused by the drying component of the cyclic ageing and hence bowing/warping leading to cracking. The random 2-D distribution of fibre and the fine aggregate included in commercial composites would help restrain the shrinkage more evenly. The commercial samples in the programme subjected to cyclic ageing (section 5.3) displayed no bow or cracking after 28 days.

Note also that the chemical composition of the matrices was changed considerably by cyclic ageing (section 4.6).

5.4.2.3. Carbonation.

The most noticeable effect of the carbonation regime was the substantial increase in the matrix strength of the matrix O composites (Figs. 5.27 cf. 5.1). This is of obvious interest to composite designers and (together with the possible chemical [section 4.6] and bond [section 7.4.2] advantages that might be conferred by carbonation) is worthy of further study.

The pre-cracking suffered by the new matrix composites and the bow suffered by all composite samples could, as with cyclic ageing, be attributed to unequal fibre distribution and lack of fine aggregate. In this case the driving force is the shrinkage caused by the carbonation. The 'true' matrix strength of the matrix C and M composites may also have increased, but the pre-cracking means that no evidence of this was exhibited in the stress/strain curves.

5.4.3. Comparison of results with Litherland ageing model.

To formulate the Arrhenius plot characterising the ageing process (Fig. 2.5) at the heart of the model according to Litherland *et al.* (1981) and Oakley *et al.* (1982), a similar strength loss must be observed at different times for at least two different

ageing temperatures. Since no significant composite strength loss was observed at the lower ageing temperatures (20 and 38°C), no direct comparison with the model could be made.

However, the model specifies (via the Arrhenius plot) the acceleration factors that apply when comparing any two (or more) temperatures *vis a vis* their ageing severity. This allows data from samples aged at different temperatures to be 'normalised' with respect to a standard temperature (for example, local mean annual temperature) and plotted on an 'equivalent time' axis. For example, if 20°C is taken as the standard temperature, from the Arrhenius plot the 'acceleration factors' of 38 and 65°C with respect to 20°C are 8.2 and 130 respectively. Hence results from a sample aged for 28 days at 65°C could be normalised and plotted as 28 x 130 = 3640 days (10 years) at 20°C; 28 days at 38°C could be plotted as 28 x 8.2 = 230 days at 20°C.

In order to provide some comparison with the model, the results from the 20, 38 and 65°C aged samples were normalised (by factors of 0.034, 0.28 and 4.4 respectively, derived from the Arrhenius plot in Fig. 2.5) to their 50°C time equivalents; this temperature was used by Litherland *et al.* as the standard. These were compared with the published 50°C log(time) vs. strength data used in the formulation of the model, represented in the plots that follow (Figs. 5.32 to 5.35) by the dotted line. The data pertaining to each pre-normalisation ageing temperature has been grouped in lines.

The strength values for both sets of data were normalised by representing the strength as a proportion of its "initial" value. The initial strength (MOR) of the Litherland data was taken as the first point on the plot at ≈1 day. The initial strength of the 20, 38 and 65°C aged samples was taken as the 28 days at 20°C strength (which is equivalent to 1 day at 50°C according to the model).

Figure 5.32. Matrix O: Normalised ageing behaviour cf. Litherland data.

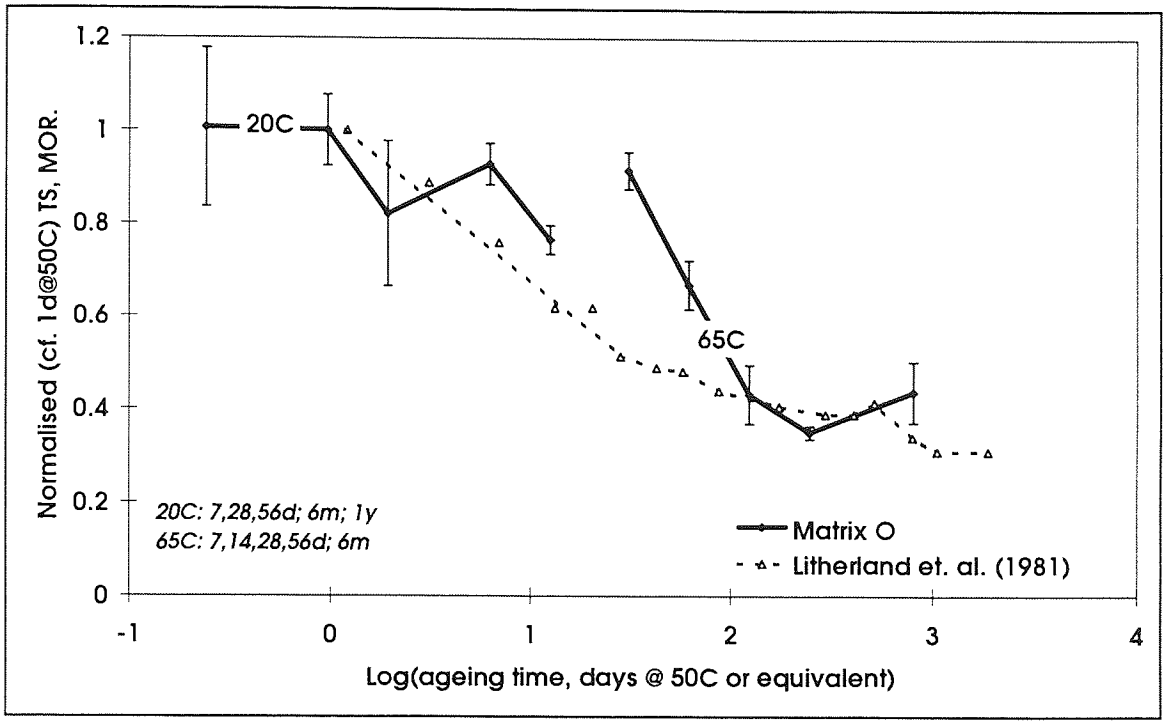

Figure 5.33. Matrix M: Normalised ageing behaviour cf. Litherland data.

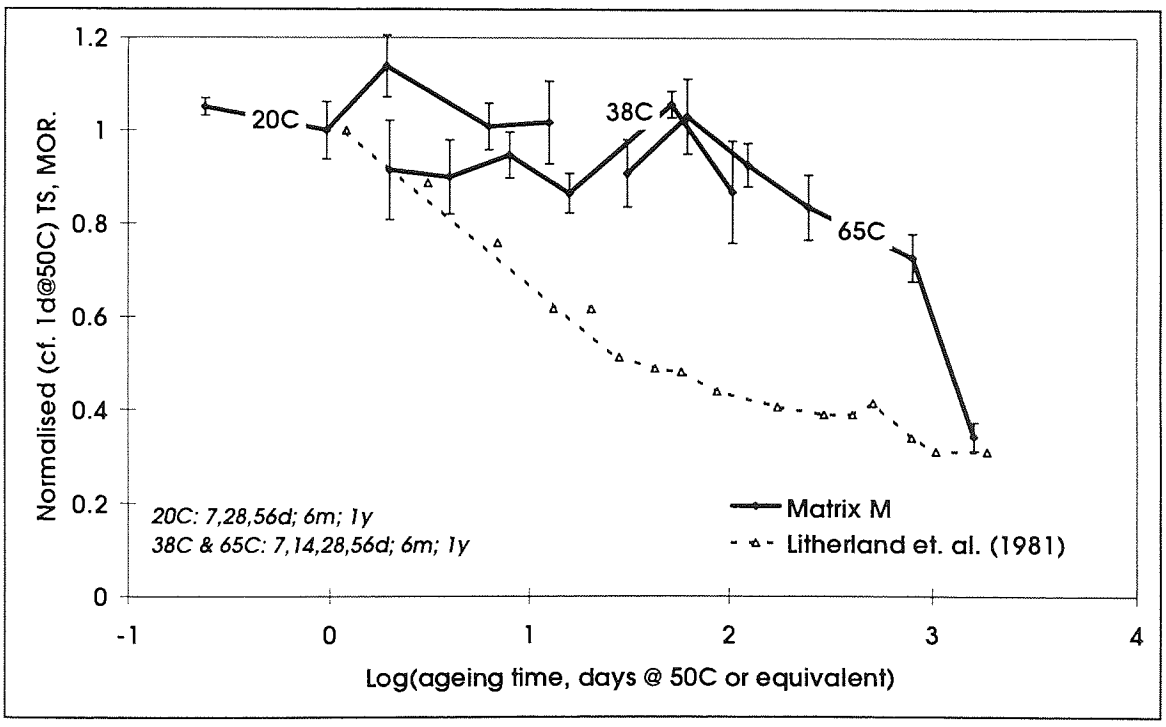

Figure 5.34. Matrix C: Normalised ageing behaviour cf. Litherland data.

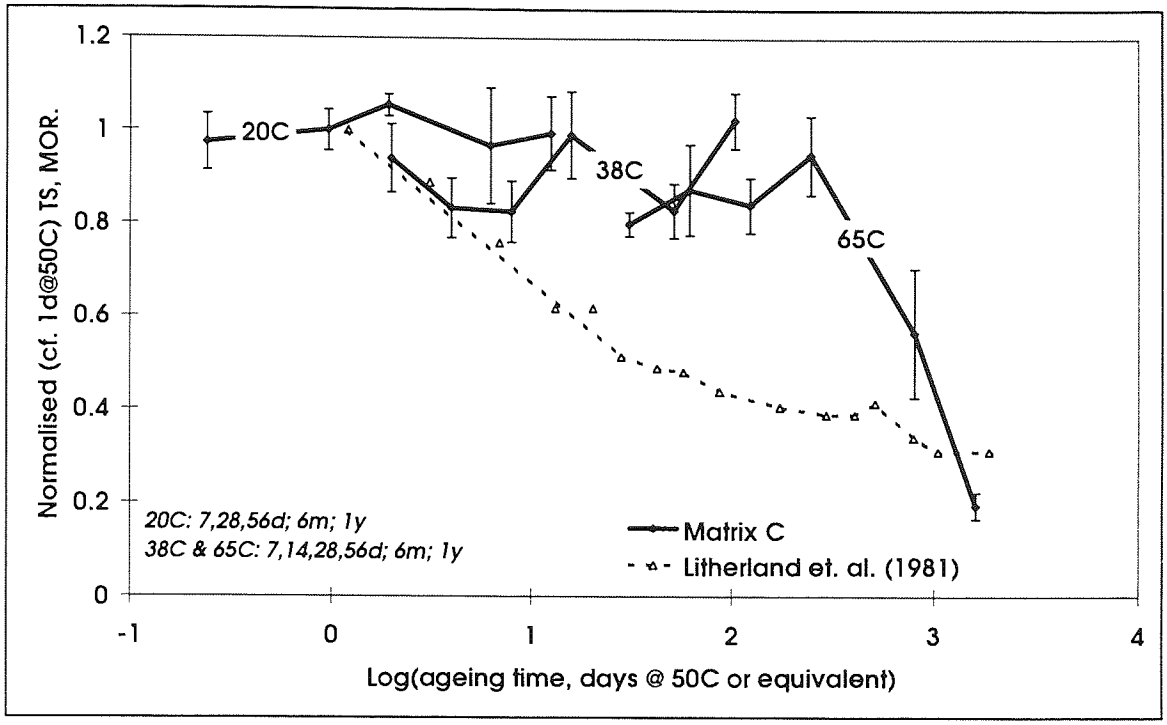

If the model were wholly valid, we would have expected a reasonable fit between the time-normalised experimental data and the Litherland data. Small discrepancies were expected since the model is based on flexural strength rather than tensile strength and was formulated using first-generation AR fibre (CemFIL I) rather than currently available fibres (although Litherland [1985] later compared results from second-generation fibre composites favourably with the model).

For matrix O (Fig. 5.32) it would be difficult to interpret the normalised 20°C data and the later normalised 65°C data as following the trend of the Litherland data; in particular, the samples aged for 7 and 14 days at 65°C appeared to perform rather better than suggested by the model. A more pronounced departure from the model predictions was evident for the new matrix composites (Figs. 5.33, 5.34) due to the additional 38°C data bridging the gap between the other data. Neither matrix M or matrix C composite behaviour could be interpreted as fitting the model at any stage. One interpretation might be that there is a pseudo-dormant period of negligible strength loss prior to the onset of degradation.

Further evidence for the invalidity of the model, especially with respect to the new matrix composites, was obtained by comparing the experimental data for composites aged at 65°C with Litherland's data for composites aged at 60°C on the same (i.e. not normalised) time axis (Fig. 5.35). The MORs of the Litherland data have been normalised to the first point of the data (≈2 days) and the experimental data to the 0 day values (which cannot be plotted on the log scale). The error bars have been omitted for clarity.

If the composites behaved in the same way as those used in Litherland's model, the difference in temperature should mean that their strength/time curves should be parallel and slightly below the Litherland curve.

Figure 5.35. Composite ageing behaviour at 65°C cf. Litherland (1981) data for ageing at 60°C.

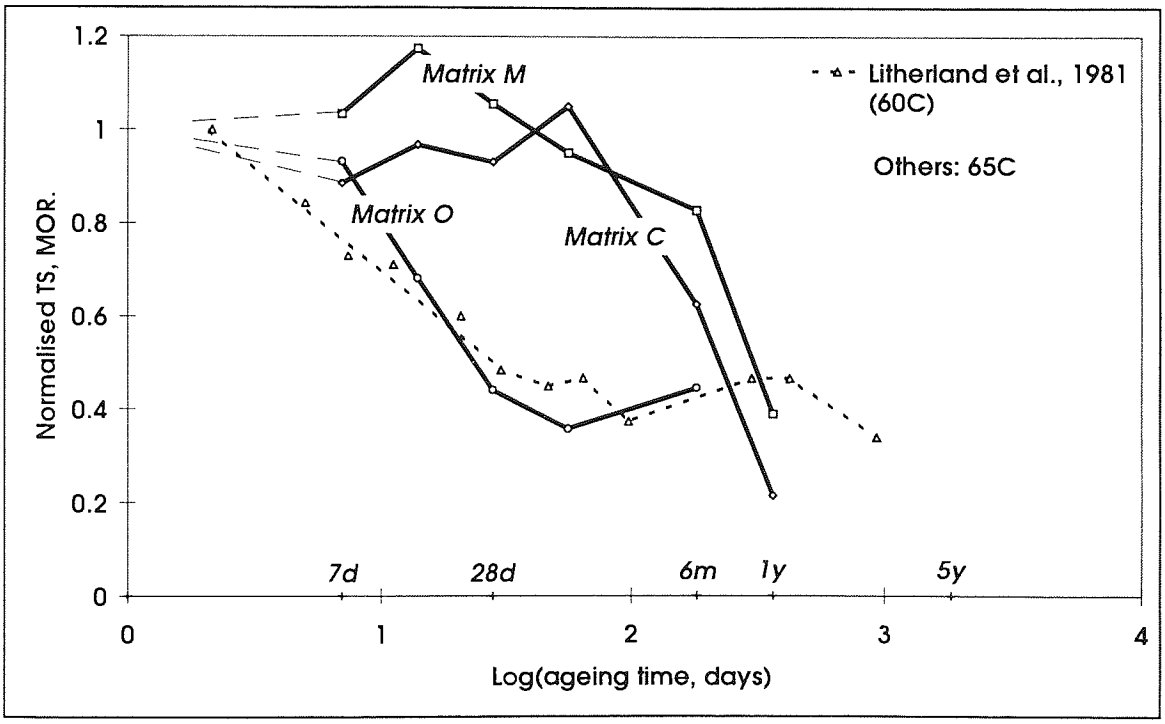

For matrix O, the fit was reasonable although the early strength was higher than in the Litherland data. The new matrix composites again did not agree with the data used in the model. For matrix C, a pseudo-dormant period was clearly evident (up to about 2 months). For matrix M, it was less clear although there was definitely a more complex relationship than strength $\propto$ 1/log[time] in evidence.

The introduction of a pseudo-dormant period to account for these departures from the predictions is inelegant; furthermore it is not clear what physical significance such a period would have. It is more likely that there is a non-linear dependence between strength and log[time] i.e. there is no single thermal rate determining step controlling the degradation process and the Arrhenius relationship (Fig. 2.5) does not hold. An alternative approach is discussed in Chapter 8.

5.5. Summary of main findings.

The main findings of the mechanical testing programme were;

- None of the composites exhibited any significant degradation of primary mechanical properties after 1 years immersion at 20°C.
- The new matrix composites also exhibited no degradation after 1 year at 38°C; this surprising result precluded the direct comparison of the accelerated ageing regimes with the existing model.
- Under ageing at 65°C, all composites were completely degraded; matrix O composites after 28 days, matrix C and M composites between 6 months and 1 year. The time taken for a 50% degradation of the primary mechanical properties to be effected ($t_{50\%}$) was 8 to 11 times longer for the new matrix composites than for matrix O composites.
- The cyclic ageing regime (and in the new matrix composites, the carbonating regime) caused substantial matrix damage and a corresponding loss of pre-cracking properties and the multiple cracking region. This was most likely due to the nature of the samples used in this project and would most likely not be observed in commercial composites, as suggested by the behaviour after cyclic ageing of the pre-fabricated material supplied to the project.
- Matrix O composites showed a marked increase in matrix strength after 4 months of accelerated carbonation.
- Although direct comparisons with the 'Litherland' accelerated ageing model could not be made (see above), indirect comparison was effected by normalising the times at different ageing temperatures on to a single time axis and comparing results with the data used in the formulation of the model. The comparison shows

that matrix O composite results could be loosely interpreted as fitting the model. The results for the new matrix composites however did not fit the model at all. There appeared to be a pseudo-dormant period before the onset of significant strength loss that is not accounted for by the model.

6. RESULTS; MICROSTRUCTURE.

Note: the figures are presented at the end of each section.

6.1. Thin section microscopy.

In the petrological microscope, light passes first through a polarising plate (the lower polar), then through the sample stage, through a second polariser (oriented at right angles to the first, called the analyser) and into the eyepiece for observation. The field of view will be black if no sample is on the stage. If a thin section is placed on the stage, coloured images of any crystalline forms in the sample will generally be seen.

This is due to the polarised light passing through the sample being doubly refracted and split into two rays by the crystals. The two rays have travelled through the crystal in two different directions and since the refractive index of the crystal is different for each direction, they will emerge out of phase. They will also have planes of vibration at 90° to each other. The difference between the two refractive indices is known as the birefringence of the crystal.

When the two rays enter the analyser, only their components in its polarisation plane can be transmitted. The two rays therefore emerge vibrating in the same plane but out of phase. The resultant interference is interpreted by the eye as a *polarisation colour.* The colour obtained is dependent on the birefringence of the material and the thickness of the section. Since each crystalline material has a particular birefringence, if samples are cut to a known thickness (generally 30μm) then the polarisation colours observed can be used to identify materials.

The sample stage is generally able to be rotated and graduated in degrees to exploit another polarisation phenomenon, extinction. As the stage is rotated, one or other of the polarisation planes in the crystal becomes parallel to that of the lower polar. Light from the lower polar passes straight through the crystal and is consequently cut out by the analyser. The crystal will appear completely dark four times during each complete revolution of the stage. Generally, extinction occurs when some crystallographic direction is parallel to the cross hairs in the eyepiece. Some minerals exhibit

extinction at an angle to the cross-hairs and this angle can be measured and used diagnostically.

(For a more rigorous explanation, see e.g. Blyth & De Freitas, 1990; St John *et al.*, 1998).

6.1.1. Application to GRC.

When examining GRC then, in principle:

- The glass fibre strands should appear as a group of black circles.
- The resin used to impregnate the samples should also appear black.
- Calcium hydroxide crystals should appear bright yellow.
- Calcite crystals have a very high birefringence generally manifesting itself as very pale pastel colours or white.

6.1.1.1. Departure from ideal conditions.

The first departure from these ideal cases was caused by 'strain birefringence'. If the resin in the sections contains any residual stress the polymer molecules become partially aligned, causing it to polarise the light transmitted through it, and it will appear bright rather than dark. Strained resin could be clearly distinguished under the microscope from crystalline material by its non-uniform extinction and its characteristic colour (bluish grey). However, in the photographs the distinction is less clear and where confusion might occur over the nature of inter-filamental material it has been described. Less frequently, strain birefringence was exhibited by the fibres, characterised by a substantial variation in brightness across the fibre, especially with the shift plate in. In the extreme, the fibres cross-section may appear 'domed'.

The other main departure was that during preparation, the difference in hardness between the glass fibres and the cement matrix resulted in non-uniform thickness of the slides. Often, crystals associated with the fibre bundles appeared 'over-thick' and the polarisation colours, particularly of portlandite, appeared 'higher' than expected tending towards red or purplish. The opposite effect was occasionally observed away from the fibres. Thus, the identification of minerals by colour had to be undertaken with some care.

It should also be noted that compared with normal geological sections, the crystals in the matrix are very small, often much smaller than the 30μm standard slide thickness. The background matrix away from large crystals therefore appears generally dark and often amorphous, as at any point of interest there may be a number of very fine crystals stacked randomly on top of one another which will transmit no polarised light. To study individual cement matrix crystals, very thin sections must be prepared.

6.1.1.2. Specific techniques.

Two specific techniques were applied to aid the study of GRC samples.

Since both the matrix and the fibre bundles appeared dark under normal petrological examination conditions, the images captured were lacking in contrast. By slightly de-crossing the analyser and polariser so they were crossed at about 75-80° rather than 90° the fibre bundles transmitted a little light providing some contrast to the matrix. The crystalline material retained its polarisation colours, albeit slightly 'diluted' by the extra light.

Where de-crossing did not provide enough contrast, particularly at high magnification, 'shift-plates' could be used to highlight the non-crystalline material. The plate most used in this study shifted the wavelength of all the light entering the eyepiece by 530nm, giving the non-crystalline material a bright cerise red colour. The colours of crystalline material with low or medium polarisation colours were also changed.

The crossing angle of the polars and the use of the shift plate is noted along with each description, e.g. (+75°) represents polars crossed at 75°.

6.1.2. Matrix O.

Fig 6.1a, (+75°), 0 day. No deposits were seen either on or between the fibres. There was very little ingress of general matrix material into the strand. Unhydrated clinker and portlandite crystals could be seen throughout the matrix (the crystal seen just

above the strand is portlandite. Note that the colour is not just yellow as expected but contains blues and red owing to the slide over-thickness near the strands).

Fig. 6.1b, (+75°), 56 days immersion at 20°C. Isolated well formed portlandite deposits could be seen within or associated with the outer filaments of the strands, particularly where the fibres are well dispersed. There was little ingress of general matrix material (i.e. 'groundmass' material other than unhydrated clinker or portlandite) into closely packed strands although dispersed filaments are well surrounded. This figure also shows an unusally well dispersed strand.

Fig. 6.1c (+78°), 1 year immersion at 20°C. More extensive crystalline deposits are apparent within the strands, these being identified as finely crystalline calcium carbonate, probably as calcite but possibly aragonite. There was still some void space between the fibres. The matrix appeared to be more uniform with fewer large inclusions, and in more intimate contact with the fibres although it had not completely penetrated the strands. In general, the strands appeared to be more closely packed than in younger samples. At higher magnifications, it was possible to see that some fibres, especially those close to the calcite deposits, exhibited slight strain birefringence indicating that they were under stress.

Fig. 6.2a, (+77°), 56 days immersion at 65°C. Portlandite deposits were observed within the fibre bundles, similar to but slightly more extensive than those observed after 56 days at 20°C. Many strands also exhibited fine portlandite deposits along much of the fibre/matrix interface. Ingress of general matrix material into the strands was not extensive and in this respect was similar to that at 56 days at 20°C.

Fig. 6.2 b & c, (530nm shift plate in [note pink colour of fibres]), 1 year immersion at 65°C. The strands were well penetrated both by matrix material and crypto-crystalline calcite or aragonite. Occasional large crystals of calcite could often be seen associated with the strand (Fig. 6.2c). Many of the fibre cross-sections no longer appeared circular, probably indicating substantial fibre corrosion. Some fibres

exhibited slight strain birefringence. The matrix was well hydrated with very few distinct crystals or inclusions.

Fig. 6.3a, (+78°), 56 days of cyclic ageing. No crystalline deposits were observed in the strands but they were generally well penetrated by the matrix. The matrix was well carbonated and no distinct portlandite crystals were observed.

Fig. 6.3b, (+78°), 4 months of carbonation. The matrix was similar to the cyclically aged sample but a rim of fine, well crystallised calcite was associated with the strand perimeters. There appeared to be little matrix ingress or material between the fibres. Quite distinct strain birefringence of the fibres was often observed.

Figure 6.1. Matrix O thin sections, 20°C ageing.

a.

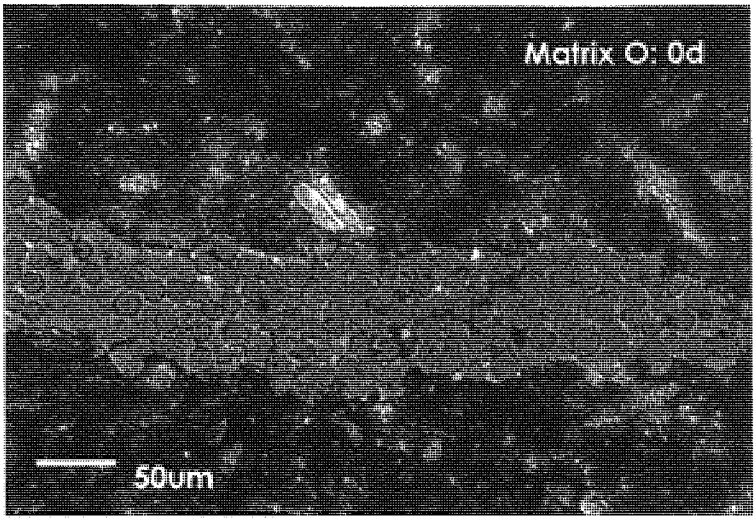

b.

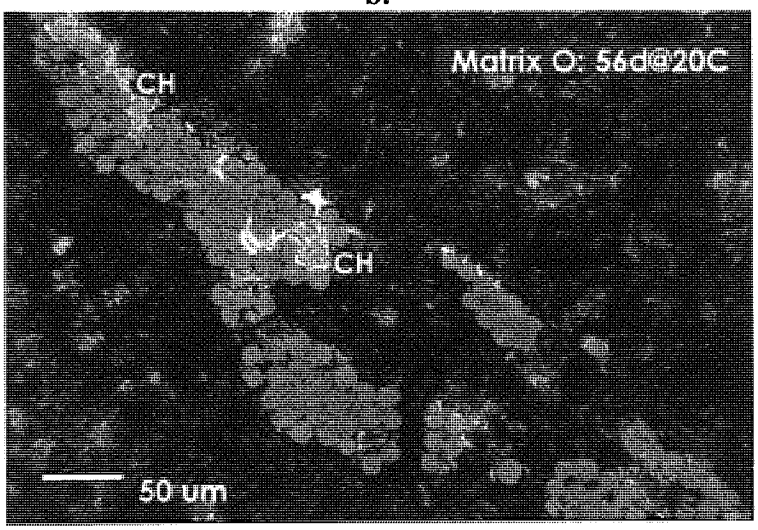

c.

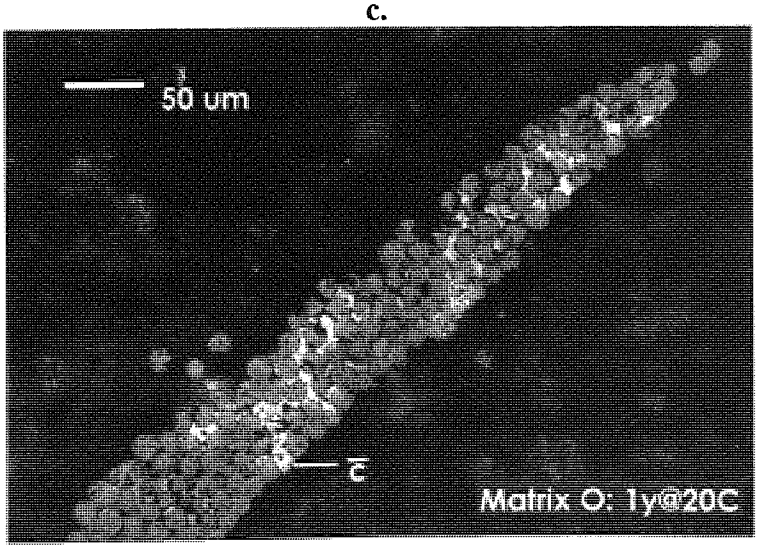

Figure 6.2. Matrix O thin sections, 65°C ageing.

a.

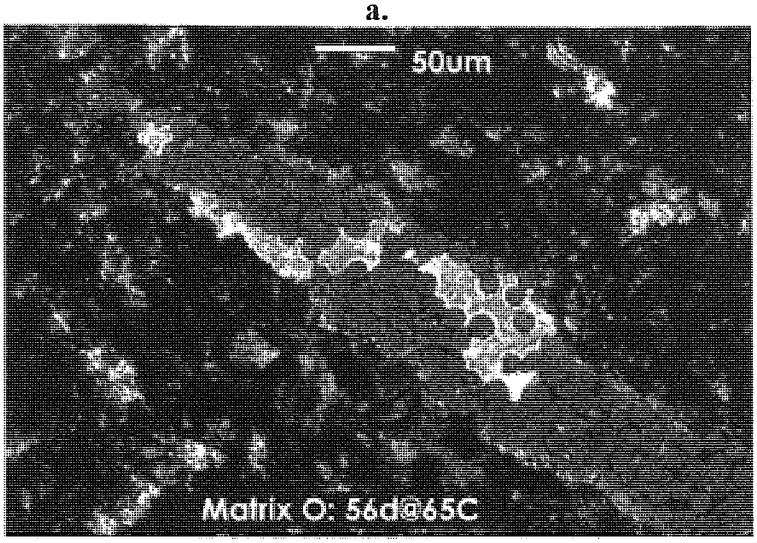

b.

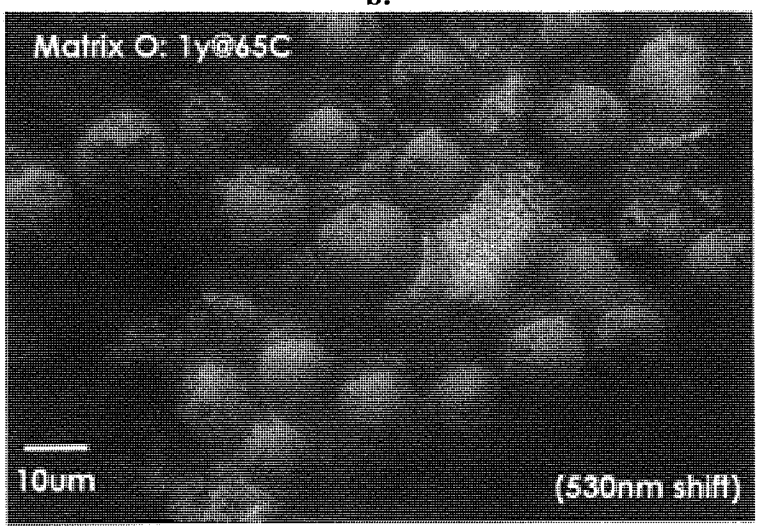

c.

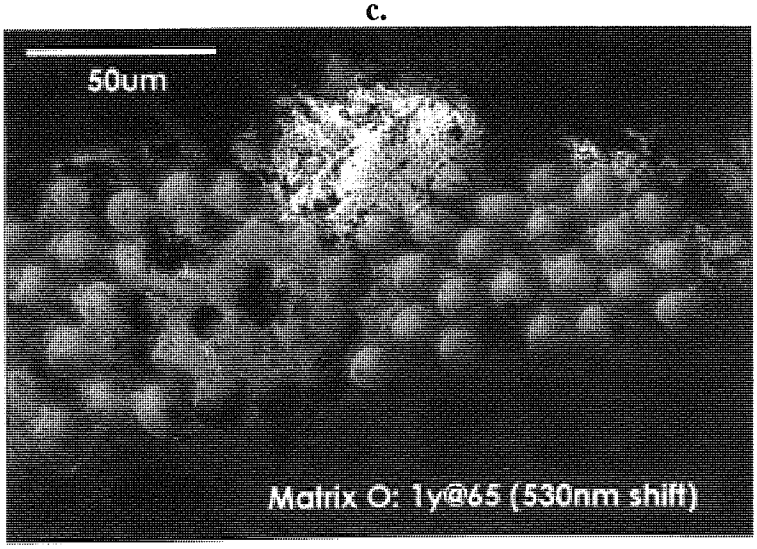

Figure 6.3. Matrix O thin sections, cyclic ageing and carbonation.

a.

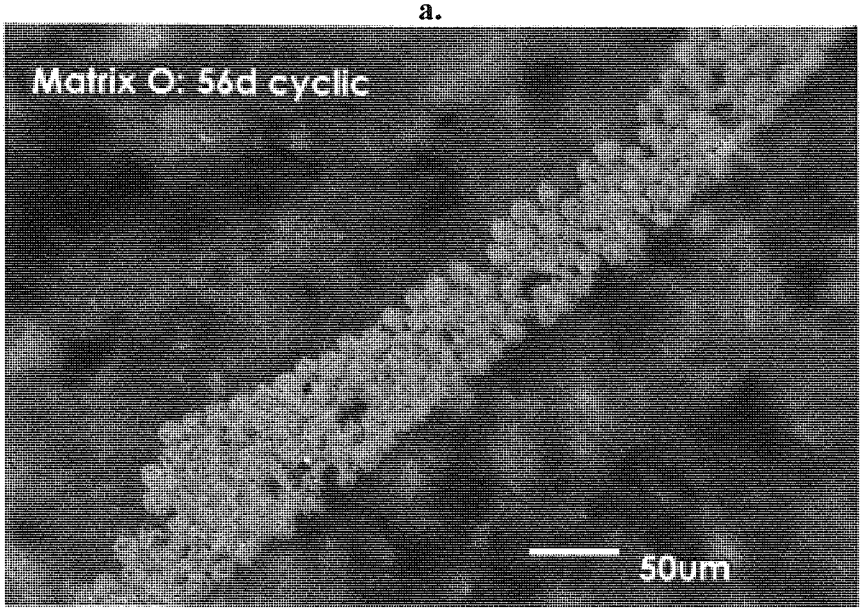

b.

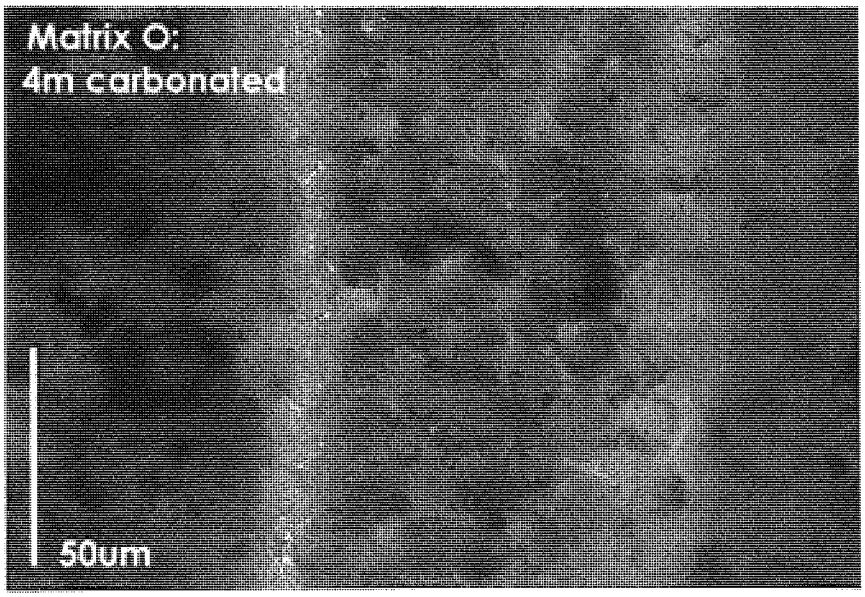

6.1.3. Matrix M.

Fig. 6.4a, (+80°), 0 day. The matrix, compared to matrix O, appeared to consist of fewer, smaller distinct crystals embedded in a very finely crystalline groundmass. The matrix had not penetrated the strands and a fine rim of portlandite enriched matrix was associated with the strand perimeters. No crystals were observed between the fibres; the bright spots seen in the image are due to strain birefringence of the resin. Some fine, dark inter-filamental material can be seen (top right of strand) which may be unreacted meta-kaolin.

Fig. 6.4b, (+80°), 56 days immersion at 20°C. A very prominent 'halo', about 50μm in width, was observed around all the strands. The halo appeared to consist of interspersed very fine crystals of calcite and portlandite. No crystals were observed between the fibres except where the halo encroached into larger gaps between the filaments, although the dark inter-filamental material is still present.

Fig. 6.4c, (+80°) 1 year immersion at 20°C. The halo was narrower but brighter and appeared to consist solely of fine calcite crystals. The matrix was more featureless than at 0 days and the clinker was well hydrated. Some ingress of matrix into the strands could be observed.

Fig. 6.5a, (+80°) 56 days immersion at 65°C. The matrix was rather more featureless than at 0 days and appeared dense. A slight halo of mostly carbonated material was evident around most of the strand. Where it was absent, matrix ingress was enhanced. The dark inter-filamental material appeared to have been incorporated into the penetrant, being morphologically massive rather than as isolated particles.

Fig 6.5b, (+78°) 1 year immersion at 65°C. The matrix was very dense and featureless apart from dark flecks, probably unreacted metakaolin. Partial halos of carbonation were apparent. Matrix ingress was substantial. Under high magnification, the fibres appear marked which may be indicative of corrosion or other damage.

Fig. 6.6a, (+75°), 56 days of cyclic ageing. The matrix was well hydrated but extensively cracked. The crack paths tended to intercept strands; the bright material in the cracks and within the strands is resin exhibiting extreme strain birefringence. Little carbonation appeared to have taken place (despite the XRD and DTA/TG evidence that carbonation was well advanced [Chapter 4]) and few strands had any halos. There was little ingress of matrix into the strands.

Fig. 6.6b (530nm shift plate) 4 months of carbonation. The carbonated sample shows the advancement of the carbonation front in that the the light areas of carbonated matrix are separated from the uncarbonated matrix by the fibre strands. Again, the matrix is cracked although less so than in the cyclically aged samples, and there is little matrix ingress into the strands.

Figure 6.4. Matrix M thin sections, 20°C ageing.

a.

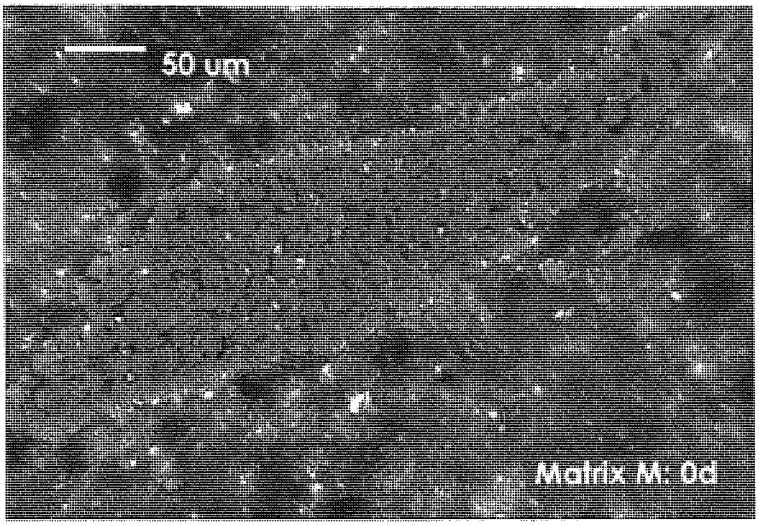

b.

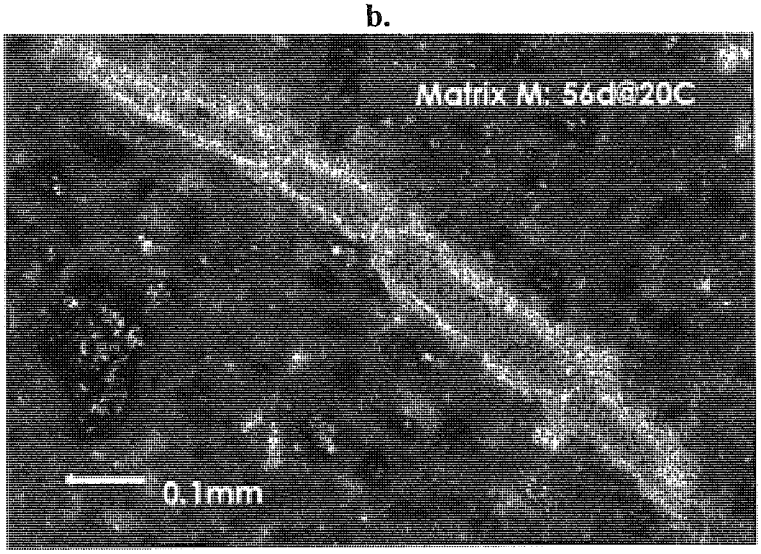

c.

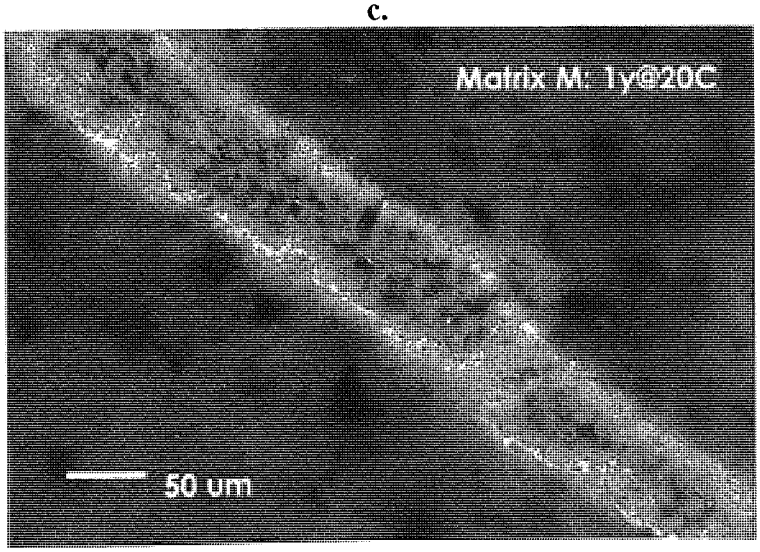

Figure 6.5. Matrix M thin sections, 65°C ageing.

a.

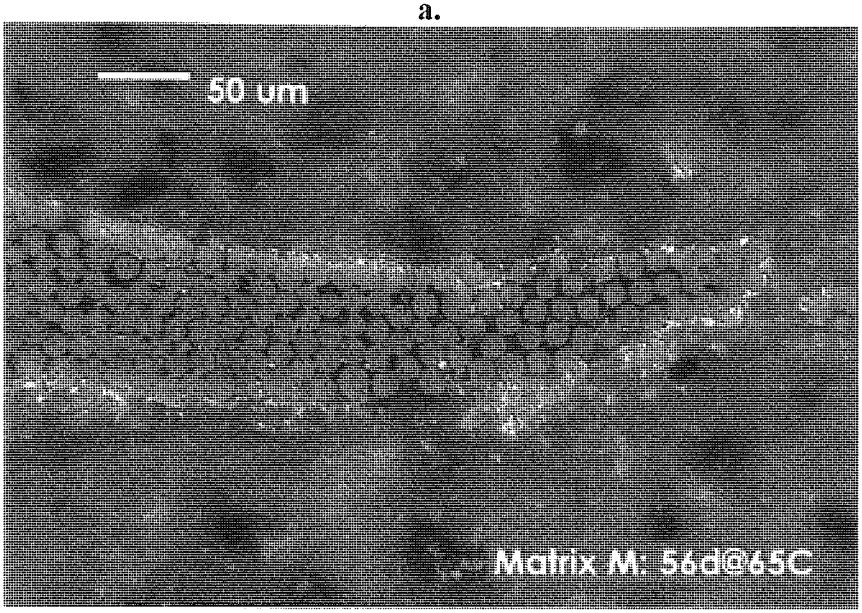

b.

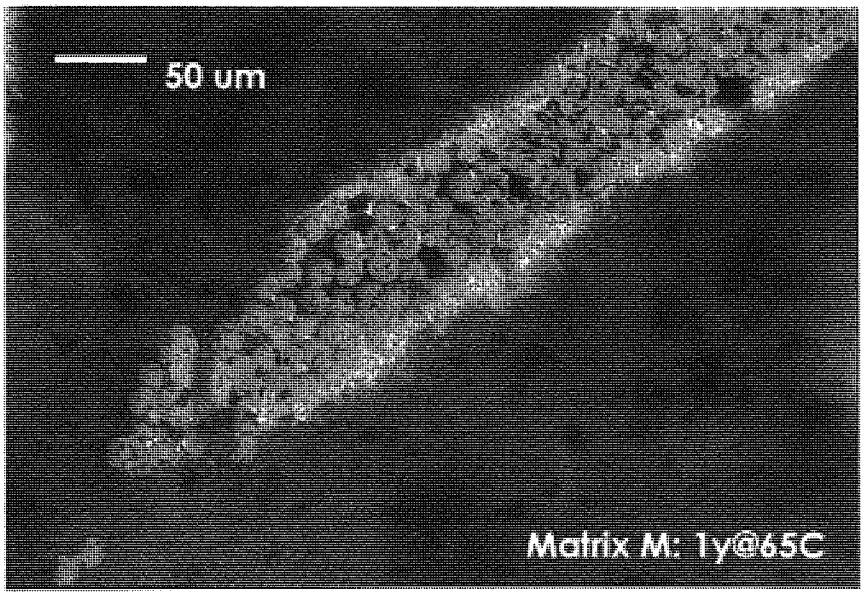

Figure 6.6. Matrix M thin sections, cyclic ageing and carbonation.

a.

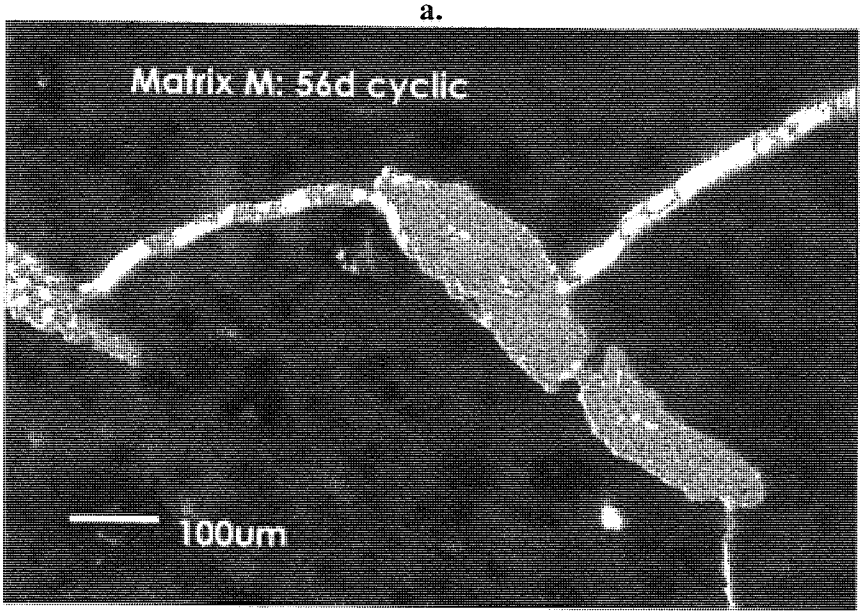

b.

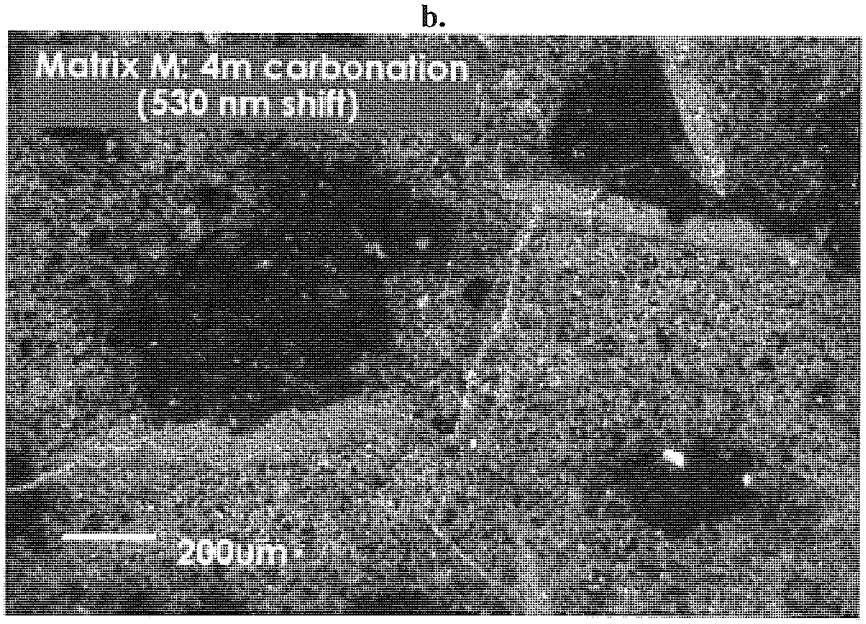

6.1.4. Matrix C.

Fig. 6.7a, (+75°), 0 day. Matrix C has an even finer, featureless groundmass, and is less granular than either of the other matrices. The matrix had penetrated well into the strands and the inter-filamental material appeared no different to the general matrix. No halos or other interfacial phenomenon were observed. No distinct portlandite crystals were observed in the matrix.

Fig. 6.7b, (+80°), 56 days immersion at 20°C. No significant differences to the 0 day samples were observed. This figure also shows a strand that has debonded during tensile testing - a distinct band of resin can be seen between the outer filaments and the matrix and the coastline of the matrix clearly shows that it was previously in intimate contact with the strand perimeter. Note that the debonded strand still contains a substantial amount of inter-filamental matrix material (the bright inter-filamental material is strained resin). This shows that the reinforcement acts as a strand rather than as individual filaments even when the void space is almost completely filled and that taking the strand perimeter as the reinforcement perimeter is justified.

Fig. 6.7c, (+80°), 1 year immersion at 20°C. No significant differences between this and the previous two samples was observed apart from the increased homogeneity of the matrix.

Fig. 6.8a, (+80°) 56 days immersion at 65°C. These samples were also very similar to those described above.

Fig. 6.8b, (+75°) 1 year immersion at 65°C. It can be seen that the fibre bundles were completely filled by the matrix after a year at 65°C. As with the matrix M samples after similar ageing, there may have been some evidence of fibre corrosion. The groundmass is very homogeneous and accounts for most of the matrix.

Fig. 6.9a, (+78°) 56 days of cyclic ageing. The matrix was more granular than in the 0 day samples and was extensively cracked. Most fibres appeared debonded. However, there was very little matrix material between the fibres compared with 0

days which is surprising as one would not expect the interfilamental material deposits at 0 days to be removed by cyclic ageing. The matrix appeared carbonated on a fine scale. More extensive carbonation was observed in a fine layer at the edges of cracks and the debonded fibre/cement interface.

Fig. 6.9b, (+78°), 4 months of carbonation. Broad carbonated zones were often associated with the fibre strands although in a less obvious manner than in the matrix M composites (Fig. 6.6b). The most striking feature was large amounts of very dark inter-filamental material, especially where several strands were in close proximity, similar to that seen in the matrix M composites (6.1.3.2 above) but on a larger scale.

Figure 6.7. Matrix C thin sections, 20°C ageing.

a.

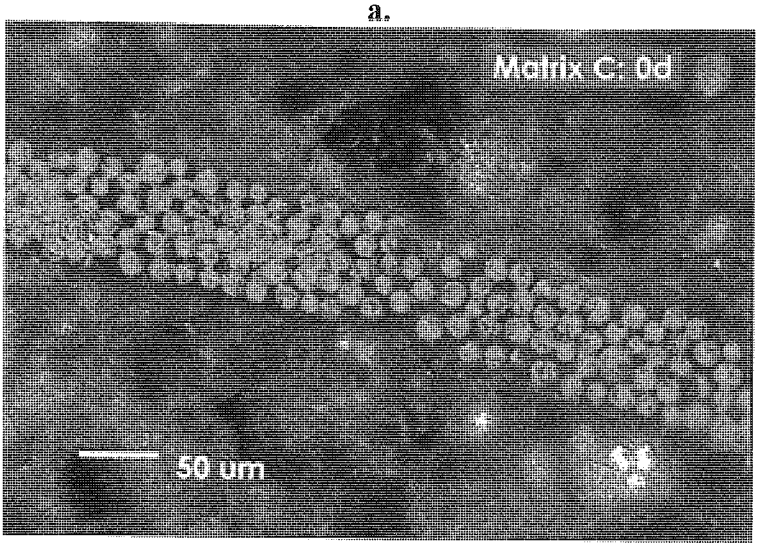

b.

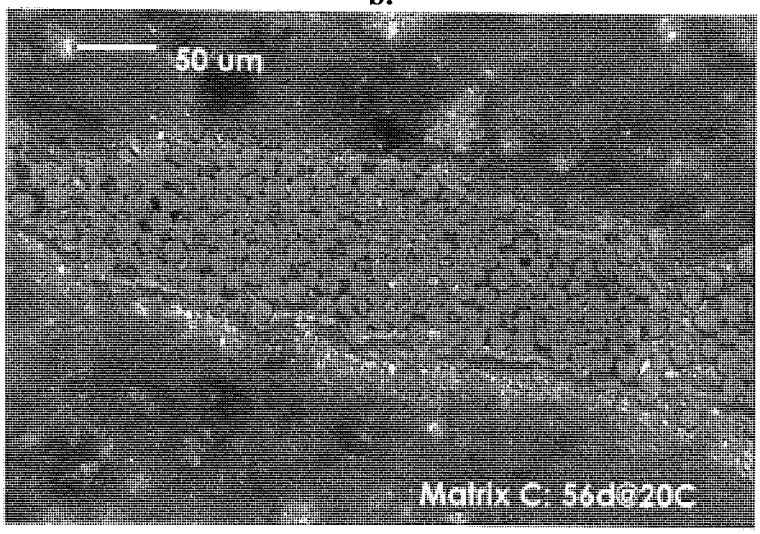

c.

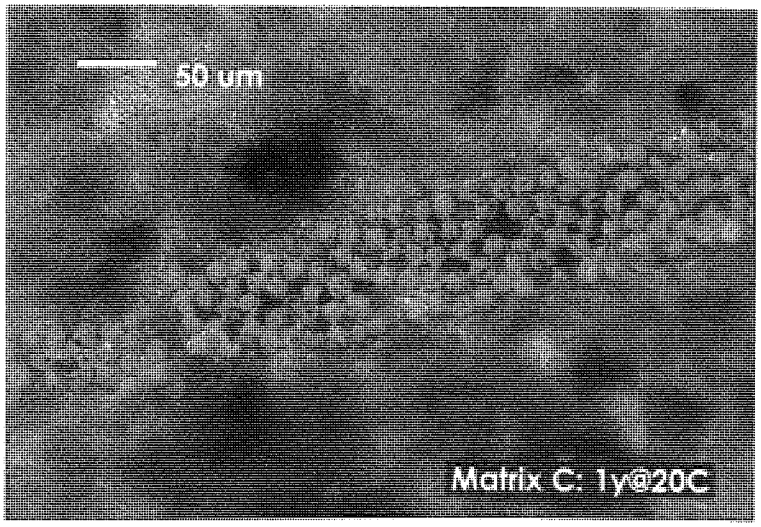

Figure 6.8. Matrix C thin sections, 65°C ageing.

a.

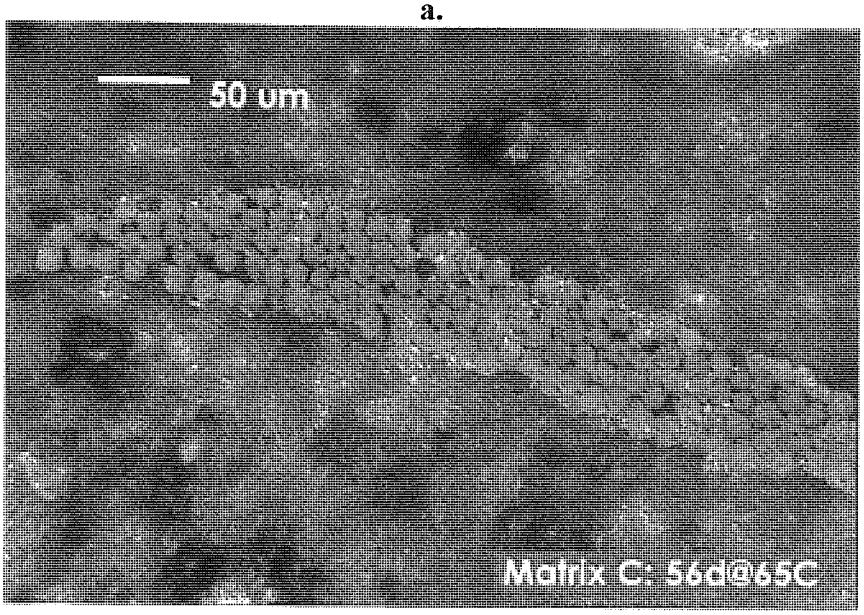

b.

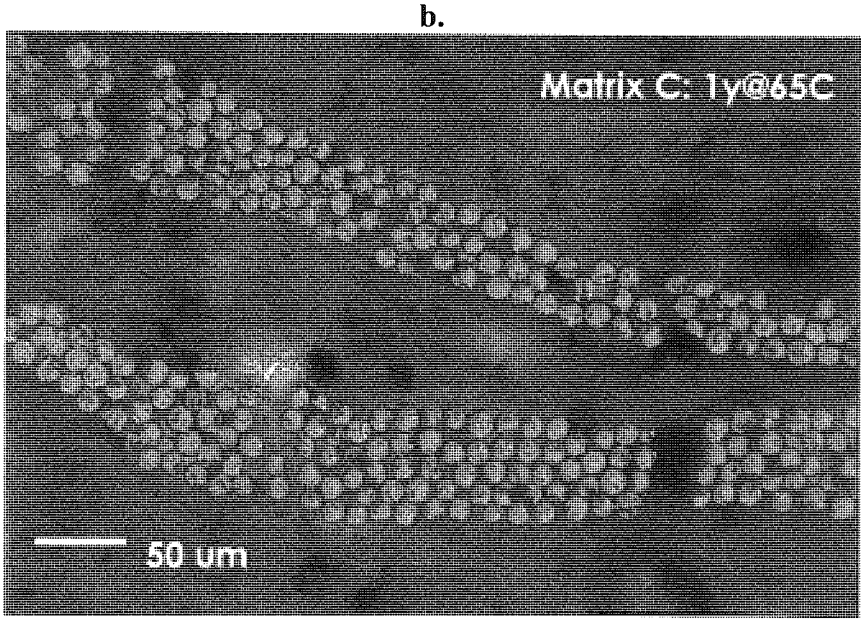

Figure 6.9. Matrix C thin sections, cyclic ageing and carbonation.

a.

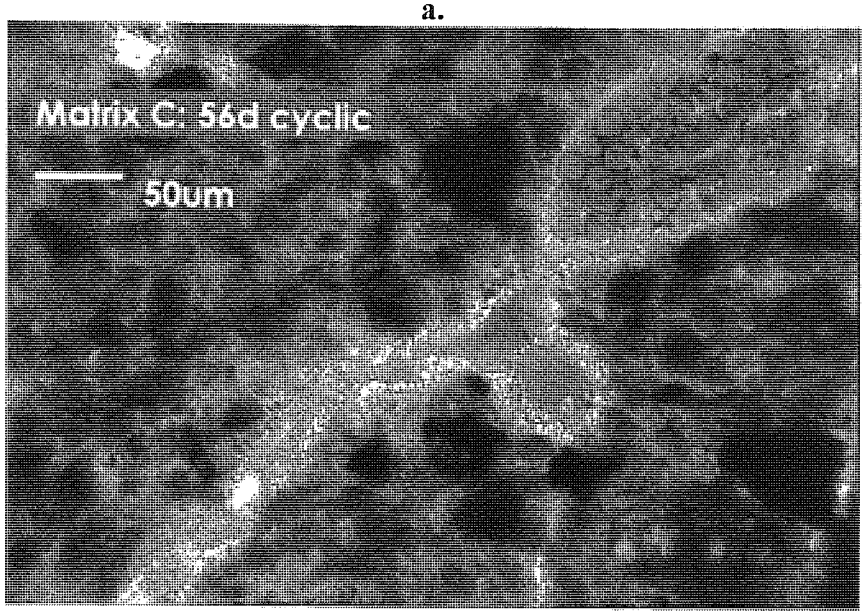

b.

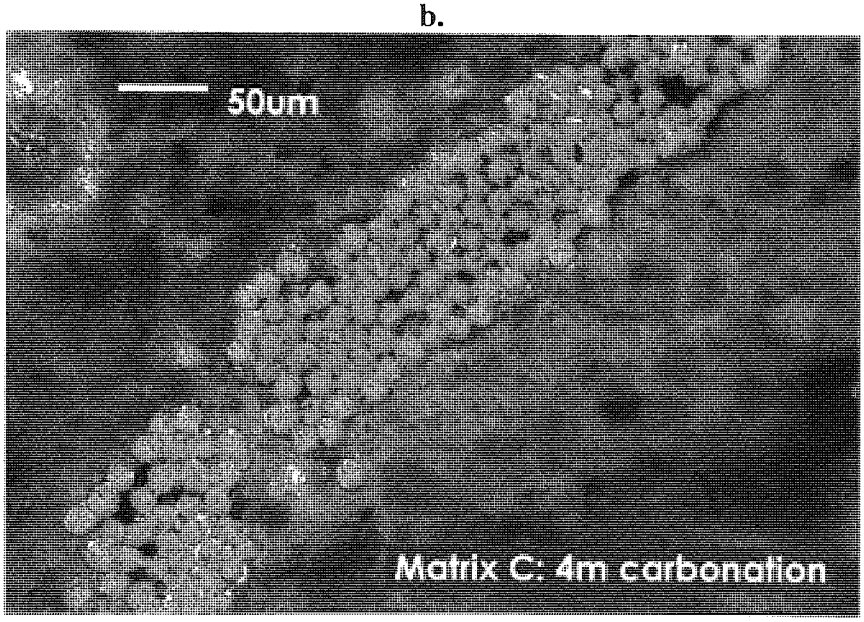

6.2. SEM.

A number of problems were encountered during the SEM studies of the composites. Early images (up to 28 days old) were captured photographically from 'true' fracture surfaces i.e. normal to the fibres. One disadvantage of this method was that relatively large samples had to be used, which proved difficult to dry (without using heat). This caused problems during gold sputter coating and subsequent examination; both processes require the sample chamber to be pumped down to quite hard vacuum and residual moisture in the samples greatly hindered this. Also, the unsupported fibres protruding from the fracture surface tended to 'wobble' as the camera shutter was activated causing blurring of the photographs.

Later (1 year and 6 month cyclic) SEM samples were made by artificially delaminating the samples i.e. fracturing parallel to the fibres to expose their length. This allowed smaller samples to be used which proved easier to evacuate. Since the fibres were now supported along their length they also had less tendency to wobble. Images were captured digitally (a facility only available in the later stages of the project) drastically reducing the exposure time and hence the likelihood of blurring. Another advantage of digital image capture was that the image captured was identical to that seen on the screen and the inevitable vagaries of photographic processing were eliminated.

Despite these improvements, the problem of poor gold coating proved difficult to avoid. In SEM, a beam of electrons is fired at a sample. Samples are coated in a very thin layer of conductive material (usually gold) to conduct away the charge build-up to earth. If the coating is not complete and uniform, then charge builds up at poorly coated spots on the sample. This phenomenon, known as 'charging' causes bright spots on the resultant image and can reduce overall image contrast. In the extreme, the charge build up may actually 'burn' the sample. The highly irregular and convoluted surface of the GRC specimens was not conducive to ease of coating. Two or three attempts normally had to be made to coat the sample sufficiently.

Note that carbonated samples were not examined by SEM; no fibre damage was expected due to the short (4 month) ageing period and the low temperature (RT).

From previous work, the samples seemed morphologically and chemically very similar to the cyclically aged samples, which were examined.

6.2.1. Matrix O.

The 0 day samples (Fig. 6.10a) showed a non-intimate interface and no deposits between the fibres. There was no evidence of any fibre damage. After 28 days at 65°C (Fig. 6.10b) some 'loose' inter-filamental material was observed and the interface was more intimate than at 0 days. (Some fibres on the right of the image show features which may be indicative of either a fine surface layer or slight damage).

After 1 year at 20°C (Fig. 6.10c) isolated deposits about 50-100μm in length could be seen clinging to the fibres as well as widespread smaller deposits seen in the close-up (Fig. 6.10d). No evidence of fibre damage was observed. After 1 year at 65°C (Fig. 6.10e) substantial quantities of dense inter-filamental material and adherent particles were observed. Fibre damage in the form of isolated pits (Fig. 6.10f) could be clearly seen although the general fibre surface remained smooth.

After 6 months of cyclic ageing (Figs. 6.10g,h), no evident fibre corrosion or massive inter-filamental deposits were observed. In close-up the fibres appeared coated with very fine material.

6.2.2. Matrix M.

The 0 day samples were very similar to those for matrix O. The image (Fig. 6.11a) shows the substantial fibre pullout - the protruding fibres had to be trimmed to allow them to fit in the SEM sample chamber. No significant differences between the 0 day samples and those aged for 28 days at 65°C were observed (Fig. 6.11b). Note the bright areas in the image, caused by charging (6.2 above).

After 1 year at 20°C large quantities of fine granular inter-filamental material were observed (Fig. 6.11c). The close-up (Fig. 6.11d) shows the fine nature of the material and the extent to which it coats the fibres. No fibre damage was observed. After 1 year at 65°C (Fig. 6.11e) this material appeared to have coalesced into distinct coatings

around the fibres. Under higher magnification (Fig. 6.11f) the coating can be seen to have been up to 3 or 4 microns in thickness and varying in nature from cotton-wool like material to thin veils normal to the surface. There was no direct evidence of fibre damage but the coating would have hidden any obvious signs.

Cyclically aged samples (Figs. 6.11g,h) also displayed fine granular material adhering to the fibres although on a lesser scale than under hot water ageing. No evidence of fibre damage was observed.

6.2.3. Matrix C.

The 0 day matrix C samples (Fig. 6.12a) appeared different to those for matrices O and M, the interface being more intimate. This was demonstrated by the tendency of the outer fibres of a strand to break close to the surface rather than pull out. After 28 days at 65°C (Fig 6.12b) this tendency has been slightly enhanced, producing the 'telescopic pullout' mode of failure described by Bartoš (1985; Zhu & Bartoš, 1993).

After 1 year at 20°C (Fig. 6.12c,d) inter-filamental material was observed, more than in matrix O but less than in matrix M composites. However, the delamination process appeared to have removed a lot of intimate interfacial material, of which the 'stripes' on the fibres are evidence. No fibre damage was observed. After 1 year at 65°C (Fig. 6.12e) large quantities of inter-filamental material were observed. In the bottom right of the image the 'channels' left by a fibre having been stripped by the delamination can be seen, showing the close contact between fibre and matrix. The rather poorly contrasted close-up image (Fig 6.12f) shows the end of a fractured fibre embedded in the matrix. As with the matrix M composites, evidence of fibre damage was likely to have been obscured.

Cyclically aged samples (Figs. 6.12g,h) showed little inter-filamental material but a rough fibre coating could be seen in close-up.

Figure 6.10 a-d. Matrix O SEM.

a.

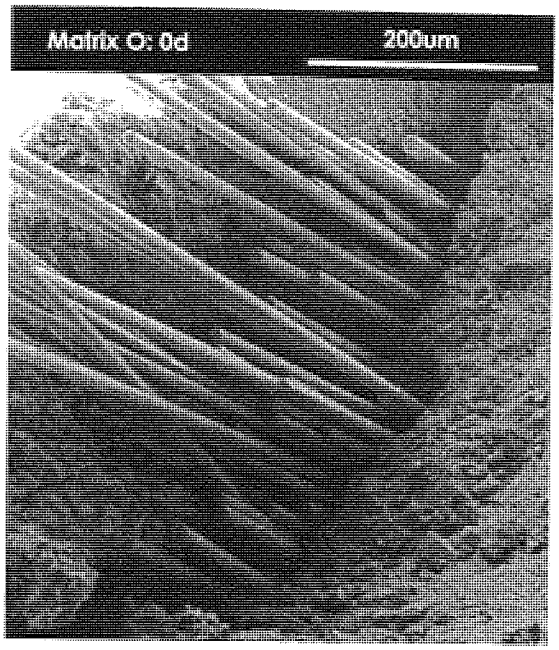

b.

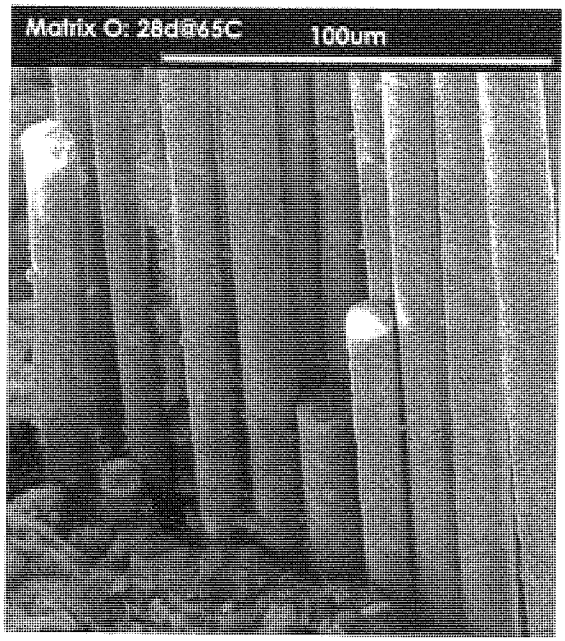

c.

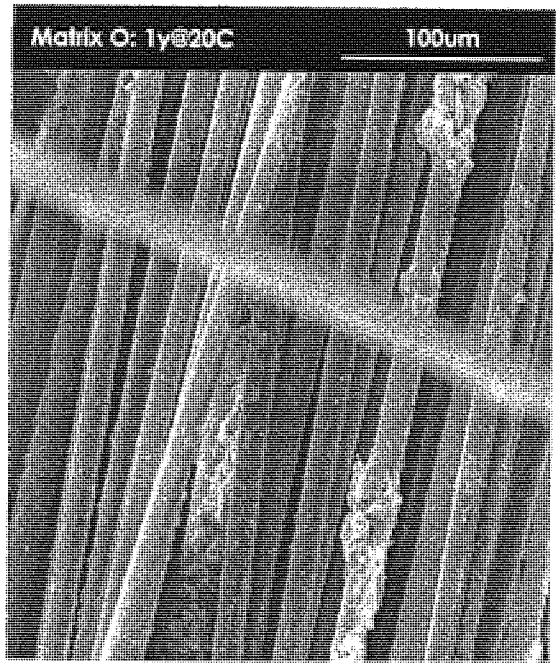

d.

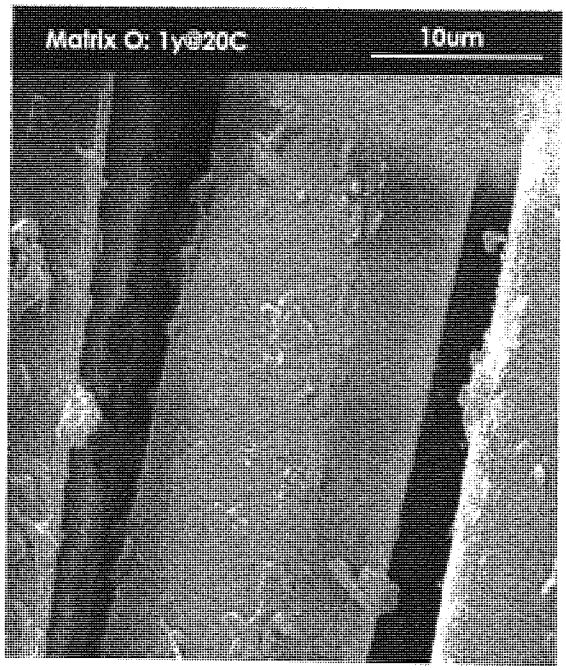

Figure 6.10 e-h. Matrix O SEM.

e.

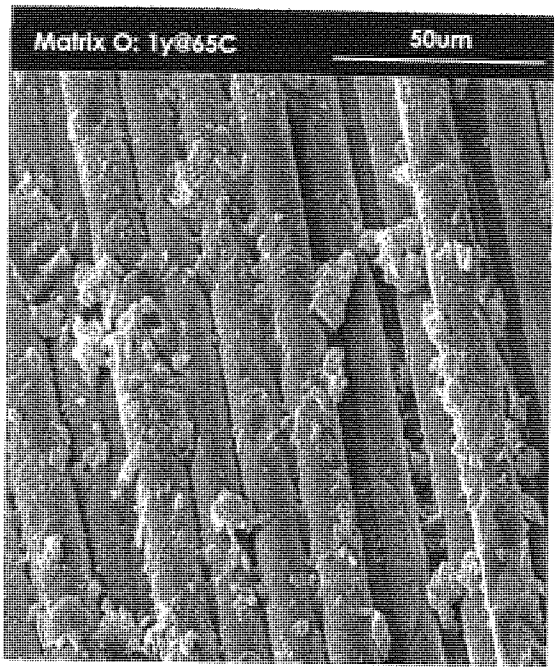

f.

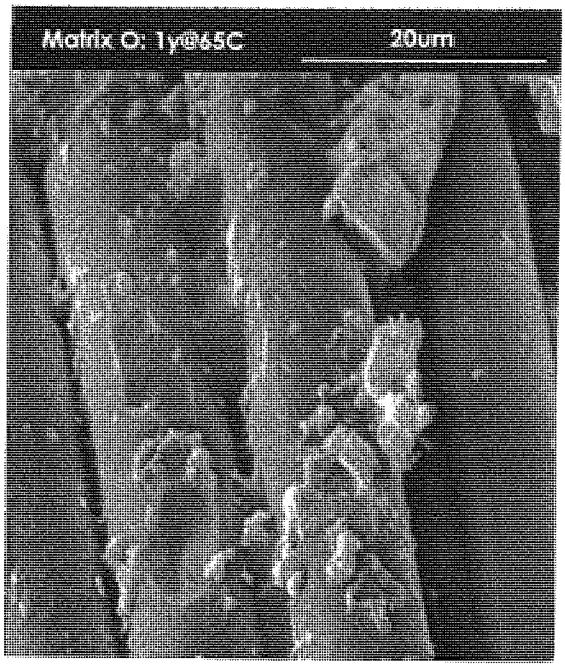

g.

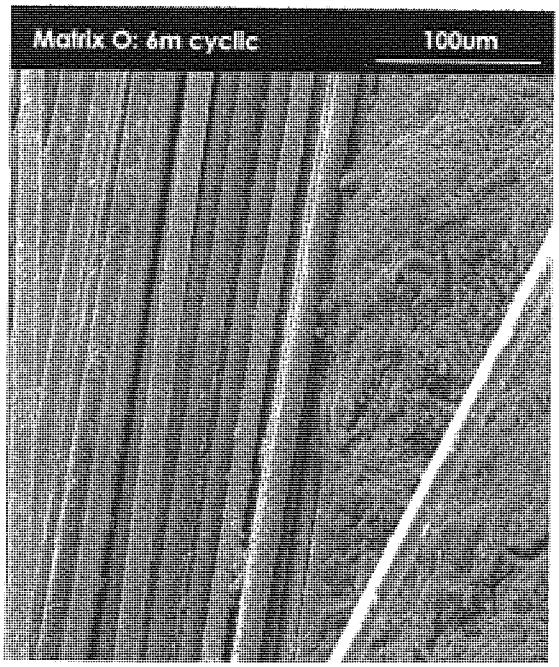

h.

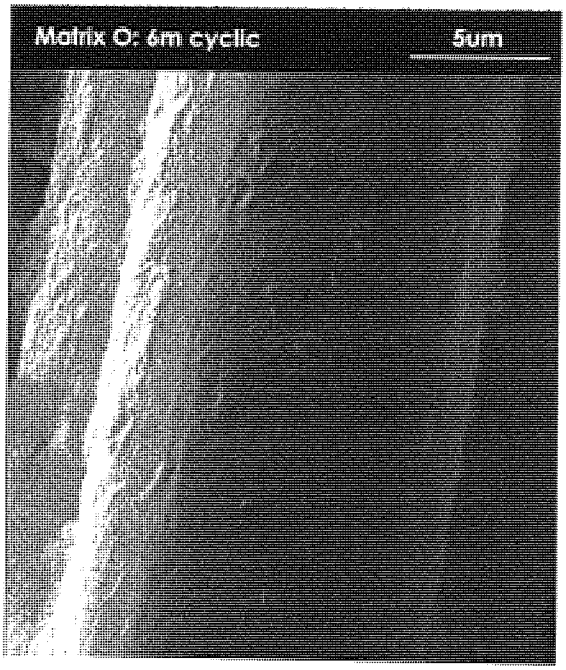

Figure 6.11 a-d. Matrix M SEM.

a.

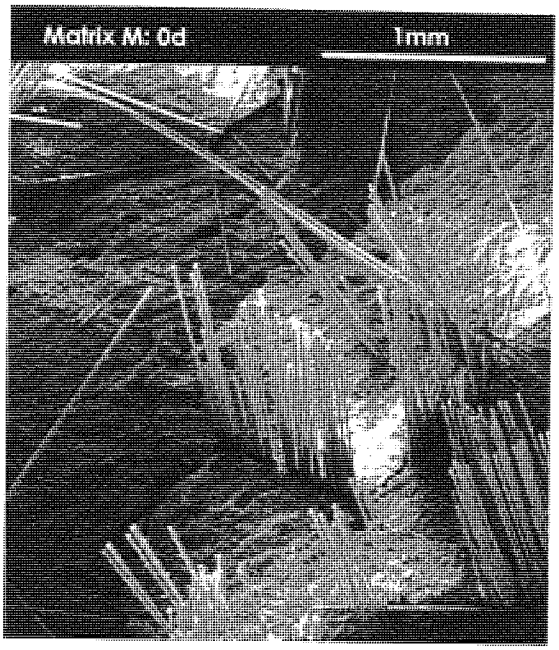

b.

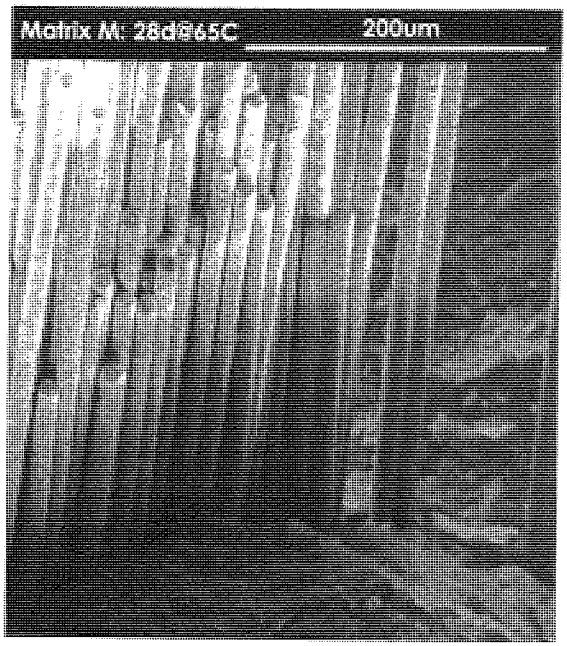

c.

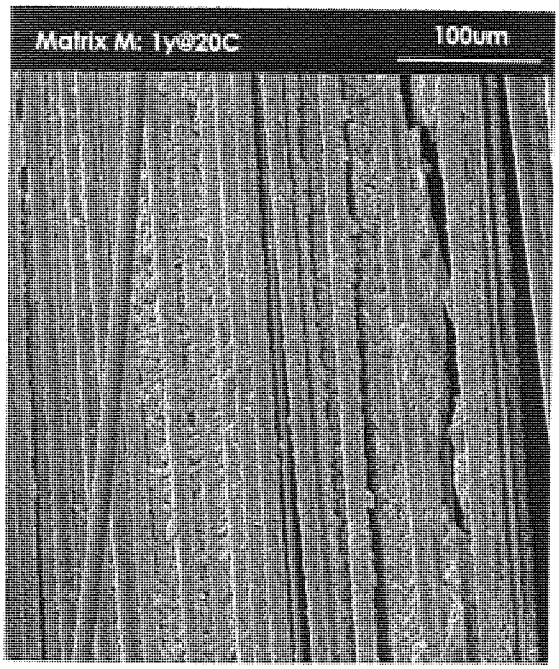

d.

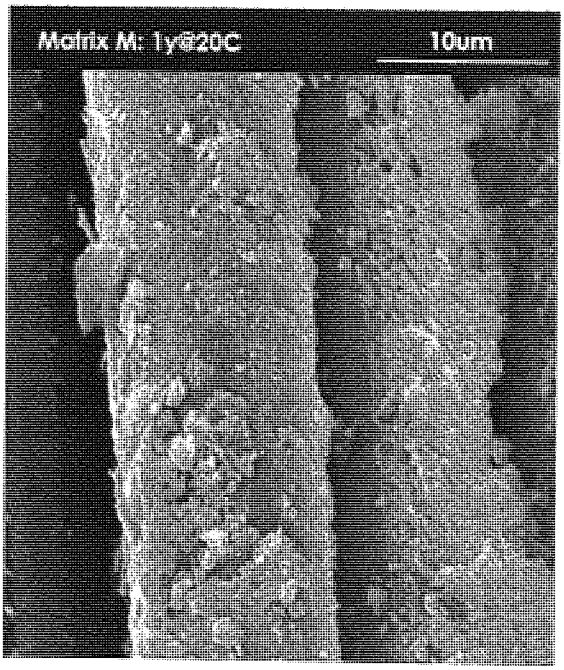

Figure 6.11 e-h. Matrix M SEM.

e.

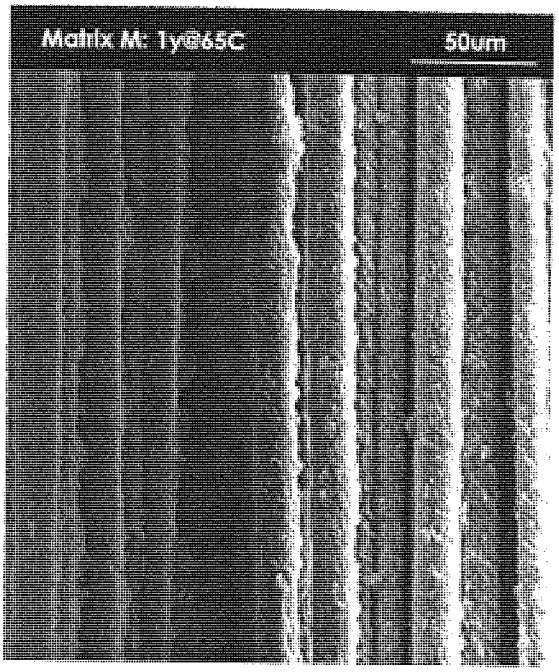

f.

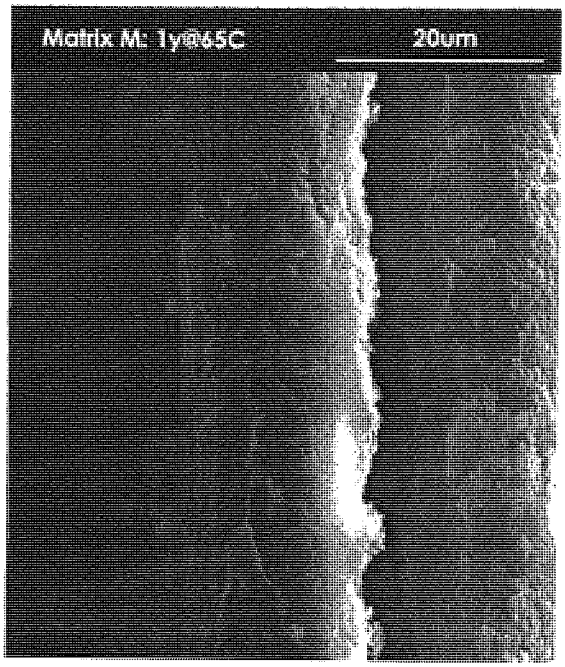

g.

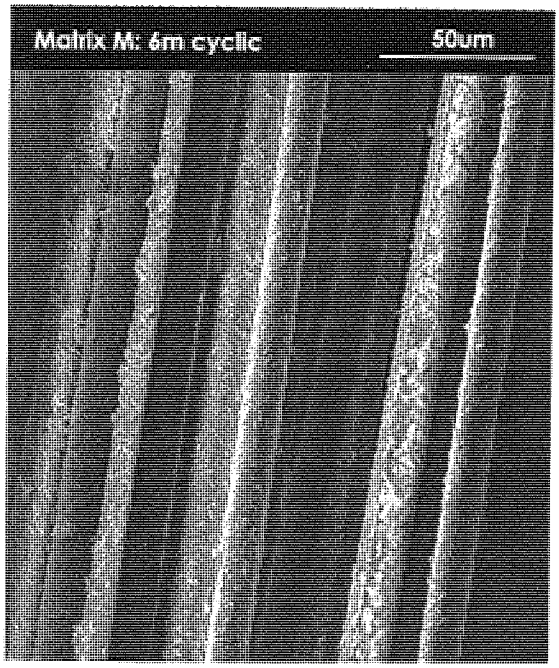

h.

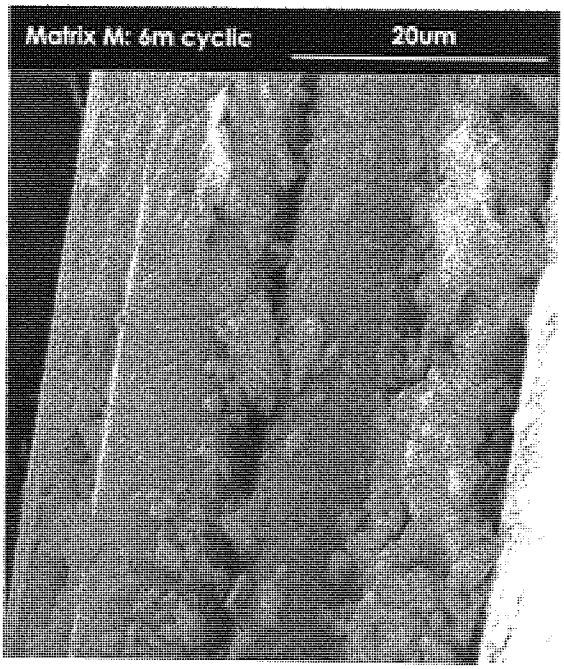

Figure 6.12 a-d. Matrix C SEM.

a.

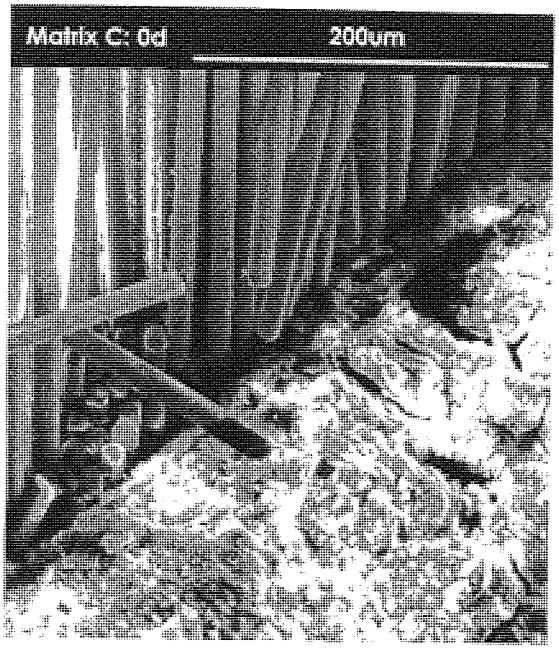

b.

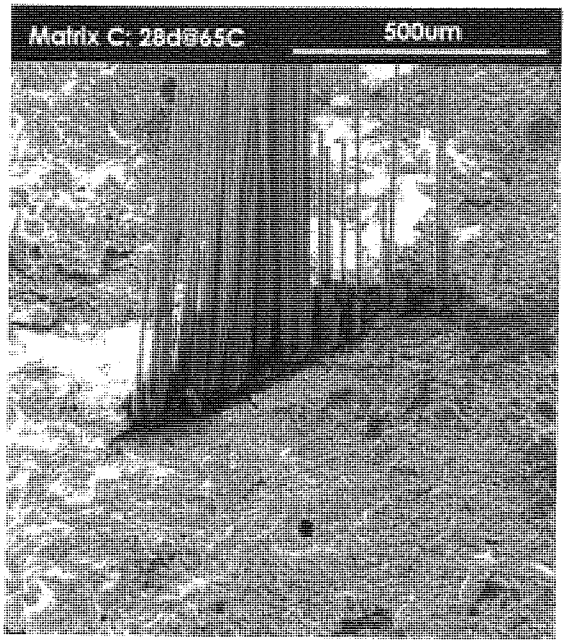

c.

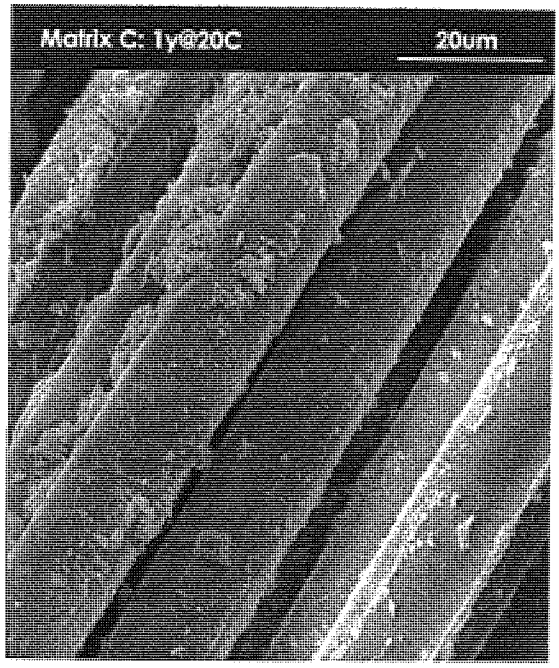

d.

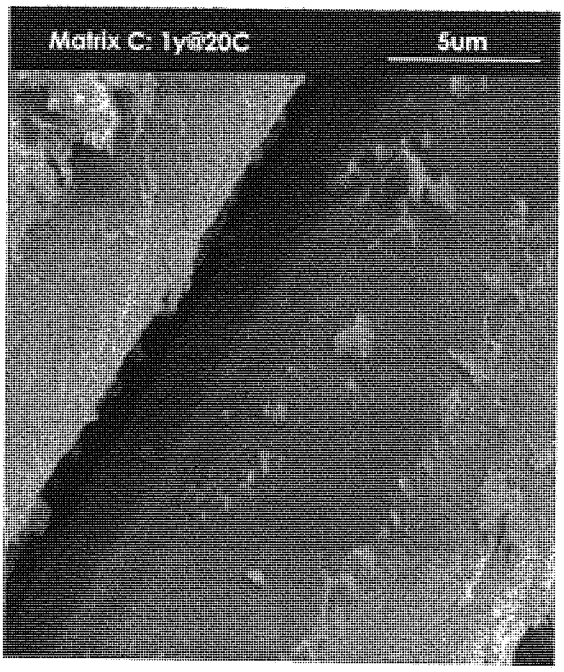

Figure 6.12 e-h. Matrix C SEM.

e.

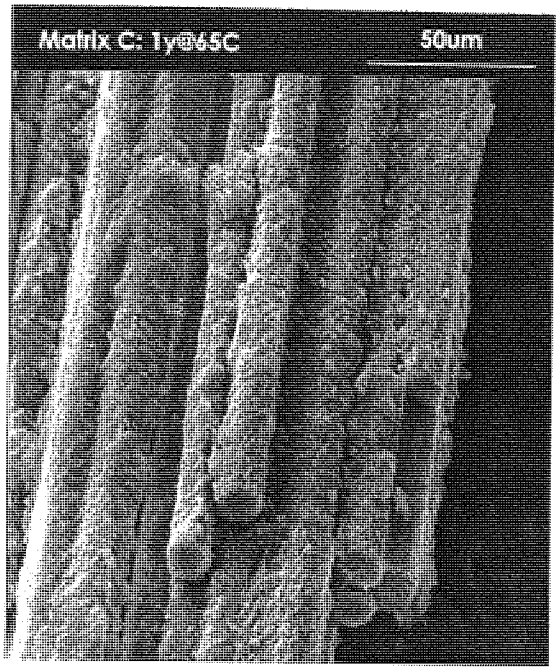

f.

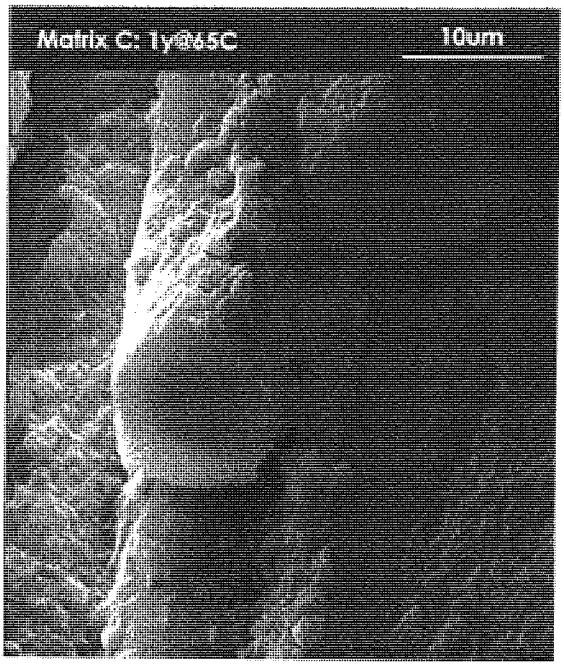

g.

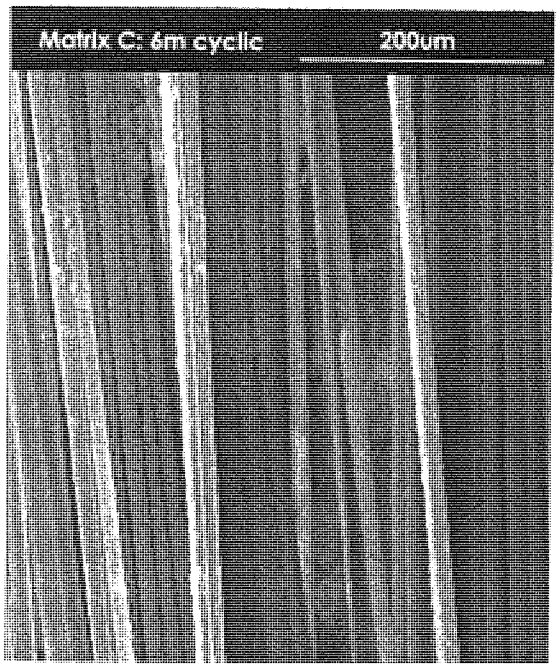

h.

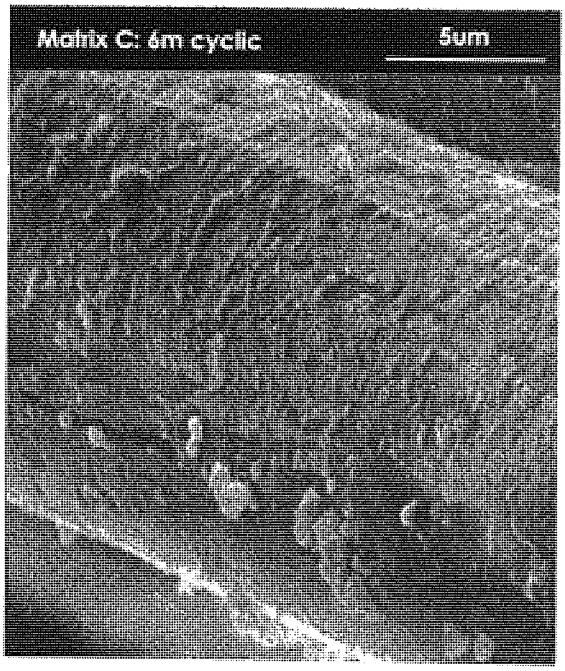

6.3. Discussion of microstructural results.

6.3.1. General comparisons.

The initial interface morphologies of matrices O and M composites were broadly similar with a 'loose' interface, little deep interfilamental material and extensive pullout during fracture (Figs. 6.1a, 6.4a, 6.10a, 6.11a). The much more intimate interface morphology and substantial matrix ingress in the matrix C composites (Fig. 6.7a) did not completely hinder pullout but filaments at the edges of strands tended rather to fracture (Fig. 6.12a). Figures 6.7 to 6.9 also show that the matrix C interface underwent little morphological change throughout ageing, whereas the matrix O and M fibre/matrix interfaces were much more intimate after ageing (Figs. 6.1 to 6.3, 6.4 to 6.6).

The most noticeable difference between the interfacial microstructures of matrix O and the new matrix composites was in the nature of the interfilamental deposits under hot water ageing. In matrix O, the material observed between the filaments was generally distinct from the general matrix material i.e. portlandite (Figs. 6.1b, 6.2b) changing to calcite at later ages (Figs. 6.1c, 6.2c - the change is discussed in section 6.3.3.) In the new matrix composites, where interfilamental material was observed it tended to be very similar to the general matrix material. In the SEM photos, the interfilamental material in the new matrix composites appeared more granular than that seen in matrix O composites (Figs. 6.10 to 6.12).

Although preferential segregation of portlandite was not observed between the fibres in matrix M composites, it was seen in the striking halos seen surrounding the strands at early ages (Fig. 6.4b) despite the small amounts of portlandite detected in the matrix analysis (Chapter 4). It would seem that even these small amounts of portlandite tend to preferentially precipitate near to the AR fibres. It is possible that the fine dark interfilamental material observed in the thin sections (which is probably unreacted metakaolin) prevented portlandite deposition between the fibres and forced it to precipitate in the area around the strand. The conversion of portlandite to calcite at later ages was common to both matrices O and M; this is discussed further below. Portlandite segregation was not observed in matrix C composites.

Fibre corrosion was only observed under the severest ageing regime, 1 year at 65°C, and was only definitely confirmed for matrix O composites (Figs. 6.10e,f) although there was some evidence that the other composites may have been affected to a lesser extent (Figs. 6.5, 6.8).

The correlation between these results and the mechanical and bond behaviour of the composites is discussed in Chapter 8.

6.3.2. Comparisons with published microstructural observations.

Ubiquitous throughout the GRC literature are SEM photographs of strands completely filled with monolithic portlandite deposits (e.g. Bentur, 1985; Diamond, 1985; Hommertgen & Odler, 1991; Majumdar & Laws, 1991) after less than a year of wet ageing, often cited as the primary reason for OPC composite deterioration. This complete strand filling was not observed in any sample in this study, either by SEM or in thin section. Most of these SEM photos are of composites made with first generation AR glass fibre. It would appear that the inhibitive size with which the second generation fibres used in this study are impregnated substantially retards the deposition of portlandite within the strands. However, it does not completely prevent it, as noted by Majumdar & Laws (1991).

6.3.3. Preferential carbonation.

As has been previously noted, after longer periods of hot water ageing any interfacial or inter-filamental deposits were of calcite rather than portlandite (e.g. Figs. 6.1c, 6.2c, 6.4c, 6.5c). The matrix M halos (Fig. 6.4b) also contained substantial amounts of calcite. This would have been formed by carbonation of the portlandite deposits formed at early ages.

It is noteworthy that calcite was found associated with the fibres even when the general matrix material was uncarbonated. This rules out carbonation caused during the preparation of the thin sections. Furthermore, the samples were aged underwater and exposed to laboratory atmosphere (which is far from an ideal carbonating environment) only for the brief period between tensile testing and section preparation.

The action of atmospheric carbon dioxide on the NaOH and KOH in the curing water (formed by leaching of Na and K ions out of the cement matrix) will cause sodium and potassium carbonate to be formed therein. The continuous strands, via a wicking action, may provide a pathway for the efficient distribution of these carbonate ions to areas of enhanced CH content i.e. the inter-filamental spaces (matrix O) or the 'halos' (matrix M) where they react to form calcium carbonate.

The phenomenon was clearest in matrix O and matrix M composites. The early filling of the strands by matrix material in matrix C seemed to largely prevent the preferential transport of carbonate ions, although evidence of faint calcite halos can occasionally be observed, especially where some debonding has taken place (Fig. 6.7b).

6.3.4. Strand compaction and strain birefringence of fibres.

It was noticed (at a qualitative level) that fibre groups in well aged samples were more compacted (i.e. there was less 'void space') than in younger samples, indicating that the fibres were being pushed together by continued matrix hydration. Many fibres in older samples also displayed degrees of strain birefringence. This strain birefringence tended to be stronger in fibres adjacent to infill material or interface deposits (Figs. 6.1c, 6.2c, 6.4c, 6.5b). It was also particularly noticable in cyclically aged samples. Although the possibility of stress having been induced in the fibres during section preparation cannot be ruled out, since strain birefringence was rarely observed in younger samples it would appear that fibres in well aged samples were subjected to lateral compressive stress by continuing matrix hydration.

6.3.5. Investigative techniques - SEM vs. thin sections.

Previous investigators have almost exclusively used SEM as the primary microstructural investigative technique during GRC studies. In this study, thin section optical microscopy has proved by far the more valuable technique, especially for observing and characterising interfacial and interfilamental deposits.

The main reasons for the preference for SEM in previous investigations are that fracture surfaces can be viewed directly, samples require minimal (and hence

inexpensive) preparation compared with thin sections and the images obtained are striking and encourage easy intuitive interpretation. Since many SE microscopes are equipped with rapid spot elemental analysis facilities (e.g. EDXA), elemental characterisation of very small areas (i.e interfaces) can also be performed. The images obtained tend to be monochrome and therefore acceptable to general publications.

However, the area generally observed in SEM studies, the fracture surface, is by definition the area where the feature of primary interest, i.e. the interface, is the most disturbed. This is especially true where pullout has occured, dragging fibres over the interfacial areas. Notice in the normal fracture surface photos (Figs. 10a,b to 12a,b) the apparent hole or trench at the interface - this is where fibres have pulled out and are now protruding from the corresponding fracture surface. Similarly, in the photos where the samples have been delaminated to prevent the problems described in Section 6.2, the interface material has been largely stripped away, leaving mainly debris between the fibres (Figs. 10c-h to 12c-h).

Thin sections can be taken from areas well away from fracture surfaces without gross disturbance of interfacial material. The preparation of the samples involves no thorough drying or hard vacuum and is less likely to disturb fragile hydrates. Although characterisation of crystalline deposits must be undertaken with care, it does allow identification of distinct minerals as opposed to relative element abundance as performed by SEM-EDXA analysers. Another advantage is that the images produced, being of a 2-D section, can be used with image analysis techniques to derive quantitative information. The slides produced are also rather easier to store and archive for future examination than SEM samples, and multiple complete cross sections can be included on one slide; samples for SEM generally have to be quite small. The main disadvantage of the technique is its diagnostic reliance on colour images, which publishers are reluctant to accept.

In summary, the two techniques are of most benefit when used in a complementary manner. Specifically, thin sections are more use for interface characterisation, tracking morphological development and producing images for quantitative analysis. SEM is most useful for observing fibre damage and the nature of the fracture mechanisms.

6.4. Summary of main findings.

The main findings of the microstructural investigations were;

- Matrix O and M composites had similar initial microstructures with no interfilamental material; matrix C composites displayed strands almost filled with matrix material even at 0 days. The interface in matrix O and M composites developed progressively while that of matrix C appeared to be little affected by ageing.
- Matrix O composites displayed distinct portlandite deposits between filaments after short periods of hot water ageing. Matrix M composites displayed striking halos of portlandite enhanced material around *but not within* the strands. Interfacial and interfilamental material in matrix C composites was very similar to the matrix groundmass, as was any interfilamental material in matrix M composites.
- Fibre corrosion was only detectable after 1 year at 65°C.
- After longer periods of hot water ageing, any interfilamental (matrix O) or halo (matrix M) portlandite became carbonated, despite samples not having been exposed to carbonating conditions and the general matrix remaining uncarbonated i.e. preferential carbonation was associated with the fibres.
- Thin section microscopy has proved a more powerful GRC investigative technique than SEM.
- A wide variety of strand and filament dispersions was observed although the classic lens-shaped strand cross-section was most common.

7. RESULTS; CRACK SPACING AND BOND STRENGTH.

A note on the presentation of crack spacing and bond strength results: *The results in this chapter are presented in similar style to those in Chapter 5. All error bars indicate ± 1 standard error.*

7.1. Normalisation.

Variation in thickness will cause a departure from the nominal V_f, since each sample contains a fixed quantity of fibre, as discussed in section 5.1. The equation relating bond strength (τ) and crack spacing (X) contains a V_f term;

$$\tau = 1.364(V_m/V_f).(\sigma_{mu}/X).(A_f/P_f) \qquad 2.12$$

In order that results from samples of varying thickness could be compared, it was decided to normalise the crack spacing results. These normalised crack spacings were also used in the bond strength calculations, negating the need to re-evaluate V_m/V_f for each sample. The normalisation algorithm was designed to use the same correction factor k = 6.1/T, derived for use with the tensile testing results, see section 5.1.

If we define the "true", measured crack spacing as **X**, the nominal (i.e. normalised) crack spacing as Ξ, the nominal fibre volume fraction as $\mathbf{V_{fn}}$ and **R** as $1.364(\sigma_{mu}/\tau)(A_f/P_f)$ then we can write;

$$\Xi = \mathbf{R(1-V_{fn})/V_{fn}} \qquad 7.1.$$

Since $V_f = kV_{fn}$ we can also write;

$$\mathbf{X = R(1-kV_{fn})/kV_{fn}} \qquad 7.2.$$

and hence;

$$\Xi/X = k(1-V_{fn})/(1-kV_{fn}) \qquad 7.3.$$

When k is close to unity and V_{fn} is small, the right hand term of equation 7.3 approximates to k and hence;

$$\Xi \approx kX \qquad 7.4.$$

i.e. the normalised crack spacing equals the observed crack spacing times the correction factor. For the values of k (0.7-1.3) and V_{fn} (1.5% i.e. 0.015) encountered in this project, the approximation was accurate to within 1%.

7.2. Crack spacing.

As discussed in section 5.2.5.1, the cyclic ageing regime caused considerable surface damage in all the composites. This made it impossible to derive crack spacing data for cyclically aged composites as any multiple cracking could not be distinguished from the surface crazing. Crack spacing data are presented below for the hot water and carbonation ageing regimes. Note that the carbonation ageing regime also induced some pre-cracking in matrix C and possibly in matrix M (5.2.6). The validity of the crack spacing data for these matrices is therefore open to question but is presented for completeness.

Figures 7.1 to 7.3 show the variation in the crack spacing of the composites with ageing time for each regime.

Figure 7.1. Variation of crack spacing with ageing time at 20°C.

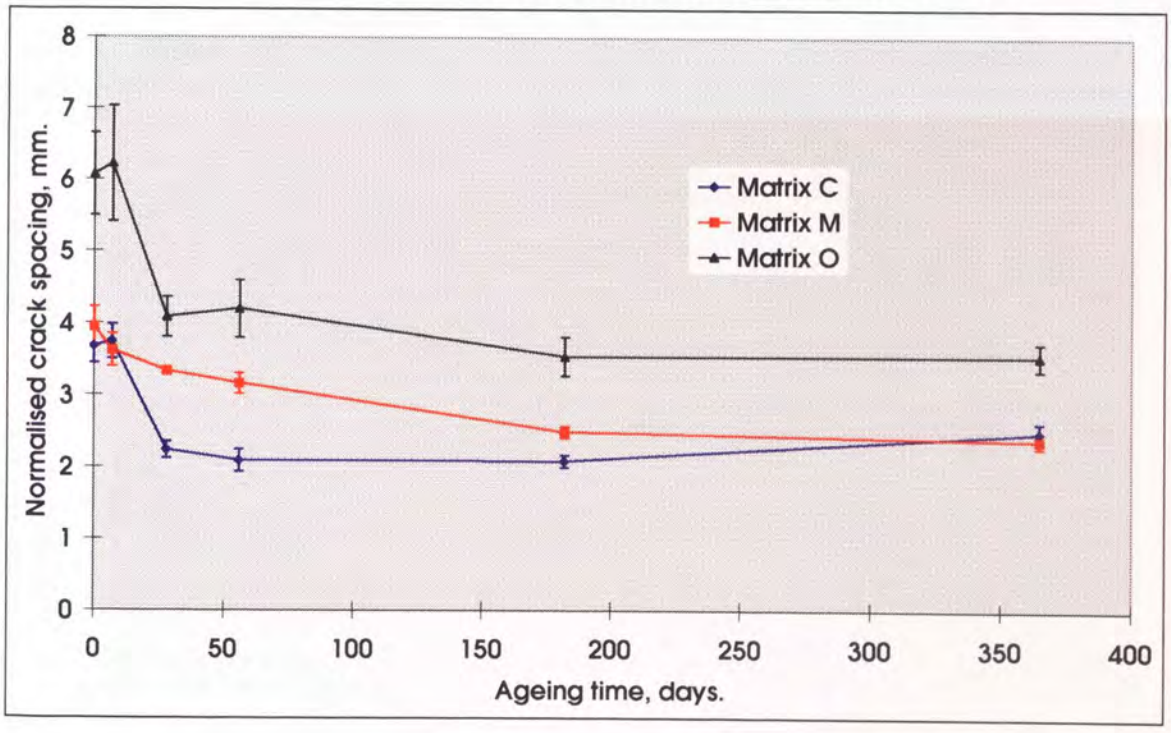

Figure 7.2. Variation of crack spacing with ageing time at 38°C.

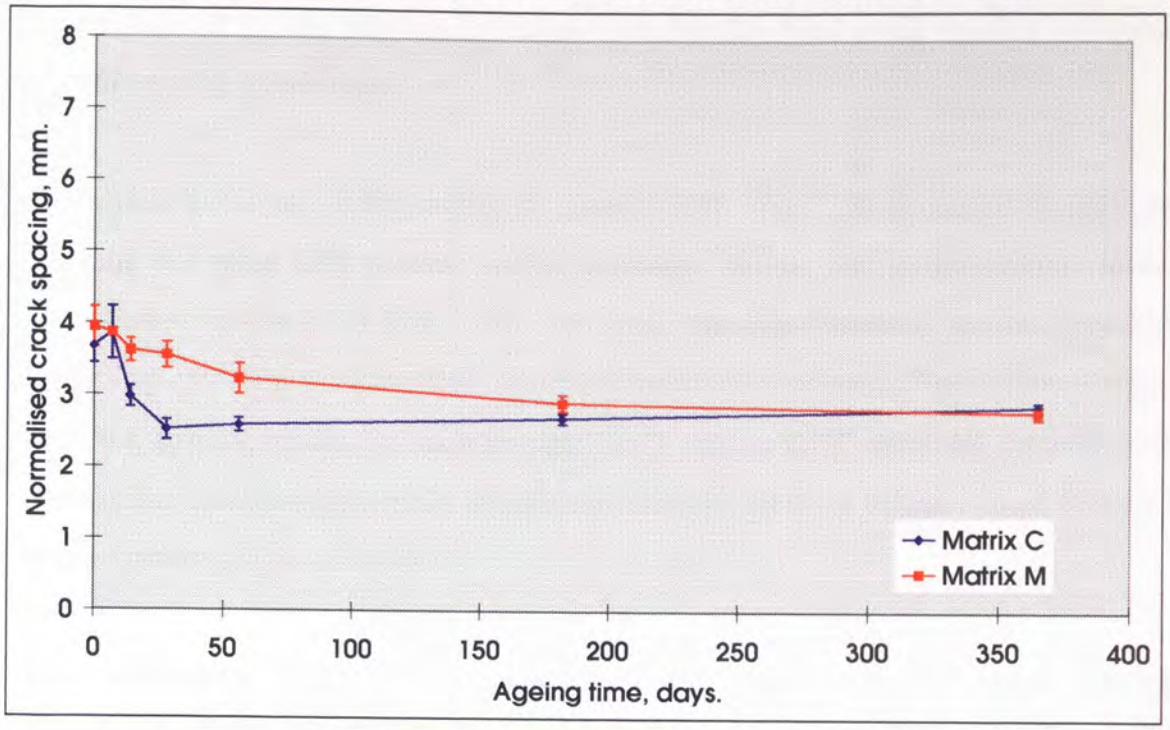

Figure 7.3. Variation of crack spacing with ageing time at 65°C.

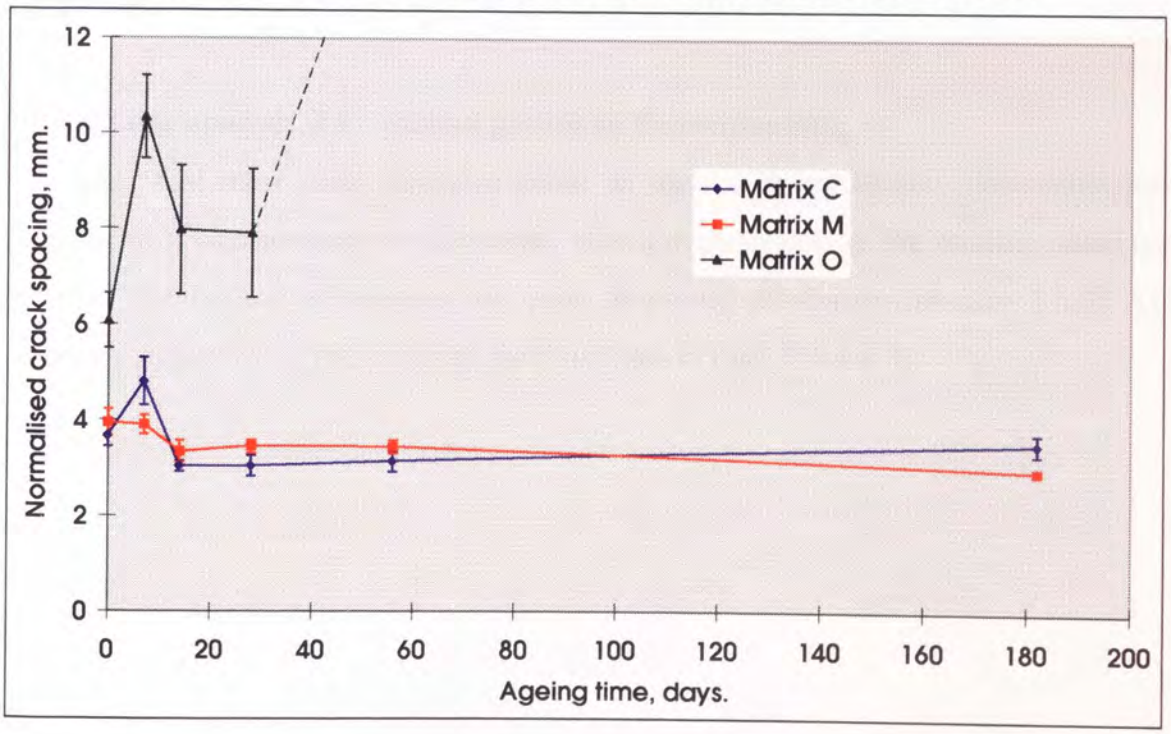

Under the all the hot water ageing regimes, crack spacing was reduced with ageing time. Matrix O under 20°C ageing (Fig. 7.1) and matrix C under all regimes appeared to exhibit three-stage behaviour. The crack spacing remained stable up to 7 days, then underwent a rapid reduction up to 28 days followed by a further period of stability.

Matrix M samples showed a smoother reduction curve. The general shape of the curves was not greatly affected by temperature but the final crack spacing increased with the ageing temperature.

The erratic behaviour of the matrix O curve at 65°C (Fig. 7.3) is caused by multiple cracking not being fully realised before composite failure, due to the strength losses described in section 5.2.4 (Fig. 5.12). The crack spacings therefore become generally larger (i.e. not all the cracks have formed before failure occurs). For similar reasons, no crack spacing results for samples aged for 1 year at 65°C could be derived since none of the samples displayed a significant multiple cracking region - most failed by single fracture (Figs. 5.17-19).

The carbonating ageing regime caused a slight reduction in the crack spacing compared to that at 0 days. The matrix O sample crack spacings were reduced by 19% (6.07 to 4.89mm), matrix M by 27% (3.95 to 2.90mm) and matrix C by 17% (3.67 to 3.06mm).

7.3. Image analysis (IA) - strand perimeter determination.

In order that these crack spacings could be used to quantitatively determine bond strengths, it was necessary to derive the 'effective perimeter' of the reinforcement (eq. 2.12). The method of analysis has been described previously (section 3.5.3). The various stages for a typical image are illustrated in Figs. 7.4 a to f.

Figures 7.4a., Original image and 7.4b., Re-mapped grey image.

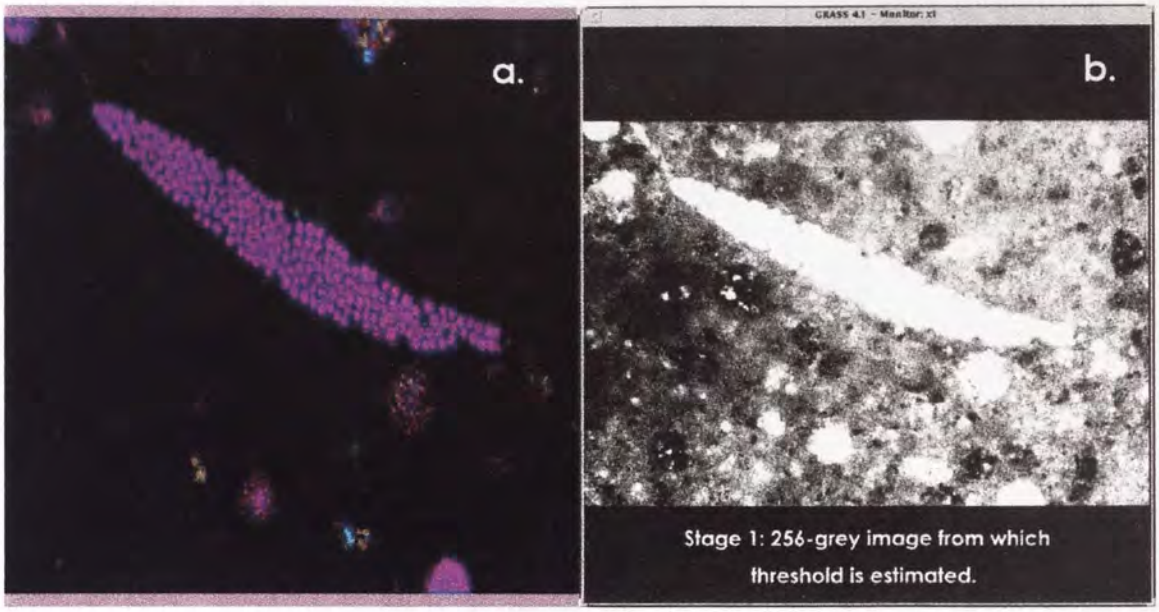

Note that the distortion in the original square image (Fig. 7.4a) has been corrected by the GRASS software. The area represented by the image is 1.011mm across by 0.689mm deep.

The cursor was run over the interface area of the remapped grey image (Fig. 7.4b) and the software displayed the grey value (brightness) of each pixel selected. A typical threshold grey value was chosen (between 0 [black] and n where n is the value of the brightest pixel, maximum 255 [white]). The density sliced image (Fig. 7.4c) is based on this threshold value, with brighter pixels in red and darker pixels in yellow. Figure 7.4d shows the image after 'clumping'; each group of red pixels has been assigned a unique value, represented as different colours.

Figures 7.4c., Density slice and 7.4d., Clumped image.

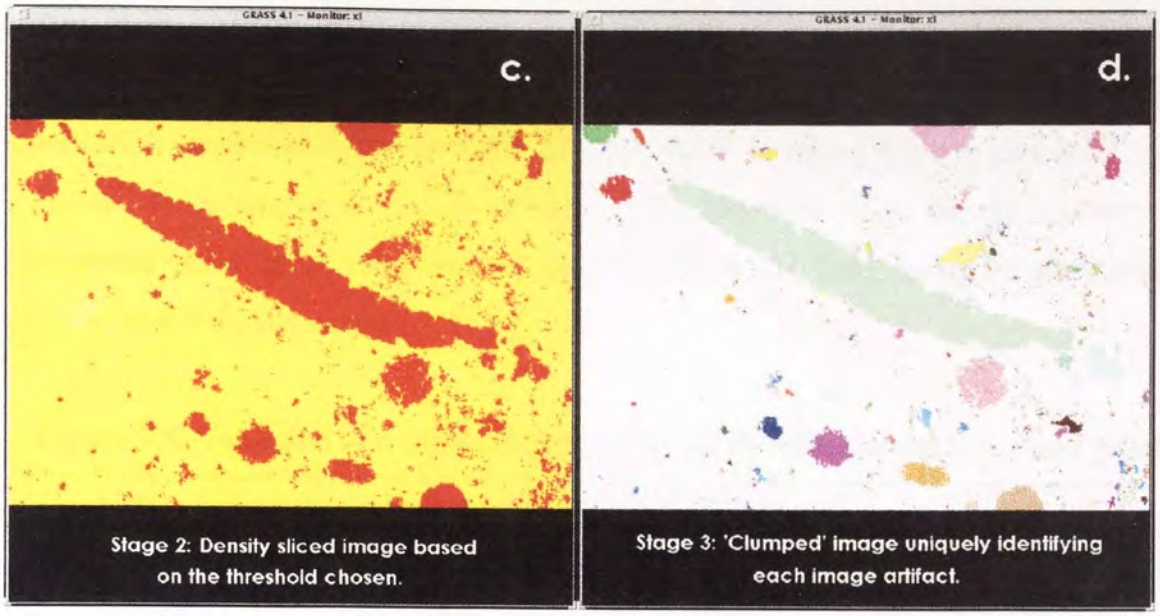

The image in Fig. 7.4e contains just the clump representing the strand cross section. The perimeter pixels forming the perimeter were then isolated (Fig. 7.4f). This image was then vectorised i.e. converted from a bitmap by drawing a line joining the centres of all the pixels. The length of this line was taken as the perimeter.

Figures 7.4e., Reclassed image and 7.4f., Isolated perimeter.

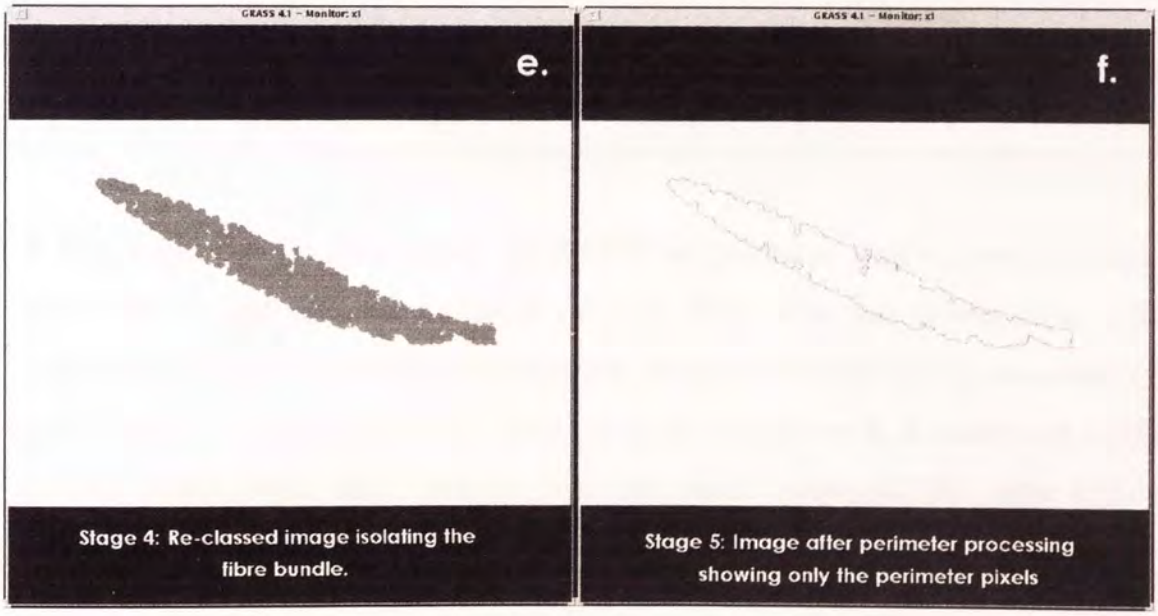

7.3.1. Threshold values.

The process at this point still involved one subjective step; the choosing of the threshold value. Since the boundary between fibre and matrix was not uniquely defined, a judgement had to be made as to the 'best' threshold value to choose. It was decided to determine the effect of varying the threshold value on the number of perimeter pixels extracted (which is proportional to the final measured perimeter). Some typical results are shown in Fig. 7.5.

Figure 7.5. Variation of number of perimeter pixels with chosen threshold value.

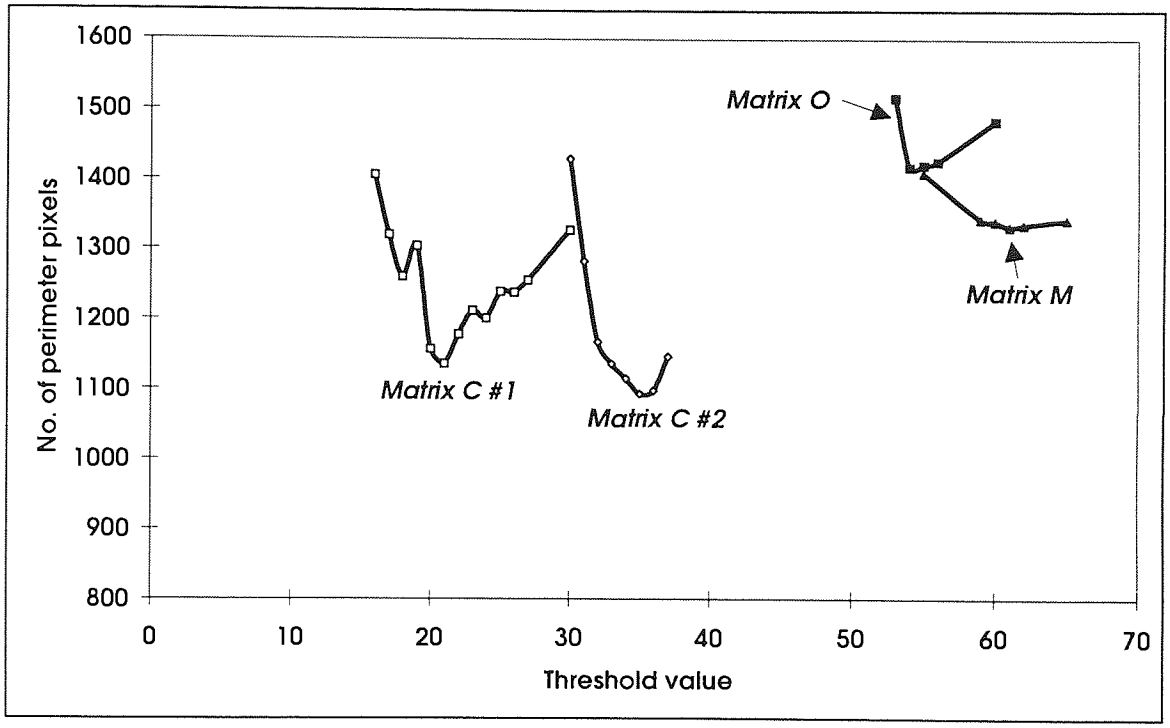

It was found that for all samples, the number of perimeter pixels passed through a minimum at some optimum threshold value T_0. This value was always close to the value chosen intuitively in the initial analysis. It was also found that T_0 was unique to each image i.e. a single threshold value could not be applied to a number of similar images despite them being derived from the same composite, the same lighting conditions, the same instrument etc. It is not a materials parameter.

T_0 was determined for each sample, and the corresponding measured perimeter was taken as the actual perimeter. Since this could be applied consistently across all samples, the subjectivity involved in manually choosing a threshold value was

eliminated. The average perimeter was found to be **2.34mm** with a standard deviation of 0.37mm, maximum 2.99mm and minimum 1.83mm. There were no significant differences in measured perimeter between the different matrix composites and so this value was applied to all samples.

The area contained within the perimeter was found to be **0.0519mm^2** with a standard deviation of 0.0066mm^2. The area occupied by the filaments (calculated either by multiplying the number of filaments by the average filament area or from the tex and density of the fibre) is 0.029mm^2 indicating that about 40-50% of the area within the perimeter is (initially) void space.

7.4. Bond strength.

7.4.1. Bond strength - a misnomer.

Although the "τ" term derived from eq. 2.12 is usually termed a bond strength and quoted in MPa (Oakley & Proctor, 1975; Kakemi *et al.,* 1996), this is something of a misnomer. The ACK theory from which the equation is derived requires that load transfer between the fibre and matrix is frictional in nature, with no elastic bond. Strictly speaking, τ in eq. 2.12 is a frictional shear stress transfer rate; the term 'bond strength' (and its quotation in MPa) implies this bond would resist separation of the components by forces normal to the interface. Obviously, a 'frictional bond' could only resist separation by forces parallel to the interface (i.e. sliding as opposed to pulling apart). Since 'frictional shear stress transfer rate' is a rather cumbersome expression, frictional bond has been used from hereon to denote the same quantity. It has been quoted in units of N/mm^2 i.e. load transferred per unit surface area of reinforcement.

7.4.2. Results.

Since no crack spacing data could be derived for the cyclically aged material, it was not possible to determine its frictional bond. Although crack spacings were measured for the carbonated matrix C and matrix M specimens, the samples had clearly undergone pre-cracking (Fig. 5.27). The BOP could not be therefore be reliably determined. Together with the uncertainty of the crack spacing data it was considered

that any frictional bond figures advanced for these specimens would be unreliable. The frictional bond of the carbonated matrix O could however be determined.

The variation of frictional bond with ageing time for all other regimes is presented in Figures 7.6 to 7.8. Note that no frictional bond data are presented for 1 year at 65°C; all samples failed by single fracture.

Figure 7.6. Variation of frictional bond with ageing time at 20°C.

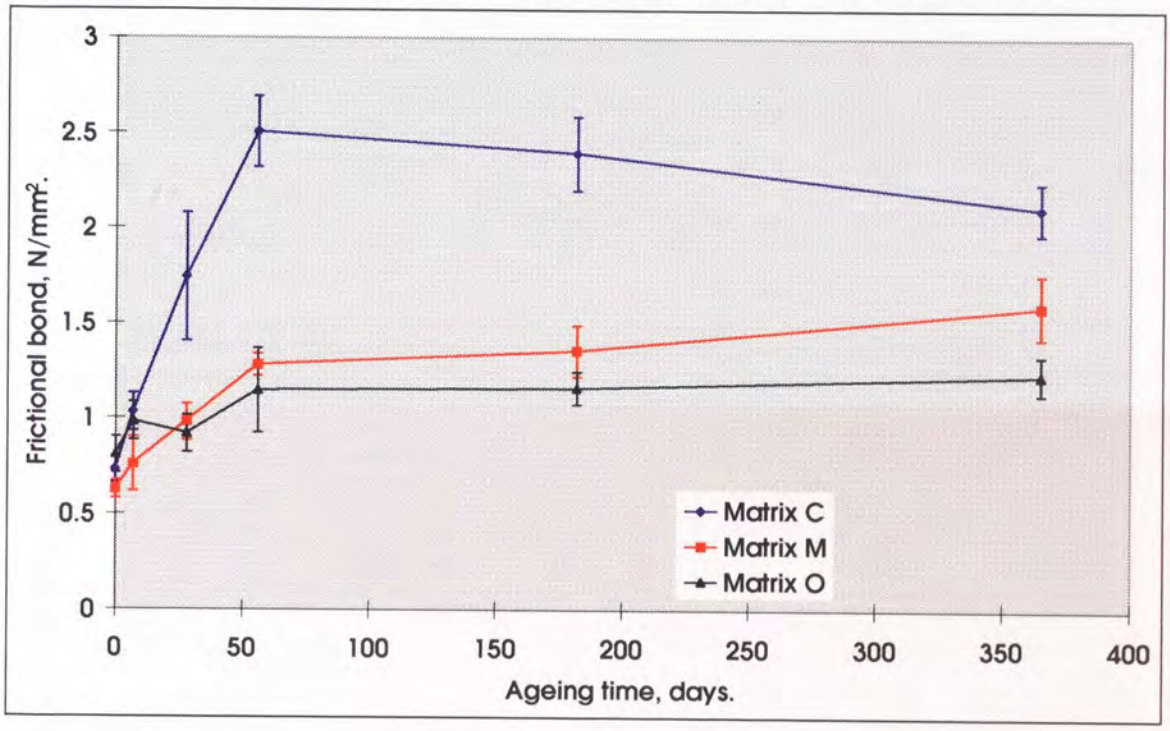

Figure 7.7. Variation of frictional bond with ageing time at 38°C.

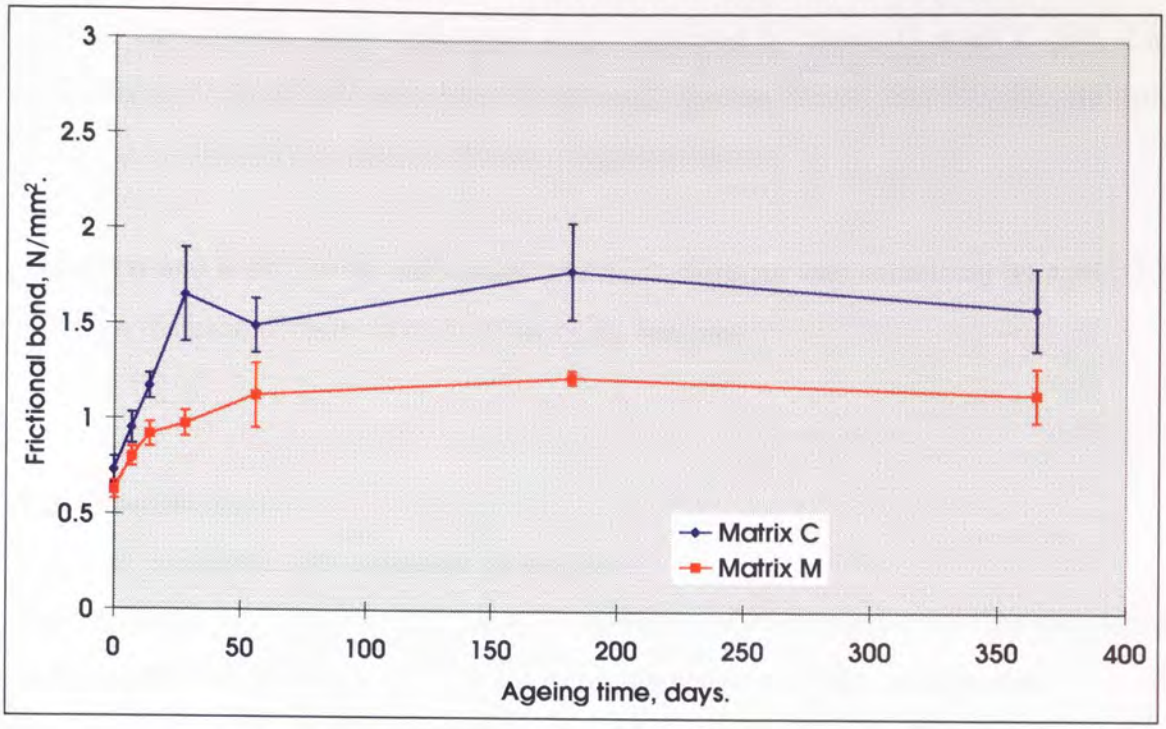

Figure 7.8. Variation of frictional bond with ageing time at 65°C.

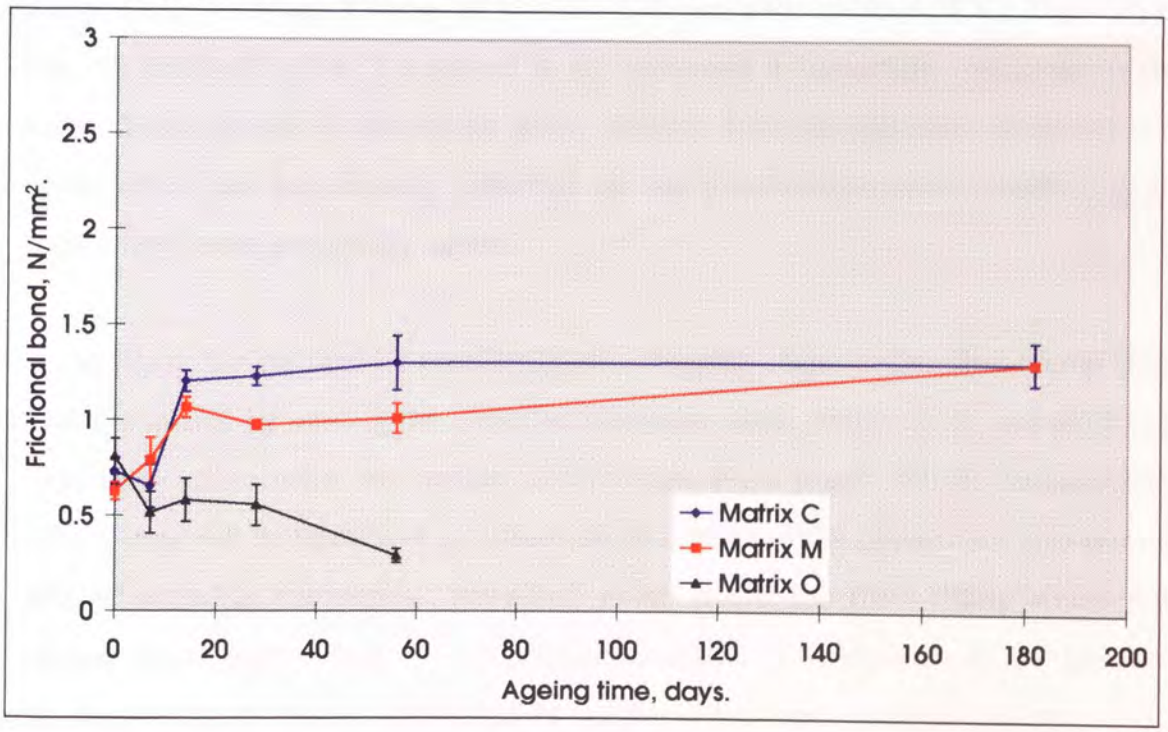

The frictional bond generally behaved as indicated by the crack spacing results; a rapid increase in frictional bond followed by a more stable period. The change point between the rising and stable portions of the curves was reached earlier at higher temperatures, but the terminal frictional bond attained was higher at 20°C (Fig. 7.6)

than at 38 or 65°C (Figs. 7.7, 7.8). This effect was most clearly seen in the matrix C curves. The apparent drop in frictional bond displayed by matrix O at 65°C (Fig. 7.8) is analogous to the erratic behaviour of the crack spacing curves (Fig. 7.3) i.e. multiple cracking not being fully realised before composite failure.

The frictional bond for the carbonated matrix O samples was calculated as about 1.3 MPa, an increase of about 60% over the 0 day samples.

7.5. Discussions.

7.5.1. IA perimeter determination technique.

The technique described in 3.5.3 and illustrated in 7.3 represents the first published fully objective method for determining strand perimeters in GRC composites.

7.5.1.1. Justification for minimum perimeter value method.

The primary justification for using the minimum perimeter method (7.3.1, Fig. 7.5) is that the threshold value (T_0) derived at this perimeter is invariably very close to the value chosen intuitively during the initial analysis. Also the minimum perimeter is a point which can be uniquely identified on the threshold/perimeter curves for all images and hence universally applied.

It can be further justified by considering the changing shape of the fibre clump (Fig. 7.4b,c) isolated by varying the choice of threshold value. When $T<T_0$, we are being 'less fussy' about what we include in the image. More pixels will be included, the fibre clump will be larger and the measured perimeter will be higher. We also run the risk of including extraneous, 'non-fibre' pixels within the fibre clump which will further inflate the perimeter. As we approach the limit ($T\rightarrow 0$), nearly all the pixels in the image will be classed as fibre and the measured perimeter rises very quickly.

When $T>T_0$, we are being 'more fussy'. Fewer pixels will be included, but the coastline of the fibre clump will become more convoluted, increasing its perimeter. This convoluted coastline may not accurately represent the contact perimeter between the strand and the cement. As we further increase T, small groups of pixels

representing single filaments or small groups will become severed from the main clump; care must be taken not to exclude these from the analysis. In the limit, the measured perimeter will approach the sum of the perimeters of the filaments.

T_0 represents the balance point between exclusion of noise and ensuring a realistic perimeter morphology. During the initial determination of T_0, it should be realised that the error in over-estimating T_0 is rather less than that of under-estimating it.

7.5.1.2. Modification of the technique.

Although the images in this project were directly captured from optical microscopy of thin sections, the principles of the technique could be applied to any digital image of a strand cross-section e.g. those captured from SEMs or scanned in from paper photographs of polished sections. The software used in the analysis (GRASS) is public-domain, open-system software developed by the U.S. Army Construction Engineering Laboratory (CERL) (Shapiro *et al.*, 1993) that can be set up on any UNIX workstation.

The technique could also be applied to quantifying other micro-structural parameters in GRC such as the distribution patterns of reinforcement throughout the matrix or the degree of dispersion of the strands or filaments.

7.5.2. Perimeter results.

It is perhaps surprising that no significant differences were displayed between the strand perimeters for the different matrices considering their distinct interface morphologies, observed (subsequent to the image analysis) in section 6.2. This may be due to the number of samples analysed (3 per matrix, 9 in all). The spread of the data was however similar to that observed by Kakemi *et al.* (1996) for 33 strands each of 100 filaments; mean 1.097mm, SD 0.143mm, range 0.802-1.363mm. The average perimeter was also similar to that derived by other authors (see section 2.2.3.1).

Although the 'classic' lens-shaped strand cross-section was most common, a large variety of degrees of dispersion was observed (section 6.3). Attempts were made to include a variety of cross-section shapes in the image analysis study, but it was not

clear at that point how varied the degrees of dispersion were. A study of a much larger number of different shaped strands would perhaps contrast strand perimeters between the matrices, but the general diversity of cross-section morphologies encountered in all samples may render these differences trivial.

7.5.3. Frictional bond results.

The initial frictional bonds for all three composites were very similar (Fig. 7.6). At 20°C, matrices O and M displayed similar frictional bond behaviour, although the terminal bond formed was higher for matrix M than for matrix O. Matrix C composites formed bond far more rapidly, and the frictional bond at 6 months was twice that of matrices O and M. At 38°C, the difference between matrices M and C was less marked. At 65°C, they behaved in a similar manner. This behaviour will be discussed further in Chapter 8.

7.5.3.1. Temperature/bond relationship.

The slowing or halting of frictional bond development with ageing time was not an unexpected result. More curious was the dependence on the ageing temperature of the terminal bond developed; higher temperature ageing appeared to inhibit frictional bond development, as shown in Figure 7.9.

The terminal frictional bond for matrix O aged at 65°C could not be derived owing to the incomplete realisation of the multiple cracking region, hence no matrix O curve is shown in Fig. 7.9. However, matrix O composites aged for 7 days at 65°C showed only a small loss of strength and multiple cracking should have been fully realised. The calculated frictional bond for 7 days at 65°C was lower than for 7 days at 20°C (0.58 N/mm^2 cf. 0.98 N/mm^2) and was also lower than the 0 day value. Other authors have previously noted similar trends in less detail (Laws *et al.*, 1986). The same inverse relationship between bond and ageing temperature may also be valid for OPC.

Figure 7.9. Terminal frictional bond vs. ageing temperature.

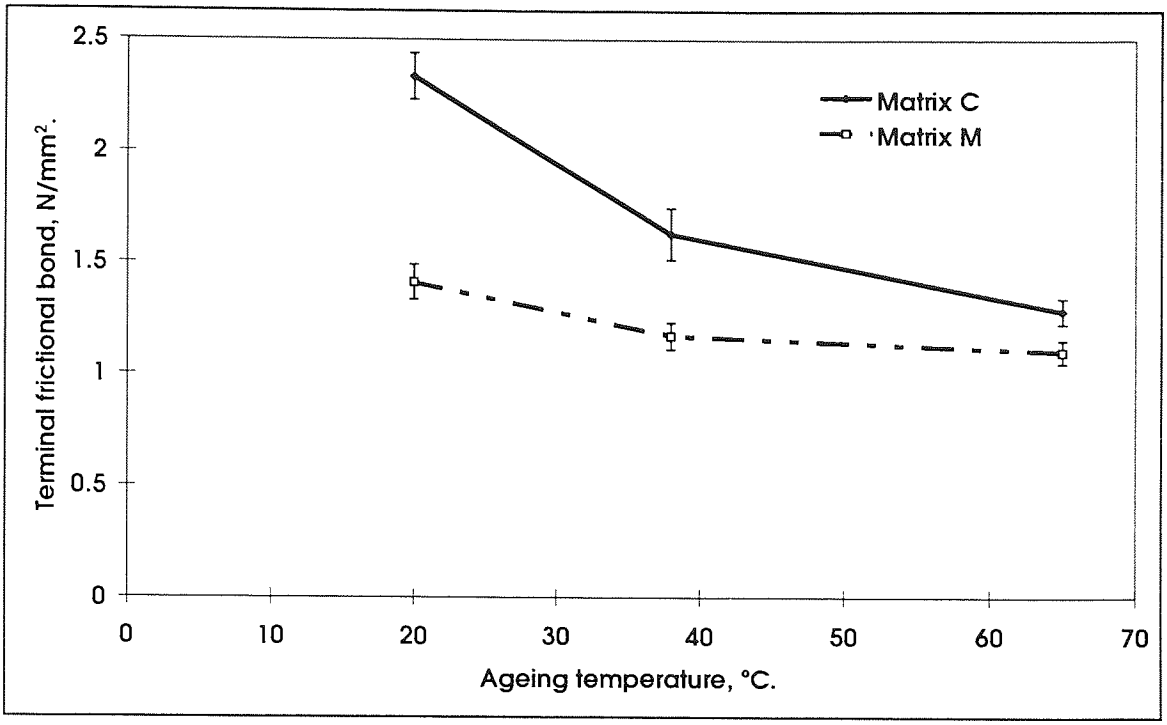

This inverse relationship is the opposite of what would be expected if short periods of high temperature ageing were analogous to long periods of low temperature ageing, as assumed during accelerated ageing tests. We would expect the terminal frictional bonds reached to be similar under both conditions, and that they be reached faster at higher temperatures. In fact the rate of frictional bond development is similar at all ageing temperatures. This is particularly well demonstrated in the matrix C composites by plotting the frictional bond vs. time curves for all three hot water ageing regimes one one graph (Fig. 7.10, error bars omitted for clarity).

Figure 7.10. Matrix C: Frictional bond vs. time under various hot water ageing temperatures.

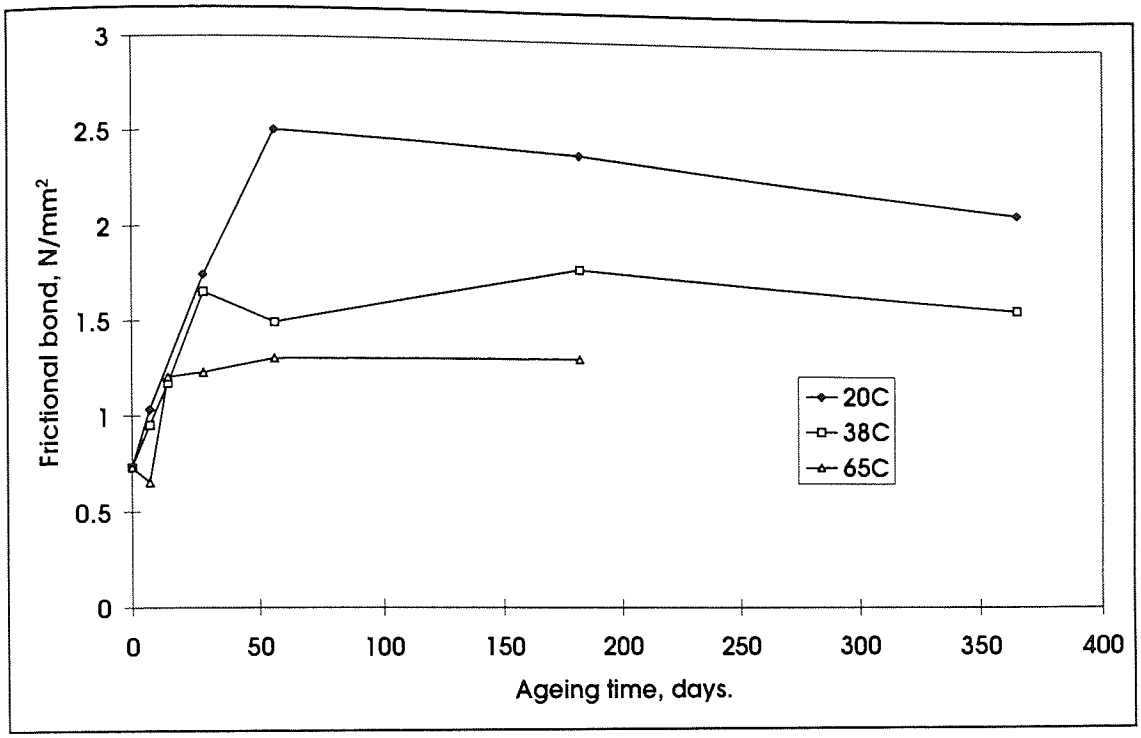

The reasons for this inverse relationship are unclear. A discussion of some possible causes is included in Chapter 8.

7.5.3.2. Matrix C: drop in frictional bond.

Figures 7.6 and 7.10 show a small but significant progressive reduction in the matrix C composite frictional bond under 20°C ageing after the maximum is reached (i.e. 56 days to 1 year), also reflected in the rise in crack spacing over a similar period (Fig. 7.1). This frictional bond drop was not observed during any other ageing regime, or for the other matrix composites. It cannot be attributed to the incomplete development of the multiple cracking region (as for matrix O at 65°C) as no corresponding strength losses were observed. The reason for the apparent drop is open to speculation.

7.5.4. Validity of the model.

The primary drawback of the model, in particular its application as eq. 2.12 to the results of this project, is that it is a predictive model. In order to verify the model, it would be necessary to independently derive strand/matrix frictional bonds (perhaps from pull-out tests), use them to predict e.g. crack spacings and compare with

observed values. It might be argued that the bond values returned by the model are simply the values required to force the model to fit.

Furthermore, the model requires that the 'bond', i.e. stress transfer between fibre and matrix, is purely frictional in nature. Many studies, in particular those by Bartoš (e.g. 1980, 1985) have clearly demonstrated that elastic bond and the relationship between elastic and frictional bonding all contribute to the bond behaviour of GRC.

In defence of the ACK model, more recent models appear to further complicate rather than solve the problem outlined above, since some of the parameters they require would be at least as difficult to independently measure as bond strength and are certainly more difficult to visualise. These models generally invoke fracture mechanics principles to model debonding as crack propagation along the interface.

The Shah (1985) model requires a knowledge of the shear modulus of the matrix and relies on spacing factor concepts to predict the bond strength. The model advanced by Naaman *et al.* (1991) purports to model the entire stress/strain behaviour in terms of 5 parameters including the bond modulus, the 'end slip' of the fibres at onset of full debonding and a compound factor 'ξ' which involves end slips, fibre length and an empirical double exponential parameter 'η'. The extension of the Shah model (Li *et al.* 1992) involves fracture mechanics of alarming complexity from which it is very difficult to extract useful materials parameters.

The ACK model is relatively easy to visualise. It uses readily quantifiable parameters such as matrix strength and crack spacing to predict a 'global bond' strength. The other models require parameters which are difficult to measure or derive and in general give behavioural predictions which are not wildly different from the basic ACK predictions. The variability of the results (unavoidable during tensile testing of these essentially brittle materials) further questions the applicability of the more complex models in practical situations.

Although the absolute values of bond returned are open to discussion, the information on the changes in the global bond parameters with ageing time and temperature are

still of great interest. With regard to the model's dependence on frictional load transfer, many authors have shown that certainly in the post-first-crack stage, frictional bond is more important than elastic bond (Aveston & Kelly, 1973; Laws, 1982; Naaman *et al.*, 1992). Bartoš (1985) has also pointed out that if the elastic bond is low then debonding may occur before first crack and the frictional bond will control the pre-cracking behaviour of the composite.

7.6. Summary of main findings.

The main findings of the crack spacing and bond strength investigations were;

- Using fundamental image analysis, a fully objective method for deriving reinforcement perimeters has been established. The method can also derive other microstructural parameters e.g. void/glass ratio in strands.
- There was no significant difference in the measured strand perimeters between the matrices. The same value was therefore used for all samples.
- The initial frictional bond was similar for all composites. Frictional bond increased with ageing time, reaching a terminal value at <56 days ageing. Under 20°C ageing, this terminal value was similar for matrix O and M composites but rather higher for matrix C composites.
- The terminal bond formed was decreased by increased ageing temperature. The effect was clearly demonstrable for matrix C and M composites and was probably also apparent in matrix O composites.

8. GENERAL DISCUSSION.

The main objective of the project, the determination of factors controlling the long-term durability of GRC, may be split into two primary facets;

i. elucidation of the mechanisms governing the time dependent property changes and
ii. assessment of the relevancy of standard accelerated ageing tests.

Discussion of these points occupies the bulk of this chapter. At the end of the chapter are discussions of some of further interesting phenomena encountered during the course of the investigations.

8.1. Degradation mechanisms.

As described in section 2.3.2, three mechanisms are thought to control composite strength loss *viz.* fibre corrosion, matrix densification and interfilamental precipitation. Each of these is discussed in relation to the results from this study in the following sections.

8.1.1. Fibre corrosion.

The first mechanism to be considered is reduction in fibre strength by corrosion in the alkaline pore solution. A possible manifestation of this, strength loss through reduced section, can be discounted. Even after 1 year at 65°C only slight loss of section was observed; degradation of the composites being complete long before this time. In addition, the section losses observed were nowhere near those required to account for the composite strength loss.

A more likely explanation concerns the fact that glass fibre strength is strongly dependent on the population and size of surface flaws. Figure 8.1 shows the relationship between critical fibre stress (i.e. fibre strength) with critical surface flaw size (i.e. the flaw size which will cause failure at a given stress). The bold line represents flaw size calculated using the simple edge-crack equation;

$$\sigma_{f,\,crit} = K_{ic} / 1.12(\pi a)^{0.5} \qquad 8.1.$$

where **a** is the flaw size. The virgin filament (**a.**) and industrial strand (**b.**) strengths were taken from the manufacturers data as 3.5 and 1.7 GPa respectively; these values are in good agreement with those typically encountered in the literature (e.g. Majumdar & Laws, 1991).

Figure 8.1. Critical fibre stress vs. critical flaw size.

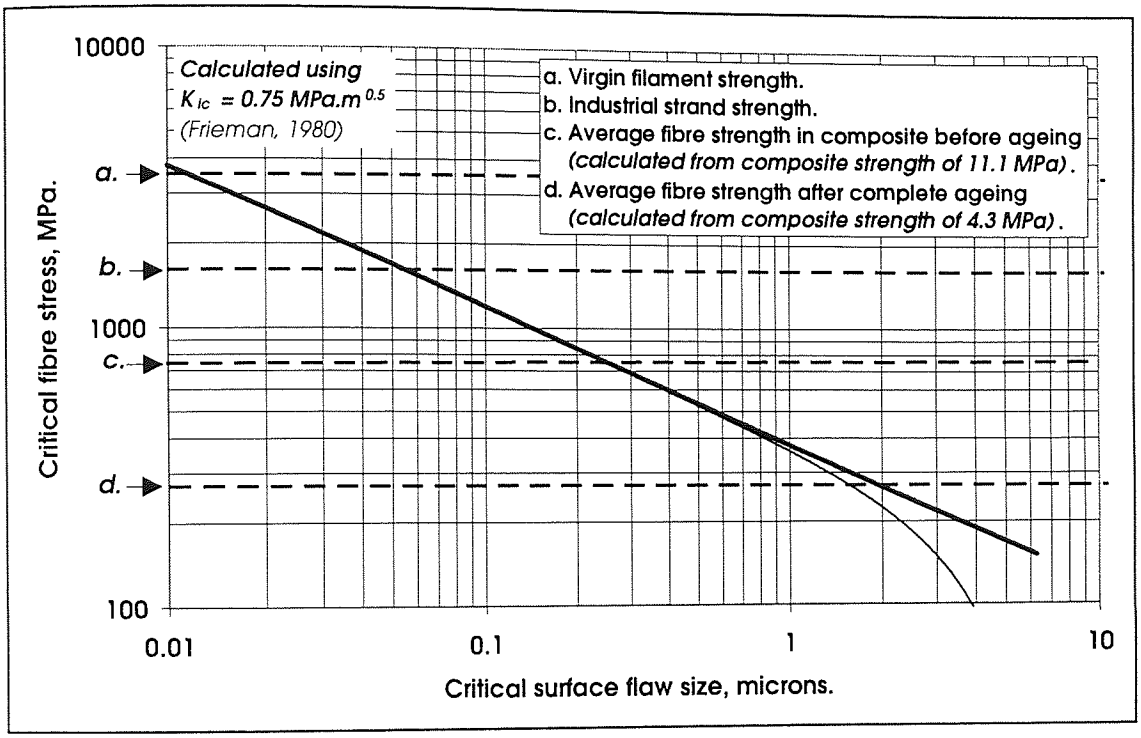

The value of the critical stress intensity factor K_{ic} (0.75 MPa.m^{½}) was calculated from a summary of data taken from Frieman (1980). The lighter line represents a more complex equation modelling a circumferential edge crack in a bar under tensile stress (adapted from Sih, 1973) which may more realistically model fracture behaviour for cracks longer than about 1μm.

Note that between filament drawing and strand manufacture (*a.* to *b.*, Fig. 8.1), flaws with a maximum size of about 0.05μm would appear to have been introduced. Composite manufacture (*c.*) would appear to have introduced further flaws of the order of 0.2μm. In order for the average fibre strength to fall to a value where the fibres cannot withstand the load transferred to them upon matrix cracking the maximum flaw size should be increased ten-fold to about 1.5μm (*d.*).

It should be noted at this point that 1.5μm is the theoretical *maximum* flaw size per single filament after complete ageing; any other flaws on the fibre will be smaller. It is also probable, especially in non-aligned composites, that some filaments are under a greater than average stress and their critical flaw size will be correspondingly lower; they will fracture prematurely, instigating a tearing effect. This will reduce the 'effective' critical flaw size to sub-micron levels. This goes some way to explaining why the fibre surfaces in completely aged composites often appear smooth under SEM examination, leading many authors to dismiss fibre corrosion; the average flaw size is less than the resolution of the images, and the distribution of critical magnitude flaws is so sparse that the small lengths of fibre examined are unlikely to contain any.

The mechanism of fibre strength loss would then appear to be extension of the pre-existing ≈0.2μm flaws or microcracks introduced during composite manufacture (***b.*** to ***c.***, Fig. 8.1). A possible process for this is a stress corrosion effect normally termed 'static fatigue' in glass technology literature. (The term 'static' is used as gradual strength loss occurs without any cyclic load; a more correct term, as used by Frieman [1980] would be delayed failure).

If a glass is under stress less than its fracture stress in a corrosive environment, the siloxane network bonds will be preferentially broken at a crack tip owing to the stress concentration there (Phillips, 1972); the crack thus becomes longer (Fig. 8.2). This slow or sub-critical crack growth may *in extremis* cause spontaneous failure of glass components and is a well known phenomenon (e.g. Ashby & Jones, 1986; Frieman, 1980).

Under hot water ageing of coupons, the necessary stress for static fatigue may be provided by the mismatch in thermal coefficient of expansion between the fibres and cement.

Figure 8.2. Flaw growth caused by OH ion attack (after Ashby & Jones, 1986).

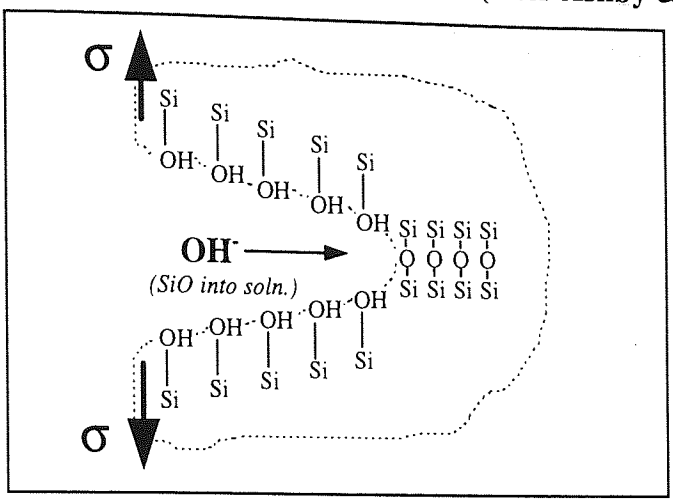

According to Majumdar & Laws (1991), the thermal coefficient of expansion of AR glass fibre is 7.5 x 10^{-6} per °C (7.5μ.°C^{-1}); for hardened Portland cement paste, it is between 12 and 20μ.°C^{-1}. Assuming a value of 70 GPa for the fibre modulus, a rise in temperature from 20 to 65°C could theoretically produce a tensile stress in the fibres of about 25 MPa. Although we might expect some of this stress to be dissipated by local slip between the fibre and matrix, it can be seen that a mechanism capable of providing an appreciable stress for sub-critical crack growth exists.

(Note: At lower temperatures this induced stress will be of course be lower. For actual structural GRC components, their dead loads will provide a driving stress for sub-critical crack growth. These points are discussed further in section 8.2.2).

If we assume there is an unrestricted supply of OH ions to the reaction zone at the crack tip then we might expect the rate of dissolution of material from the crack tip (and hence the flaw growth rate) to be proportional to [OH^-];

$$da/dt = kC_0 \qquad 8.2.$$

where C_0 is the [OH^-] of the pore solution and k is a constant. If we assume for a first approximation a simple model where the bulk pore solution alkalinity remains constant with time and integrate eq. 8.2 with respect to t, then;

$$a = \tfrac{1}{2}kC_0t + a_0 \qquad 8.3.$$

where a_0 is the initial flaw size which can be obtained from Fig. 8.1 or eq. 8.1. The rate constant k will have units of $m.°C^{-1}.s^{-1}$ and will be dependent on the temperature and the magnitude of the load driving the stress corrosion process.

If the reaction between the glass and the pore solution is first order with respect to OH^- (e.g. $SiO_2 + OH^- \rightarrow HSiO_3^-$ *via* the formation of an SiO_2-OH^- adsorbed complex) then k could be written;

$$\mathbf{k = k_{sc}.e^{(-\Delta G^*/RT)}} \qquad \textbf{8.4.}$$

where k_{sc} = proportionality constant dependent on the stress driving the stress corrosion process, R = gas constant (8.314 $JK^{-1}\,mol^{-1}$), T = absolute temperature and ΔG^* = activation energy of the formation of the adsorbed complex. Since we do not know ΔG^* with any confidence at this stage, the discussion will continue without substitution of eq. 8.4 into eq. 8.3.

Note that k is likely to be very sensitive to temperature; an increase in hot water ageing temperature would have a 'double' effect, increasing k by its involvement in the exponential term in eq. 8.4 and by increasing the induced thermal expansion stress and hence k_{sc}.

We can calculate k values for the 65°C hot water ageing regime by substituting the initial pore solution alkalinities for C_0, the $t_{50\%}$ values in seconds (section 5.4.2.1) for t and deriving the flaw size required to produce a strength drop of 50% from eq. 8.1. The values obtained were 0.3 x 10^{-12} for matrices M and C, and 1.3 x 10^{-12} $m.°C^{-1}.s^{-1}$ for matrix O.

If we substitute eq. 8.3 into eq. 8.1 and assume that the composite strength equals the fibre strength multiplied by the fibre volume fraction ($\sigma_c = V_f\sigma_f$) then we can obtain an expression for composite strength vs. time;

$$\sigma_c = 0.893 V_f K_{ic}(\tfrac{1}{2}\pi k C_0 t + \pi a_0)^{-\frac{1}{2}} \qquad \textbf{8.5.}$$

Note that values for k could also be found by substituting failure stresses and the corresponding ageing times into eq. 8.5. rather than using $t_{50\%}$ values in eq. 8.3. Similar values were obtained from the data by both methods.

Figure 8.3. Equation 8.5 strength vs. time model cf. real data; 65°C hot water ageing.

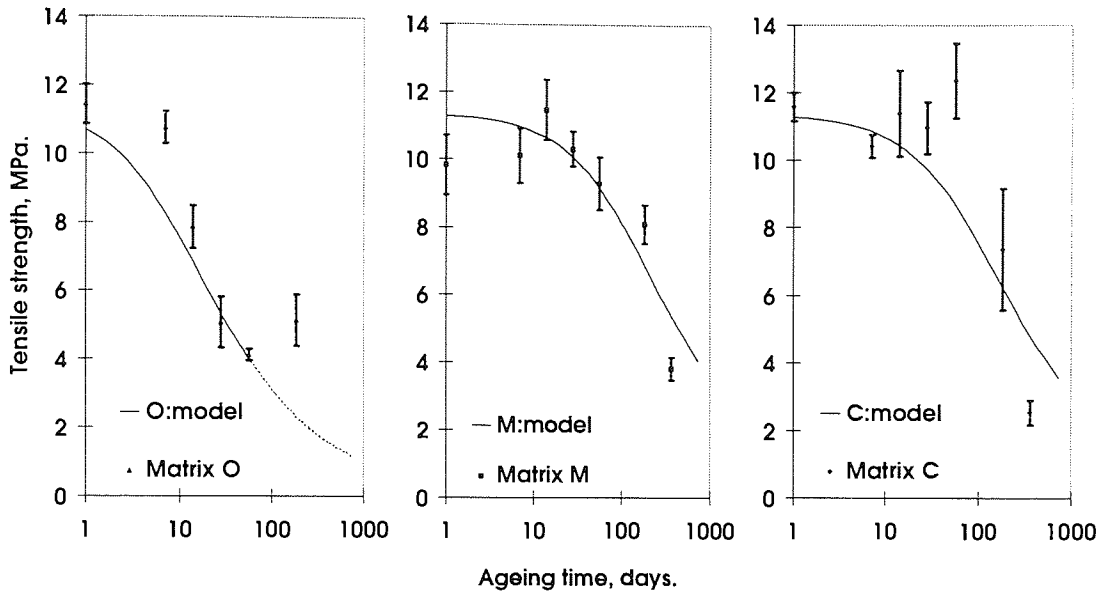

Notes:

- *a: '1 day' data on graphs are derived by interpolation between 0 day and 7 day results since '0 days' cannot be plotted on a log scale. For all matrices, the differences between the 0 and 7 day strengths were insignificant.*
- *b: Note that the model curves will have a 'cut off' point where the fibre strength becomes insufficient for the strands to carry the load transferred to them upon first matrix crack (i.e. the composite strength falls to the BOP value); a model of the complete process would be to combine the strength loss model curve with the BOP vs. time curve.*

Figure 8.3 compares the model with the results from the tensile tests. Although the fit is only reasonable at best, the shape is encouraging. It would appear to be a better representation than the strength $\propto$ 1/log[time] relationship used in the Litherland model in that it shows the rate of strength loss increasing with log[time] and also predicts the 'psuedo-dormant period' described in section 5.4.3 and Fig. 5.34.

As indicated above, the value of k for matrix O is rather higher than for the new matrices (1.3×10^{-12} cf. 0.3×10^{-12} $m.°C^{-1}.s^{-1}$). This suggests that the increased

degradation rate of matrix O composites at 65°C is not solely a consequence of their higher pore solution alkalinity, but that the induced load driving the stress corrosion process is also higher. Either the coefficient of thermal expansion is substantially greater for matrix O then for the new matrices (which seems unlikely), or some additional mechanism is inducing a load.

The most obvious phenomenon unique to matrix O composites was the preferential precipitation of well crystallised calcium hydroxide around and between the filaments. Many authors have long argued that the pressures exerted by crystals growing in confined spaces may be considerable (e.g. Warnes, 1926; Correns, 1949; Winkler and Singer, 1972; Xie & Beaudoin, 1992) and their arguments are based on the Riecke principle which states that "under linear pressure, a crystal has a... greater solubility than an unpressed crystal." (Correns, 1949). Some doubt exists as the precise magnitude of these pressures, but the derivations express the pressure in the following terms;

$$P_c = (RT/V_s).\ln\Psi \qquad 8.6.$$

where T = temperature (K), V_s = molar volume of the crystal (3.30×10^{-5} $m^3 mol^{-1}$ for portlandite) and Ψ is a scaling factor. According to Ping and Beaudoin (1992), this scaling factor is the ratio of the solubility product of the crystal at P_c to that at atmospheric pressure. According to Correns (1949) and Winkler & Singer (1972), it is the 'super-saturation ratio' i.e. the ratio of the pore solution concentration to the saturation concentration, a relationship which Correns confirmed experimentally for supersaturation ratios below about 2. The two scaling factors may in fact represent the same thing; there appears to be some confusion as to whether the variations in ionic activity products or molecular activities with pressure should be considered in the derivation. In either case, Ψ must be greater than unity for a pressure to be exerted. The pre-scaling factor pressure for $Ca(OH)_2$ (i.e. RT/V_s) at 65°C is 85 MPa.

Xie and Beaudoin (1992) did not attempt to quantify the scaling factor. Winkler and Singer (1972) gave some indication of its likely value by considering the critical dependence of nucleation rate on supersaturation ratio (i.e. Ψ). According to Stumm and Morgan (1981), the nucleation rate in nuclei per cm^{-3} can be calculated as a

function of Ψ for given values of temperature, interfacial energy and a factor related to the efficiency of collisions between ions or molecules. Inserting typical values for these parameters they showed that if Ψ=10, the nucleation rate is such that nucleation should not occur within geological timescales (i.e. 1 nucleus cm^{-3} per 10^{70} seconds; the age of the observable universe is $<10^{18}$ seconds) and if Ψ=100, nucleation is practically instantaneous (10^5 nuclei cm^{-3} sec^{-1}). Since portlandite is clearly being deposited within appreciable timescales we might expect Ψ to be at least 10 even if the nucleation rate is being accelerated by heterogeneous nucleation at flaws. Hence the pressure exerted by the growing crystals is likely to be a multiple rather than a fraction of RT/V_s (85 MPa).

The surprising attraction of $Ca(OH)_2$ to AR glass in preference to other precipitation substrates has been previously noted (Mills, 1981); it would be reasonable to assume that the crystals are likely to preferentially nucleate at surface flaws. As they grow, they may induce a local tensile stress at the flaw by two mechanisms. Firstly, the crystal may, constrained by the flaw geometry and the matrix, apply a 'wedge' action forcing apart the flaw faces; in this case we would not expect the full stress given above to be applied owing to local yielding of the constraint applied by the relatively weak matrix. However, if supersaturated pore solution is drawn by capillary action into the depths of small crack-like flaws (i.e. those with high depth:width aspect ratios) and nucleation occurs deeper within the crack, the constraint will be firmer (controlled by the glass strength not the matrix strength), and pressures approaching that given above could be generated. Directly applied pressures of these magnitudes would greatly accelerate crack growth and hence composite degradation.

A consequence of this model would be that for matrix O composites, an increase in ageing temperature would have three accelerating effects;

- increased reaction rate between the OH ions and the Si-O bonds in the glass,
- increased stress induced by thermal expansion coefficient mismatch,
- increased stress induced by crystal growth ($P \propto T$ in eq. 8.6).

This may explain why no degradation was observed under 20°C hot water ageing despite the pore solution alkalinity and the amount of portlandite deposition being of similar magnitude; k for matrix O composites is likely to be even more sensitive to temperature than for the new matrix composites.

This aggravation of the decay by deposition of portlandite in the confined spaces within the fibre/matrix interfacial area may also explain why many investigators have failed to observe significant damage or strength loss in fibres stored in hot alkaline or cement extract solutions (section 2.3.2.1); in a solution, any crystals deposited can grow unhindered by matrix.

8.1.2. Matrix densification.

The primary aspect of GRC durability related to matrix densification is increased bond strength reducing the critical fibre length and changing the failure mode from fibre pullout to fibre fracture. In theory, this does not apply to continuous uni-directionally reinforced composites. However, a brief discussion of the bond strength results in relation to critical fibre lengths is justified here.

Figures 7.6 to 7.8 show that the frictional bond strength increased with time, reaching a terminal value very quickly relative to the likely service life of GRC components. If these terminal values are used in design then embrittlement caused by a decrease in critical fibre length should not be encountered.

The terminal bond values (under 20°C ageing) were 2.3, 1.4 and 1.2 $N.mm^{-2}$ for matrices C, M and O respectively. The critical length l_c is defined as the minimum length required for the fibre to reach its breaking strain (Majumdar & Laws, 1991);

$$l_c = 2\sigma_{fu}a / p\tau \qquad 8.6.$$

Where σ_{fu} is the strength of the strand, **a** is the cross-sectional area, **p** is the perimeter and τ is the bond strength. From the image analysis results, p = 2.34mm, and a = $0.029mm^2$. The fibre strength σ_{fu} should be taken as the *in-situ fibre strength* (740 MPa) rather than the original strand strength (i.e. c., not b. in Fig. 8.1) to ensure pull-out is achieved. The critical fibre lengths thus calculated are 8, 13 and 15mm

respectively for matrices C, M and O. Typical values quoted in the literature are about 12 to 15mm (e.g. Majumdar & Laws, 1991; Bartoš, 1980; Oakley & Proctor, 1975), hence of the composites studied only matrix C would need special attention during design with regard to choosing fibre lengths and calculating efficiency factors (which are dependent on l_c [section 2.2.2.1]).

The secondary matrix densification effect is fully described in section 2.3.2.2. The ability of the matrix to locally yield adjacent to a bending fibre is reduced as the matrix hydrates. This decreases the radius of curvature of the fibre and increases the induced stress, causing premature failure.

Theoretically this does not apply when aligned fibres are used as reinforcement and samples are tested in direct tension. In practice, some fibre mis-alignment is inevitable and even fibres crossing a crack at right angles may undergo local flexure due to shifting crack paths (Bentur, 1985), so the effect should still manifest itself in some way.

The likely magnitude of the effect is difficult to quantify; however, it can be seen in the matrix C and M curves in Fig. 8.3 that the composite strengths after 1 years immersion at 65°C are somewhat less than those predicted by the fibre corrosion model. This may be a manifestation of the matrix densification effect; at later ages the matrix is dense enough to prevent local yielding and cause premature bending failure in already weakened fibres. The preferential carbonation of the interfacial area discussed in section 6.3.3 is likely to substantially aggravate this effect; calcium carbonate is a relatively hard material, and if the area under a bending fibre was carbonated we would expect it to be less capable of yielding.

(Note: The exaggerated strength loss is not seen on the matrix O curve, probably because by the time the matrix has densified sufficiently the fibres are already severely damaged by the alkalinity and the calcium hydroxide precipitation [section 8.1.1]).

The reduction of local yielding by matrix densification, even if aggravated by interfacial carbonation, would not however appear sufficient to cause substantial degradation alone; similar degrees of matrix strength enhancement (i.e. BOP, Figs. 5.5, 5.10 and 5.15) and interfacial carbonation were observed after 1 years immersion ageing at all temperatures. However, the 30% loss of toughness and strain to failure observed in the matrix O samples subjected to the accelerated carbonation regime may be due to matrix densification, especially considering the substantially enhanced matrix strength (Fig. 5.27).

8.1.3. Interfilamental precipitation.

Deposition of portlandite within the fibre bundles, transforming the strand from a flexible to a monolithic reinforcement unit, is often cited as a major cause of composite degradation. Again, it could be argued that for composites made with aligned reinforcement tested in direct tension the effect of bundle filling will not be apparent. In practice, the effect may still manifest itself for the same reasons discussed in section 8.1.2.

As noted in section 6.3.2, the complete filling of strands with monolithic portlandite deposits was not observed in any of the microstructural studies in this project. In agreement with the findings of Majumdar and Singh (1990), the inhibitive size applied to the second generation CemFIL 2 fibre appeared to substantially reduce the amount of portlandite deposited within the strands compared to composites made with first generation AR fibre.

For matrix O and matrix M composites after 1 years immersion ageing at 20°C, a substantial proportion of the void space within the fibre strands was seen to be filled with hydration products, either general matrix material (groundmass) or a mixture of calcite and groundmass (Figs. 6.1c, 6.4c). This appeared to have no effect on the composite properties. In matrix C composites, the void space was practically completely filled with groundmass from the outset (Fig. 6.7a), again with no effect on the properties. It would appear that interfilamental precipitation of material other than portlandite is not necessarily deleterious to GRC.

Fibre notching by portlandite crystals has been described by Yilmaz & Glasser (1991a). The term 'notching' infers a mechanical indentation of the fibre by the growing portlandite crystals. This seems unlikely given the relative hardness of glass compared with portlandite. The micrographs published purporting to show this notching could equally well be interpreted as partial envelopment of the fibre by portlandite crystals. The "...accelerated attack [that] takes place where relatively large $Ca(OH)_2$ crystals develop in contact with the fibres..." is more likely to be due to the enhanced sub-critical crack growth described for matrix O composites in section 8.1.1. In a later paper (Yilmaz & Glasser, 1991b) showed more convincing evidence of the damage caused to fibres by massive adjacent $Ca(OH)_2$ deposits, especially that caused by cracks in the massive deposits continuing into the fibre. It should be noted that both these papers are concerned with first-generation AR fibre reinforcement; second generation fibre does not seem to become associated with these massive deposits.

8.2. Relevancy of accelerated ageing regimes.

Discussion of the relevancy of accelerated ageing has three aspects;

- the accuracy of the Litherland (*et al.*, 1981) model for hot water ageing,
- the pertinence of hot water ageing in general and,
- the application of other accelerated ageing regimes.

8.2.1. Relevancy of the Litherland model.

Direct comparison could not be made between our results and the Litherland ageing model for reasons discussed in section 5.4.3. The discussion of its relevancy is therefore limited to comparing the trends observed during the tensile testing with those of the data used to formulate the model.

The central assumption of the model is that up to the point where ageing is completed (presumably where the composite strength has been decreased to the BOP) the composite strength is inversely proportional to log[time]. Hence a family of strength vs. log[time] curves obtained at different ageing temperatures will be a series of parallel straight lines (Litherland *et al.*, 1981). This does not hold for the data obtained

during this project, which would appear to be better represented by a strength $\propto 1/\sqrt{[A.time+B]}$ relationship (Fig. 8.3). In fact, the Litherland data could also be well represented by a family of strength vs. time curves of this nature with different values for k (which is primarily dependent on the ageing temperature [section 8.1.1]), since the 'middle' portions of the curves are similar to a series of parallel lines when plotted on a log scale (Fig. 8.4).

Figure 8.4. Comparison of families of stress corrosion model and Litherland model curves.

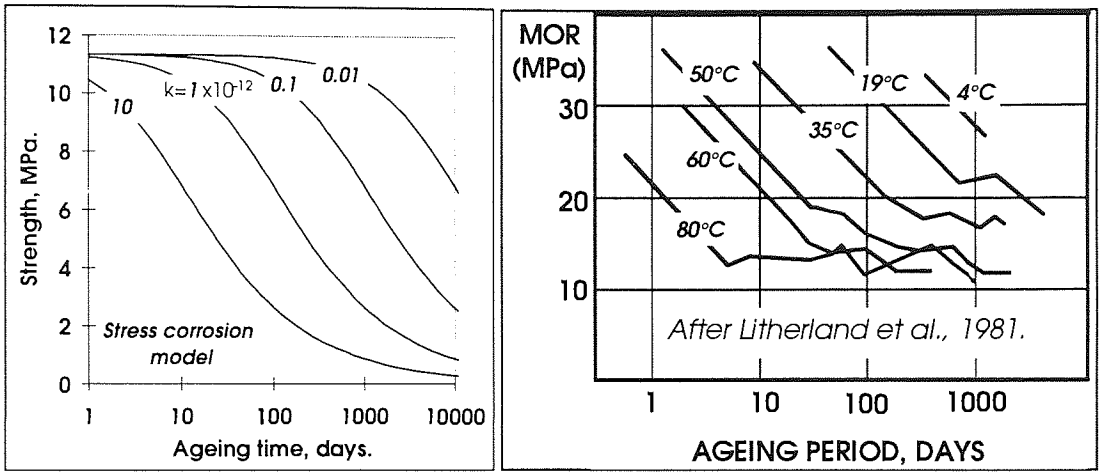

Because the central assumption of the model does not appear relevant for the new matrix composites, any long term strength predictions such as "immersion in water at 60°C for 40 days...[is] equivalent to 30 years natural exposure" (Gartshore *et al.*, 1991) or "28 days accelerated ageing at 50°C...would correspond to 7.8 years [conditions in Eastern Canada]" (Bentur & Diamond, 1985) for these composites should be treated with a great deal of caution.

8.2.2. Relevancy of hot water ageing.

Although the detail of the Litherland model (i.e. the acceleration factors, Table 2.3) may well be irrelevant for the new matrix composites, the basic premise (i.e. that short periods of hot water ageing are equivalent to longer periods of natural exposure), particularly with regard to strength, may be valid. As the formulators of the model themselves state (Litherland *et al.*, 1981) the only unequivocal way of confirming or refuting such a relationship is by comparison with very long term data obtained from

in service material; this data is simply not available for the new matrix composites. However, a number of the results from the various avenues of this study suggest that ageing at elevated temperatures changes the nature of the composites in ways that lower temperature or natural ageing would not.

In the new matrix composites aged underwater at 65°C, large quantities of C_3ASH_4 hydrogarnet was progressively formed, apparently replacing the ettringite formed during initial curing. Matrix M also contained monosulphate after long periods at 65°C. No traces of hydrogarnet (or monosulphate) were found in the samples aged at lower temperatures; according to Lea (1970), these hydrogarnets are unlikely to form below 50°C. Hence high temperature ageing has changed the composition of the new matrices. Matrix O hydration was little affected by temperature (section 4.6.2.2).

The terminal frictional bond formed between the fibre and the matrix is affected by temperature (Fig 7.10) in the opposite way to that which we might expect; higher ageing temperature produces lower eventual bond. The effect is clear for the new matrix composites and is probably present in matrix O composites (section 7.5.3.1). Although this has little bearing on the behaviour of continuously reinforced GRC, for short fibre reinforced material it will affect the critical length and hence the transition between fibre pull-out and fibre fracture modes of composite failure. As an example, the critical fibre length for matrix C composites aged at 20°C is 8 mm (section 8.1.2). The eventual bond formed at 65°C is about half that formed at 20°C; the critical length would therefore be about 15 mm. If the bond/temperature relationship is extrapolated to average UK exposure temperature (≈10°C), the critical length for in-service composites would less than 8 mm, possibly as low as 5mm.

If a matrix C composite were manufactured with a fibre length of 10 mm, aged for 28 days underwater at 65°C (purportedly equivalent to about 20 to 25 years of natural exposure and at a point prior to the onset of degradation owing to fibre corrosion) and mechanically tested, the failure mode would be pull-out and pseudo-ductility would be retained. If the same composite were then placed in an ambient temperature, natural weathering environment, after less than a year the bond would have developed to the

point where the fibre length is less than the critical length. The composite would fail upon loading with no pull-out behaviour and hence reduced toughness, despite an accepted accelerated ageing test predicting long-term retention of pseudo-ductility.

The complete lack of deterioration observed in composites aged at 20 and 38°C compared with the rapid total degradation at 65°C might suggest that there is a 'critical' temperature below which no degradation occurs. A common concept in static fatigue theory is that of a static fatigue limit i.e. a stress below which sub-critical crack growth will not occur. If the stress driving the sub-critical flaw growth in the composites is generated by the mismatch in the coefficients of thermal expansivity and is hence proportional to temperature then a critical temperature effect would be expected.

Regardless of the argument above, it will be seen from the model (section 8.1.1) that up to three separate effects are accelerated by increased temperature and the value of k is likely to be extremely sensitive to temperature. For example, for the model curve to fit within the standard error of the 38°C immersion strength data for matrix M, k must be increased by at least a factor of ten compared to 65°C; an 8% rise in absolute temperature produces *at least* a 1000% rise in k. There is likely to be a temperature below which strength loss becomes too slow to measure whether the fatigue limit principle applies or not.

Finally, an in service component at ambient temperature will be subject to dead loads and hence a possible driving stress for the sub-critical flaw growth process in addition to that provided by temperature variations; a coupon aged at ambient temperature will be under no such stress. Hence the behaviour of coupons aged at ambient temperature may well be different from that of components subject to similar conditions.

8.2.3. Relevancy of other accelerated ageing regimes.

Substantial matrix damage was suffered from the earliest stages by tensile test samples subjected to the cyclic ageing regime (sections 5.2.5, 5.4.2.2). No such damage was observed in similarly aged pre-fabricated GRC (section 5.3). Since it would appear that our samples were far more susceptible to cyclic ageing than real GRC, no

meaningful assessment of the likely comparison between cyclic and real component ageing can be advanced in this study.

One observation that can be made is that for the new matrix composites, cyclic ageing seemed to affect the post-cracking properties in much the same way as 65°C immersion ageing, while for matrix O composites the cyclic regime was clearly less deleterious.

The effect of the carbonating ageing regime has already been discussed (sections 5.2.6, 5.4.2.3, 4.6.2.3).

8.3. Other discussions.

The most interesting of the secondary phenomenon observed during the studies involved the bond strength behaviour. Matrix C composites formed (at 20°C) a much higher terminal frictional bond than the other composites (Fig. 7.6). At first glance one might attribute this to the increased apparent interfacial contact area for matrix C composites (Figs.6.1, 6.4 & 6.7). However, this cannot be the reason, since the unaged composite bond strengths were very similar yet the initial interfacial morphologies (matrix C cf. matrices O and M) were very different, and the interfacial morphology of matrix C composites developed least yet the bond developed most.

One reason may be linked with the strand compaction observed during the microstructural studies (section 6.3.4). As the matrix hydrates and begins to fill void space, the loosely packed fibre strands appear to become more compact with time; they are being 'squeezed'. In matrix O and M composites, the interfilamental void space is largely empty, filaments can easily be pushed together and little net force is developed. In matrix C composites, the void space is filled with hydration product from an early age and the strand will therefore resist being squeezed. This will result in a compressive 'hoop' stress being applied by the matrix on the strand; since the bond is frictional in nature, a higher bond strength will be manifested.

It is of course possible that the interface between the fibre and matrix on a much finer scale than observed in the thin section work differs between the matrices, although

this seems unlikely since similar hydration products were developed by all three matrices under 20°C immersion ageing and the initial frictional bonds were similar.

The reasons for the inverse relationship between hot water ageing temperature and terminal frictional bond (Figs. 7.9, 7.10) are similarly unclear. Fundamentally, the magnitude of the frictional bond is controlled by three parameters; the contact area between the fibre and matrix surfaces (A´), the 'normal force' applied at the interface (P´) and the coefficient of friction between the surfaces (μ) (i.e. the intrinsic nature of the interface). Since the bond strength does not increase indefinitely, we might not expect the eventual magnitude of the first two parameters to be greatly changed by increased ageing temperature; the squeezing effect described above (controlling P´) and A´ are likely to be a function of the degree of hydration of the matrix, and this will merely be accelerated by increased ageing temperature. Hence the fundamental nature of the interface is being changed at increased ageing temperature, the most likely reason being that the interfacial matrix material is different.

Both matrices C and M developed different hydration products at higher temperature (section 4.6.2.2) which might validate this theory; however, matrix O composites may also have developed lower frictional bond at higher ageing temperatures yet no different high temperature hydration products were observed. It may be possible that at higher ageing temperatures the adherent fibre surface layers observed by some authors (e.g. Cohen & Constantiner, 1985; Yilmaz & Glasser, 1991) control the bond between fibre and matrix. The results of this study are insufficient to completely explain the mechanism of fibre-cement bond in GRC.

9. CONCLUSIONS AND FURTHER WORK.

9.1. Conclusions.

The major conclusions of the project are set out below, together with references to the relevant discussion sections.

- **The new matrix composites perform substantially better than OPC composites in 65°C hot water and cyclic accelerated ageing tests.** *(5.4.2)*

- **The primary mechanism of composite degradation is fibre weakening caused by the enlargement of pre-existing flaws; this process has been successfully modelled based on stress corrosion/static fatigue principles and provides a closer fit to experimental data than existing models.** *(8.1.1)*

- **The improved performance of the new matrix composites is attributed partly to their lower pore solution alkalinity cf. OPC but more importantly to the lack of portlandite crystal growth at their fibre/cement interfaces, which aggravates the decay mechanism.** *(4.6.1, 6.3.1)*

- **Hot water ageing is useful in allowing distinctions between the time dependent behaviour of different composites to be observed and has aided formulation of the model. However, a body of evidence has been accumulated which suggests elevating the ageing temperature changes the intrinsic nature of the composites rather than simply accelerating hydration and interaction processes.** *(8.2.2, 7.5.3, 4.6.2.2)*

- **Cyclic ageing is not suitable for composites with no fine aggregate.** *(5.4.2.2)*

- **A constant 'terminal' bond is quickly developed in GRC; this should increase confidence in the derivation of the major design parameters of commercial short fibre GRC (critical length and the efficiency factors).** *(7.4.2, see also 2.2.2.1)*

9.2. Further work.

A number of points raised during this work merit further study:

Immersion ageing of composites at additional temperatures between 20 and 65 °C:

Immersion at 38°C should, for OPC composites, fall neatly between the 20°C regime (where no degradation was observed) and the 65°C regime (where rapid degradation was observed). This would allow the variation of the 'k' parameter in the model (8.1.1) with temperature to be derived. It would also confirm or deny whether the bond-temperature relationship holds for OPC GRC. Since it has been suggested that k is very sensitive to temperature, ageing at additional temperatures between 20 and 65°C for all composites would allow the applicability of the model to be tested for all composites.

Manufacture and ageing of Matrix D composites:

Matrix D displayed an exceptionally low pore solution alkalinity compared to all the other matrices; it also had no calcium hydroxide. It would then appear chemically ideal as a GRC matrix, and composites made thereof should have enhanced durability compared to the other matrix composites. Armed with the correct mix design, it should be possible to manufacture and test these composites and because of the very low matrix alkalinity the results should further elucidate the role of alkalinity in composite degradation.

Further investigation of the effect of carbonation on OPC composites:

Substantial additional matrix (i.e. pre-cracking) strength appears to be conferred on OPC composites by carbonation. Since the pre-cracking region is often of primary importance to component designers, any extension of this region is of great interest. Carbonation may also improve the chemical compatibility of OPC with glass fibres by removing portlandite from the matrix and reducing the pore solution alkalinity. In particular, if methods could be found to effect this carbonation in hours or minutes rather than months, carbonation treatment of components would become attractive to manufacturers. The use of supercritical carbon dioxide to speed up the process might prove useful in this respect.

Cyclic ageing of samples containing fine aggregate:

Although cyclic ageing had a profoundly deleterious effect on the matrix properties and serviceability of the composites prepared for this study, its effect on the post-cracking properties was less dramatic. Commercial GRC samples did not suffer matrix damage during cyclic ageing, probably due to the fine aggregate content. Hence although cyclic ageing proved unsuitable for the composites in this study, it is still worthy of further investigation using more robust composites, especially since standards are being drawn up for its application without any fundamental knowledge of the parameters affected by it.

Collection of new and review of existing long term mechanical property vs. time data:

Although it is not frequently stated, the fact remains that the only way to validate accelerated ageing models is by comparison with long-term real-time weathering data. For OPC composites, a lot of data exists in the literature. This data could be reviewed with a view to applying it to the model described in section 8.1.1 to help derive the relationship between k and temperature, and to form an accelerated ageing model based on the more realistic strength $\propto 1/\sqrt{[A.time+B]}$ relationship rather than the strength $\propto$ log[time] relationship used in the Litherland model. Similarly, long-term natural ageing programmes for the new matrix composites must be implemented to allow accelerated ageing predictions to be advanced with more confidence for these composites.

Refinement of the new model:

The new model (section 8.1.1) relies on a number of assumptions about the nature of the flaw growth process, primarily;

- that flaw growth rate is directly proportional to pore solution alkalinity.
- the reaction between the OH ions and the glass is a single first order reaction and
- that the pore solution alkalinity is constant with time.

Furthermore, k is a 'compound' constant, a function of the reaction rate between the pore solution and the glass at any given temperature and the induced load driving the

stress corrosion process. Substantial further refinement is possible and necessary if the model is to apply to all composites in all conditions, as must be the aim of its eventual derivation. Finite element analysis techniques may prove useful during the refinement, particularly in deriving the stresses exerted by thermal mismatch and portlandite crystal growth. Determination of the activation energy in eq. 8.4 would allow the stress related effects to be isolated, simplifying their study.

Diversification of the image analysis technique:

The image analysis technique used in this study proved successful in deriving strand perimeters. In its current form, it could be also be used to quantify the strand compaction observed in section 6.1; this is believed to be related to bond development. It could however be quite simply adapted to determine other parameters in GRC composites such as degrees of strand dispersion, volume fractions, variation in strand morphologies and patterns of fibre alignment in short fibre composites. The only radical adaptation necessary would be automation of some of the time consuming elements of the process (i.e. initial threshold value determination, manually repeated binary slicing and ensuring that any segmentation of the strand image is accounted for) so that far more samples could be quickly analysed to provide a stronger statistical basis for any findings. The public domain GRASS software used in this project is freely available, extremely adaptable and well supported by the image analysis community and should prove ideal for further development of the application of image analysis to GRC.

The basic principles behind the image analysis technique are not only applicable to GRC, but could easily find similar applications over a wide range of materials. More general applications might include determination of such parameters as porosity, aggregate/cement contents, aggregate or grain size distributions; in fact any parameter which is manifested by contrasting areas in a section. It should also be noted that the section does not have to be a thin section; it could be a polished surface or cut face. Neither does the image have to be captured digitally in the first instance; a traditional photograph could be scanned into a computer for analysis.

Investigations into workability and hydration kinetics.

All the new matrices displayed much lower workability than OPC and had to be used with superplasticiser. Although some exploratory work was carried out, a more detailed investigation of the changing rheological characteristics of the slurries, both with time and superplasticiser addition level, would be useful. Similarly, the new matrices tended to set quicker than OPC, matrix C remarkably so. This could be further investigated, using calorimetric techniques, to determine the early setting behaviour of these new matrices and the effect of the chemical retarders used in industry.

10: REFERENCES.

ASHBY, M.F. & JONES, D.R.H. (1986): Engineering Materials 2, An Introduction to Microstructures, Processing and Design; UK, Oxford, Pergamon Press 369pp.

ASKELAND, D.R. (1990): The Science and Engineering of Materials, 2nd Ed. London, Chapman & Hall. 880pp.

AVESTON, J. & KELLY, A. (1973): Theory of multiple fracture of fibrous composites; Journal of Materials Science, v.8, pp352-362.

AVESTON, J., COOPER, G.A. & KELLY, A. (1971): Single and multiple fracture; Proc. NPL Conf. The Properties of Fibre Composites pp15-27. UK, IPC Science and Technology Press.

AVESTON, J., MERCER, R.A. & SILLWOOD, J.M. (1974): Fibre reinforced cements - scientific foundations for specifications; Proc. NPL Conf. Composites - Standards, Testing and Design pp93-103. UK, IPC Science and Technology Press.

BALL, H.P. Jr. & WACKERS, M (1993): Performance of polymer modified GFRC; Proc, 9th Biennal Cong. GRC Assocn., Copenhagen, Denmark paper 2/3 - 16pp.

BARTOŠ, P. (1980): Analysis of pull-out tests on fibres embedded in brittle matrices; Journal of Materials Science v.15, pp3122-3128.

BARTOŠ, P. (1985): Effects of changes in fibre strength and bond characteristics due to ageing on fracture mechanism of GRC; Proc. PCI Symp. Durability of Glassfiber Reinforced Concrete, Illinois, USA pp136-146. ed. S. Diamond.

BARTOŠ, P.J.M. & ZHU, W. (1996): Effect of microsilica and acrylic polymer treatment on the ageing of GRC; Cement and Concrete Composites v. 18 pp31-39.

BENTUR, A. & DIAMOND, S. (1985): Effects of direct incorporation of microsilica into GFRC composites on retention of mechanical properties after ageing; Proc. PCI Symp. Durability of Glassfiber Reinforced Concrete, Illinois, USA pp337-351. ed. S. Diamond.

BENTUR, A. & MINDESS, S. (1990): Fibre Reinforced Cementitious Composites; 449p, London, Elsevier Science Publishers .

BENTUR, A. (1985): Mechanisms of potential embrittlement and strength loss of glass fiber reinforced cement composites; Proc. PCI Symp. Durability of Glassfiber Reinforced Concrete, Illinois, USA pp108-123. ed. S. Diamond.

BIRYUKOVICH, K.L., BIRYUKOVICH, Yu. L. & BIRYUKOVICH, D.L. (1964): Glass Fibre Reinforced Cement; Budevelnik, Kiev; Translation no. 12, Civil Engineering Research Assoc. 1965.

BLYTH, F.G.H. & de FREITAS, M.H. (1990): A Geology for Engineers (7th ed.); 325pp, London, Edward Arnold.

CANHAM, I., PAGE, C.L. & NIXON, P.J. (1987): Aspects of the pore solution chemistry of blended cements related to the control of alkali silica reaction; Cement and Concrete Research v.17 n.5, pp839-844.

CEMFIL NEWS No. 48 (1995): Cem-FIL International Ltd., Merseyside WA12 0JQ, England.

CEMFIL NEWS No. 49 (1996): ibid,.

CHAKRABORTY, M., DAS, D., BASU, S. & PAUL, A. (1979): Corrosion behaviour of a ZrO_2-containing glass in aqueous acid and alkaline media and in a hydrating cement paste; International Journal of Cement Composites v.1 n.3 pp103-109.

COHEN, E.B. & DIAMOND, S. (1975): Validity of flexural strength reduction as an indication of alkali attack on glass fibre in reinforced cement composites; Proc. of RILEM Sympos. , Fibre reinforced Cement and Concrete, pp315-326. UK, Lancs., Construction Press.

COHEN, M.D. & CONSTANTINER, D. (1985): Morphological developments of high and low alkali cement paste at the glass fiber-cement interface; Proc. PCI Symp. Durability of Glassfiber Reinforced Concrete, Illinois, USA pp158-173. ed. S. Diamond.

COLEMAN, N.J. & PAGE, C.L. (1997): Aspects of the pore solution chemistry of hydrated cement pastes containing metakaolin; Cement and Concrete Research v.27 n.1 pp147-154.

CORRENS, C.W. (1949): Growth and dissolution of crystals under linear pressure; Discussions of the Faraday Society n.5 pp267-271.

DANIEL, J.I. & SCHULTZ, D.M. (1985): Durability of glass fiber reinforced concrete systems; Proc. PCI Symp. Durability of Glassfiber Reinforced Concrete, Illinois, USA pp174-198. ed. S. Diamond.

DATTA, A.B., GUPTA, A.P. & PAUL, A. (1986): Alkaline durability of glass fibre containing SiO_2, PbO and Al_2O_3; Journal of Materials Science v.21 n.8, pp2633-2642.

DIAMOND, S. (1985): The GFRC durability problem : Nature, characteristics, and test methods; Proc. PCI Symp. Durability of Glassfiber Reinforced Concrete, Illinois, USA pp199-209. ed. S. Diamond.

DUCHESNE, J & BERUBE, M.A. (1994): Available alkalies from supplementary cementing materials; ACI Materials Journal v. 91 n. 3, pp289-299.

DUCHESNE, J. & BERUBE, M.A. (1994): The effectiveness of supplementary cementing materials in suppressing expansion due to ASR: Another look at the reaction mechanisms Part 2: Pore solution chemistry; Cement and Concrete Research, v. 24 n.2, pp221-230.

FRANKE, L. & OVERBECK, E. (1987): Loss in strength and damage to glass fibres in alkaline solutions and cement extracts; Durability of Building Materials v.5 n.1, pp73-79.

FRIEMAN, S.W. (1980): Fracture Mechanics of Glasses: Chap. 2 *in* Glass Science and Technology Volume 5, Elasticity and Strength in Glasses ed. D.R.Uhlmann & N.J.Kreidl; UK, London, Academic Press, pp21-75.

GAMBLES, C. (1997): The durability of glass fibres in GRC using new cement matrices; Final Year Research Project Report, Aston Uni., U.K..

GARTSHORE, G.C., KEMPSTER, E. & TALLENTIRE, A.G. (1991): A new high durability cement for GRC products; Proc. 8th Biennal Cong. GRC Assocn, Maastrict, Neth. pp3-12.

GERE, J.M. & TIMOSHENKO, S.P. (1990): Mechanics of Materials (2nd SI Ed.), London, U.K., Van Nostrand Reinhold (International) Co. Ltd.

GILL, T. (1996): Final Year Research Project Report; Aston University, Birmingham.

GLINICKI, M.A., VAUTRIN, A., SOUKATCHOFF, P. & FRANCOIS-BRAZIER, J. (1993): Impact performance of glass fibre reinforced cement plates subjected to accelerated ageing; Proc. 9th Biennal Cong. GRC Assocn., Copenhagen, Denmark pp1/1/I to 1/1/X.

GRAY, R.J. (1984): Analysis of the effect of embedded fibre length on fibre debonding and pullout from an elastic matrix, Part 1: Review of theories; Journal of Materials Science v.19, pp861-870.

HANNANT, D.J. (1978): Fibre Cements and Fibre Concretes; Chichester, U.K., John Wiley & Sons.

HOMMERTGEN, C. & ODLER, I. (1991): Glass fiber composites made with a cement based on a hydraulically active CaO-SiO_2-Al_2O_3 glass: Proc. Materials Research Soc. Symp. Fiber-Reinforced Cementitious Materials, Mass., USA, ed. S. Mindess & J. Skalny v. 211, pp93-104. USA, Pittsburgh, MRS.

HUANG, C.M., ZHU, D., CONG, X-D., KRIVEN, W.M., LOH, R.R. & HUANG, J. (1997): Carbon-coated-glass-fiber-reinforced cement composites: 1, Fiber pushout and interfacial properties; Journal of the American Ceramics Soc. v.80 n.9 pp2326-32.

JARAS, A.C. & LITHERLAND, K.L. (1975): Microstructural features in glass fibre reinforced cement composites; Proc. of RILEM Sympos., Fibre Reinforced Cement and Concrete, pp327-334. UK, Lancs., Constuction Press.

KAMEKI, M., HANNANT, D.J. & MULHERON, M. (1996): Techniques for determining some microstructural parameters in glass reinforced cement; Magazine of Concrete Research v.48 n. 176 pp229-236.

KELLY, A. & ZWEBEN, C. (1976): Poisson contraction in algned fibre composites showing pullout; Journal of Materials Science v.11 (Letters), pp582-586.

KUMAR, A. & ROY, D.M. (1985): Microstructure of glass fiber/cement paste interface in admixture blended Portland cement samples; Proc. PCI Symp. Durability of Glassfiber Reinforced Concrete, Illinois, USA pp147-156. ed. S. Diamond.

LARBI, J.A., FRAAY, A.L.A. & BIJEN, J.M.J.M. (1990): The chemistry of the pore fluid of silica fume-blended cement systems; Cement and Concrete Research v.20 n.4, pp506-516.

LAWRENCE, P. (1972): Some theoretical considerations of fibre pull-out from an elastic matrix; Journal of Materials Science v.7 pp1-6.

LAWS, V. (1982): Micromechanical aspects of the fibre-cement bond; Composites, v.113 n.2, pp145-151.

LAWS, V. (1971): The efficiency of fibrous renforcement of brittle matrices; Journal of Physics D: Applied Physics v.4 pp1737-1746.

LAWS, V., LANGLEY, A.A. & WEST, J.M. (1986): The glass fibre/cement bond; Journal of Materials Science v.21 n.1, pp289-296.

LEA, F.M. (1970): The Chemistry of Cement and Concrete (3rd Ed.) London, U.K., Edward Arnold Ltd. 727pp.

LI, S.H., LI, Z., MURA, T. & SHAH, S.P. (1992): Multiple fracture of fiber-reinforced brittle matrix composites based on micromechanics; Engineering Fracture Mechanics v. 43, n. 4, pp561-579.

LITHERLAND, K.L. & PROCTOR, B.A. (1985): The effect of matrix formulation, fibre content and fibre composition on the durability of glassfibre reinforced cement; Proc. PCI Symp. Durability of Glassfiber Reinforced Concrete, Illinois, USA pp124-135. ed. S. Diamond.

LITHERLAND, K.L. (1985): Test methods for evaluating the long term behaviour of GFRC; Proc. PCI Symp. Durability of Glassfiber Reinforced Concrete, Illinois, USA pp210-221. ed. S. Diamond.

LITHERLAND, K.L., OAKLEY, D.R. & PROCTOR, B.A. (1981): The use of accelerated ageing procedures to predict the long term strength of GRC composites; Cement and Concrete Research, vol. 11, pp455-466.

MAJUMDAR, A.J. & LAWS, V. (1991): Glass Fibre Reinforced Cement; Oxford, U.K., BSP Professional Books 197p.

MAJUMDAR, A.J. & RYDER, J.F. (1968): Glass fibre reinforcement for cement products; Glass Technology v.9 pp78-84.

MAJUMDAR, A.J. & SINGH, B. (1990): Long term durability of GRC; Proc. of V International Conf.,Durability of Building Materials and Components, ed. J.M. Baker *et al* pp651-658. UK, Cambridge, Chapman & Hall 1991.

MAJUMDAR, A.J. (1992): Fibre reinforced cement - thin sheets; Proc. 9th International Congress on the Chemistry of Cement, New Delhi, India pp737-774. New Delhi, National Council for Cement and Building Materials.

MAJUMDAR, A.J. (1974): Modification of GRC properties; Proc. NPL Conf. Composites - Standards, Testing and Design pp108-110. UK, IPC Science and Technology Press.

MAJUMDAR, A.J. (1974): The role of the interface in glass fibre reinforced cement; Cement and Concrete Research (a) v.4 pp247-266.

MAJUMDAR, A.J. (1975): Properties of fibre cement composites; Proc. of RILEM Sympos., Fibre Reinforced Cement and Concrete, pp279-314 . UK, Lancs., Construction Press.

MARKOU, B. (1996): Final Year Research Project Report; Aston University, Birmingham.

MILLS, R.H. (1981): Preferential precipitation of calcium hydroxide on alkali resistant glass fibres; Cement and Concrete Research v.11 n.5/6, pp689-697.

MOLLOY, H.J., JONES, J. & HARMON, T. (1993): Glass fiber reinforced concrete with improved ductility and long term properties; Proc. 9th Biennal Cong. GRC Assocn., Copenhagen, Den. paper 2\1 - 9pp.

MORRISON, J.K., SHAH, S.P. & JENQ, Y-S (1988): Analysis of fiber debonding and pullout in composites; Journal of Engineering Mechanics ASCE, v.114 n.2, pp277-294.

MURAT, M. & Al CHEIKH, A. (1989): Behaviour of E-glass fiber in basic aqueous medium resulting from the dissolution of mineral binders containing metakaolinite; Cement and Concrete Research v.19 n.1, pp16-24.

NAAMAN, A.E. & SHAH, S.P. (1979): Fracture and multiple cracking of cementitious composites; Proc. of XII National Symp. on Fracture Mechanics (ASTM), ed. S.W. Freiman pp183-201. USA, Pa. ASTM Spec. Tech. Publication 678.

NAAMAN, E.A., NAMUR, G.G., ALWAN, J.M. & NAJM, H.S. (1991): Fiber pullout and bond slip. II: Experimental validation; Journal of Structural Engineering v. 117 n. 9, pp2791-2800.

OAKLEY, D.R. & PROCTER, B.A. (1975): Tensile stress-strain behaviour of glass fibre reinforced cement composites; Proc. of RILEM Sympos., Fibre Reinforced Cement and Concrete, pp347-360. UK, Lancs., Construction Press.

OHIGASHI, T. (1978): Measurement of effective fracture energy of GRC; Proc. of RILEM Symp., Testing and Test Methods of Fibre Cement Composites, ed. RN Swamy pp67-78. UK, Lancs., Construction Press.

PAGE, C.L. (1982): Microstructural features of interfaces in fibre cement composites; Composites, April, pp140-144.

PERA, J. & AMBROISE, J. (1994): Durability of glass-fibre reinforced composites - influence of metakaolin and polymer; Proc. NSF/Univ. of Sheffield Workshop on Fibre Reinforced Cement and Concrete, Sheffield, UK., ed. R.N.Swamy & V. Ramakrishan pp78-87.

PERA, J., DEJEAN, J. & AMBROISE, J. (1993): Modelisation du comportement mecanique de composites ciment-fibres de verre en liason avec la natures des interfaces; Proc. of RILEM International Conf., Interfaces in Cementitious Composites, ed. JC Maso pp?? . London, E&FN Spon/Chapman and Hall.

PHILLIPS, C.J. (1972): Fracture of Glass, Chapter 1 *in* Fracture: An advanced treatise Volume 7, Fracture of Non-Metals and Composites, ed. H. Liebowitz; UK, London, Academic Press pp2-38.

PLAS, Ir. C. van der (1991): The many improvements of GRC by polymer modification; Proc. 8th Biennal Cong. GRC Assocn., Maastricht, Neth. pp13-21.

PROCTOR, B.A. & YALE, B (1980): Philosophical Transactions of the Royal Society London, A294, pp427-??.

PROCTOR, B.A. (1985): The development and technology of AR fibres for cement reinforcement; Proc. PCI Symp. Glassfiber Reinforced Concrete, Illinois, USA pp64-77. ed. S. Diamond.

PROCTOR, B.A., OAKLEY, D.R. & LITHERLAND, K.L. (1982): Developments in the assessment and performance of GRC over 10 years; Composites, v.13, pp173-179.

RAMACHANDRAN, V.S. (1969): Applications of Differential Thermal Analysis in Cement Chemistry; New York, Chemical Publishing Co. Inc. 308p.

ROMUALDI, J.P. & BATSON, G.B. (1963): Mechanics of crack arrest in concrete; Journal of the Engineering Mechanics Divn. ASCE, v.89 n.EM3, pp147-168.

SHAPIRO, M., WESTERVELT, J., GERDES, D., LARSON, M. & BROWNFIELD, K.R. (1993): GRASS 4.1 Programmers Manual, U.S. Army Construction Engineering Research Laboratory, Champaign, Illinois 61801, U.S.A.

SIH, G.C. (1973): Handbook of Stress Intensity Factors for Researchers and Engineers; USA, Pennsylv., Bethlehem Lehigh University.

SOUKATCHOFF, P. & RIDD, P.J. (1991): High durability glass-fibre reinforced cement using a modified cementitious matrix; Proc. 8th Biennal Cong. GRC Assocn, Maastrict, Neth. pp37-44.

St JOHN, D.A., POOLE, A.B. & SIMS, I. (1998): Concrete Petrography: A handbook of investigative techniques; London, U.K., Arnold, 474pp.

STUCKE, M.S. & MAJUMDAR, A.J. (1976): Microstructure of glass fibre-reinforced cement composites; Journal of Materials Science v.11 pp1019-1030.

STUMM, W. & MORGAN, J.J. (1981): Aquatic Chemistry: An Introduction Emphasizing Chemical Equilibria in Natural Waters, 2nd Ed.; Chichester, U.K. J. Wiley & Sons, 780pp.

SWAMY, R.N., MANGAT, P.S. & RAO, C.V.S.K. (1974): The mechanisms of reinforcement of cement matrices; *in* Fiber Reinforced Concrete, ACI-SP 44. Detroit, American Concrete Institute pp1-28.

THIERY, J., VAUTRIN, A. & FRANCOIS-BRAZIER, J. (1991): High durability glass-fiber reinforced modified cementitious matrix: Proc. Materials Research Soc. Symp. Fiber-Reinforced Cementitious Materials, Mass., USA, ed. S. Mindess & J. Skalny v. 211, pp79-91. USA, Pittsburgh, MRS.

VANIS, M. & KOMLOS, K. (1985): Contribution to methods of determining the chemical resistance of glass fibres in alkaline media; Proc. PCI Symp. Durability of Glassfiber Reinforced Concrete, Illinois, USA pp222-229. ed. S. Diamond.

WECHARATANA, M. & SHAH, S.P. (1983): A model for predicting fracture resistance of fiber reinforced concrete; Cement and Concrete Research, v.13 n.6, pp819-829.

WINKLER, E.M. & SINGER, P.C. (1972): Crystallization pressures of salts in stone and concrete; Bulletin of the Geological Society of America, 1972 pp3509-12.

XIE, P. & BEAUDOIN, J.J. (1992): Mechanism of sulphate expansion I. Thermodynamic principle of crystallization pressure; Cement and Concrete Research, v.22 n.4 pp631-640.

YILMAZ, V.T. & GLASSER, F.P. (1991a): Reaction of alkali-resistant glass fibres with cement. Pt.1 - Review, assessment and microscopy; Glass Technology v.32 n.3 pp91-98.

YILMAZ, V.T. & GLASSER, F.P. (1991b): Reaction of alkali-resistant glass fibres with cement. Pt.2 - Durability in cement matrices conditioned with silica fume; Glass Technology v.32 n.4 pp138-147.

YOUNG, J.F. (1985): Aspects of cement hydration relevant to the manufacture and performance of GFRC; Proc. PCI Symp. Durability of Glassfiber Reinforced Concrete, Illinois, USA pp78-89. ed. S. Diamond.

ZHU, W. & BARTOŠ, P.J.M. (1993): Effects of combined fibre treatments and matrix modifications on toughness of aged GRC; Proc. 9th Biennal Cong. GRC Assocn., Copenhagen, Den. paper 1\4 - 10pp.

APPENDIX 1: Example of stoichiometric 'Bogue' calculation. (re: Section 4.1.)

This example calculation is that used to derive the compound composition for OPC (4.1.1.)

(molar mass)	56.1	60.1	102.0	159.7	80.1	
	CaO	**SiO_2**	**Al_2O_3**	**Fe_2O_3**	**SO_3**	**%ww**
1. Oxide composition.	63.4	19.3	5.14	2.91	3.28	
2. Recast as moles/100g	1.130	0.321	0.050	0.018	0.041	
3. Eliminate SO_3 as gypsum and adjust CaO accordingly	1.089	0.321	0.050	0.018	-----	7.04
4. Eliminate Fe_2O_3 as C_4AF and adjust CaO and Al_2O_3	1.016	0.321	0.032	-----	-----	8.84
5. Eliminate remaining Al_2O_3 as C_3A and adjust CaO	0.919	0.321	-----	-----	-----	8.70
6. Correct for 'free lime', given as 1.6%	0.890	0.321	-----	-----	-----	1.6

Assume remainder consists of x moles of C_3S (molar mass 228.3) and y moles of C_2S (172.3);

1.	3x	+	2y	=	0.890 (ie. total combined CaO)	
2.	x	+	y	=	0.321 (ie. total SiO_2)	
3.	2x	+	2y	=	0.642 (2.x2)	
4.	x			=	0.248; x 228.3 (C_3S) =	56.6
			y	=	0.073; x 172.3 (C_2S) =	12.6

From oxide analysis: MgO = 1.36%, alkalies = 0.90% and minor phases = 2.13%.

These are then re-cast to sum to 100%;

C_3S	**C_2S**	**C_3A**	**C_4AF**	**CaO**	**MgO**	**Gypsum**	**Alkalies**	**Minors**
56.6	**12.6**	**8.7**	**8.8**	**1.6**	**1.4**	**7.0**	**0.9**	**2.1**

Cement chemistry notation key:

C	**CaO**
S	**SiO_2**
A	**Al_2O_3**
F	**Fe_2O_3**
Š	**SO_3**
H	**H_2O**

CO_3 is occasionally represented by ' **c** ' (lower case c) or $\overline{C}$ but is usually written out in brackets.

APPENDIX 2: XRD TRACES.

Figs. A2.1 to A2.11: Matrix O.
Figs. A2.12 to A 2.22: Matrix M.
Figs. A2.23 to A2.33: Matrix C.
Figs. A2.34 to A2.37: Matrix D.

Key:

All compounds are indicated in cement chemistry notation (see Appendix 1) except;

ETT Ettringite

Q Quartz

$\mathbf{C\overline{C}_C}$ Calcite

$\mathbf{C\overline{C}_A}$ Aragonite

$\mathbf{C\overline{C}_V}$ Vaterite

$\mathbf{Af_m}$ Monosulphate

MK 26.7° 2θ peak used to track meta-kaolin consumption in matrix M (see Fig. A2.12).

All traces have been corrected for baseline drift.

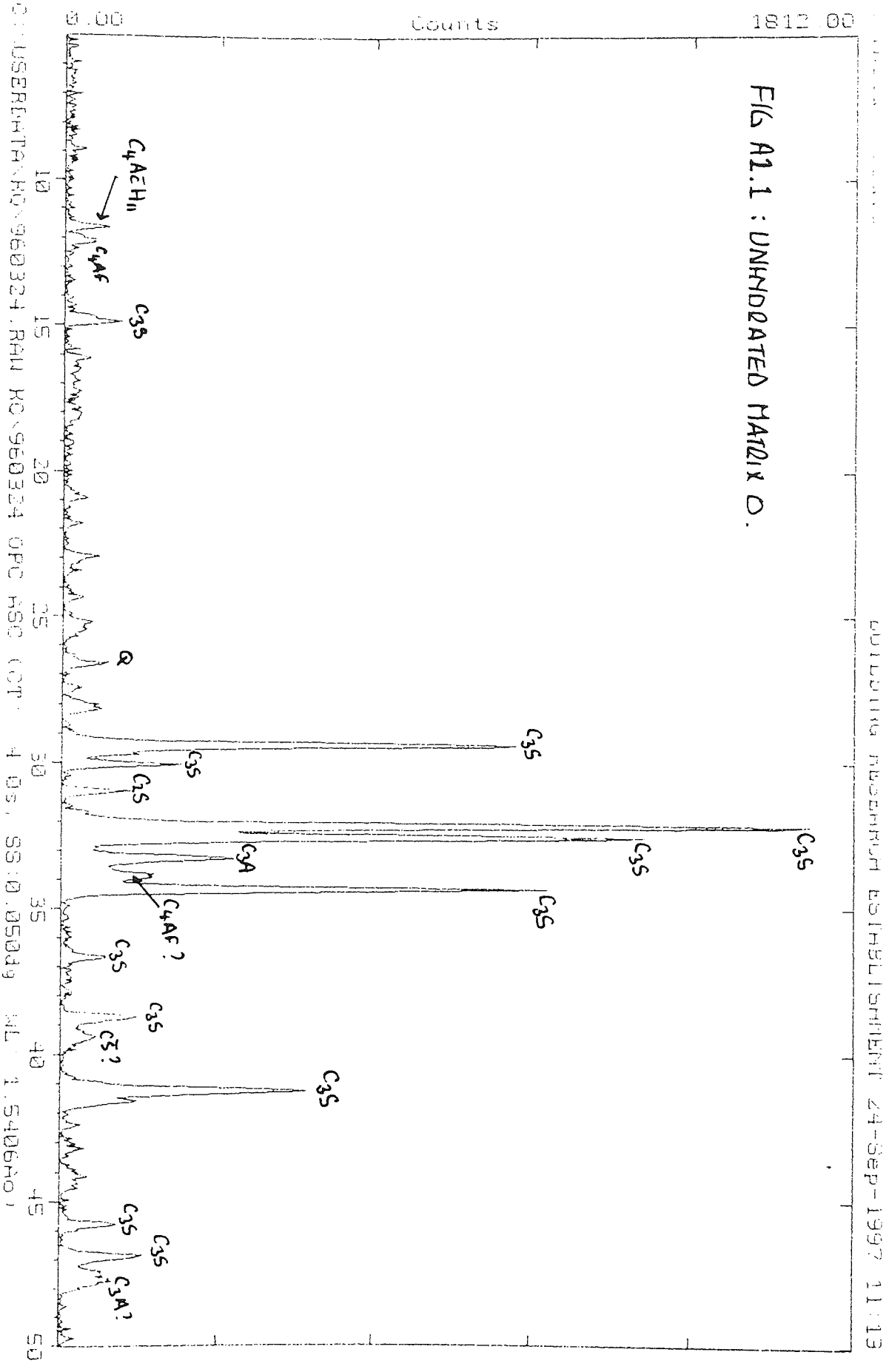
0.00
Counts
1812.00
FIG A1.1 : UNHYDRATED MATRIX O.
C4AEH11
C4AF
C3S
Q
C3S
C3S
C3S
C3A
C3S
C4AF ?
C3S
C3S
C3S
C3S ?
C3S
C3S
C3A ?
10
15
20
25
30
35
40
45
50

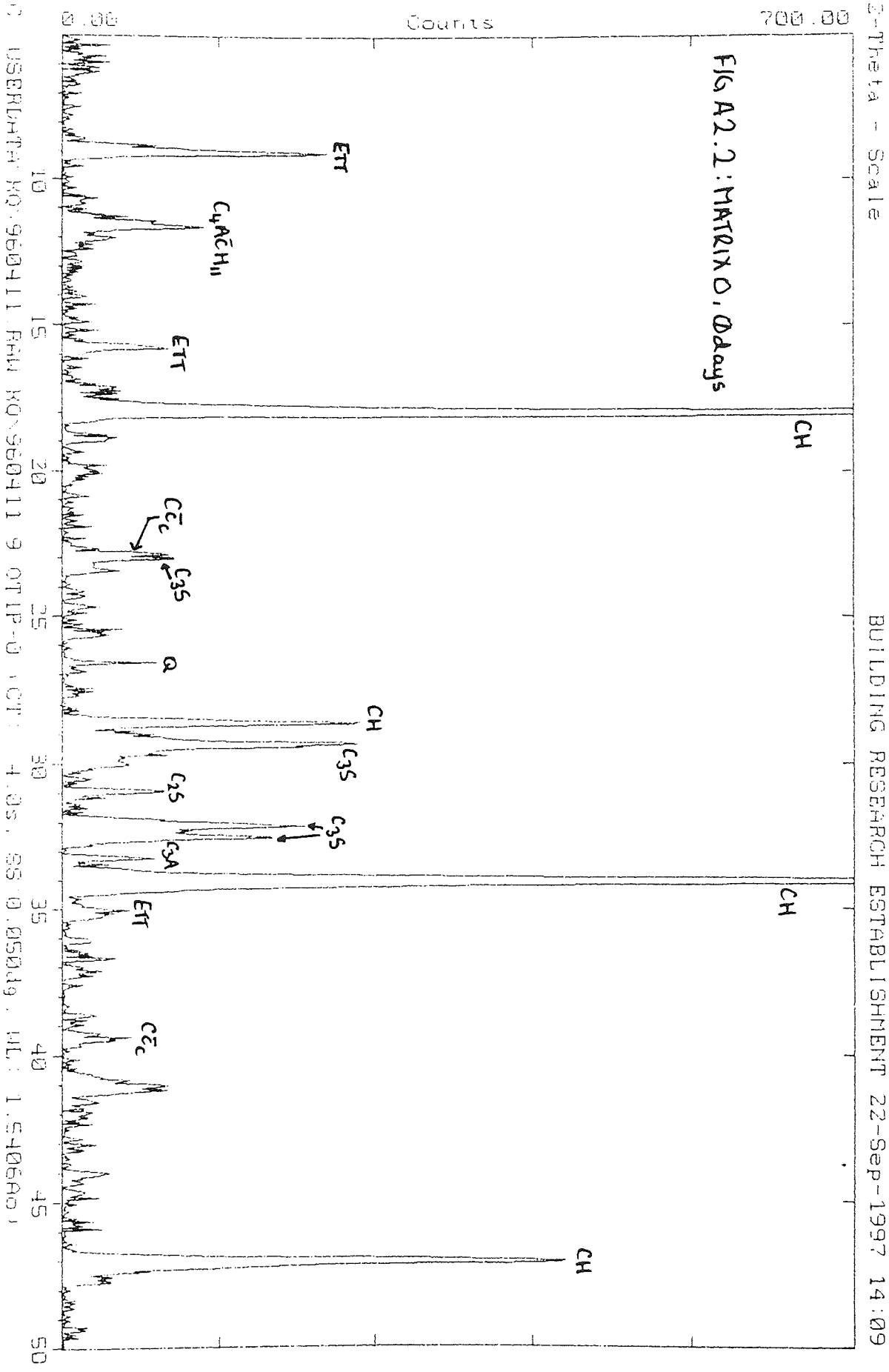
2-Theta - Scale
Counts
0.00
700.00
FIG A2.2: MATRIX 0, 0days
ETT
C4AH11
ETT
CH
CC
C35
Q
CH
C35
C25
C3S
C3A
ETT
CH
CC
CH
10
15
20
25
30
35
40
45
50
BUILDING RESEARCH ESTABLISHMENT 22-Sep-1997 14:09
USER/PETER KQ-960411 RAW KQ-960411 9 0TIP-0 .CP 4.0s, 0S 0.05000, WL: 1.54060

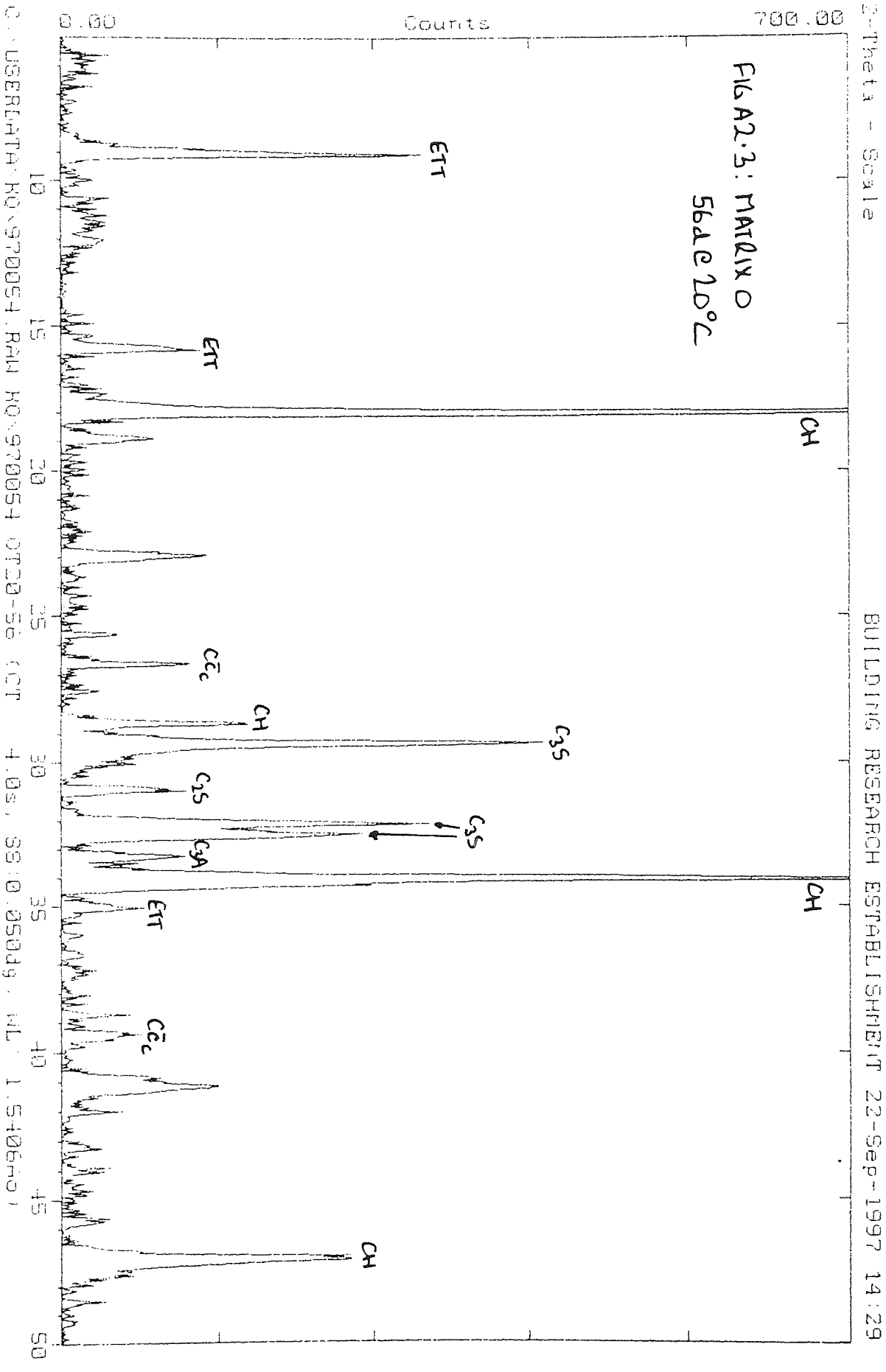
FIG A2.3: MATRIX O
56d @ 20°C
0.00
Counts
700.00
2-Theta - Scale
BUILDING RESEARCH ESTABLISHMENT 22-Sep-1997 14:29
C:\USERDATA\XQ\970054.RAW XQ\970054 OPC20-55 (OPT +0.05) SS:0.050d9 WL: 1.54060
ETT
CH
$C\bar{C}_c$
C_3S
C_2S
C_3A

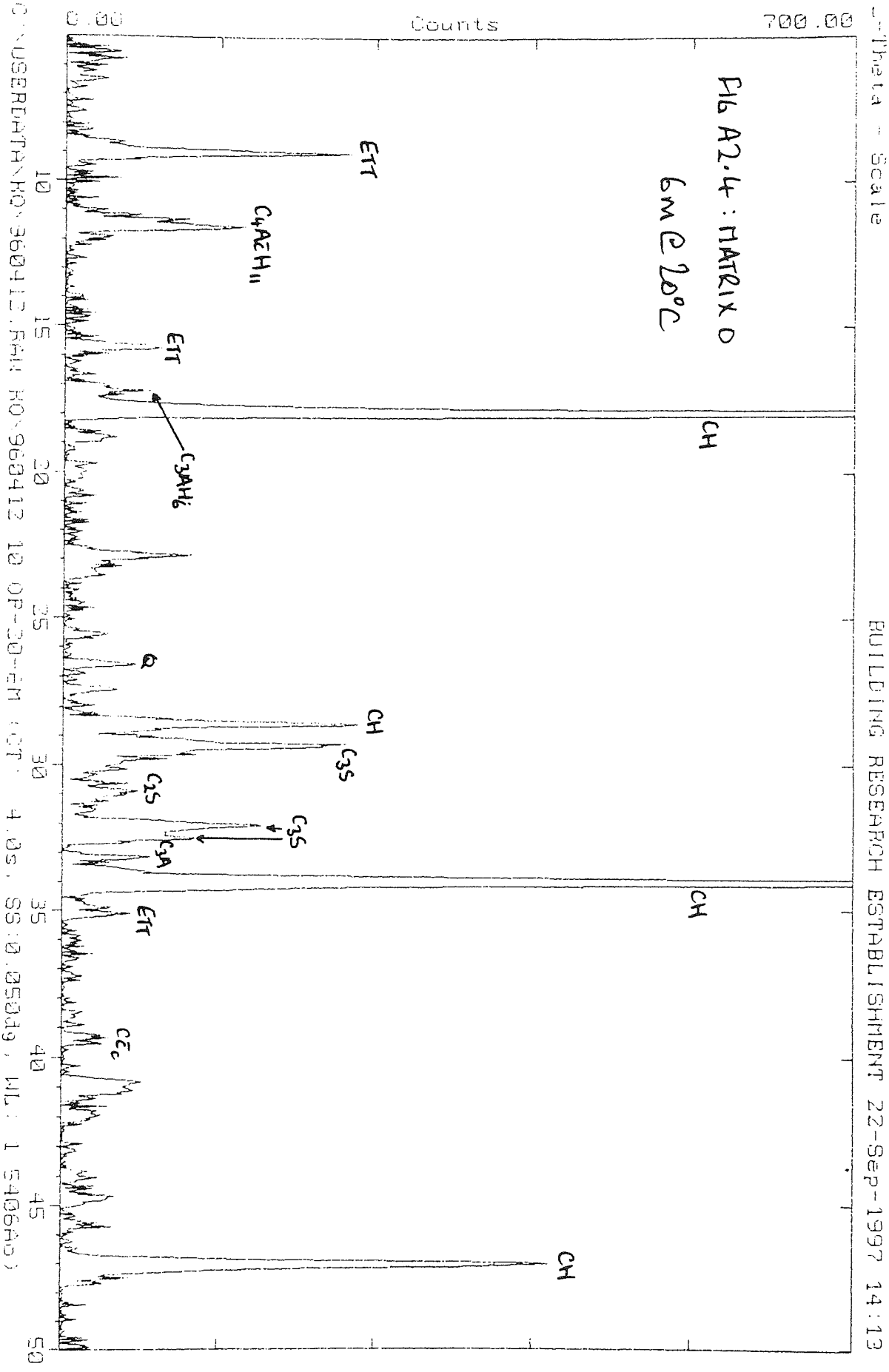
0.00
Counts
700.00
P16 A2.4 : MATRIX 0
6m @ 20°C
ETT
C4AH11
ETT
C3AH6
CH
Q
CH
C2S
C3S
C3S
C3A
CH
ETT
CEC
CH
-Theta - Scale
BUILDING RESEARCH ESTABLISHMENT 22-Sep-1997 14:13
C:\USERDATA\RQ\960412.RAW RQ\960412 10 OP-30-EM :CT: 4.0s, SS:0.050d9, WL: 1.54060

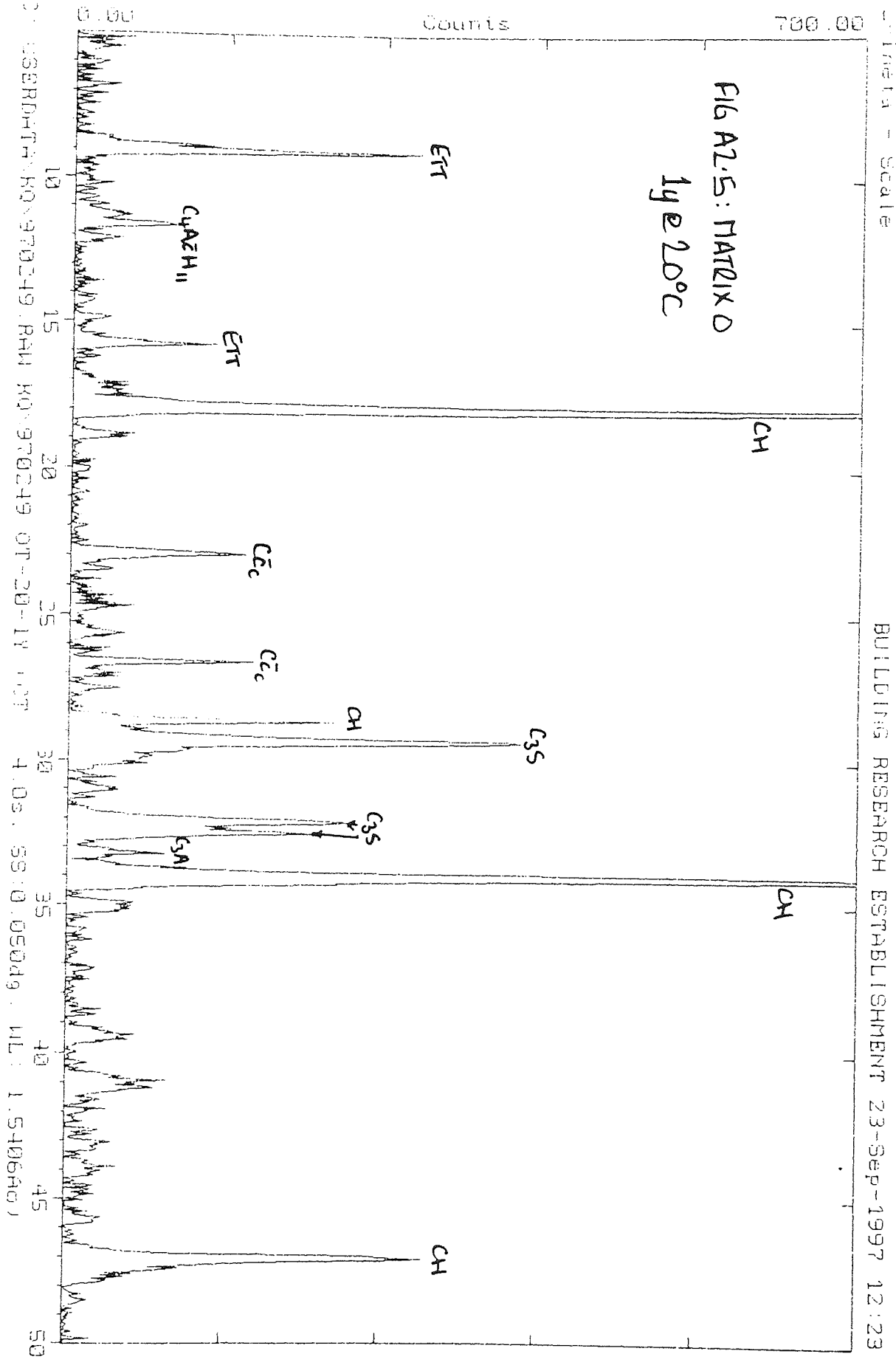
FIG A2.5: MATRIX O
1y @ 20°C
Counts
0.00
700.00
Linear - Scale
BUILDING RESEARCH ESTABLISHMENT 23-Sep-1997 12:23
E$\bar{T}\bar{T}$
$C_4A\bar{c}H_{11}$
E$\bar{T}\bar{T}$
CH
$C\bar{c}_c$
$C\bar{c}_c$
CH
C_3S
C_3S
E_3A
CH
CH
10
15
20
25
30
35
40
45
50

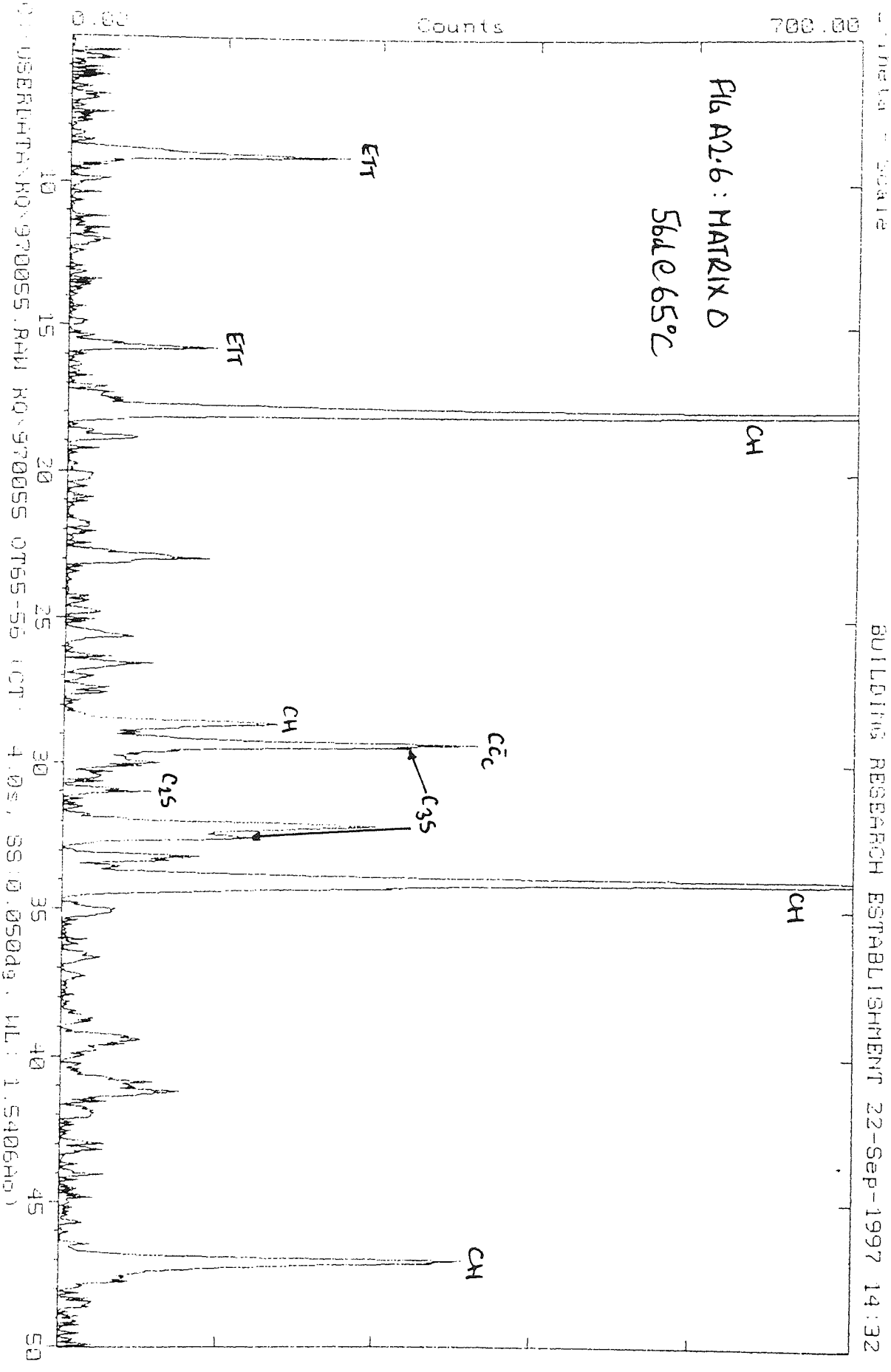
Counts
700.00
0.00
AG A2.6 : MATRIX D
56d @ 65°C
ETT
ETT
CH
CH
CC̄C
C35
C15
CH
CH
CH
BUILDING RESEARCH ESTABLISHMENT 22-Sep-1997 14:32
10
15
20
25
30
35
40
45
50

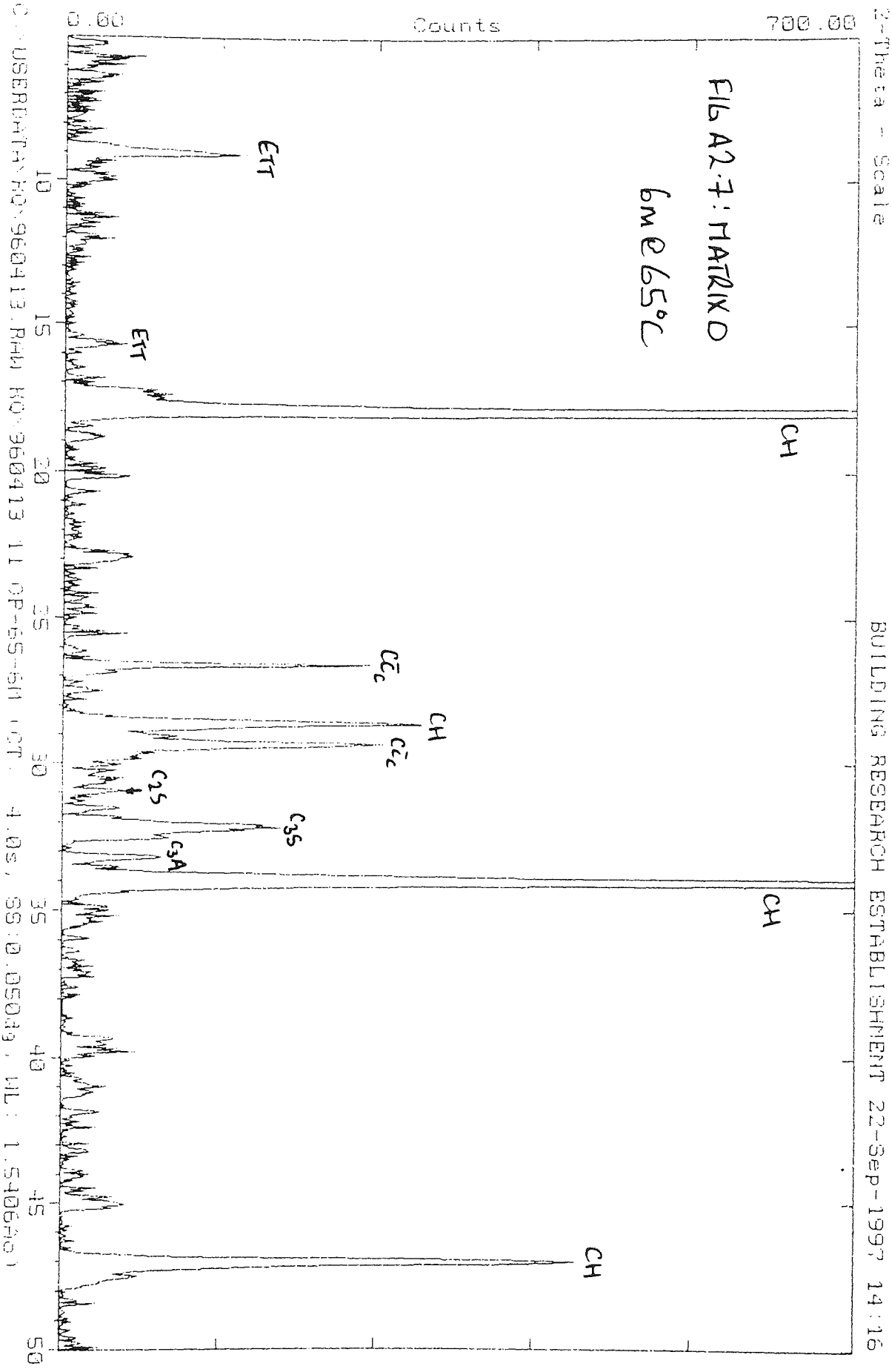
FIG A2.7: MATRIX
6m @ 65°C
Counts
0.00
700.00
2-Theta - Scale
BUILDING RESEARCH ESTABLISHMENT 22-Sep-1997 14:16
ETT
CH
$C\bar{C}_c$
$C\bar{C}_c$
C_2S
C_3S
C_3A
10
15
20
25
30
35
40
45
50

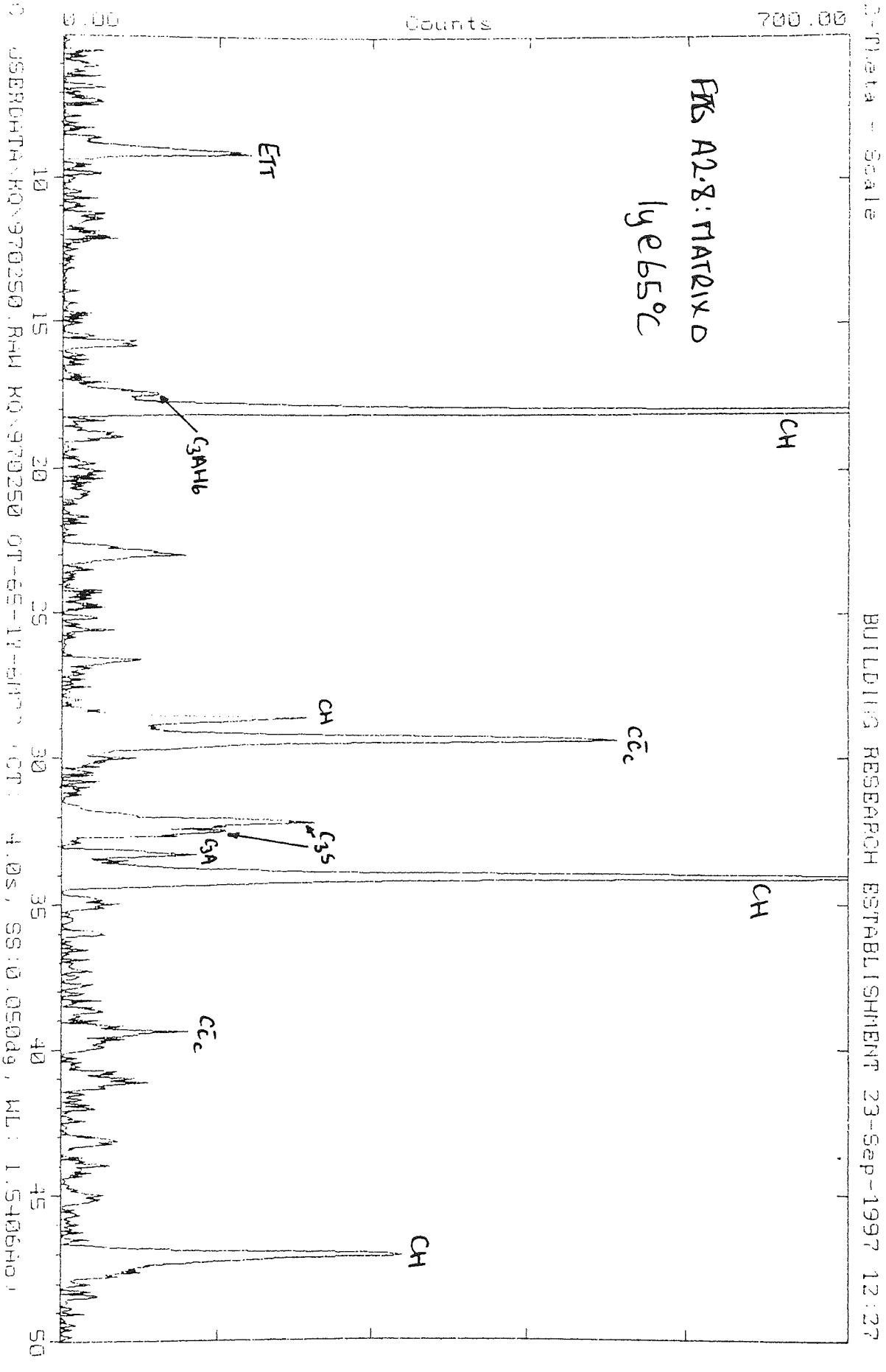
Data - Scale
BUILDING RESEARCH ESTABLISHMENT 23-Sep-1997 12:27
0.00
Counts
700.00
FIG A2.8: MATRIX D
lye 65°C
ETT
C3AH6
CH
CC̄C
C3S
C3A
10
15
20
25
30
35
40
45
50

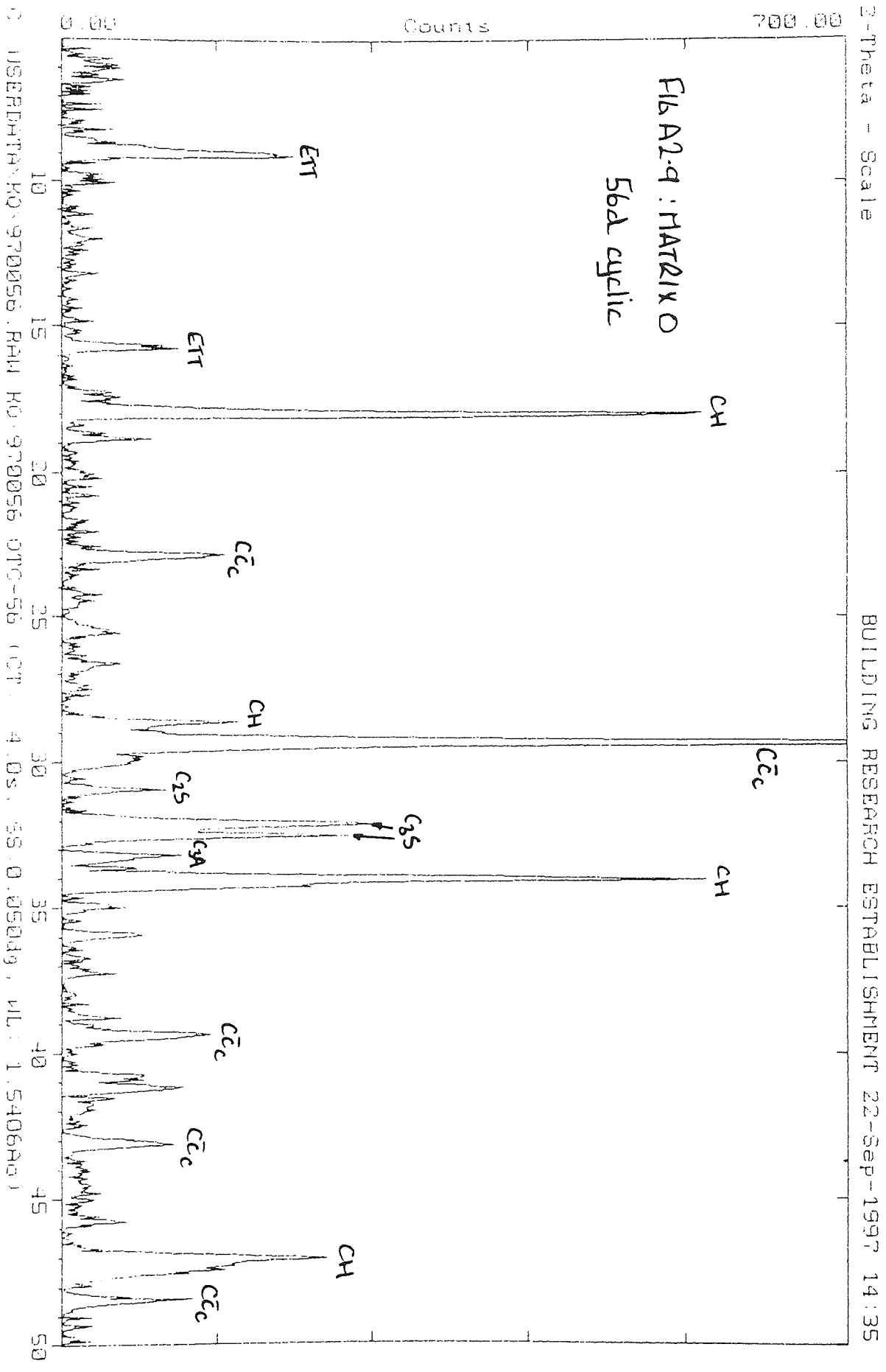
Fig A2-9 : MATRIX O
56d cyclic
Counts
0.00
700.00
2-Theta - Scale
BUILDING RESEARCH ESTABLISHMENT 22-Sep-1997 14:35
C:\USERDATA\XRD\970056.RAW XRD-970056 OTC-56 (OT 4.0s, 55 0.05009, WL: 1.5406Ag)
ETT
ETT
CH
CC̄C
CH
CC̄C
C2S
C3S
C3A
CH
CC̄C
CC̄C
CH
CC̄C
10
15
20
25
30
35
40
45
50

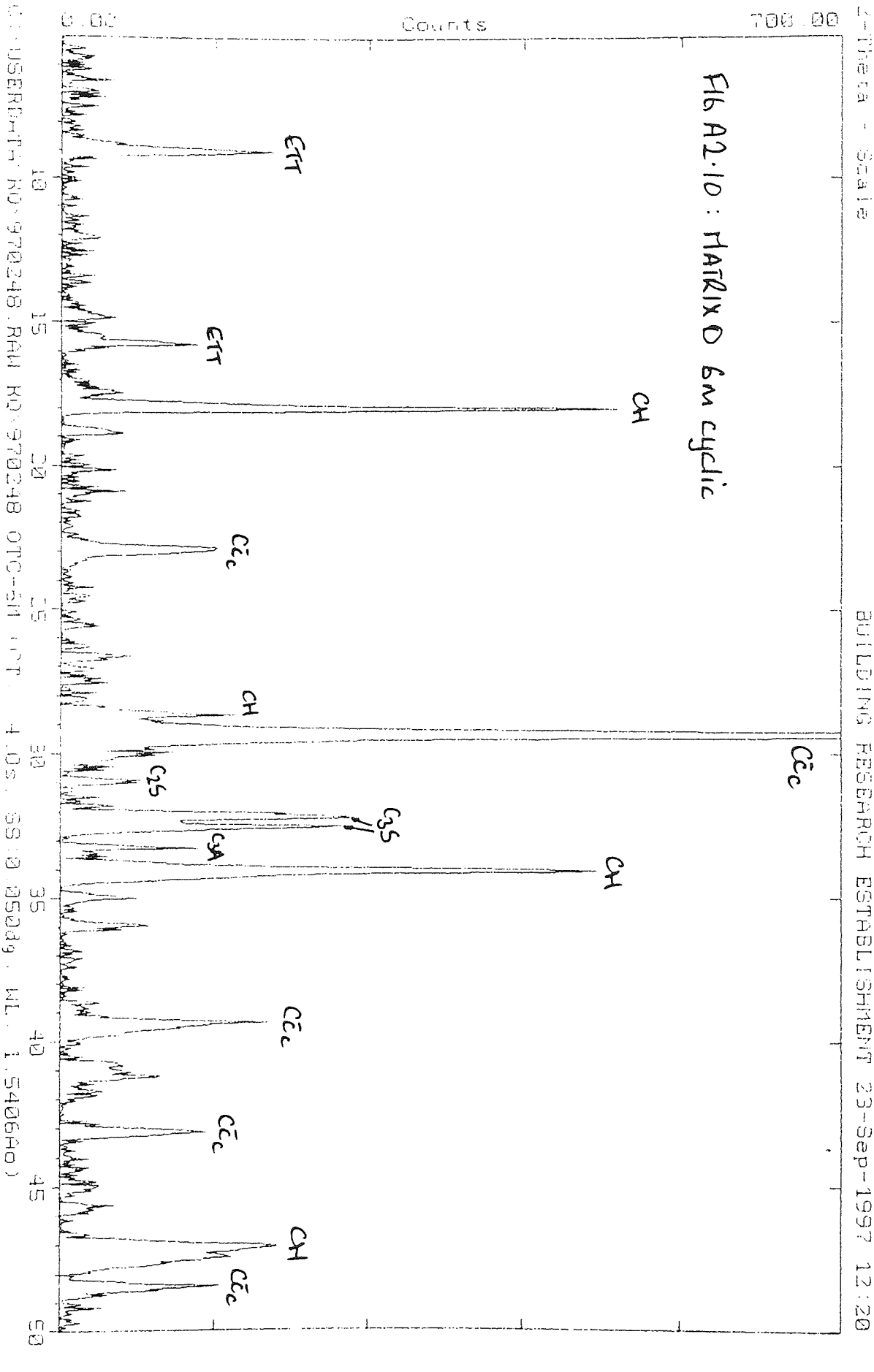
2-Theta - Scale
BUILDING RESEARCH ESTABLISHMENT 23-Sep-1997 12:20
Counts
0.00
700.00
FIG A2.10 : MATRIX D 6m cyclic
ETT
ETT
CH
CC̄c
CH
C2S
C3S
C3A
CH
CC̄c
CC̄c
CH
CC̄c
10
15
20
25
30
35
40
45
50
C:\USERDATA\RD\970248.RAW RD:970248 OTC-SM (CT 4.0s SS:0.05000 WL: 1.540600)

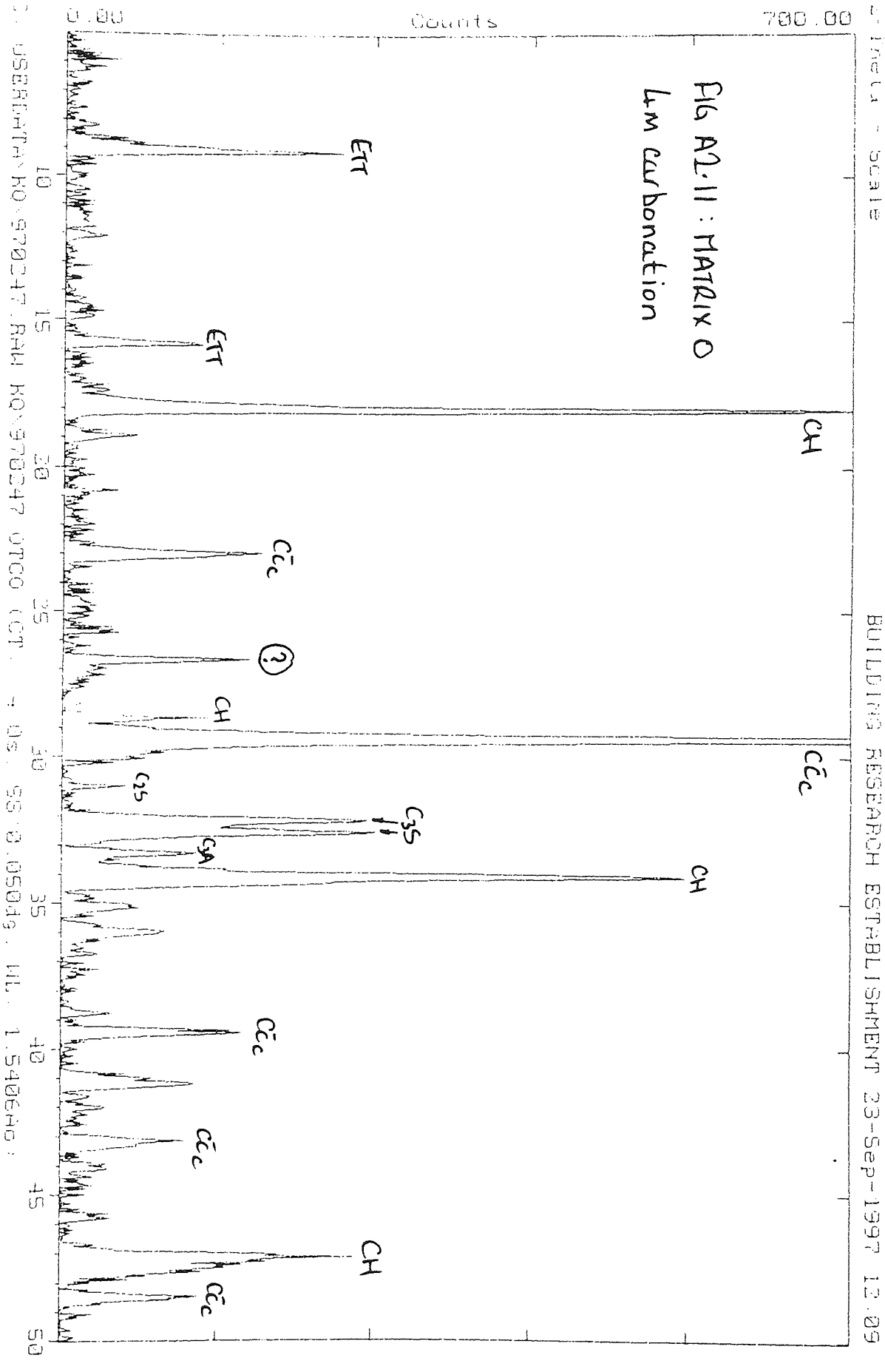
FIG A2.11 : MATRIX O
4m carbonation
Counts
0.00
700.00
ETT
ETT
CH
CC̄C
C̄C̄C
?
CH
C25
C35
C3A
CH
C̄C̄C
C̄C̄C
CH
C̄C̄C
BUILDING RESEARCH ESTABLISHMENT 23-Sep-1997 12:09
USER:HTA\KO\970247.RAW KO\970247 OTCO (CT, 4.0s, 55.0,050dg, WL, 1.5406nm)
10
15
20
25
30
35
40
45
50

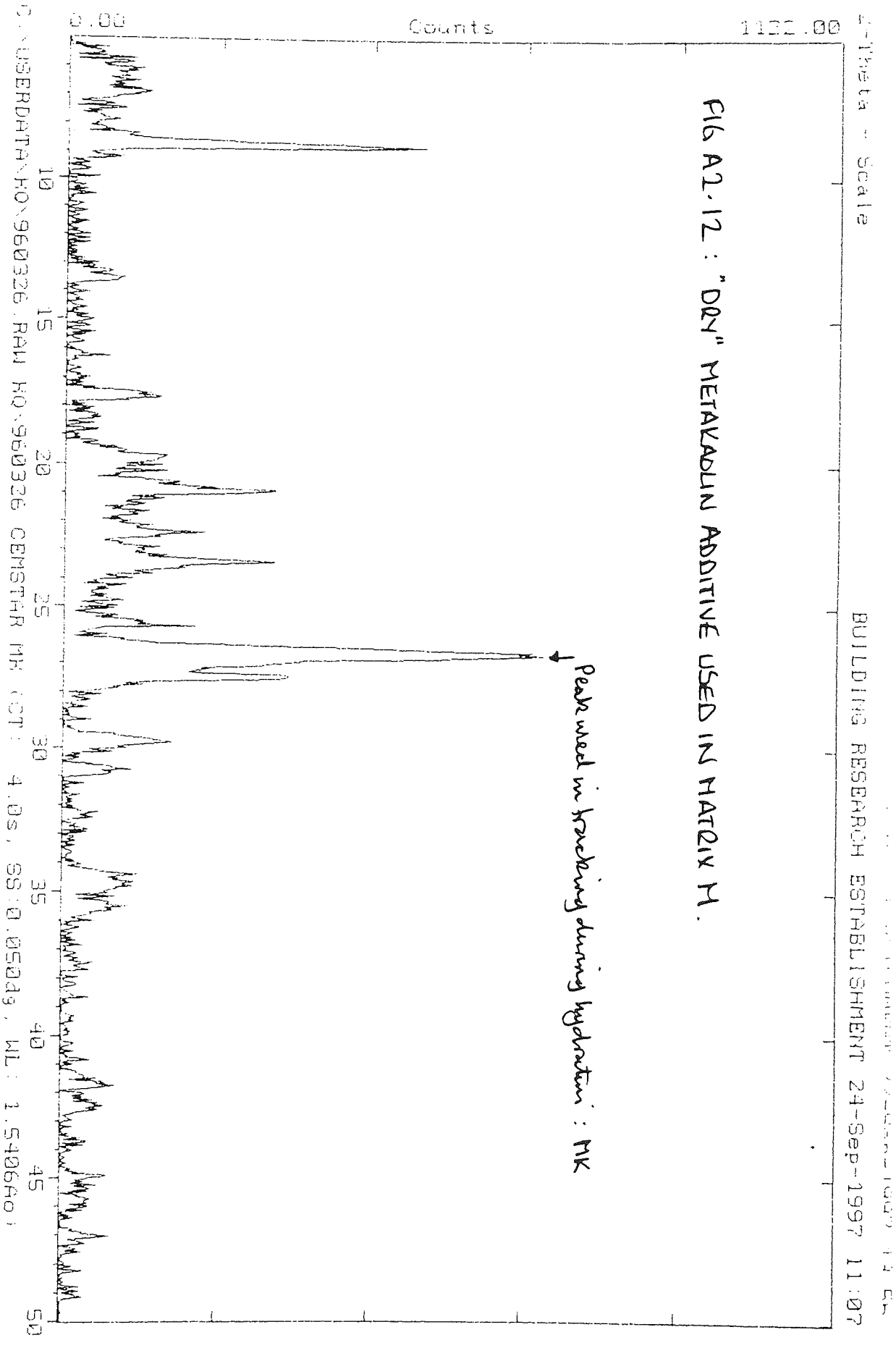

FIG A2.12 : "DRY" METAKAOLIN ADDITIVE USED IN MATRIX M.

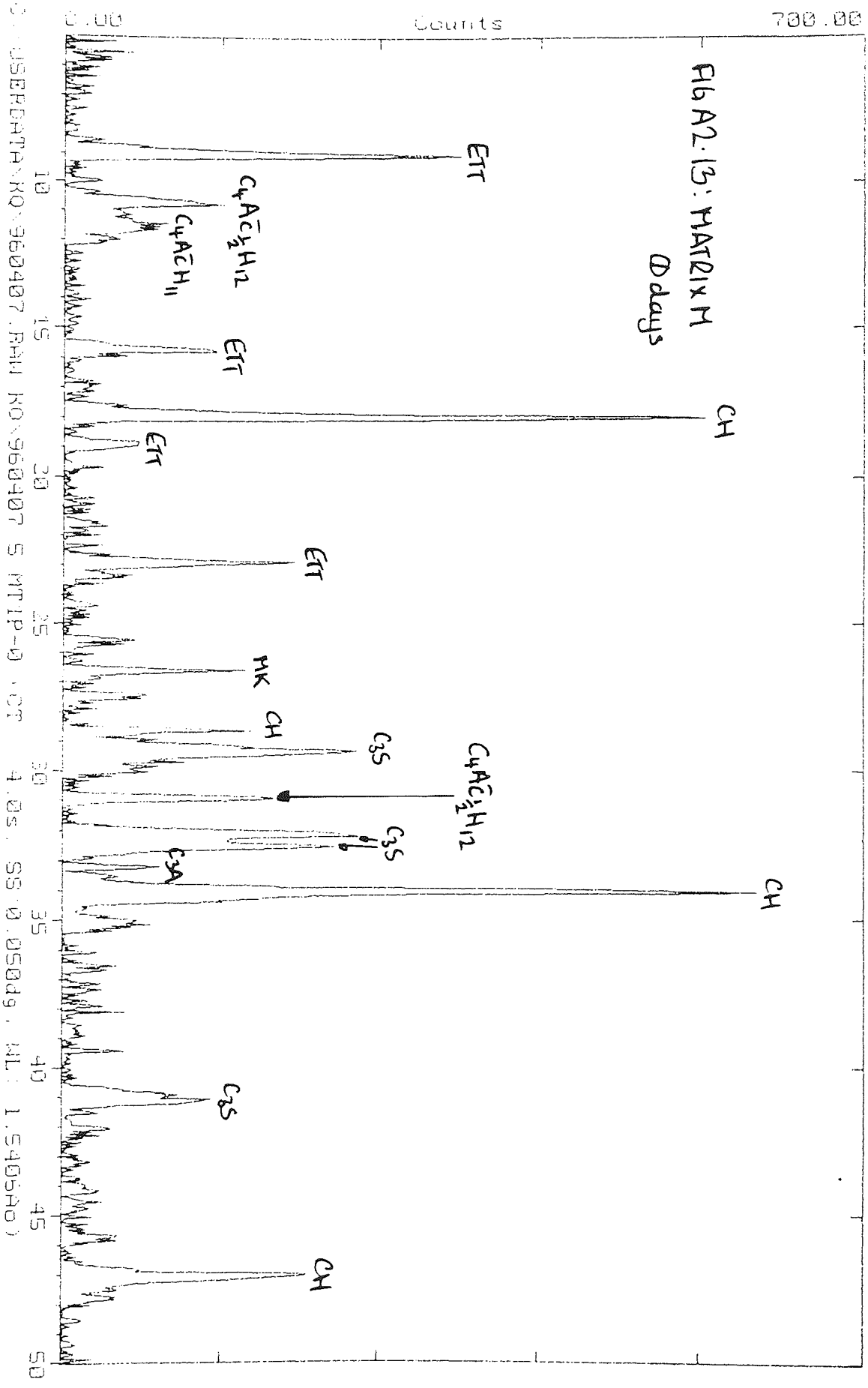
Counts
700.00
A6 A2.13: MATRIX M
0 days
ETT
$C_4A\bar{C}_{\frac{1}{2}}H_{12}$
$C_4A\bar{C}H_{11}$
ETT
CH
ETT
ETT
MK
CH
C_3S
$C_4A\bar{C}_{\frac{1}{2}}H_{12}$
C_3S
C_3A
CH
C_3S
CH
10
15
20
25
30
35
40
45
50

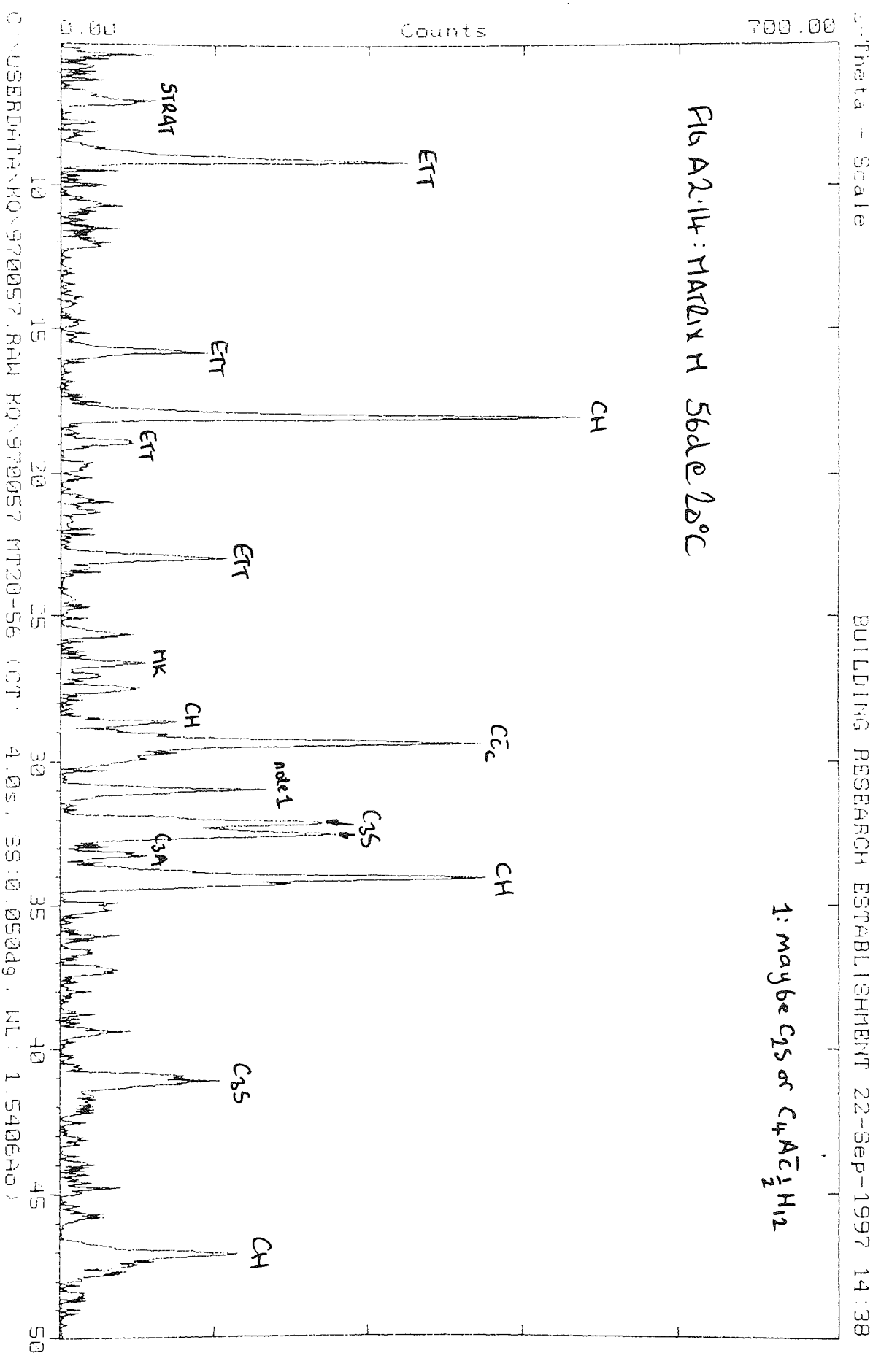
Fig A2.14: MATRIX H 56d @ 20°C
1: maybe C2S or C4AC̄½H12
2-Theta - Scale
BUILDING RESEARCH ESTABLISHMENT 22-Sep-1997 14:38
Counts
0.00
700.00
10
15
20
25
30
35
40
45
50
STRAT
ETT
ETT
ETT
ETT
CH
MK
CH
CC̄
node1
C3S
C3A
CH
C2S
CH
C:\USERDATA\KQ\970057.RAW KQ\970057 MT20-56 (CT 4.0s, SS:0.050d9, WL: 1.5406Ao)

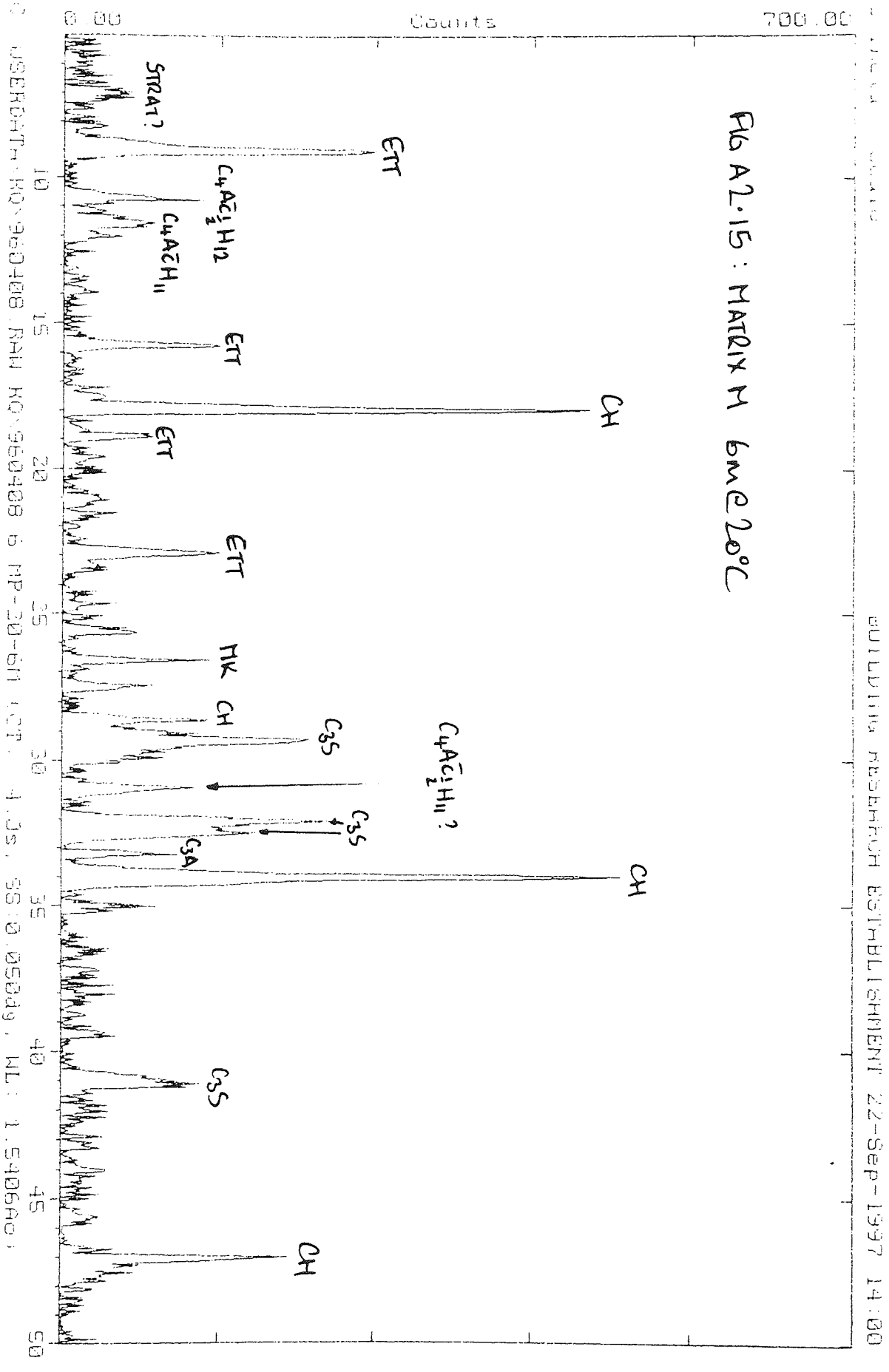
FIG A2.15 : MATRIX M 6m@20°C
Counts
0.00
700.00
STRAT?
ETT
C4AC̄2H12
C4AC̄H11
ETT
CH
ETT
ETT
MK
CH
C3S
C4AC̄2H11 ?
C3S
C3A
CH
C3S
CH
10
15
20
25
30
35
40
45
50

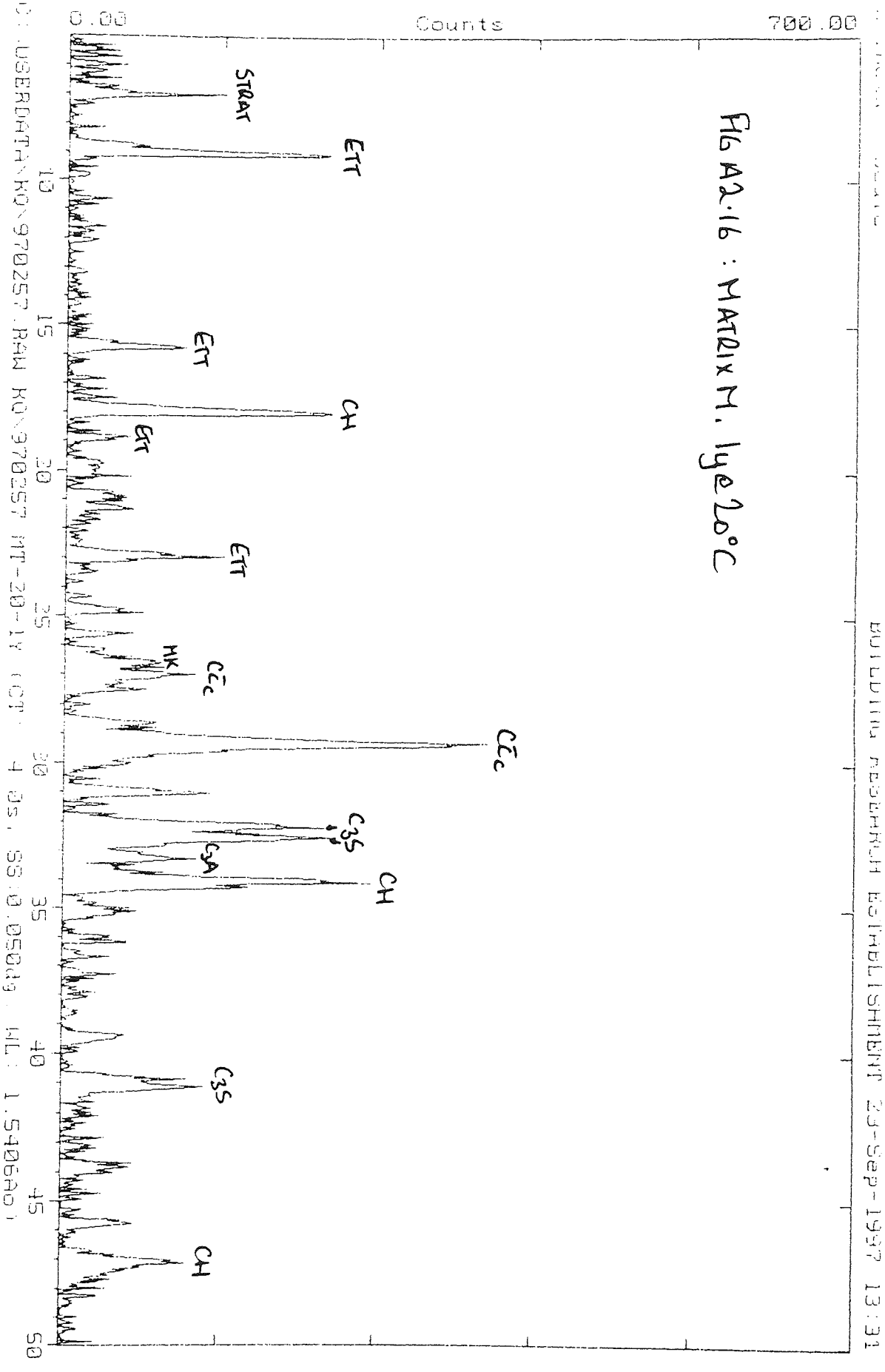
0.00
Counts
700.00
FIG A2.16 : MATRIX M. Iye 20°C
STRAT
ETT
ETT
CH
ETT
ETT
HK
CĒc
CĒc
C3S
C3A
CH
C3S
CH
10
15
20
25
30
35
40
45
50
D:\USERDATA\KQ\970257.RAW KQ\970257 MT-20-1Y (CT 4 0s, SS:0.050d WL: 1.540600
BUILDING RESEARCH ESTABLISHMENT 23-Sep-1997 13:31

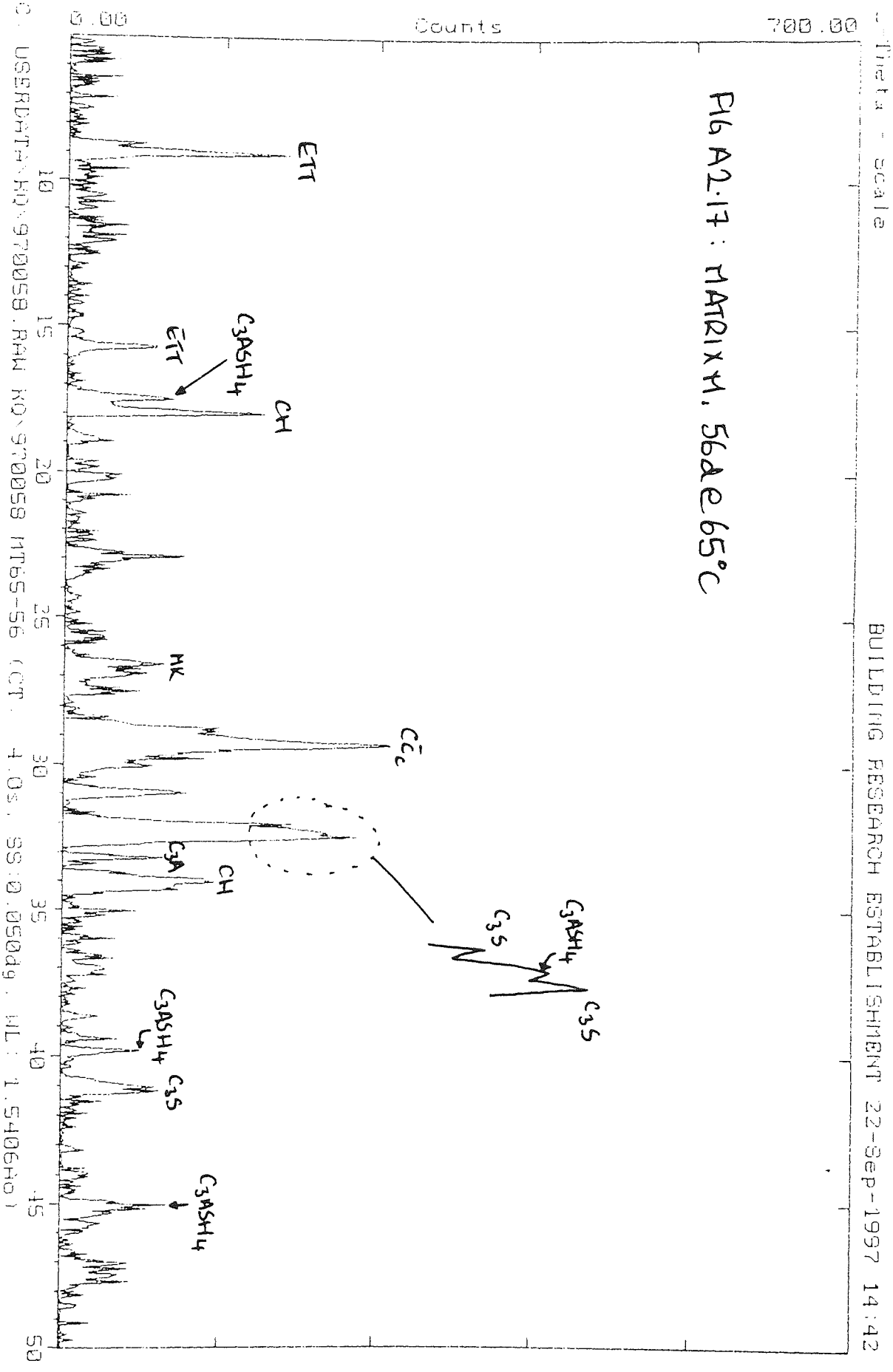
P16 A2.17 : MATRIX M, 56d @ 65°C
Counts
0.00
700.00
ETT
C3ASH4
ETT
CH
MK
CC
C3A
CH
C3S
C3ASH4
C3ASH4
C3S
C3ASH4
BUILDING RESEARCH ESTABLISHMENT 22-Sep-1997 14:42
10
15
20
25
30
35
40
45
50

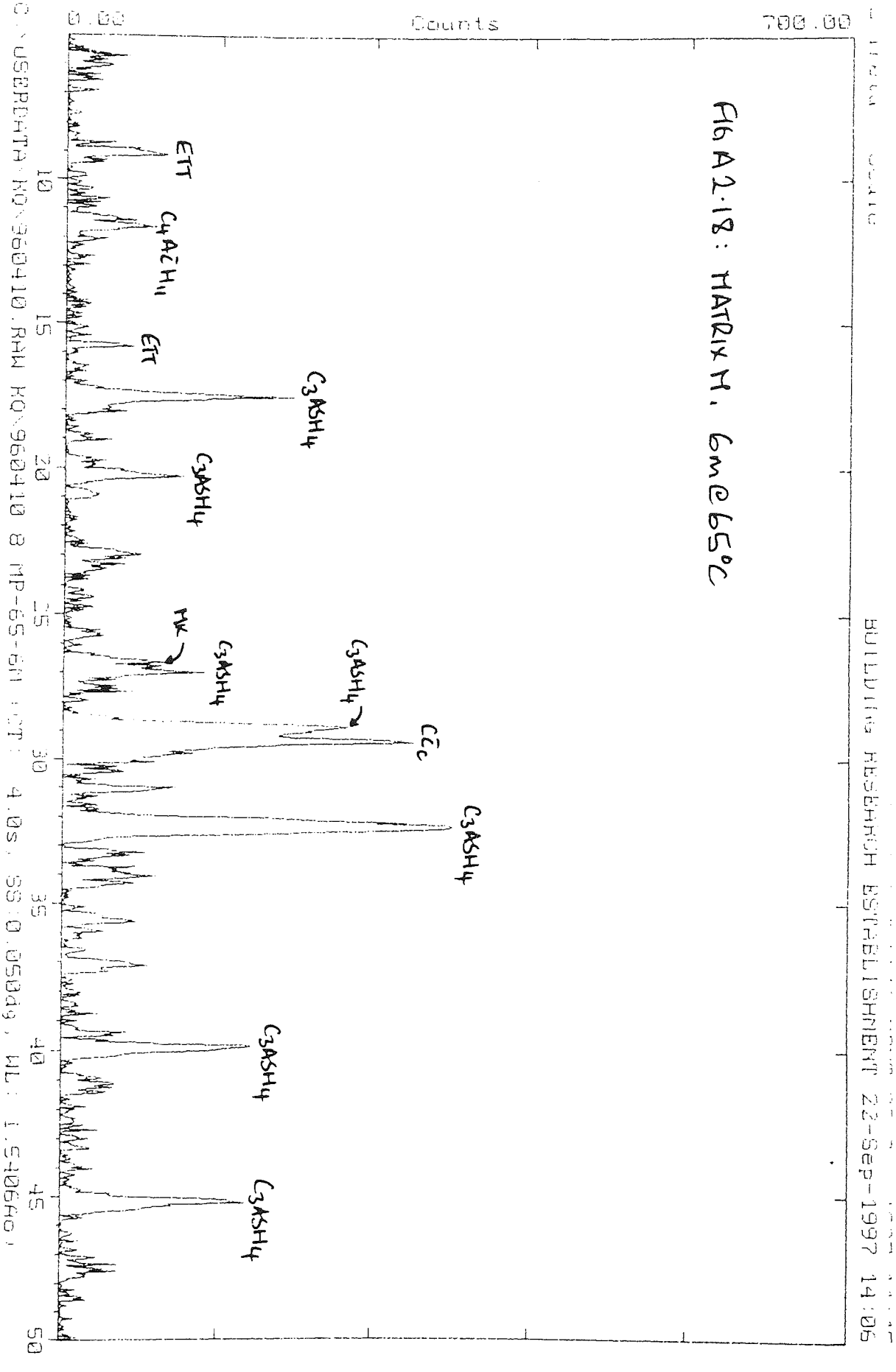
Counts
0.00
700.00
FIG A2.18: MATRIX M. 6m@65°C
BUILDING RESEARCH ESTABLISHMENT 22-Sep-1997 14:05
C:\USERDATA\KQ\960410.RAW KQ\960410 8 MP-65-6M ; CT: 4.0s, SS 0.050d, WL: 1.54060
ETT
C4AcH11
ETT
C3ASH4
C3ASH4
C3ASH4
C3ASH4
C3ASH4
C3ASH4
C3ASH4
C3ASH4
MK
CC
10
15
20
25
30
35
40
45
50

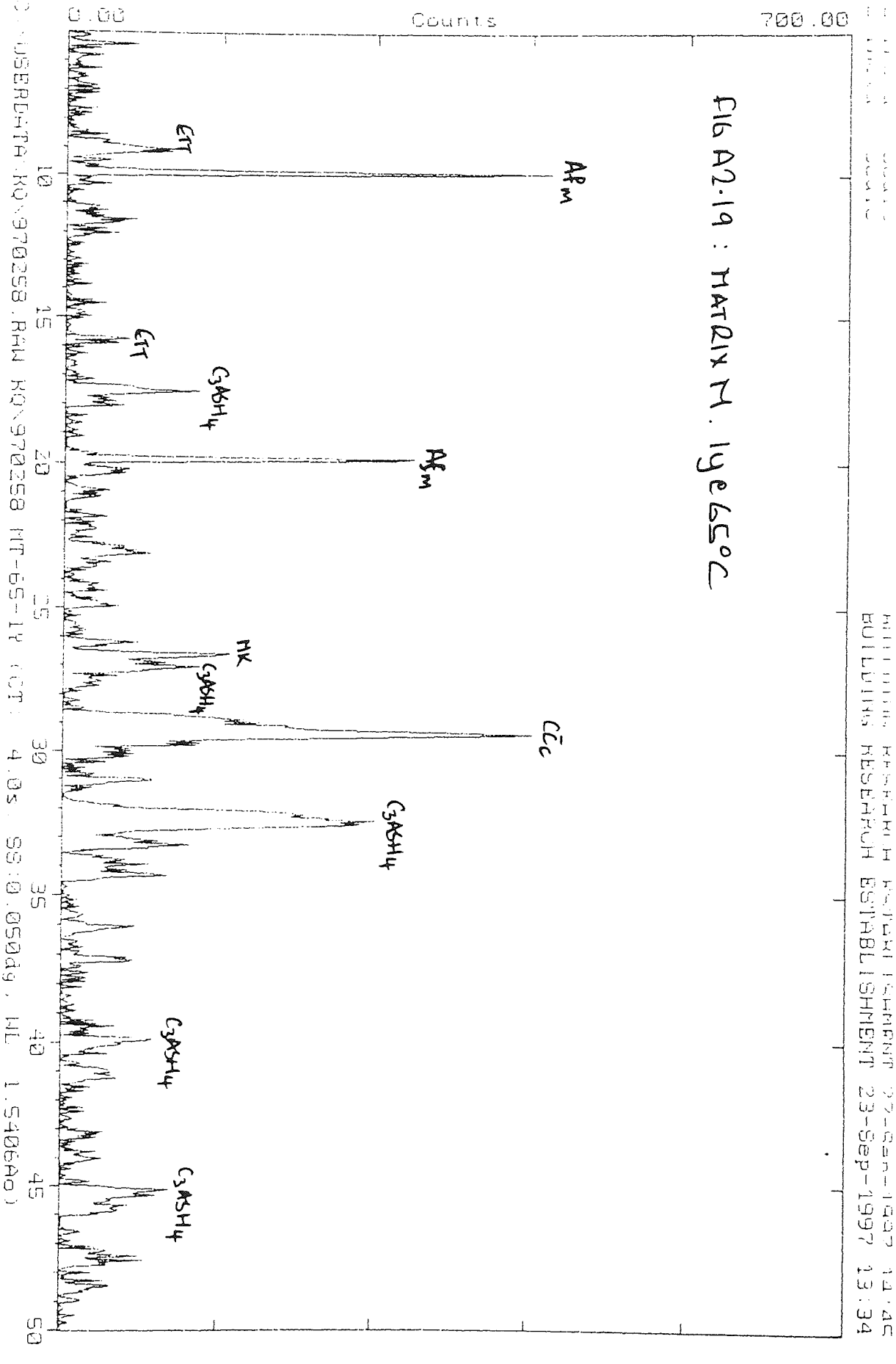
Counts
0.00
700.00
BUILDING RESEARCH ESTABLISHMENT 23-Sep-1997 13:34
Fig A2.19 : Matrix M. 1y @ 65°C
Afm
Ett
Ett
C3AsH4
Afm
Hk
C3AsH4
CCc
C3AsH4
C3AsH4
C3AsH4
10
15
20
25
30
35
40
45
50

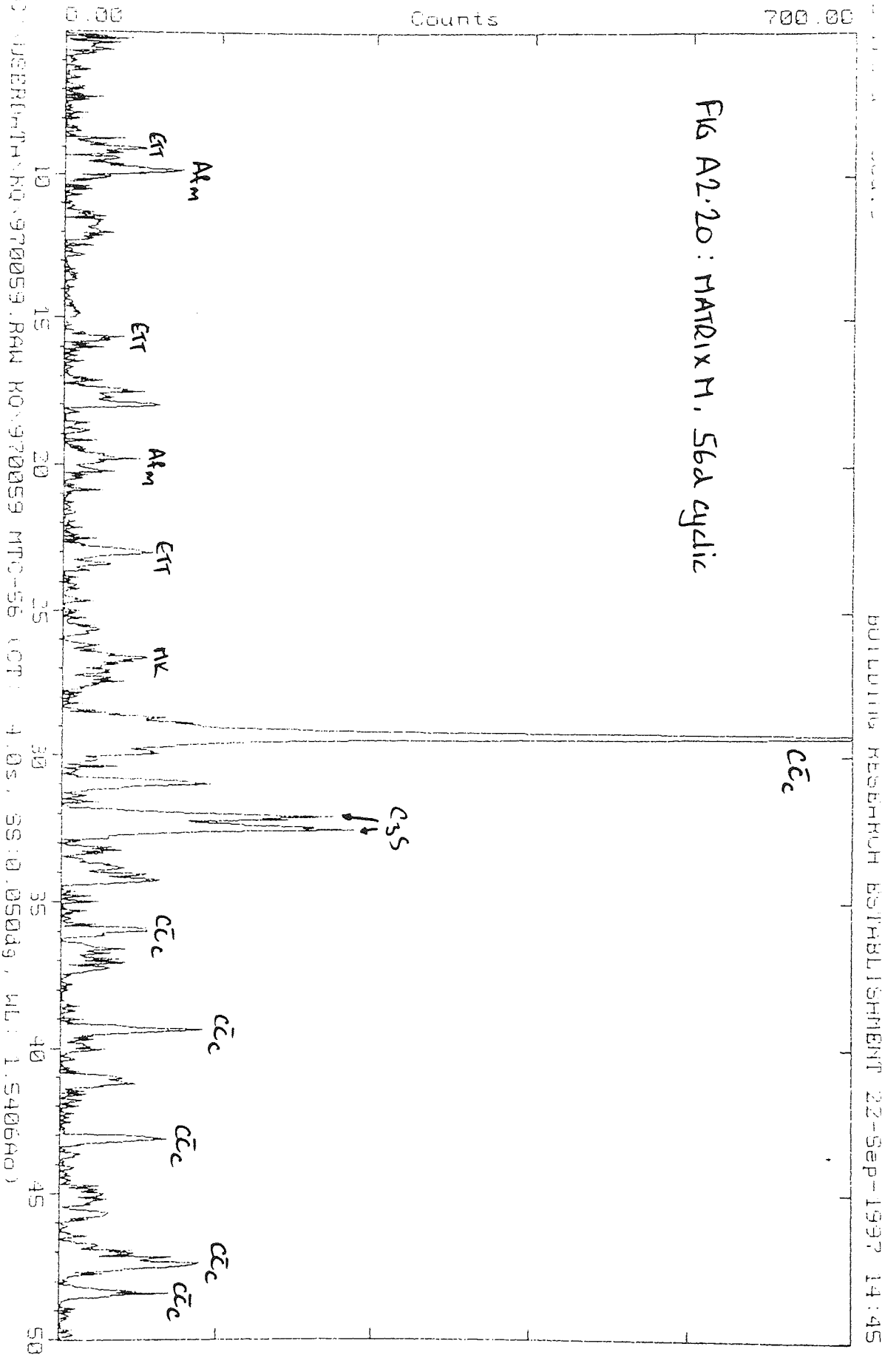
Counts
0.00
700.00
Fig A2.20 : Matrix M, 56d cyclic
BUILDING RESEARCH ESTABLISHMENT 22-Sep-1997 14:45
C:\USERDATA\KQ\970059.RAW KQ\970059 MTC-56 (OT
4.0s, SS:0.05deg, WL: 1.540600
Ett
Afm
Ett
Afm
Ett
Hk
C3S
CC̄c
CC̄c
CC̄c
CC̄c
CC̄c
CC̄c
10
15
20
25
30
35
40
45
50

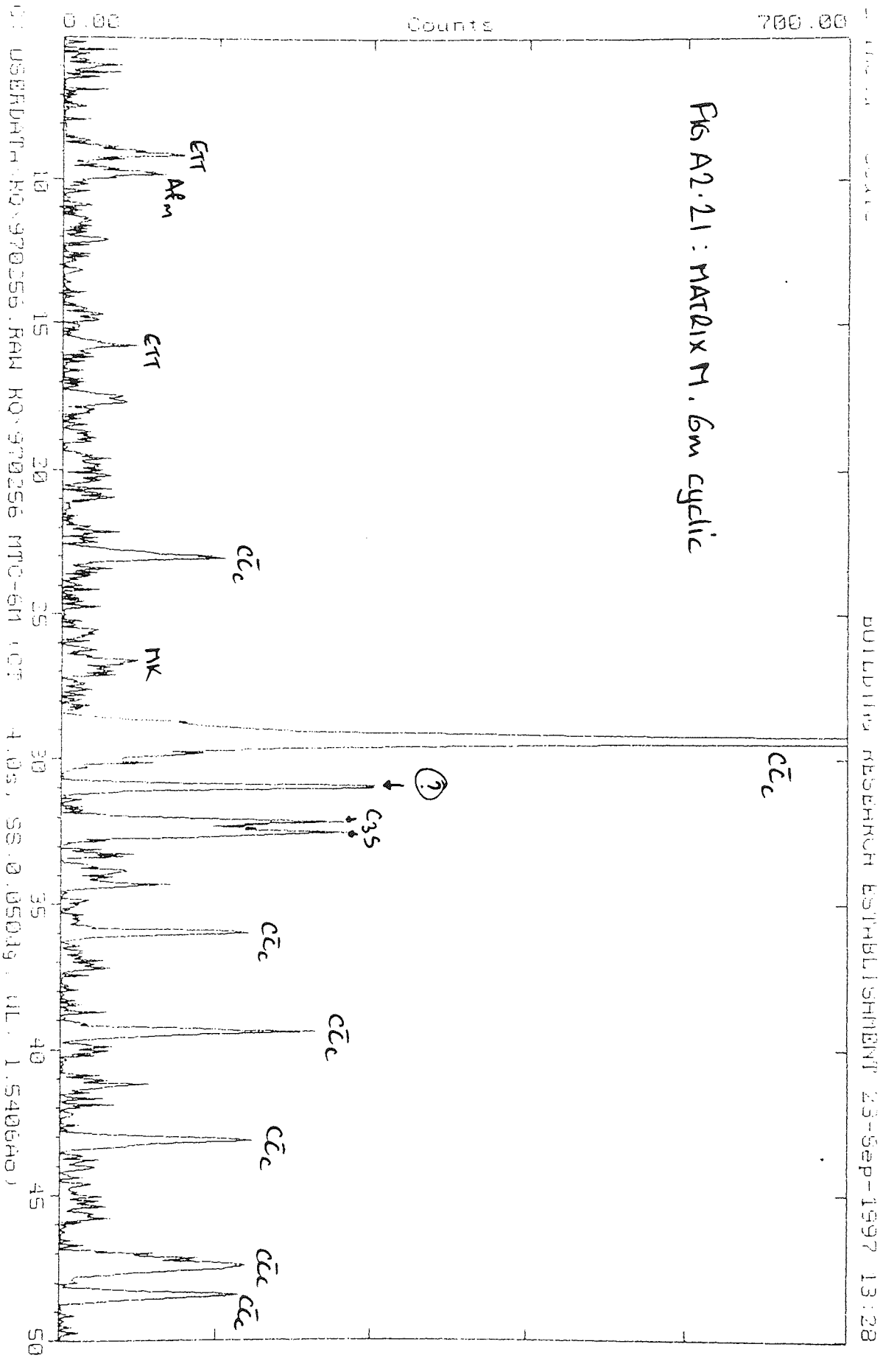
Fig A2.21 : Matrix M. 6m cyclic
Ett
Afm
Ett
CC̄c
Mk
CC̄c
C3S
CC̄c
CC̄c
CC̄c
CC̄c
CC̄c
Counts
0.00
700.00
10
15
20
25
30
35
40
45
50
BUILDING RESEARCH ESTABLISHMENT 25-Sep-1997 13:28

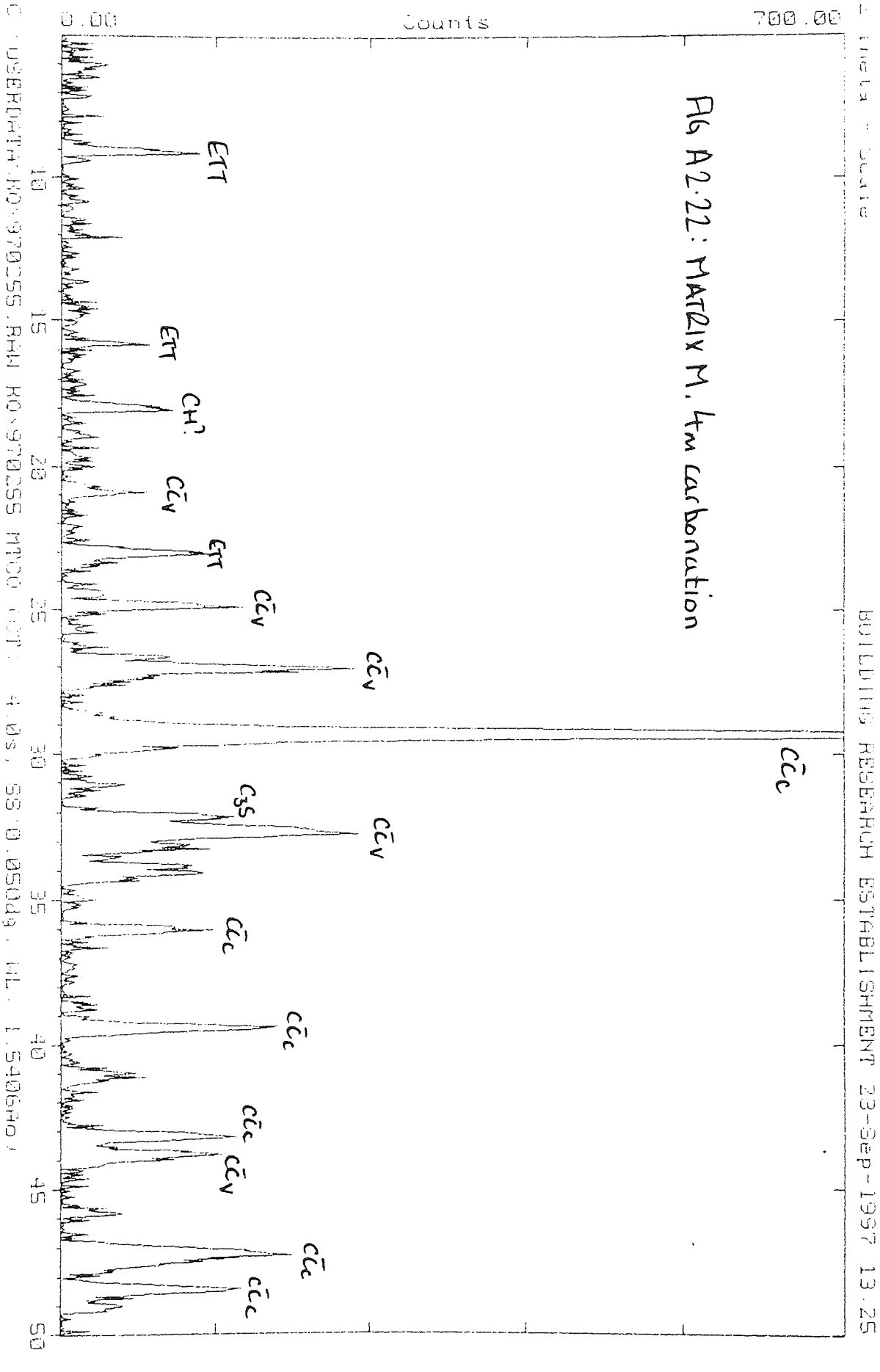
0.00
Counts
700.00
A6 A2.22: Matrix M. 4m carbonation
BUILDING RESEARCH ESTABLISHMENT 23-Sep-1997 13:25
Ettr
Ettr
CH?
Ettr
C3S
10
15
20
25
30
35
40
45
50

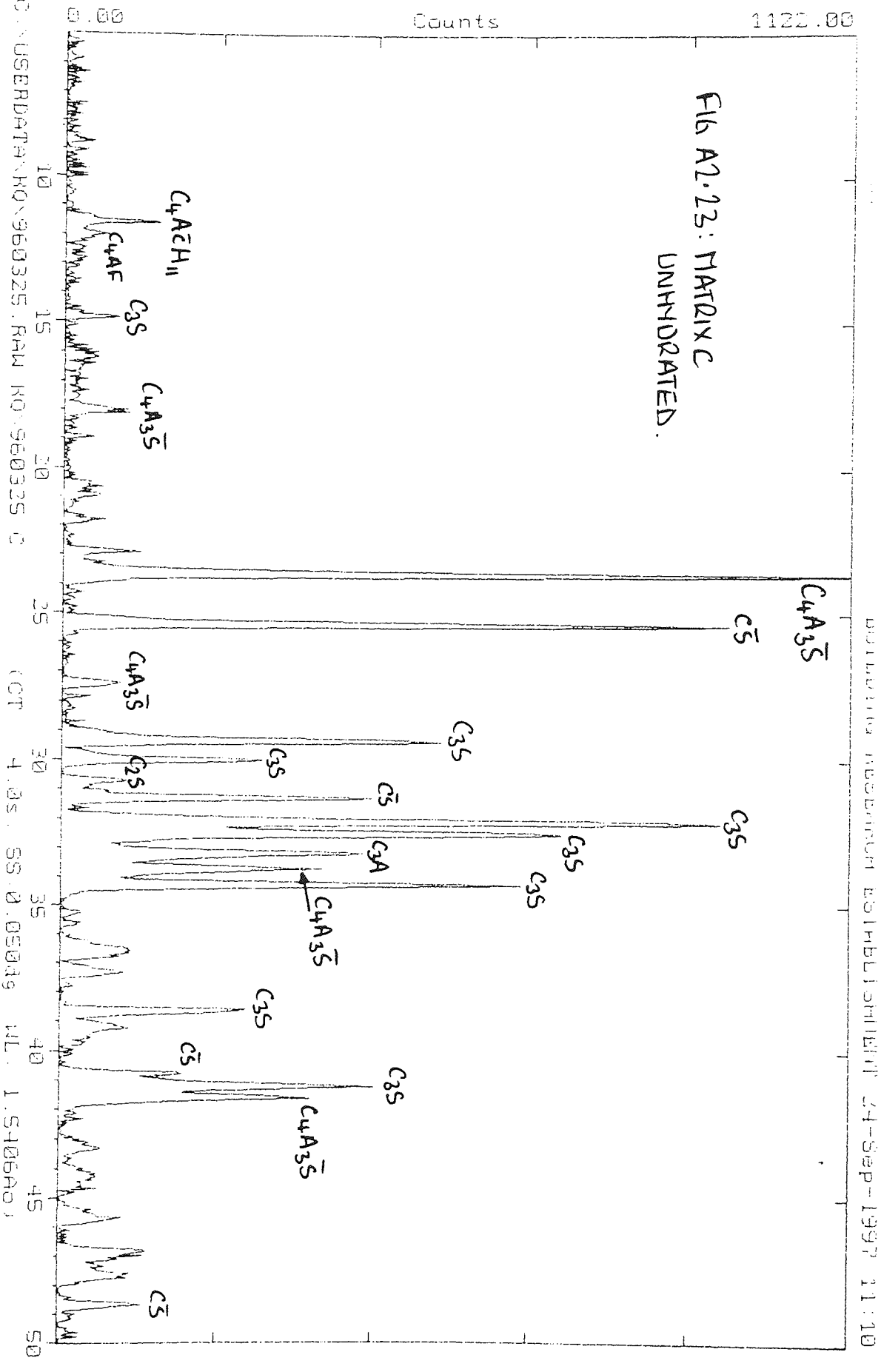
Counts
0.00
1122.00
FIG A2.23: MATRIX C
UNHYDRATED.
C4AC̄H11
C4AF
C3S
C4A3S̄
C5̄
C4A3S̄
C3S
C2S
C5̄
C3A
C4A3S̄
C3S
C5̄
C4A3S̄
C5̄
10
15
20
25
30
35
40
45
50
C:\USERDATA\KO\960325.RAW KO 960325 C
CT 4.0s SS 0.050 WL 1.5406Ao
24-Sep-1997 11:10

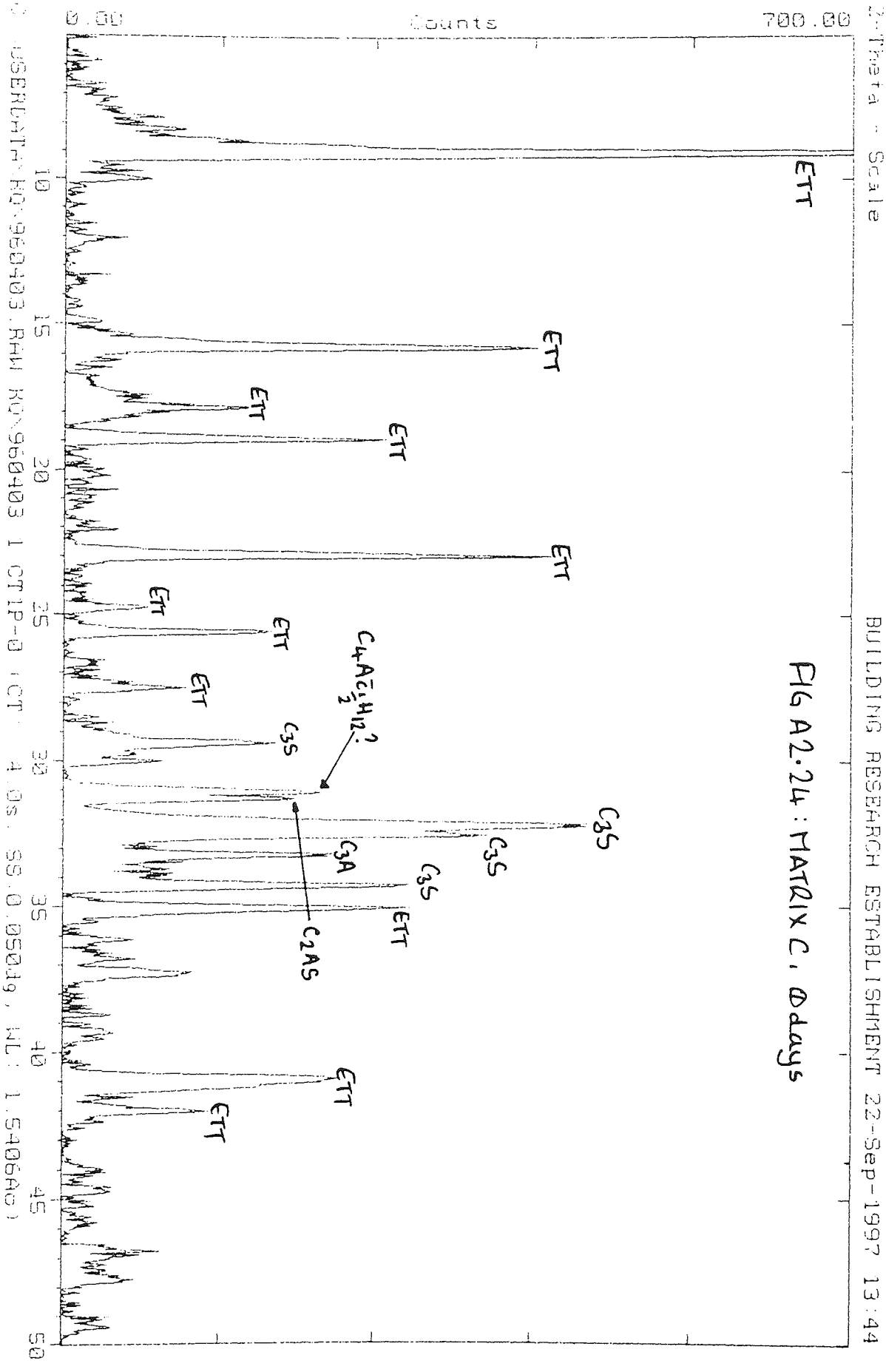
0.00
Counts
700.00
2-Theta - Scale
BUILDING RESEARCH ESTABLISHMENT 22-Sep-1997 13:44
PG A2.24 : MATRIX C, 0days
ETT
C3S
C4AC̄H12 ?
C3A
C2AS
10
15
20
25
30
35
40
45
50

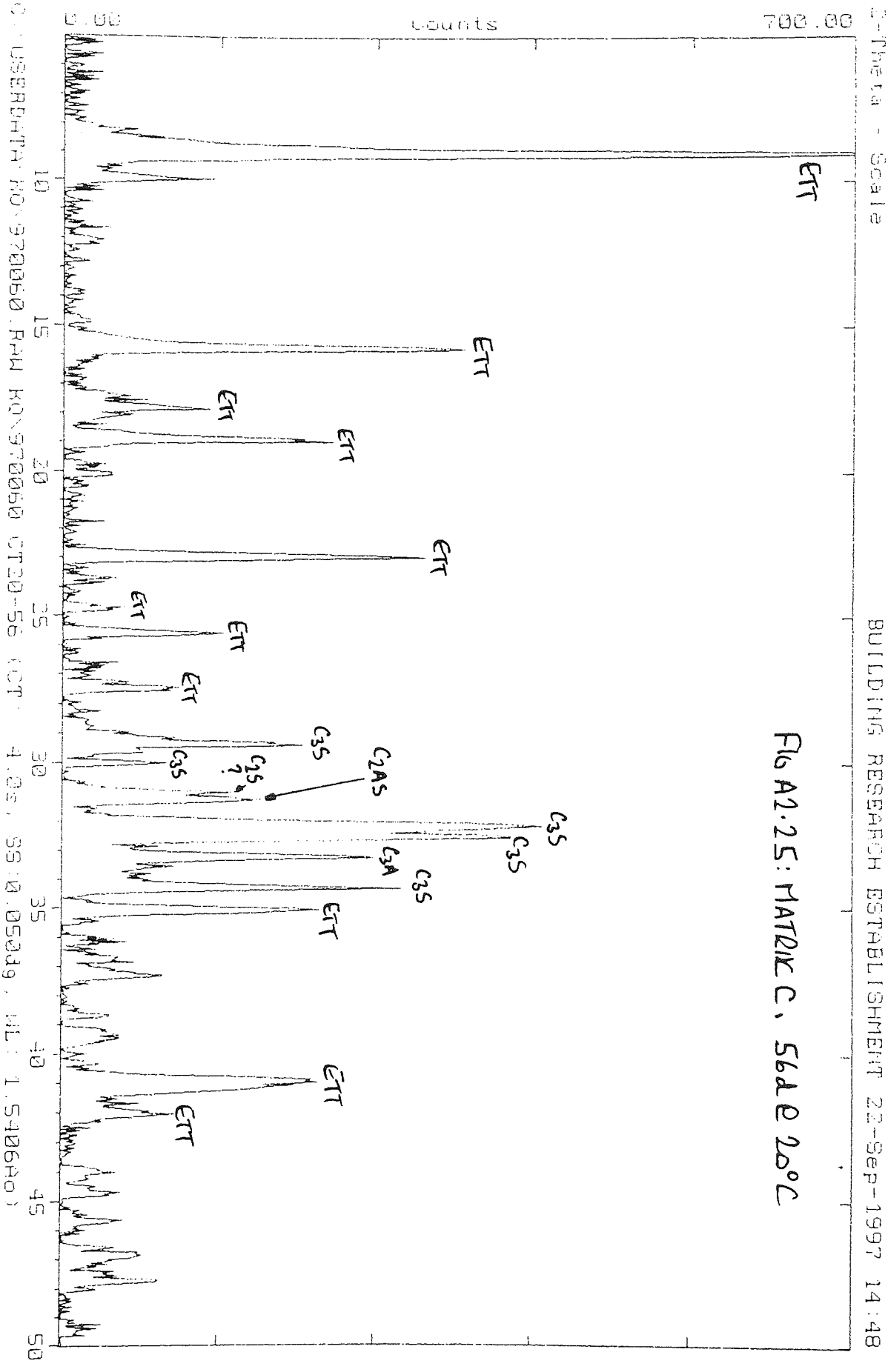
2-Theta - Scale
BUILDING RESEARCH ESTABLISHMENT 22-Sep-1997 14:48
Counts
0.00
700.00
10
15
20
25
30
35
40
45
50
C:\USERDATA\RD\970060.RAW KD\970060 CT20-56 OCT 4.0s, SS:0.05009, WL: 1.54060Ao
Fig A1.25: MATRIX C, 56d @ 20°C
ETT
C3S
C2AS
C3A

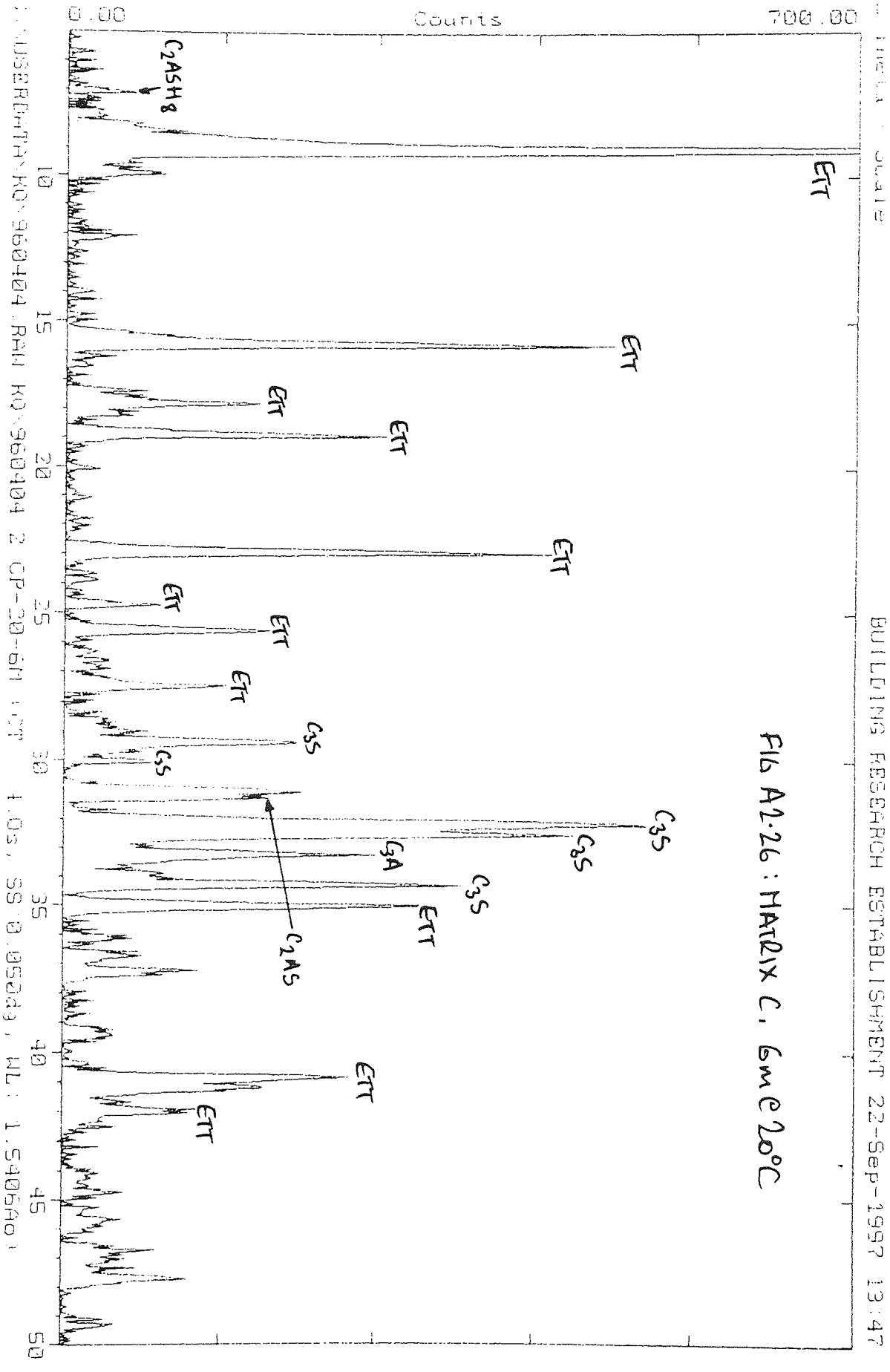
0.00
Counts
700.00
C2ASH8
ETT
C3S
C2S
C3A
C4AF
C2AS
10
15
20
25
30
35
40
45
50
BUILDING RESEARCH ESTABLISHMENT 22-Sep-1997 13:47
Fig A1.26 : Matrix C, 6m @ 20°C

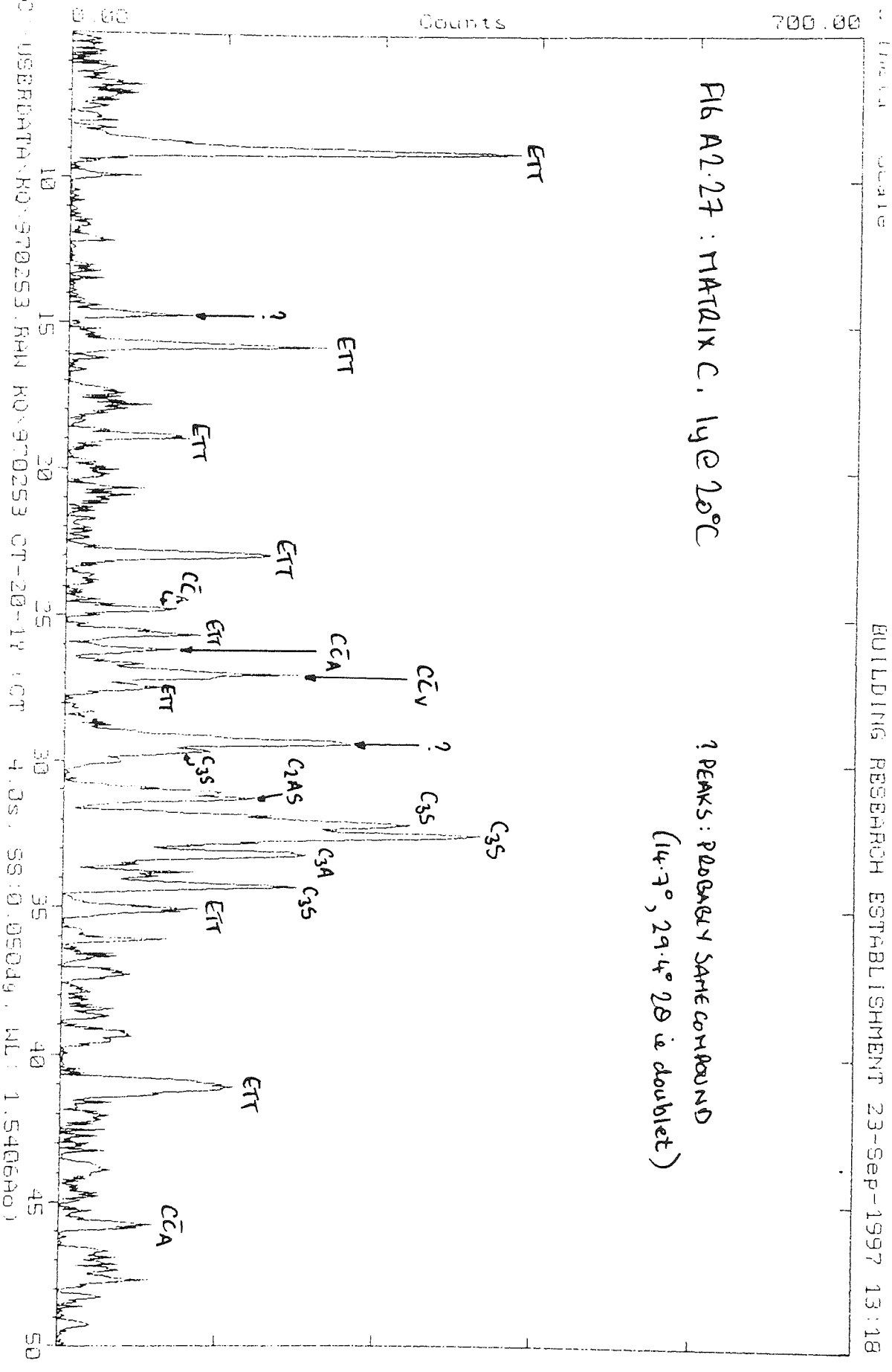
Counts
700.00
Pb A2.27 : MATRIX C, 1y @ 20°C
1 PEAKS: PROBABLY SAME COMPOUND
(14.7°, 29.4° 2θ i doublet)
BUILDING RESEARCH ESTABLISHMENT 23-Sep-1997 13:18
C:\USERDATA\RD\970253.RAW RD\970253 CT-20-1Y CT
4.3s, SS:0.050dg, WL: 1.54060Ao
ETT
?
ETT
ETT
ETT
CĀ4
ETT
CĀA
CC̄v
ETT
?
C3S
C2AS
C3S
C3S
C3A
C3S
ETT
ETT
CĀA
10
15
20
25
30
35
40
45
50

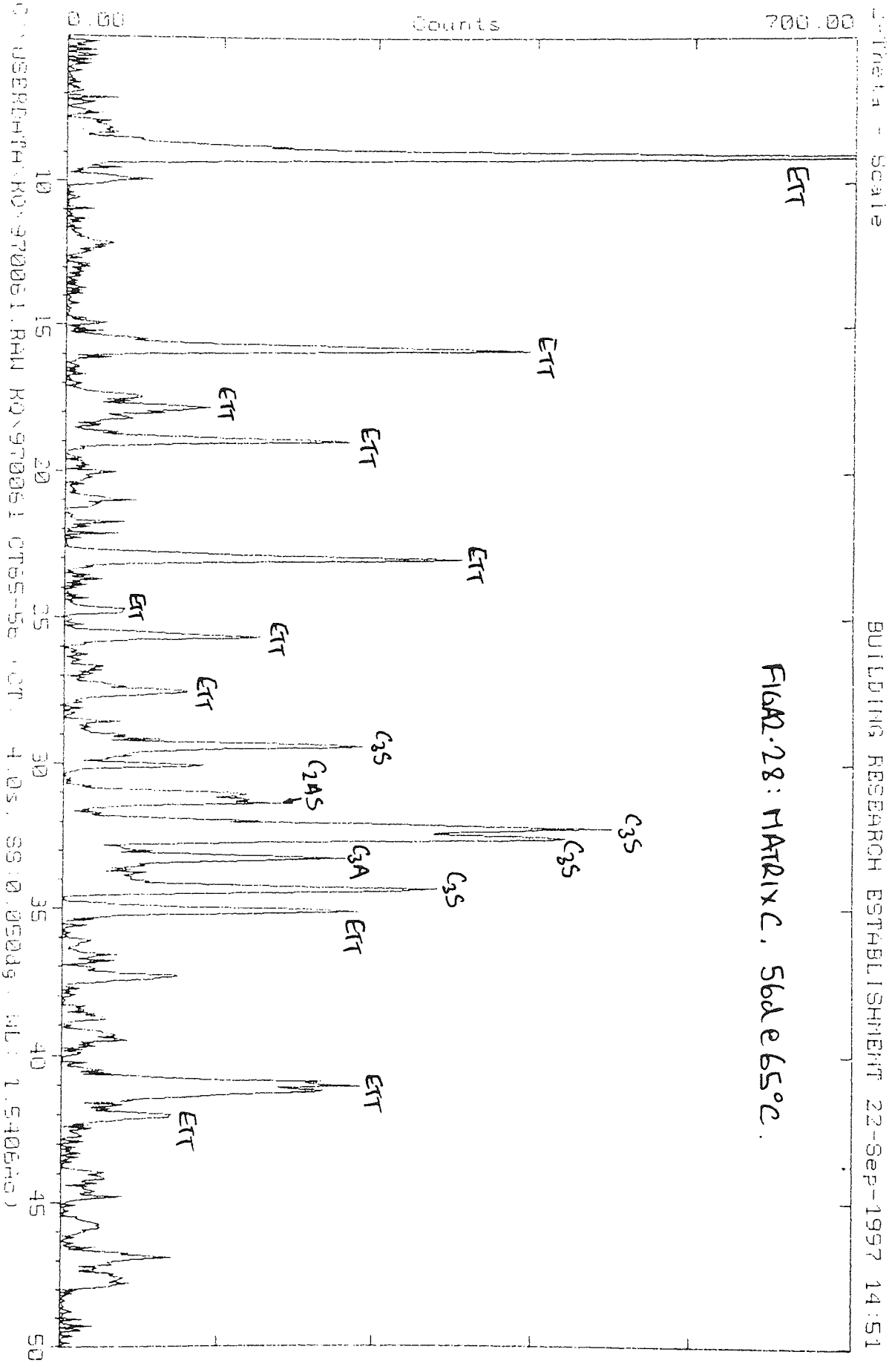
0.00
Counts
700.00
Theta - Scale
BUILDING RESEARCH ESTABLISHMENT 22-Sep-1997 14:51
FIGR2.28: MATRIX C, 56d @ 65°C.
Ett
C3S
C2AS
C3A
10
15
20
25
30
35
40
45
50

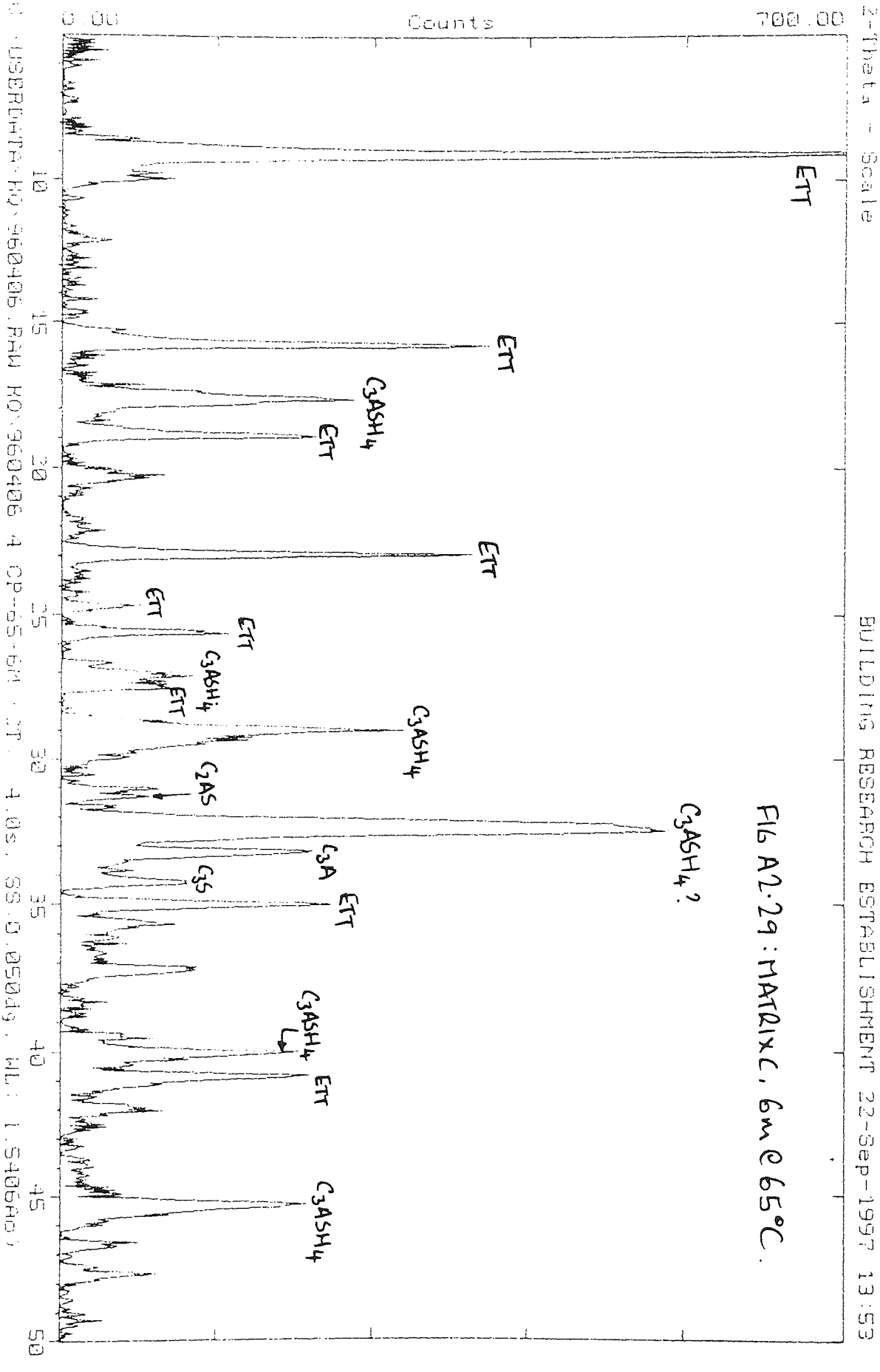
2-Theta - Scale
BUILDING RESEARCH ESTABLISHMENT 22-Sep-1997 13:53
Counts
0.00
700.00
10
15
20
25
30
35
40
45
50
ETT
C3ASH4
C2AS
C3A
C3S
C3ASH4?
FIG A2.29: MATRIX C, 6m @ 65°C.

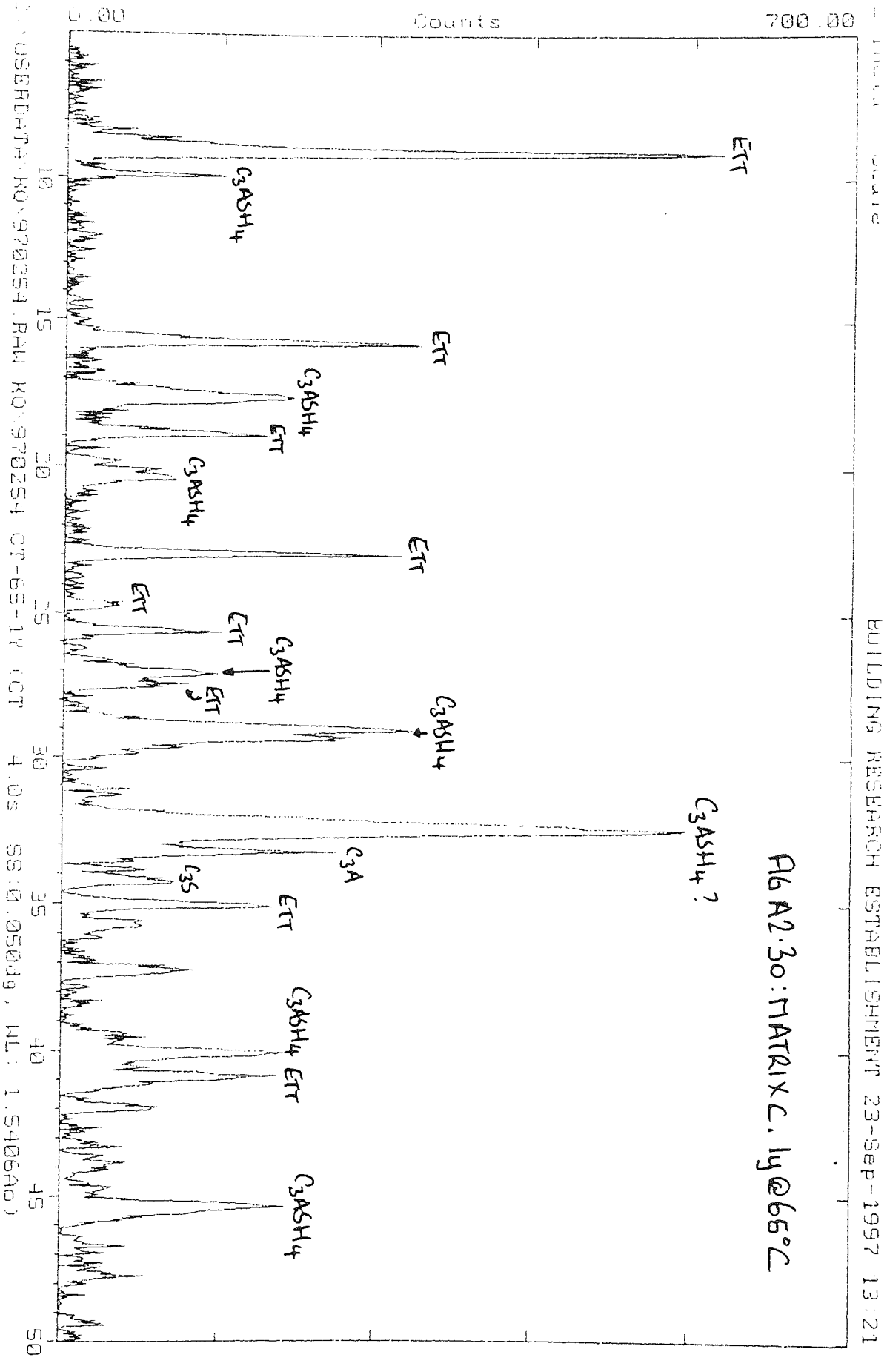
Counts
0.00
700.00
BUILDING RESEARCH ESTABLISHMENT 23-Sep-1997 13:21
A6 A2.30: MATRIX C. 1y@65°C
C3ASH4 ?
C3A
C3S
ETT
C3ASH4
10
15
20
25
30
35
40
45
50

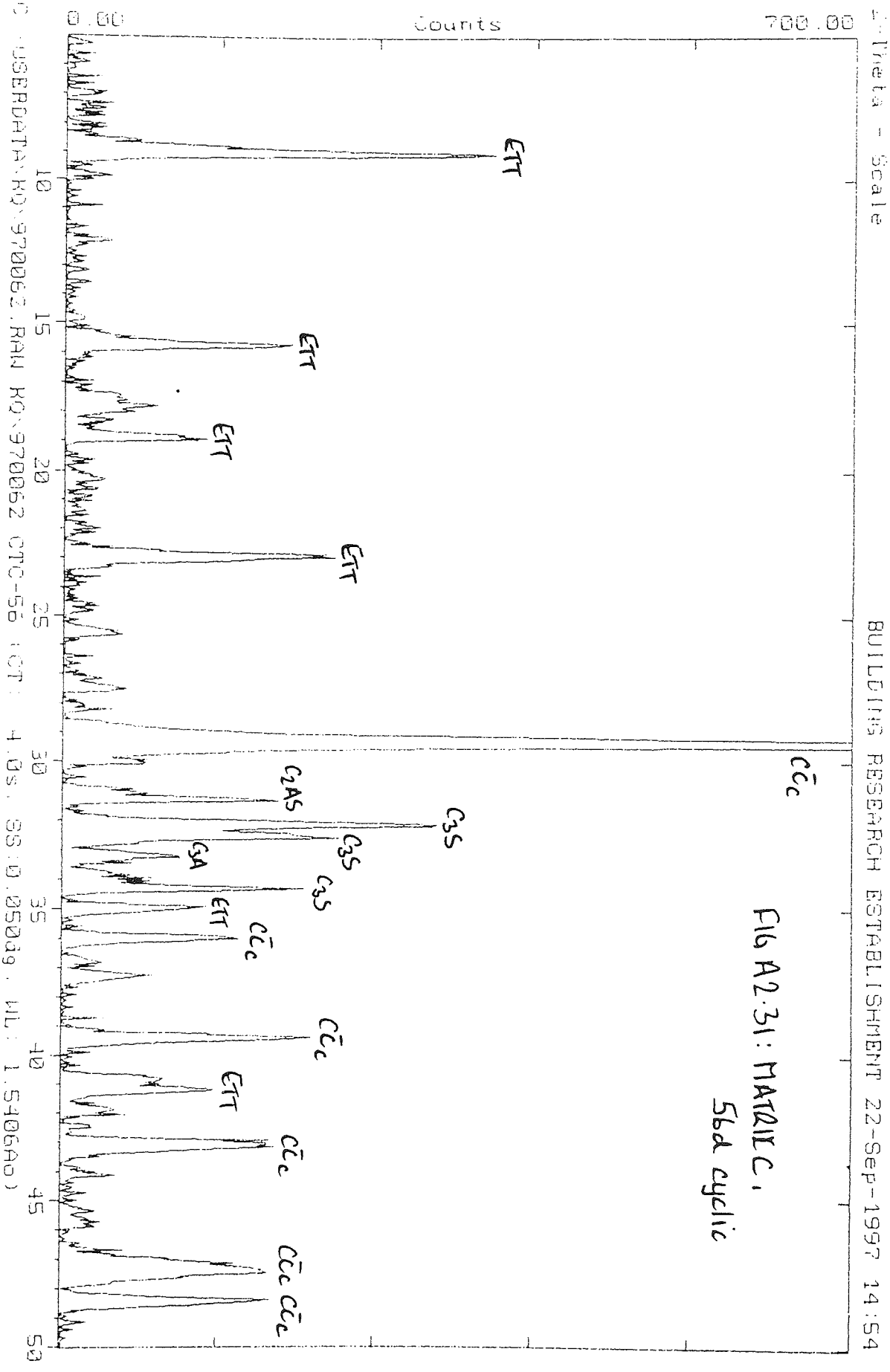
0.00
Counts
700.00
2-Theta - Scale
BUILDING RESEARCH ESTABLISHMENT 22-Sep-1997 14:54
C:\USERDATA\KQ\970062.RAW KQ\970062 CTC-56 (CT: 4.0s, SS:0.050@9, WL: 1.5406Ao)
10
15
20
25
30
35
40
45
50
Ett
Ett
Ett
Ett
C_2AS
C_3S
C_3S
C_3A
C_3S
Ett
$C\bar{C}c$
$C\bar{C}c$
Ett
$C\bar{C}c$
$C\bar{C}c$ $C\bar{C}c$
$C\bar{C}c$
Fig A2.31: MATRIX C,
56d cyclic

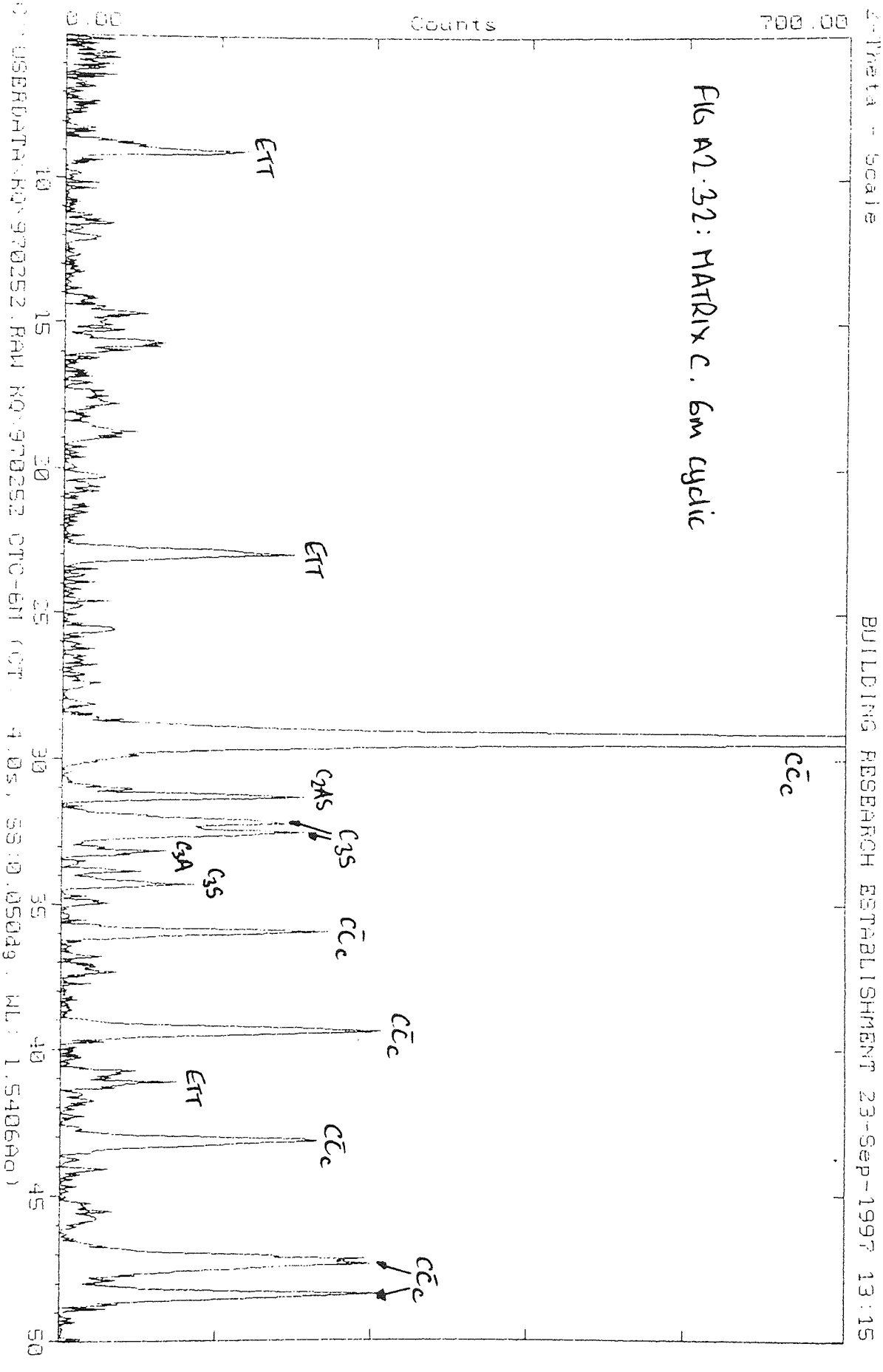
FIG A2.32: MATRIX C, 6m cyclic
Counts
0.00
700.00
BUILDING RESEARCH ESTABLISHMENT 23-Sep-1997 13:15
ETT
ETT
ETT
CC̄c
C4AS
C3S
C3A
C3S
CC̄c
CC̄c
CC̄c
CC̄c
10
15
20
25
30
35
40
45
50

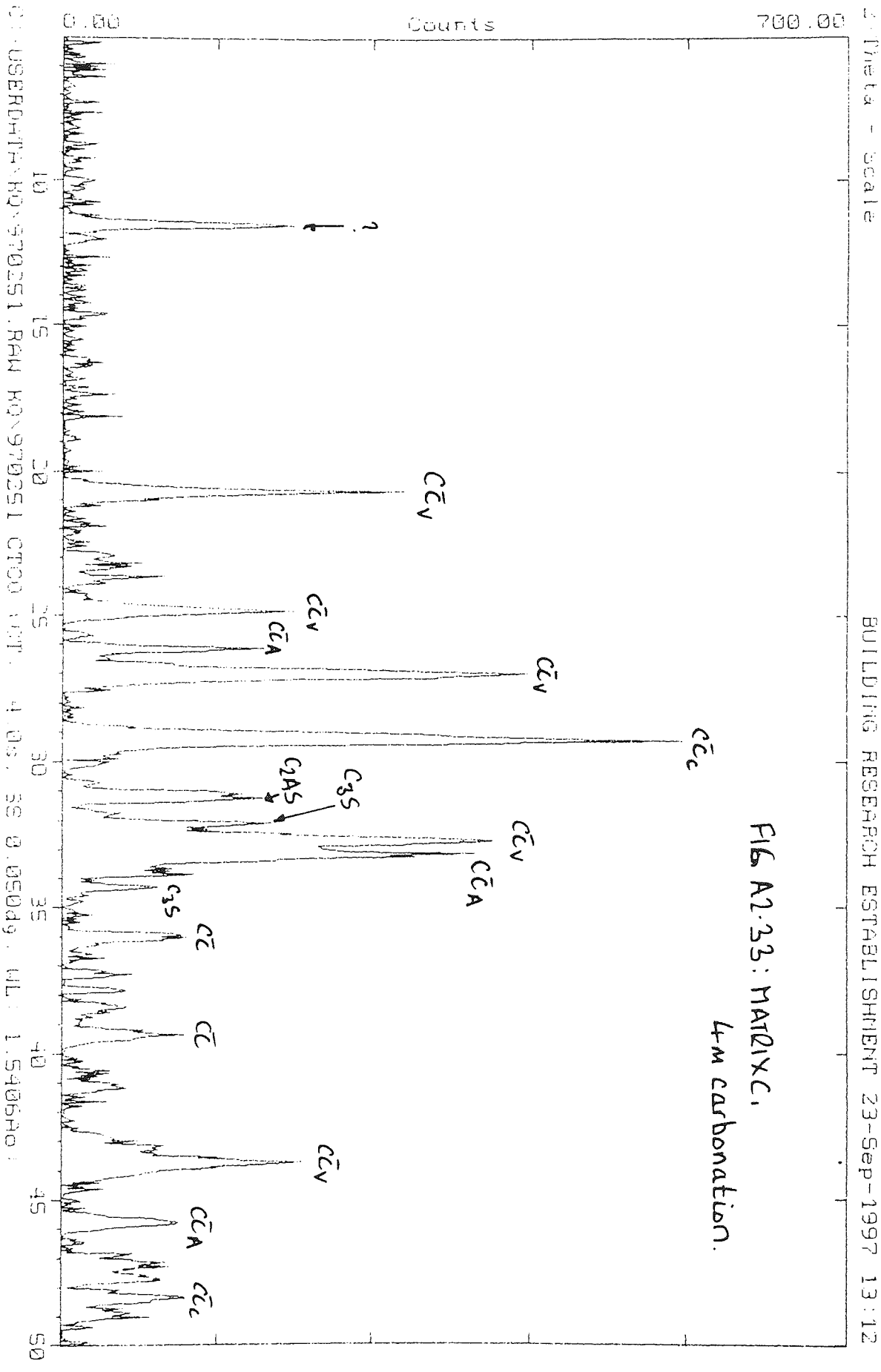
0.00
Counts
700.00
2-Theta - Scale
10
15
20
25
30
35
40
45
50
C:\USERDATA\XQ\970251.RAW XQ\970251 CTOD
BUILDING RESEARCH ESTABLISHMENT 23-Sep-1997 13:12
?
CC̄v
CC̄v
CC̄A
CC̄v
CC̄c
C2AS
C3S
CC̄v
CC̄A
C3S
CC̄
CC̄
CC̄v
CC̄A
CC̄c
FIG A2.33: MATRIX C.
4m carbonation.

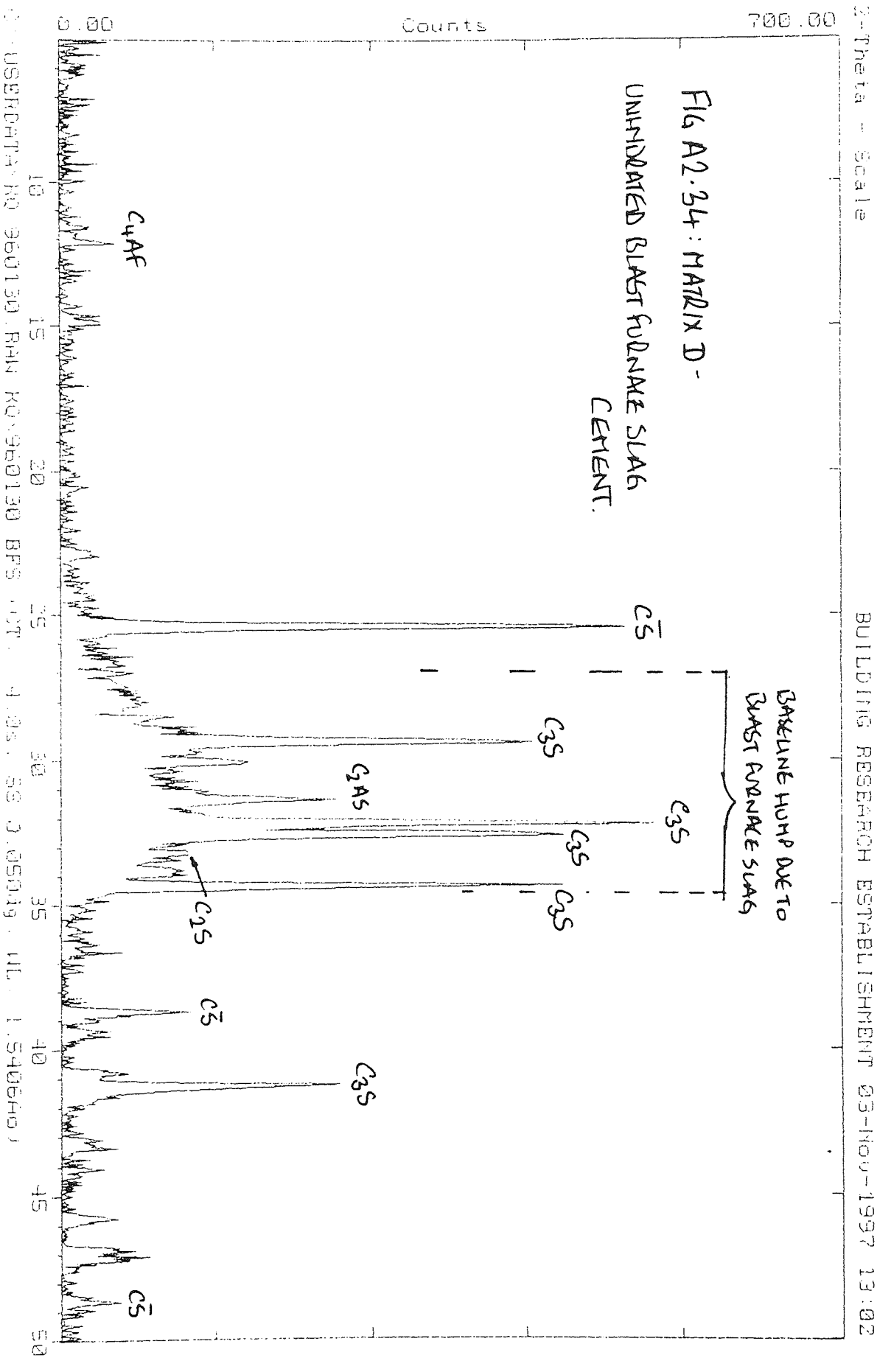
FIG A2.34: MATRIX D -
UNHYDRATED BLAST FURNACE SLAG CEMENT.
BASELINE HUMP DUE TO BLAST FURNACE SLAG
C4AF
C$\bar{S}$
C3S
C2AS
C3S
C3S
C2S
C$\bar{S}$
C3S
C$\bar{S}$
Counts
0.00
700.00
2-Theta - Scale
BUILDING RESEARCH ESTABLISHMENT 03-NOV-1997 13:02
10
15
20
25
30
35
40
45
50

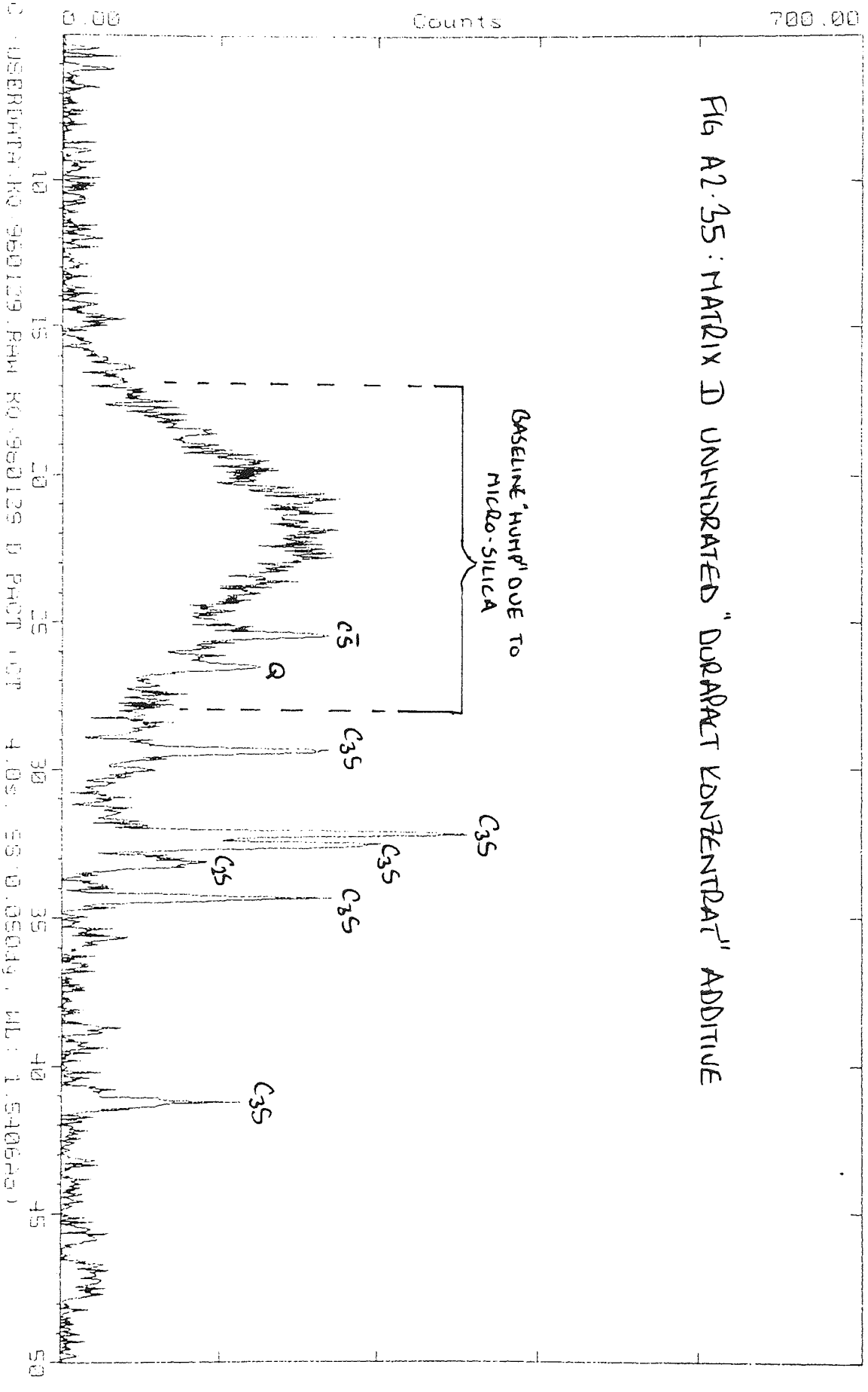

FIG A2.35: MATRIX D UNHYDRATED "DURAPACT KONZENTRAT" ADDITIVE

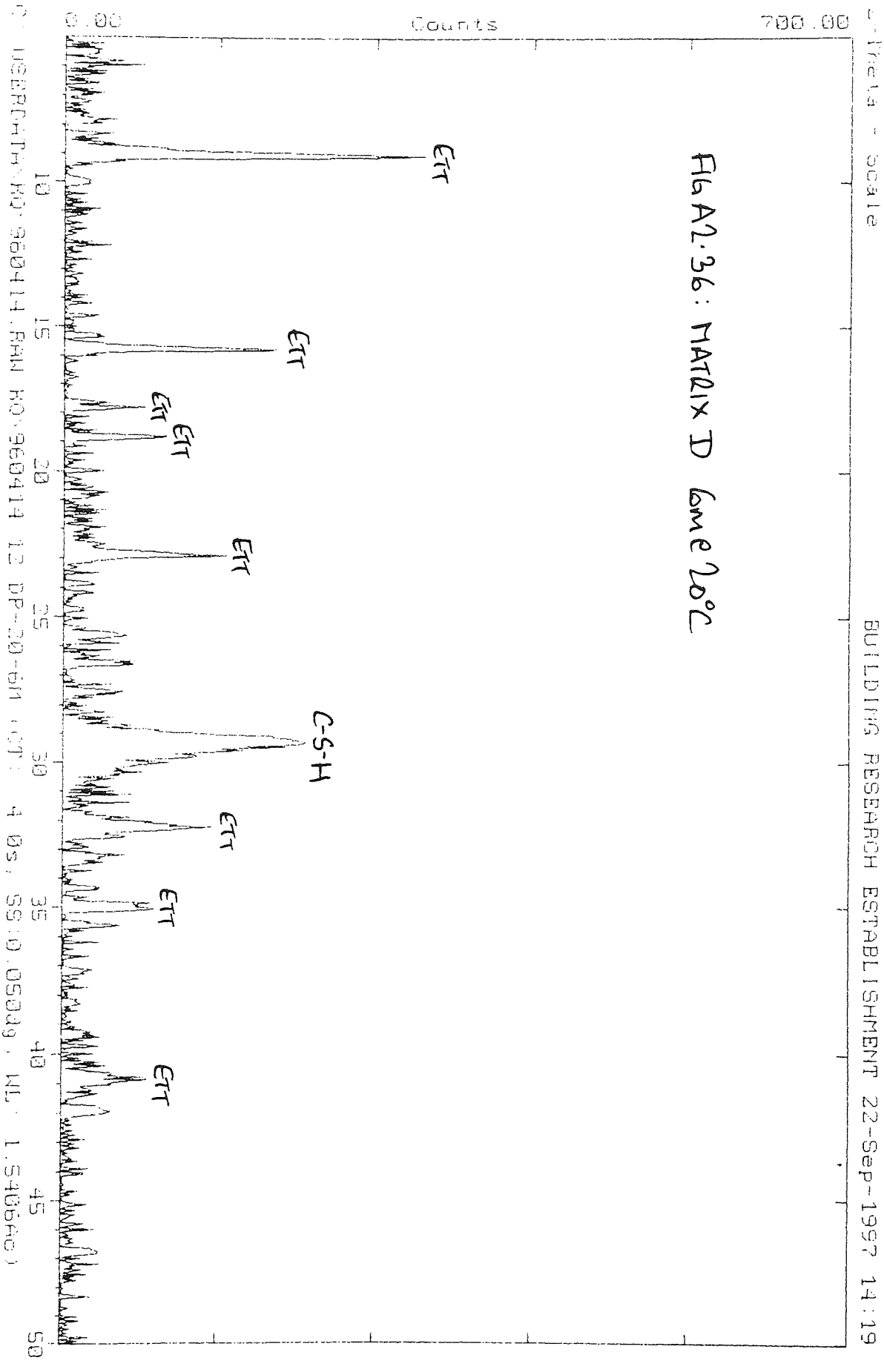
Theta - Scale
BUILDING RESEARCH ESTABLISHMENT 22-Sep-1997 14:19
0.00
Counts
700.00
HgA2.36: MATRIX D 6mc 20°C
ETT
ETT
ETT
ETT
ETT
C-S-H
ETT
ETT
ETT
10
15
20
25
30
35
40
45
50

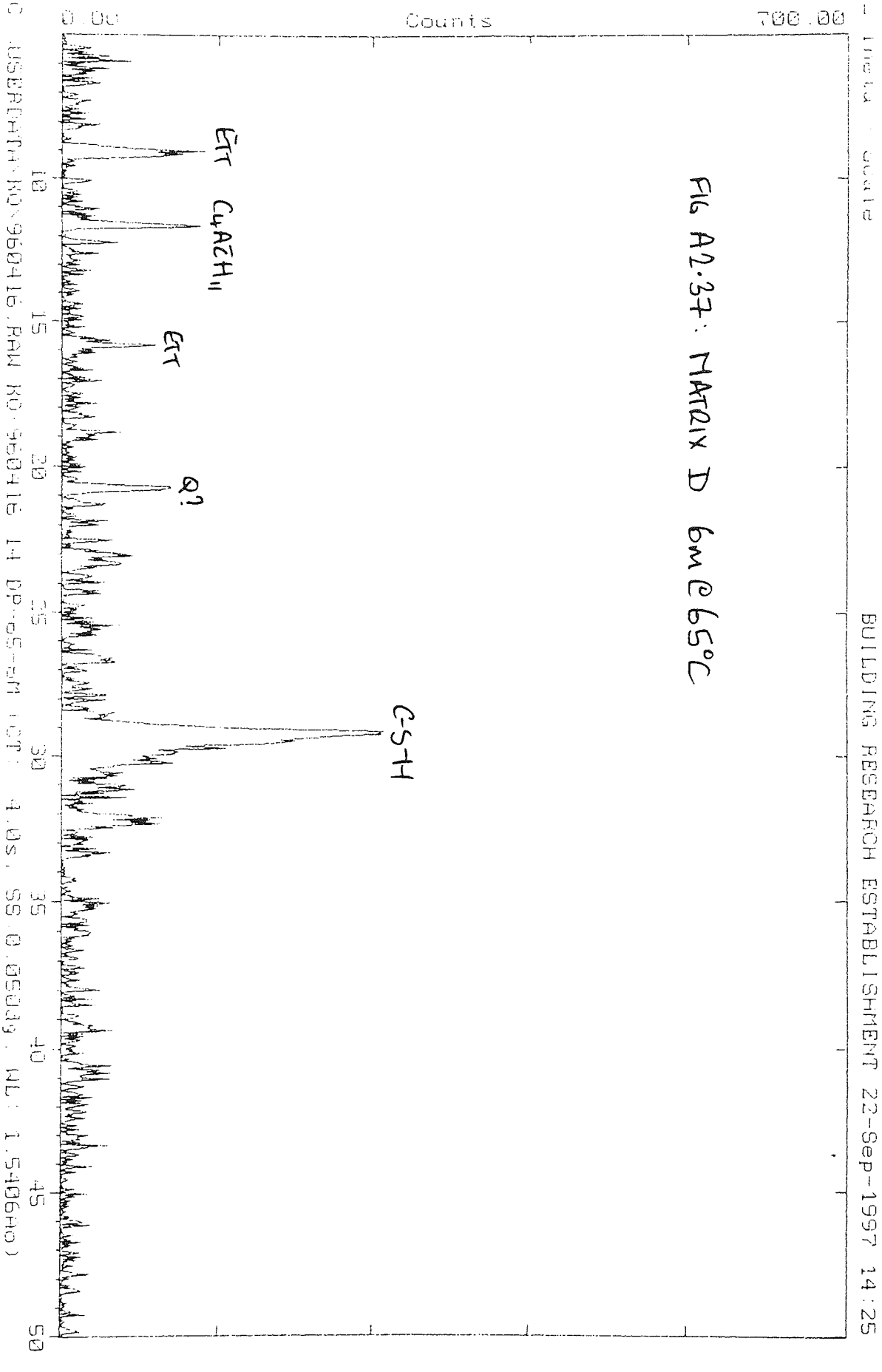
Counts
0.00
700.00
10
15
20
25
30
35
40
45
50
Ett C_4AZH_{11}
Ett
Q?
C-S-H
FIG A2.37: MATRIX D 6m @ 65°C
BUILDING RESEARCH ESTABLISHMENT 22-Sep-1997 14:25

APPENDIX 3: Derivation of section modulus for circular torus segment cross section. (re: Section 5.3. and Figure 5.27).

Figure A3.1. Circular torus segment.

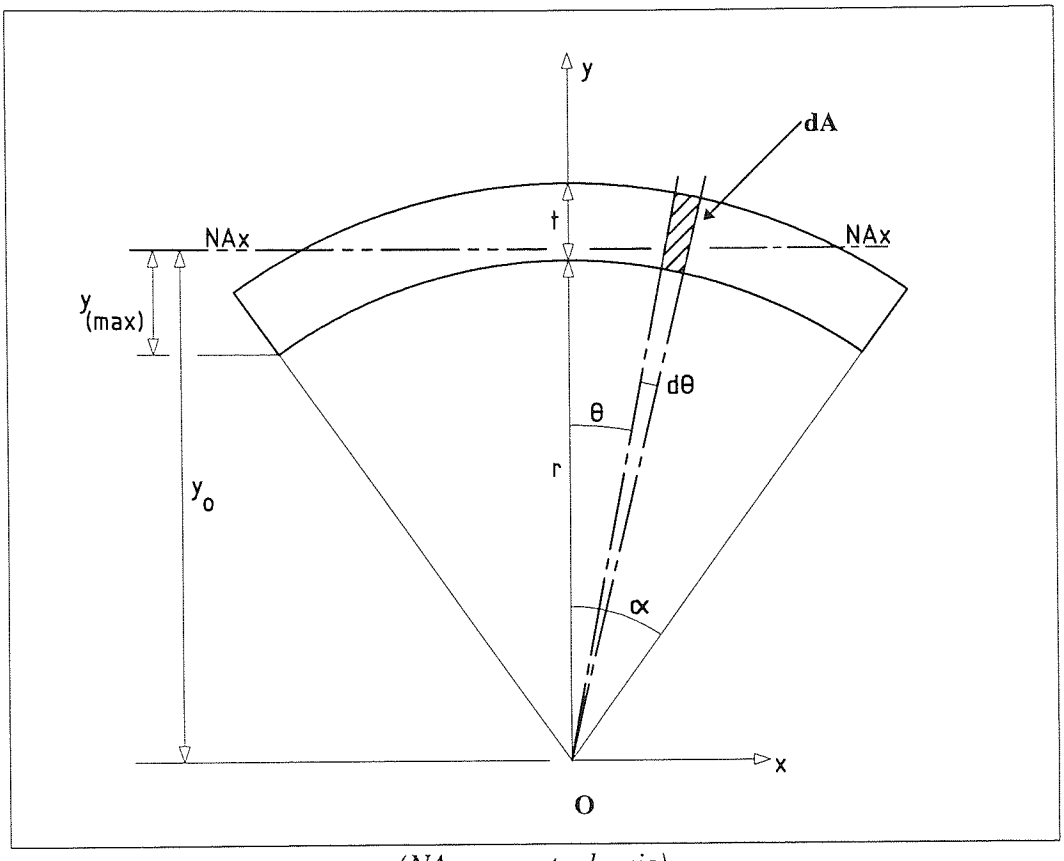

(NAx = neutral axis)

In order to calculate the section modulus ($I_{NA}/y_{(max)}$) we need to calculate the location of the neutral axis (y_o), the distance of the point of maximum stress from the neutral axis (y_{max}) and the second moment of area of the cross-section about the neutral axis (I_{NA}).

From Fig. 5.27, α and r can be derived trigonometrically as 0.621 rads (72.2°) and 45.5 mm respectively.

y_o is found from;

$$y_o = Q_x/A;\ Q_x = \int y.dA$$

We define r_o (the 'average' radius) as $r + \frac{1}{2}t$ and hence;

$$A = 2tr_o\alpha$$
$$= 426\ mm^2$$

and

$$Q_x = \int_{-\alpha}^{\alpha} r_o \cos\theta . t r_o d\theta$$

$$= t r_o^2 (\sin\alpha - \sin(-\alpha))$$

$$= 19558 \text{ mm}^3$$

hence

$$y_o = 45.9 \text{ mm.}$$

The second moment of area about the x axis through point O is given by (Gere & Timoshenko, 1990);

$$I_x = \tfrac{1}{4}.((r+t)^2 - r^2).(\alpha + \sin\alpha.\cos\alpha)$$

$$= 0.906 \times 10^6 \text{ mm}^4.$$

We must now apply parallel axis theorum to find I_{NA};

$$I_{NA} = I_x - A.y_o^2$$

$$= 8230 \text{ mm}^4.$$

The section modulus can now be computed, since $y_{max} = y_o - r + 8.5$ mm.

APPENDIX 4: Mould design diagram.

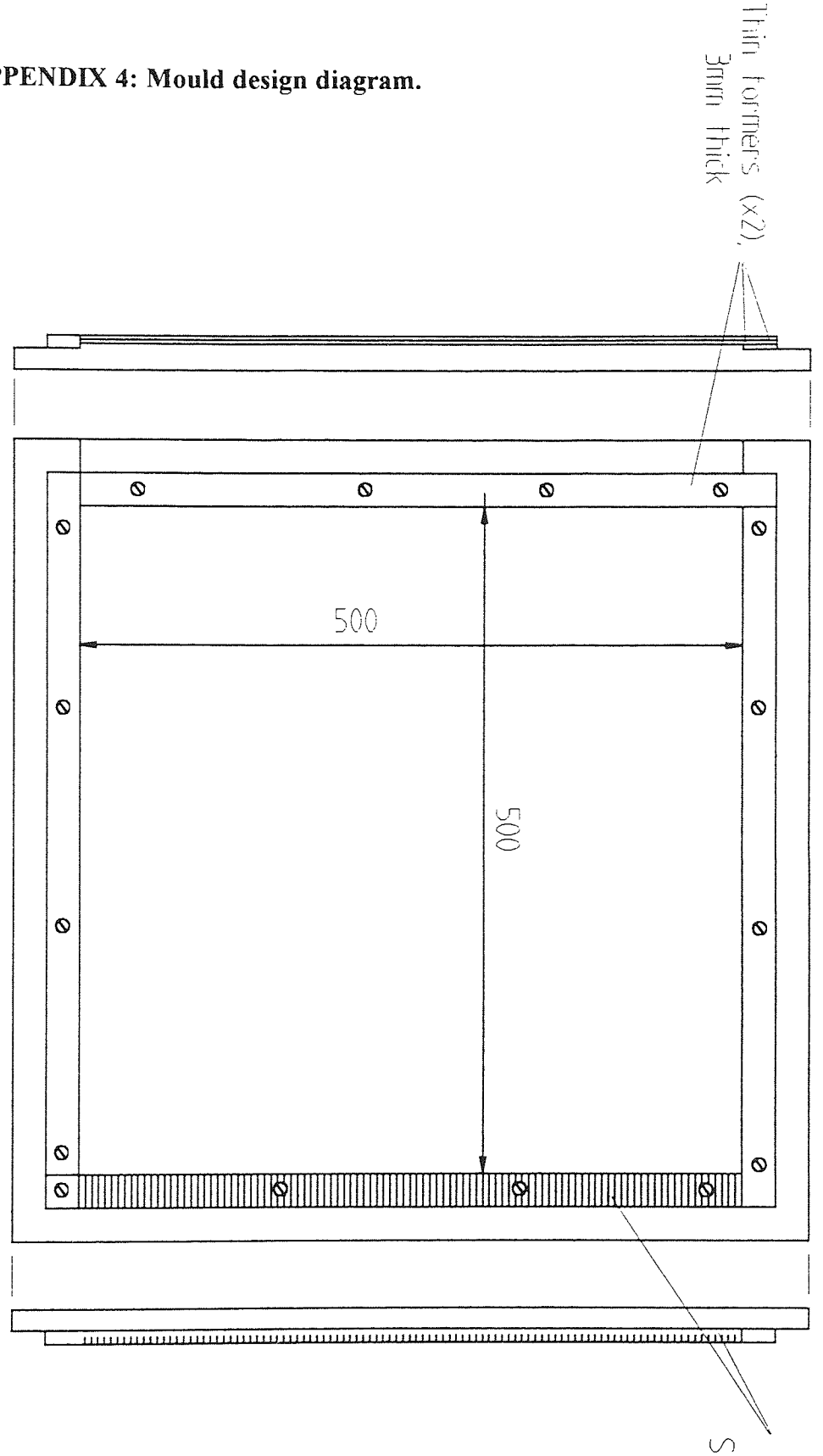

APPENDIX 5: Glossary of selected terms.

Degradation: Samples are considered degraded if their primary mechanical properties (i.e. tensile/flexural/impact strength, post-cracking modulus or toughness) have been reduced by accelerated or natural ageing to less than their initial, unaged or "0 day" values. "Complete degradation" is considered to have occurred when one or more of these properties has been reduced to a value comparable with that of the unreinforced matrix.

Groundmass: The petrographic images of the composites generally show the matrix as comprising of discrete particles (e.g. unhydrated clinker grains, portlandite crystals) set in a background of relatively dark amorphous material. This amorphous material is referred to as groundmass.

Interfacial zone: This refers to the area of matrix immediately adjacent to the outer filaments of a strand. The width of the interfacial zone varies considerably. In matrix C composites, where the matrix is almost completely homogenous, the zone may be very small, the few microns comprising the contact area between matrix and outer filaments. In matrix M composites, where the matrix near to the strand is often rather different to the bulk matrix (i.e. the 'halos') the interfacial zone may be up to 50 microns across.

Inter-filamental: This refers to the area between the filaments within the strand perimeter which would have initially been void space. This zone may or may not fill with precipitated material e.g. portlandite.

Pseudo-dormant period: A initial period during ageing where strength loss is too slow to be detected. It is a manifestation of the fact that strength is not inversely proportional to log[time] (as assumed in previous models). In actual fact the rate of strength loss increases with log[time] and is initially very slow.

Terminal [frictional] bond: The bond parameter as determined by application of ACK theory to crack spacing and matrix strength results has been shown to initially increase in magnitude until about 56 days of ageing, after which no further increase is generally apparent. The value at which this parameter stops increasing (i.e. at which the bond vs. time graph levels off) is termed the terminal bond. Since the ACK theory assumes that bond in GRC is purely frictional in nature, this value is also termed the terminal frictional bond. As explained in section 7.4.1, a more pedantic description would be the terminal frictional shear stress transfer rate; a rather cumbersome expression hence the shorthand.

Unaged: When referring to samples made specifically for this project, unaged (0 days) is clearly defined in the text. When referring to other material or results from other authors, it refers to samples taken from material prior to it being put into service which has not been subjected to any wet outdoor exposure or accelerated ageing.